272-101

REPORT DOCUMENTATION PAGE	1. REPORT NO. NSF/ENG-92004	2.	3. PB94-117611

Title and Subtitle "Evaluation of code accidental-torsion provisions using earthquake records from three nominally symmetric-plan buildings"	5. Report Date July 1992 6.
Author(s) Juan C. De La Llera and Anil K. Chopra	8. Performing Organization Rept. No. UCB/EERC-92/09
Performing Organization Name and Address Earthquake Engineering Research Center University of California, Berkeley 1301 So. 46th Street Richmond, Calif. 94804	10. Project/Task/Work Unit No. 11. Contract(C) or Grant(G) No. (C) (G) BCS-8921932
Sponsoring Organization Name and Address National Science Foundation 1800 G Street, N.W. Washington, D.C. 20550 California Dept. of Conservation CSMIP 801 K Street, MS 13-35 Sacramento, CA 95814-3531	13. Type of Report & Period Covered 14.

Supplementary Notes

Abstract (Limit: 200 words)

A procedure is presented for evaluating building code provisions for accidental torsion from analysis of earthquake-induced motions of nominally symmetric-plan buildings. This procedure is used to analyze the motions of three buildings recorded during recent California earthquakes. The results demonstrate that the accidental torsional moments specified by the Uniform Building Code are more than sufficient in representing the torsion in the recorded motions of these three buildings, a conclusion that should be applicable to almost all buildings with nominally symmetric plan. It is also demonstrated that accidental torsion need not be considered at all in the design of two of the three buildings, a conclusion that should carry over to most nominally symmetric-plan buildings, with some exceptions that are identified. These conclusions concerning accidental torsion derived for symmetric-plan buildings are expected to be appropriate also for unsymmetric-plan buildings.

17. Document Analysis a. Descriptors

b. Identifiers/Open-Ended Terms

c. COSATI Field/Group

18. Availability Statement:	19. Security Class (This Report)	21. No. of Pages
Release Unlimited	unclassified	162
	20. Security Class (This Page)	22. Price
	unclassified	

See ANSI-Z39.18) | See Instructions on Reverse | OPTIONAL FORM 272 (4-77) (Formerly NTIS-35)

PB94-117611

REPORT NO.
UCB/EERC-92/09
JULY 1992

EARTHQUAKE ENGINEERING RESEARCH CENTER

EVALUATION OF CODE ACCIDENTAL-TORSION PROVISIONS USING EARTHQUAKE RECORDS FROM THREE NOMINALLY SYMMETRIC-PLAN BUILDINGS

by

JUAN C. DE LA LLERA

ANIL K. CHOPRA

A Report to the California Strong Motion Instrumentation Program and the National Science Foundation

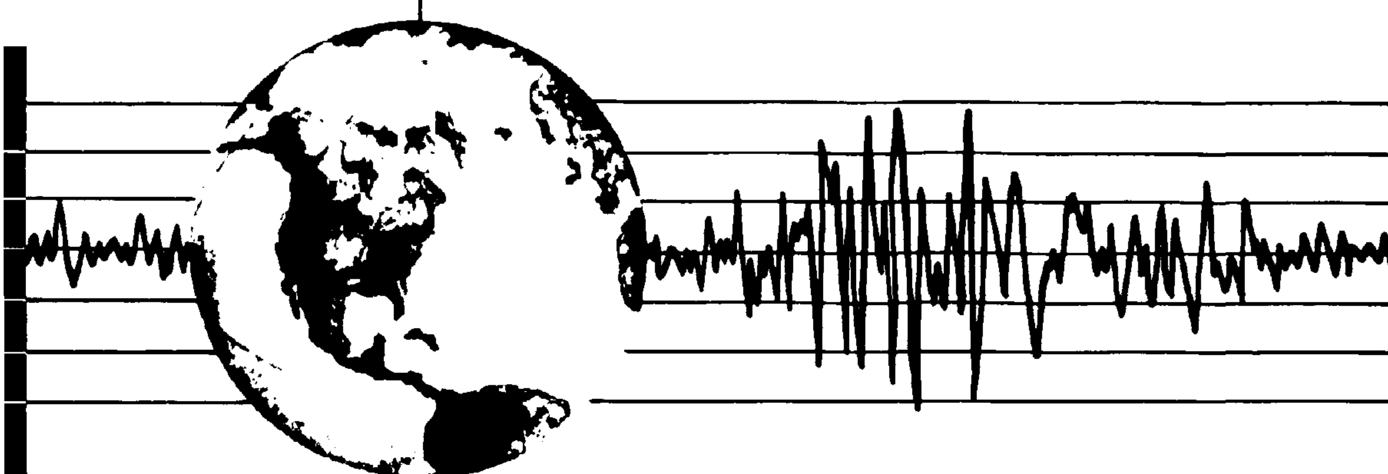

COLLEGE OF ENGINEERING

UNIVERSITY OF CALIFORNIA AT BERKELEY

For sale by the National Technical Information Service, U.S. Department of Commerce, Springfield, Virginia 22161

See back of report for up to date listing of EERC reports.

EVALUATION OF CODE ACCIDENTAL-TORSION PROVISIONS
USING EARTHQUAKE RECORDS FROM THREE
NOMINALLY SYMMETRIC-PLAN BUILDINGS

by

Juan C. De la LLera

Anil K. Chopra

A Report on Research Conducted Under
a Grant from the California Strong Motion Instrumentation Program
and
Grant No. BCS-8921932 from the National Science Foundation

Report No. UCB/EERC-92/09
Earthquake Engineering Research Center
University of California
Berkeley, California

July 1992

ABSTRACT

A procedure is presented for evaluating building code provisions for accidental torsion from analysis of earthquake-induced motions of nominally-symmetric-plan buildings. This procedure is used to analyze the motions of three buildings recorded during recent California earthquakes. The results demonstrate that the accidental torsional moments specified by the Uniform Building Code are more than sufficient in representing the torsion in the recorded motions of these three buildings, a conclusion that should be applicable to almost all buildings with nominally-symmetric plan. It is also demonstrated that accidental torsion need not be considered at all in the design of two of the three buildings, a conclusion that should carry over to most nominally-symmetric-plan buildings, with some exceptions that are identified. These conclusions concerning accidental torsion derived for symmetric-plan buildings are expected to be appropriate also for unsymmetric-plan buildings.

ACKNOWLEDGEMENTS

This investigation was supported by the Strong Motion Instrumentation Program, California Division of Mines and Geology, and the National Science Foundation under Grant No. BCS-8921932. The authors are grateful for this support and to Moh-Jiann Huang and Anthony F. Shakal for providing building plans and earthquake records. Any opinions, discussions, findings, recommendations and conclusions are those of the authors and do not necessarily reflect the views of the sponsor.

The research presented in this report will be included in Juan C. De la Llera's doctoral dissertation.

CONTENTS

INTRODUCTION

Building codes require that the effects of torsion be considered by applying the equivalent lateral forces at a distance e_d from the center of rigidity (CR), resulting in story torques in addition to shears and overturning moments. U.S. codes and design recommendations specify that the lateral force be applied at the center of mass—i.e., at a distance equal to the static eccentricity e_s from the CR—and that this force be shifted $\pm 0.05b$, where b is the plan dimension of the building perpendicular to the direction of ground motion, to obtain increased force in each structural element [1,2]. Thus, the design eccentricity e_d is equal to $e_s \pm 0.05b$. The first term, e_s, is intended to account for the coupled lateral torsional response of the building arising from lack of symmetry in plan. The additional $\pm 0.05b$, known as *accidental eccentricity*, is introduced to account for building torsion arising from discrepancies between the mass, stiffness, and strength distributions used in analysis and true distributions at the time of an earthquake; torsional vibrations induced by a rotational component of ground motion: and other sources of torsion not considered explicitly in analysis. Accidental torsion is to be considered in the design of buildings with asymmetric plans as well as symmetric plans; in the latter case, this is the total torsion to be considered.

Because this investigation is concerned only with accidental torsion provisions in building codes, it is focused on buildings with nominally-symmetric plan. The subject of accidental torsion is not amenable to investigation by traditional analytical approaches because standard dynamic analyses do not predict torsion in symmetric-plan buildings. However, it has been possible to investigate analytically the torsional response of such buildings due to rotational motion of the building's base, where this rotational motion is determined by assumptions which so far have not been verified for lack of suitable ground motion records [3]. Therefore, analysis of recorded motions of nominally-symmetric-plan buildings during earthquakes provides the most direct means of developing an understanding of the torsional responses of such buildings and for evaluation of building code provisions for accidental torsion. This is the approach adopted in this investigation.

BUILDINGS CONSIDERED AND RECORDED MOTIONS

Ideal for the purposes of this investigation would be buildings satisfying certain requirements—nominally-symmetric floor plans, rigid floor diaphragms, and negligible soil-structure interaction effects—that have experienced significant ground shaking, and three independent components of acceleration have been recorded at the ground level and at each floor. Three buildings which essentially satisfy the above requirements have been identified for the present study. A brief description of these three structures and their motions recorded during earthquakes is presented next.

Building A

Identified as CSMIP Station No. 58506, this building is located in Richmond, California. A photograph and typical framing plan of this steel structure is shown in Fig. 1. The building has a nominally-symmetric floor plan. It consists of moment-resisting frames 1 and 7 in the Y-direction. Between frame lines 3 and 6, frames A and C are also designed for lateral load resistance. All other frames with semi-rigid connections are designed to carry only gravity loads. The floor decking system is formed by a corrugated steel sheet filled with lightweight concrete. The roof deck is lighter but has additional insulating concrete. The foundation system consists of rectangular column footings interconnected by grade beams. In the Y-direction only footings for columns of frames 1 and 7 are interconnected. Additional information about this building is presented in Appendix A.

The accelerographs located as shown in Fig. 2 recorded the motion of the building during the Loma Prieta earthquake (October, 1989). These records shown in Fig. 3 include three channels of horizontal motion at the second floor, third floor, and roof levels, and two channels of motion at the first (or ground) floor level. The peak accelerations at the ground level are 0.083g in the X-direction and 0.11g in the Y-direction. These motions were amplified to 0.31g and 0.27g , respectively, at the roof level. The building experienced no structural damage during the earthquake.

Building B

Identified as CSMIP Station No. 23511, this building shown in Fig. 4 is located in Pomona, California. This reinforced concrete frame building has two stories and a partial basement, and a light penthouse structure. The building has a nominally-symmetric floor plan, as indicated by its framing plan (Fig. 4). The lateral force-resisting system in the building consists of peripheral columns interconnected by longitudinal and transverse beams. The "L"-shaped exterior corner columns as well as the interior columns in the building are not designed especially for earthquake resistance. The floor decking system is formed by a 6" concrete slab. The building also includes walls in the stairwell system—concrete walls in the basement and masonry walls in upper stories. Foundations of columns and interior walls are supported on piles. Additional information about this building is presented in Appendix B.

The accelerographs located as shown in Fig. 5 recorded the motion of the building during the Whittier (October, 1987) and Upland (February, 1990) earthquakes. These records shown in Figs. 6 and 7 include three channels of horizontal motion at the second floor and roof levels and at the basement of the building. During the Whittier earthquake, the peak accelerations at the basement level were 0.046g in the X-direction and 0.05g in the Y-direction. These motions were amplified to 0.15g in both directions at the roof level. During the Upland earthquake, the peak accelerations at the ground level were 0.12g and 0.13g in the X- and Y-directions, respectively. These motions were amplified to 0.24g in the X-direction and 0.39g in the Y-direction at the roof level. The building experienced no structural damage during either earthquake.

Building C

Identified as CSMIP Station No. 57562, this building is located in San Jose, California. The building considered is one of four similar wings around a central building. Each wing is isolated from the central building by a separation joint. A photograph and typical framing plan of this three-story steel structure is shown in Fig. 8. The triangular portion of the building (shown in dashed lines) is not part of any lateral moment-resisting frame of the structure. Thus, the building has a nominally-symmetric floor plan consisting of moment-resisting frames A, B, C, and D in the X-direction and frames 1 through 9 in the Y-direction. All other frames are designed to carry only gravity loads. The floor decking system is formed by a steel corrugated metal sheet filled with lightweight concrete. The foundation system consists of rectangular column footings interconnected by grade beams. Additional information about this building is available in Appendix C.

The accelerographs located as shown in Fig. 9 recorded the motion of the building during the Loma Prieta earthquake. These records shown in Fig. 10 include three channels of horizontal motion at each of the roof, third, and first (ground) floor levels. The peak accelerations at the ground level are 0.2g in both lateral directions, X and Y. These motions were amplified to 0.58g in the X-direction and 0.68g in the Y-direction at the roof level. The building experienced no structural damage during the earthquake. The two horizontal components of acceleration and rotational acceleration at the second floor without any accelerographs were estimated using the procedure described in Appendix C.

DYNAMIC ACCIDENTAL ECCENTRICITY

We first determine the accidental eccentricity for a nominally-symmetric-plan building with rigid floor diaphragms directly from the recorded motions. At the i^{th} floor these recorded accelerations are denoted by $a_{1_i}(t), a_{2_i}(t)$, and $a_{3_i}(t)$, and such data are assumed to be available for all floors

$i = 1, 2, \ldots, N$ (Fig. 11(a)) [1]. From the recorded motions of the i^{th} floor the X and Y accelerations components at the CM of the floor, $a_{Xi}(t)$ and $a_{Yi}(t)$, and the torsional acceleration, $a_{\theta i}$, of the i^{th} floor diaphragm can be determined by a simple geometric transformation. The associated inertia forces are $m_i a_{Xi}(t)$ and $m_i a_{Yi}(t)$ in the X and Y directions, respectively, and the associated torque is $I_{pi} a_{\theta i}(t)$ where m_i is the i^{th} floor mass and I_{pi} is the polar moment of inertia of the i^{th} floor mass about the CM of the floor (Fig. 11(b)). The shears and torques in the j^{th} story are determined by simple statics from the floor inertia forces which are known from the floor masses and recorded accelerations:

$$V_{Xj}(t) = \sum_{i=j}^{N} m_i a_{Xi}(t) \tag{1}$$

$$V_{Yj}(t) = \sum_{i=j}^{N} m_i a_{Yi}(t) \tag{2}$$

$$T_j(t) = \sum_{i=j}^{N} I_{pi} a_{\theta i}(t) \tag{3}$$

These story shears and torque are statically equivalent to each of the following force sets: (1) V_{Xj} at the CM and V_{Yj} at eccentricity e_{Xj} (Fig. 11(c)) given by

$$e_{Xj}(t) = \frac{T_j(t)}{V_{Yj}(t)} \tag{4}$$

and (2) V_{Yj} at the CM and V_{Xj} at eccentricity e_{Yj} given by

$$e_{Yj}(t) = \frac{T_j(t)}{V_{Xj}(t)} \tag{5}$$

The time-dependent quantities $e_{Xj}(t)$ and $e_{Yj}(t)$ may be interpreted as the instantaneous accidental eccentricities for the j^{th} story.

From the recorded motions shown in Figs. 3, 6, 7, and 10 these accidental eccentricities were computed for the three selected buildings. The results for the first story are presented in Figs. 12,

[1] Floors are numbered starting with 1 at the floor immediately above the ground level, which is different from the numbering used in describing recorded motions in the preceding sections.

13, 14, and 15 wherein the base shear and base torque are presented together with accidental eccentricities $e_{X1}(t)$ and $e_{Y1}(t)$. These computed eccentricity values grossly exceed the code value of $0.05b$ intermittently during the earthquake. However, this result does not imply that the code provisions are deficient.

This approach to compute the accidental eccentricity is appealing because it is based exclusively on recorded motions and does not require idealization or analysis—static or dynamic—of the structure. However, the numerical results are not especially useful because the largest peaks in the eccentricity-time plot are usually associated with small values of the base shear, and can occur even during the trailing, weak portions of the building motions. Therefore, a large value for the accidental eccentricity by itself is not meaningful and should be considered in conjunction with the instantaneous base shear value. In order to consider the combined effects of shear and torque in evaluating the code provisions, however, static analysis of the structure becomes necessary.

STRUCTURAL IDEALIZATION

The natural vibration frequencies and modes of the buildings are computed and static analyses are performed at many time instants, but no dynamic analyses were necessary. For these analyses the three buildings were idealized consistent with the ETABS computer program wherein the building mass is assumed to be lumped at the floor levels and the floor diaphragms are assumed to be rigid. The compatibility of axial deformations required in columns belonging to more than one moment-resisting frame is considered by analyzing each structure as a single three-dimensional frame with six degrees of freedom per joint (in contrast to the more common type of analysis that considers the structure as an assemblage of independent planar frames). A brief summary of the structural idealization for each building is presented next; additional details are available in the appendices.

Building A

This building was treated as fixed at the level defined by the slab on grade. Each frame was modeled with appropriate beam-column joints: moment-resistant (or rigid) connections and semi-rigid connections. The latter were divided into two groups: connections of column flanges with beams were modeled as rigid, and connections of column webs with beam webs as pinned. Computed by the ETABS program, the natural vibration frequencies and shapes of the first mode in the X-direction, the first mode in the Y- direction, and the first torsional mode are presented in Table 1. These computed results are similar to the "actual" vibration properties in Table 1 determined from the recorded earthquake motions by the procedure described in Appendix A.

Building B

This building was treated as fixed at the level defined by the base of the columns because the pile foundations are very stiff. The structural idealization considers all structural elements, including those not intended to provide lateral resistance, such as the masonry walls in the stairwell system, because they may cause torsion of the building and contribute to its accidental eccentricity. The effective moment of inertia in the beams was calculated assuming cracked sections and including the contribution of the concrete slab. The actual variation of moment of inertia along the span was considered in modeling the tapered beams along axes 2, 3, 4, and 5 (Fig. 4). The effective moment of inertia in columns was calculated assuming gross section properties.

Computed by the ETABS program, the natural vibration frequencies and shapes of the first mode in the X-direction, first mode in the Y-direction, and first torsional mode are presented in Table 1. These computed results agree reasonably well with the "actual" vibration properties determined from the recorded earthquake motions (Appendix B). As expected, the computed vibration properties are closer to the "actual" values from the less intense Whittier earthquake motions than from the more intense Upland earthquake motions. The higher intensity of shaking during the Upland earthquake, combined with the stiffness degradation during the earlier Whittier earthquake, leads to lower vibration frequencies during the Upland earthquake.

Building C

This building was treated as fixed at the level of the slab on grade. The structural idealization includes all structural elements, including those that provide little lateral resistance, such as the triangular portion of the building (Fig. 8), because they may cause torsion of the building and contribute to its accidental eccentricity. Each frame was modeled with appropriate beam-column connections: moment-resistant (or rigid) connections and pinned connections as defined in the original structural drawings of the building. Computed by the ETABS program, the natural vibration frequencies and shapes of the first mode in the X-direction , the first mode in the Y-direction , and the first torsional mode are presented in Table 1. These computed results are similar to the "actual" vibration properties in Table 1 determined from the recorded earthquake motions by the procedure described in Appendix C.

BASE SHEAR AND BASE TORQUE

As mentioned in a preceding section, the combined effects of shear and torque must be considered in evaluating the accidental torsion provisions in building codes. For each of the three buildings the base shears $V_{X1}(t)$ and $V_{Y1}(t)$ and base torque $T_1(t)$ have already been computed from the recorded accelerations using Eqs. 1-3. Consistent with the code approach of two independent lateral-force analyses in two orthogonal directions, X and Y, we consider the combined effects of V_{Y1} and T_1 separately from the combined effects of V_{X1} and T_1 ; only the first pair is considered in the following presentation and the modification for the other pair is obvious. Figure 16 shows the base shear $V_{Y1}(t)$ and base torque $T_1(t)$ for Building A during the recorded earthquake wherein each point

(+) denotes the combination of V_{Y1} and T_1 values at a particular time instant; there are as many points as the time instants considered. The point C in Fig. 16 identifies the code value of base shear $V_{code} = (ZIC\ /R_w)\,W$ and base torque which, for a nominally-symmetric building, is $T_{code} = (0.05b)\,V_{code}$ In computing the coefficient C , the fundamental vibration period T was taken equal to the "actual" value in Table 1, and R_w as 12. The fact that the base shear during the earthquake exceeds the code value of base shear at many time instants is consistent with the well known fact that the actual capacity of most buildings is much larger than the design base shear. In order to evaluate the code-accidental torsion provisions, we also show the point C_a, which denotes the maximum value of actual base shear $(V_{Y1})_o = max_t|V_{Y1}(t)|$ and $T_1 = (0.05b)(V_{Y1})_o$. However, it is by no means obvious whether the pair of actual forces $V_{Y1}(t)$ and $T_1(t)$ at a particular time instant is more or less "critical" to the structure than the amplified "code" forces denoted by C_a. Note that so far no structural analysis was necessary.

In order to resolve this issue, we determine all combinations of base shear and base torque which, when considered as static forces, produce the same member force as the amplified code forces denoted by C_a. These code-equivalent combinations shown, for example, in Fig. 16 for Building A are determined by static analysis of the building as follows:

1. The maximum value of base shear $V = (V_{Y1})_o$ determined from floor accelerations (Eq. 2) may be defined as the amplified "code" base shear.

2. Analyze the structure using a static code-type analysis considering: (a) base shear as given in Step 1; (b) heightwise distribution of lateral floor forces according to the code; and (c) accidental eccentricity, equal to $0.05b$ in the Uniform Building Code, in the most unfavorable direction for each element. The resulting base shear V and base torque T are shown as point C_a in Fig. 17(e). A member force computed by this analysis is defined as a member "design" force. The analysis required in Step 2 is shown conceptually in Fig. 17(a), where F_i (i=1,2,3)

are the lateral floor forces in the Y-direction, defined by Steps 2a and 2b. The resulting "design" shear V_{c1}^D in column 1 is obtained by applying the story lateral forces at a distance equal to $0.05b$ to the right of the CM. Analogously, the "design" shear V_{c2}^D in column 2 is obtained by applying the same floor forces at a distance of $0.05b$ to the left of the CM.

3. Determine the value of base shear and the associated lateral floor forces distributed over the building height according to the code which, applied at the CM (without any floor torques or eccentricity), produce the same member "design" force as determined in Step 2. This base shear is identified by points A_c and A'_c in Fig. 17(e). The analysis required in Step 3 is shown conceptually in Fig. 17(b). The building subjected to the lateral floor forces F_1, F_2, and F_3 of Steps 2a and 2b applied at the CM of the floors is analyzed to determine V_{c1}^S and V_{c2}^S, the shear forces in columns 1 and 2, respectively. The lateral forces F_i and base shear V multiplied by the ratio V_{ci}^D/V_{ci}^S (i=1,2) acting alone (without any floor torques or eccentricity) would produce in column "i" the shear force V_{ci}^D, which is equal to the member "design" force determined in Step 2. In the case of column 1 this base shear, $V_{c1}^o = (V_{c1}^D/V_{c1}^S)\, V$, defines the points A_{c1} and A'_{c1} in Fig. 17(e). Similarly, $V_{c2}^o = (V_{c2}^D/V_{c2}^D)V$ defines the points A_{c2} and A'_{c2} in Fig. 17(e).

4. Determine the value of base torque and the associated floor torques distributed over the building height in the same proportion as the lateral floor forces which alone (without any lateral forces) produce the same "design" force in a selected member as determined in Step 2. This torque is identified by points B_c and B'_c in Fig. 17(e). The analysis required in Step 4 is shown conceptually in Fig. 17(c). The building subjected to story torques T_i, where $T_i = 0.05b\, F_i$ and F_i are known from Steps 2a and 2b, is analyzed to determine V_{c1}^T and V_{c2}^T, the shear forces in columns 1 and 2, respectively. The floor torques T_i and base torque T multiplied by the ratio V_{ci}^D/V_{ci}^T (i=1,2) acting alone (without any lateral forces) would

produce the "design" shear force V_{ci}^{D} in column "i". In the case of column 1 this base torque $T_{c1}^{o} = (V_{c1}^{D}/V_{c1}^{T})T$ defines the points B_{c1} and B'_{c1} in Fig. 17(e). Similarly, $T_{c2}^{o} = (V_{c2}^{D}/V_{c2}^{T})T$ defines the points B_{c2} and B'_{c2} in Fig. 17(e).

5. Each point on lines $A_{c1}B_{c1}$ and $A'_{c1}B'_{c1}$ denotes a combination of base shear and base torque, each being distributed over the building height according to the code (Steps 3 and 4) which produces the same member "design" force as determined in Step 2; hence, lines $A_{c1}B_{c1}$ and $A'_{c1}B'_{c1}$ are called "code-equivalent combinations" associated with column 1. Similarly, $A_{c2}B_{c2}$ and $A'_{c2}B'_{c2}$ are the "code-equivalent combinations" associated with column 2.

If at each time instant the "actual" base shear and base torque combination falls within the region enclosed by the code-equivalent limits, this implies that, during the earthquake, the force in the selected member did not exceed the "design" value determined in Step 2. Alternatively, such a situation indicates that the accidental eccentricity of $0.05b$ is conservative during the particular earthquake. Any point in the base shear-torque plot which falls outside the region enclosed by code-equivalent combination represents, at a particular time instant, a combination of base shear and base torque that produces in the selected member a force that is larger than its "design" value. Alternatively, this situation indicates that the accidental eccentricity of $0.05b$ is unconservative at that instant of time.

The above-described procedure was utilized to determine the code-equivalent combinations of base shear and base torque for Building A, and the results are presented in Fig. 16. Analysis for Y forces with the shear forces in columns 8 and 18 selected as the member "design" forces led to the code-equivalent combinations of Fig. 16(b). Similarly, analysis for X-lateral forces with the shear forces in columns 4 and 22 selected as the member "design" forces led to the code-equivalent combinations of Fig. 16(a). These results demonstrate that all points denoting "actual" values of base shear and base torque during the earthquake fall inside the region enclosed by the code-equivalent combinations with one exception: point A in Fig. 16(a), which indicates that only at that instant of time during the earthquake, the shear force in column 22 exceeds the "design" force. This observation is consistently confirmed by examining the code-equivalent limits for the "design" shear forces and bending moments in several other beams and columns. For the recorded response of Building A during the Loma Prieta earthquake, the torsional effects are so small that it may not be necessary to consider accidental eccentricity at all. Figure 16 indicates that very few points fall outside the region enclosed by the code-equivalent combinations with zero accidental eccentricity.

Figure 18 shows the dynamic base shear-torque values, and code-equivalent combinations determined from the motions of Building B recorded during the Whittier earthquake. Similar results for the Upland earthquake are presented in Fig. 19. Analysis for X-lateral forces with the shear forces in columns 2 and 29 selected as the member "design" forces led to the code-equivalent combinations of Figs. 18(a) and 19(a). Similar analysis for Y-lateral forces with the shear forces in columns 8 and 25 selected as the member "design" forces led to the code-equivalent combinations of Figs. 18(b) and 19(b). Only at two time instants during the Whittier earthquake does the "actual" shear force in column 29 exceed the "design" force. During the Upland earthquake, the "actual" forces in all columns remain below their respective design values. In fact, the design value with zero accidental eccentricity is exceeded only once, suggesting that it is not even necessary to consider any accidental eccentricity for the recorded response of Building B during the Upland earthquake.

The actual values of the Y-component of the base shear and base torque for Building C during the Loma Prieta earthquake are presented in Fig. 20(b). This plot shows a trend towards the second and fourth quadrants which implies that the dynamic forces in structural elements located on the left side of the CM of the structure (Fig. 8), e.g. column 1, and more likely to exceed their "design" values. This speculation is confirmed in Fig. 20 which shows that at a few time instants the actual shear force in the first story exceeds the design value.

MEMBER FORCES

An alternative procedure to the one presented in the preceding section for evaluating the code-accidental torsion provisions is to compare the member "design" forces defined in Step 2 of the preceding section with the time history of the "actual" member forces during the earthquake. At each time instant the "actual" member forces during the earthquake are determined by static analysis of the building subjected to the floor inertia forces $m_j a_{xj}(t)$, $m_j a_{yj}(t)$, and $I_{pj} a_{\theta j}(t)$ at all floors, i.e., j = 1,2 and 3 (Fig. 17(d)). If at all time instants the "actual" member force is less than its "design" value, the accidental eccentricity of $0.05b$ can be interpreted to be conservative during the particular earthquake. Conversely, the accidental eccentricity of $0.05b$ is unconservative at those time instants when the "actual" member force exceeds the "design" value. The two procedures are equivalent for a symmetric one-story system but differ slightly for multistory buildings because the actual heightwise distribution of lateral forces computed from recorded accelerations and floor masses is not identical to the heightwise distribution of lateral forces specified by the code.

The time variation of the "actual" shear force in the first-story columns 22 and 18 of Building A during the Loma Prieta earthquake is presented in Fig. 21, together with the "design" values of these forces obtained by static analysis of the building for amplified code forces in the X-direction (for column 22) and in the Y-direction (for column 18). The "actual" values of these member forces do not exceed their "design" values based on the specified accidental eccentricity and barely exceed the design values ignoring this eccentricity. The results for shear force and bending moment in all columns support this conclusion (Appendix A).

The time variation of the "actual" shear force in the first-story columns 8 and 26 of Building B during the Whittier earthquake is presented in Fig. 22, together with the "design" values of these forces obtained by static analysis for amplified "code" forces in the X -direction (for column 26) and in the Y -direction (for column 8). Similar results obtained from the Upland earthquake records are presented in Fig. 23. For both earthquakes the "actual" values for these member forces do not exceed their "design" values based on the code-specified accidental eccentricity and barely exceed the design values ignoring this eccentricity. The results for shear force and bending moment in all columns in the building support this conclusion (Appendix B).

The time variation of the "actual" shear force in the first-story columns 1 and 8 of Building C during the Loma Prieta earthquake is presented in Fig. 24, together with the "design" values of these forces obtained by static analysis of the building for amplified code forces in the X-direction (for column 8) and in the Y-direction (for column 1). The "actual" value of the X-component of the shear force in the first-story column 8 does not exceed its "design" value based on the code-specified accidental eccentricity and barely exceeds the design value ignoring this eccentricity. The results for shear forces and bending moments in all columns associated with motion of the building in the X-direction support this conclusion. The "actual" value of the Y-component of the shear force in the first-story column 1 exceeds its "design" value for a small fraction of a second three times during the earthquake. The maximum value of the "actual" shear during the earthquake is ten percent greater than its "design" value. These observations are representative of other columns at the left edge of the plan (Appendix C). The "actual" forces in columns located to the right of the CM remain below their "design" values throughout the earthquake.

Accidental torsion is seen to be more significant in the response of Building C than the other two buildings. This may be the result of three factors: Firstly, the natural vibration periods of the first three—two lateral and one torsional—vibration modes are very close to each other—a situation known from forced vibration tests to create strong coupling of lateral and torsional motions even in nominally-symmetric buildings [4]. Secondly, as shown in the next section, the torsional component of the base motion contributes about forty percent of the accidental torsion. Thirdly, the restraint provided by the adjacent building may have contributed to accidental torsion.

CONTRIBUTION OF ROTATIONAL BASE MOTION

The member forces presented in the preceding section are associated with the earthquake-induced translational and torsional motions of the selected buildings. As mentioned earlier, symmetric-plan buildings may undergo "accidental" torsional motions for several reasons, including the two principal factors: the building is usually not perfectly symmetric, and the ground motion contains a rotational (about the vertical axis) component which will induce torsional motion of the building even if its plan were perfectly symmetric. Presented in this section are results that identify the member forces due only to "accidental" torsion, and the portions of these forces associated with rotational motion at the ground level of the building. Computed from the motions recorded by channels 6 and 7 in Building B (Figs. 6 and 7) and by channels 3 and 4 in Building C (Fig. 10), these rotational accelerations multiplied by half the building-plan dimensions are presented in Fig. 25. The channels of recorded motion at the base of Building A (Fig. 2) are insufficient to compute the rotational motion at the base of this building. For Building C the peak value of $b/2a_\theta(t)$, where $b = 87.9$ m, is 57.6 cm/sec^2, compared with the peak acceleration of 192.5 cm/sec^2 at channel 4 in the Y-direction. For Building B the peak values of $b/2a_\theta(t)$, where $b = 33.5$ m, are 9.2 cm/sec^2 during the Whittier earthquake and 28.3 cm/sec^2 during the Upland earthquake, compared with the peak values of 45.3 and 119.5 cm/sec^2, respectively, at channel 6 in the X-direction. It is apparent that, in the cases considered, rotational ground motion contributes twenty to thirty percent of the lateral acceleration at the edges of the building plan.

The member forces due to accidental torsion are determined at each instant of time by static analysis of the building subjected to floor inertia torques $I_{pj}a_{\theta j}(t)$ at all floors, i.e. j=1,2,...,N, determined in the preceding section. The results of these analyses, which are the same as in the preceding section, except that the floor inertia lateral forces $m_j a_{Xj}(t)$ and $m_j a_{Yj}(t)$ are excluded, are presented in Figs. 26-28. Comparing these results (Figs. 26 and 27) with the total member forces in Building B (Figs. 22 and 23) indicates that the member forces associated with accidental torsion are only two to four percent of the total forces. In contrast, a comparison of Figs. 24 and 28 for Building C shows that accidental torsion contributes about ten percent of the total shear in Column 8 and about thirty percent of the total shear in column 1. These observations that accidental torsion is much more significant in Building C than in Building B are consistent with the results of the preceding sections.

In order to determine the torsional response of Buildings B and C due only to the rotational ground motion, dynamic analyses of these buildings are necessary, something we had deliberately avoided so far in order to eliminate any discrepancies in the structural idealization for dynamic analyses relative to the actual building. The torsional response of Buildings B and C to the rotational base motions presented in Fig. 25 was determined using the structural idealizations described earlier. The mode superposition method was used to determine the response in the natural modes of torsional vibration of the buildings. The modal damping ratios were estimated as five percent and three percent for Buildings B and C, respectively, by the half-power bandwidth method applied to the transfer function for rotational accelerations.

The response history of structural member forces determined by these dynamic analyses is presented as the dashed curve in Figs. 26-28. The maximum force in a particular member due to rotational base motion is compared next with its value associated with the total torsional motions due to accidental torsion. This ratio, which is essentially the same for all structural members of a building, is twenty-five percent for Building B during the Whittier earthquake, forty-five percent for the same building during the Upland earthquake, and forty percent for Building C during the Loma Prieta earthquake. Obviously, the rotational base motion causes a significant portion of the accidental torsion of a building, which obviously depends on the intensity of the rotational ground motion.

IMPLICATIONS FOR CODE PROVISIONS

For the three buildings and their motions during past earthquakes considered in this investigation, the actual member forces exceed their "design" values based on the UBC-specified accidental torsion by less than ten percent for three or fewer times during an earthquake, each time for a small fraction of a second (Figs. 21-24). These discrepancies between the "design" force and the actual force are small when considered in the context of the many larger approximations inherent in building code provisions, and in the context of uncertainties in building idealization and material properties. Thus, the accidental torsion provisions in building codes are sufficient in representing the torsional motions of these three buildings during the particular earthquakes.

The next issue addressed in this paper is: can accidental torsion be ignored in building design? We address this question first for moderate ground motion, then for strong ground motion. During the earthquakes considered, a member design force is exceeded once for a small fraction of a second by less than three percent in Building A, once in Building B for a small fraction of a second by less than ten percent during the Whittier earthquake and thirteen percent during the Upland earthquake, and four times, each for a small fraction of a second, by less than thirty-eight percent in Building C (Figs. 21-24). Such increased force demand, except possibly the large increase in Building C, should not be a problem for most well designed buildings with nominally-symmetric floor plan for two reasons. Firstly, the overstrength relative to design values that is typical of most buildings would, for moderate ground motion, be sufficient for the building to withstand the increased force demand essentially within the elastic range. Secondly, even if the force demands exceeded structural capacity because of accidental torsion, the damaging effects of the very few and small inelastic excursions of very short duration would be very small.

During strong ground motions, most buildings would be expected to deform beyond the elastic range and accidental torsion may increase the ductility demand for some structural frames or elements of a building designed without considering accidental torsion. However, although the results presented in preceding sections are from elastic analyses, they suggest that the additional ductility demand due to accidental torsion should be small for the buildings considered, except possibly for Building C. Thus, if Buildings A and B were designed ignoring accidental eccentricity, but detailed for sufficient ductility for the design earthquake, their performance should not be adversely affected by accidental torsion.

Thus, it seems that accidental torsion need not be considered in the design of at least two of these three buildings for the recorded ground motions or reasonably amplified versions of these ground motions. Although extrapolating these observations to other situations is somewhat speculative, it is difficult to visualize that the design of many nominally-symmetric buildings would be influenced significantly by accidental torsion, or that torsional response could be a significant contributor to the damage such a building may experience during an earthquake.

On the other hand, accidental torsion may be a significant factor in several situations: (1) natural vibration periods of the fundamental lateral and torsional modes are very close to each other, as in Building C, a situation that creates strong coupling of lateral and torsional motions of the building; (2) the torsional vibration period is much longer than the lateral vibration period, as in a central shear core building or a building with cruciform-shaped plan, leading to possibly large torsional motions; (3) the building plan is especially long in one or both directions, as in Building C, in which case some of the structural elements at the edges of the building-plan can be affected significantly by accidental torsion; and (4) the earthquake causes significant rotation of the base of the building. However, these situations are not recognized by the accidental torsion provisions in building codes, with one exception. The accidental eccentricity of $\pm 0.05b$ is proportional to the plan dimension b and, hence, leads to larger torsional moments for buildings with long plan dimension.

CONCLUSIONS

Building code provisions for accidental torsion are conceptually appealing in that they account for the torsional motions of nominally-symmetric buildings which invariably occur because these buildings are not *perfectly* symmetric in plan and the base motion may contain a rotational (about the vertical axis) component. In this investigation these design provisions have been evaluated by investigating the motions of three nominally-symmetric-plan buildings recorded during earthquakes. The results presented have demonstrated that:

1. The accidental torsion provisions, based on an eccentricity equal to five percent of the plan dimension, are more than sufficient in representing the torsional motions of the three buildings during the particular earthquakes, although these motions cause as large as thirty-percent increase in member forces in one of the buildings. This conclusion should apply to almost all nominally-symmetric-plan buildings.

2. Accidental torsion need not be considered in the design of two of these buildings for the recorded ground motions or reasonably amplified versions of these ground motions. Although extrapolating this conclusion to other situations is speculative, it appears that accidental torsion would not be significant in the earthquake response of most nominally-symmetric buildings; possible exceptions are identified in the next paragraph.

3. Accidental torsion may, however, be significant if the natural vibration periods of the fundamental and torsional modes of the building are very close to each other, the torsional vibration period is much longer than the lateral vibration period, the building plan is especially long in one or both directions, or the expected ground motion can cause unusually strong rotational (about the vertical axis) motions at the base of the building. Accidental torsion may also be significant for buildings which may undergo yielding or local failures that are likely to

increase the asymmetry, e.g, buildings with masonry walls or partitions. However, the code provisions do not recognize these factors, except the one concerning the plan dimension.

4. The rotational base motion causes twenty-five to forty-five percent of the accidental torsion in the recorded earthquake motions of the three buildings considered in this investigation.

5. Although conceptually appealing, the accidental torsion provision in building codes is a refinement to represent effects that are small for most buildings, especially when considered in the context of many larger approximations inherent in structural design.

6. This investigation supports the experience of many practicing structural engineers that building design is influenced very little by considering the accidental eccentricity of $\pm 0.05b$, a code requirement that is cumbersome to implement in design practice.

7. The preceding conclusions concerning accidental torsion derived for symmetric-plan buildings are expected to be appropriate for unsymmetric-plan buildings. Torsion of such buildings arising from plan asymmetry is separately considered by buildings codes.

Recorded motions of nominally symmetric-plan buildings during earthquakes provides the most promising means for understanding the torsional response of such buildings and for evaluating building code provisions for accidental torsion. Therefore, additional buildings with nominally symmetric-plan, especially those likely to undergo significant torsional vibration, should be instrumented, e.g., buildings with fundamental lateral and torsional periods close to each other, or with torsional vibration period much longer than the lateral vibration period. Records from such buildings, especially of response in the inelastic range, would provide a basis to evaluate further the adequacy and the necessity of the accidental torsion provisions in building codes.

REFERENCES

1. Recommended Lateral Force Requirements and Tentative Commentary. Structural Engineers Association of California, 1990.

2. Tentative Provisions for the Development of Seismic Regulations for Buildings, ATC3-06. Applied Technology Council, Palo Alto, California, 1978.

3. N.M. Newmark and E. Rosenblueth. Fundamentals of Earthquake Engineering. Prentice-Hall, Inc., Englewood Cliffs, N.J., 1971.

4. P.C. Jennings, R.B. Matthiesen, and J.B. Hoerner, "Forced Vibration of a Tall Steel-Frame Building," Earthquake Engineering and Structural Dynamics, Vol. 1, No. 2, 1972, pp. 107-132.

Page Intentionally Left Blank

Table 1: Natural Vibration Periods and Mode Shapes for Buildings A, B, and C

Vibration Properties	X-lateral mode		Y-lateral mode		Torsional mode	
	Recorded	Computed	Recorded	Computed	Recorded	Computed
	Building A: Loma Prieta Earthquake					
Period (sec)	0.63	0.60	0.74	0.76	0.46	0.45
Mode Shape						
Roof	1.00	1.00	1.00	1.00	1.00	1.00
3^{rd} Floor	0.71	0.77	0.72	0.73	0.72	0.76
2^{nd} Floor	0.39	0.57	0.39	0.38	0.40	0.43
	Building B: Whittier Earthquake					
Period (sec)	0.29	0.28	0.27	0.27	0.20	0.20
Mode Shape						
Roof	1.00	1.00	1.00	1.00	1.00	1.00
2^{nd} Floor	0.62	0.61	0.39 ?	0.60	0.57	0.64
	Building B: Upland Earthquake					
Period (sec)	0.30	0.28	0.28	0.27	0.21	0.20
Mode Shape						
Roof	1.00	1.00	1.00	1.00	1.00	1.00
2^{nd} Floor	0.64	0.61	0.55	0.60	0.52	0.64
	Building C: Loma Prieta Earthquake					
Period (sec)	0.67	0.70	0.69	0.69	0.69 - 0.65	0.67
Mode Shape						
Roof	1.00	1.00	1.00	1.00	1.00	1.00
3^{rd} Floor	0.80	0.70	0.70	0.67	0.67	0.66
2^{nd} Floor	0.44	0.33	0.33	0.30	0.31	0.30

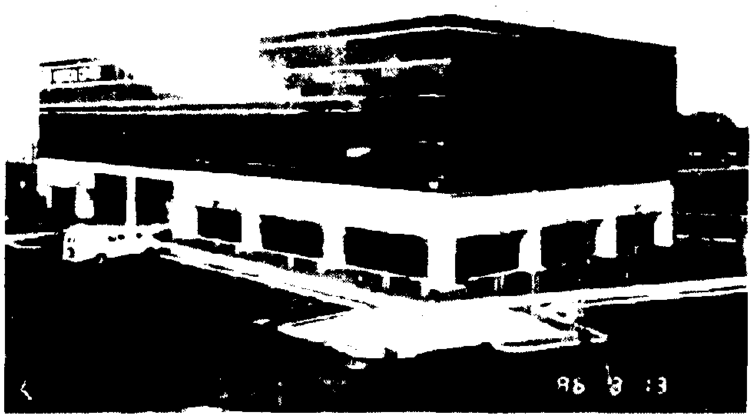

(a) Three-story Steel Frame Building, Richmond, California

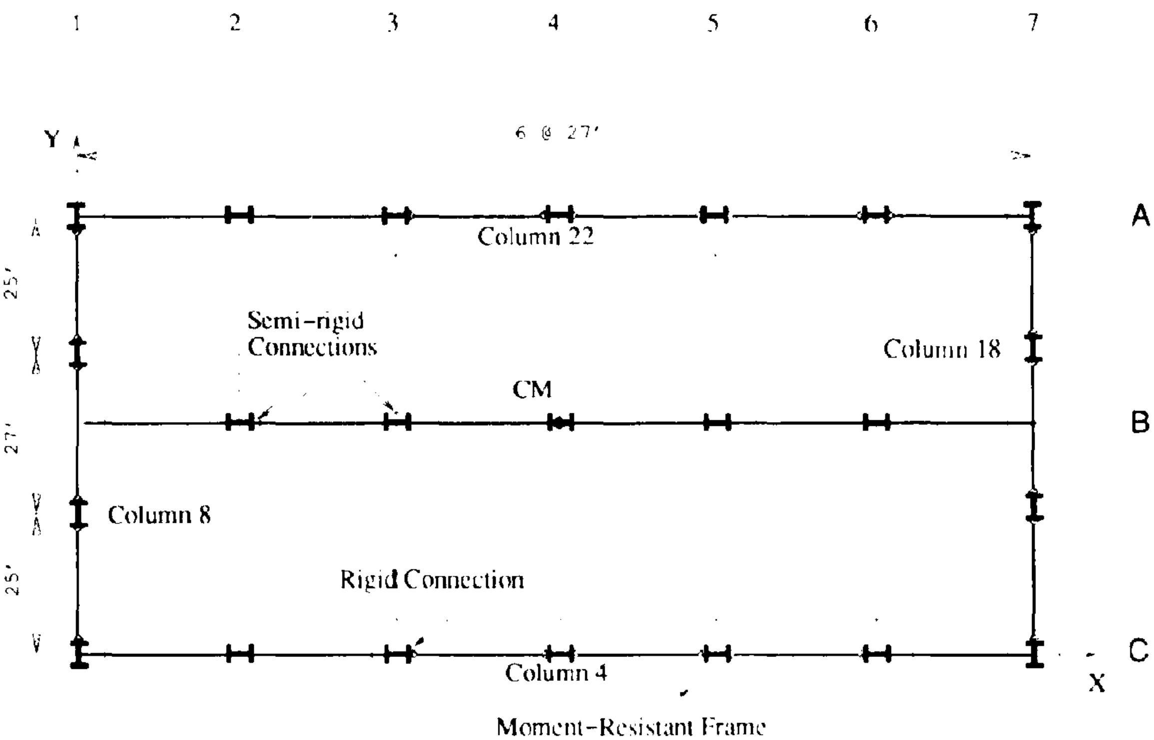

(b) Framing Plan

Figure 1: Photograph and Framing Plan of Building A

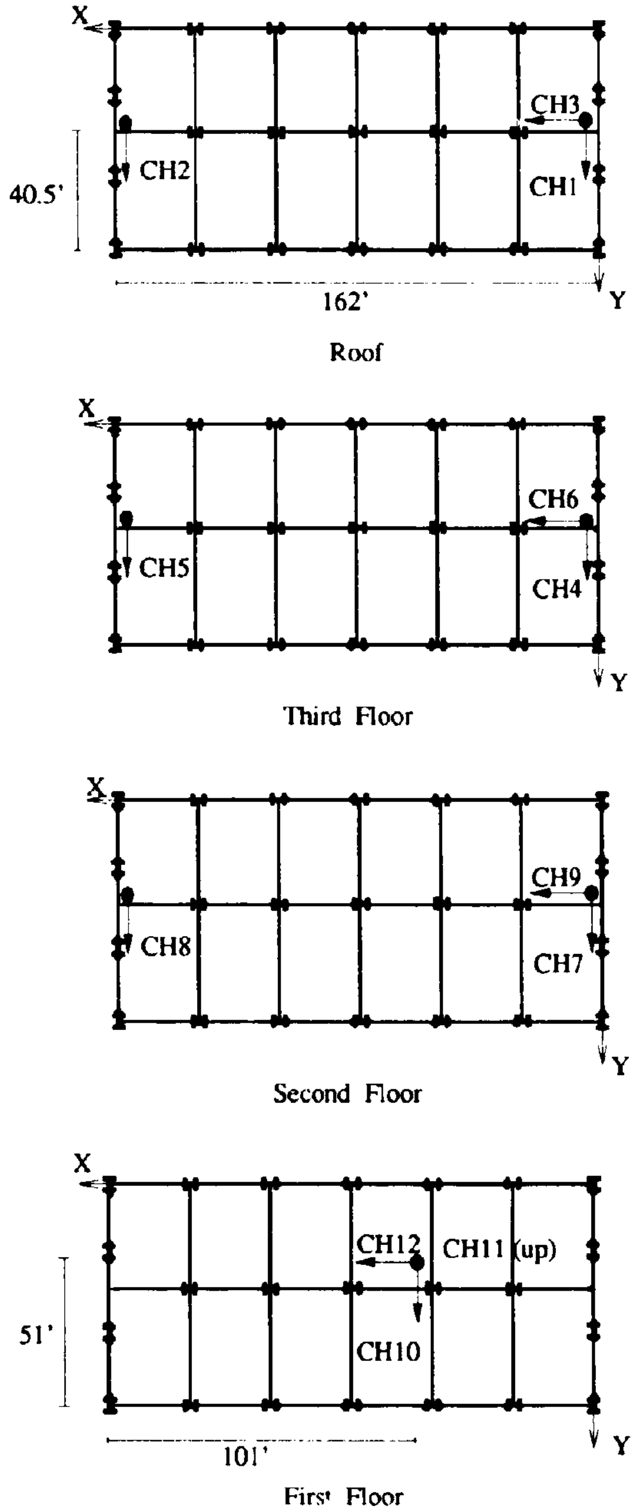

Figure 2: Accelerograph Channels

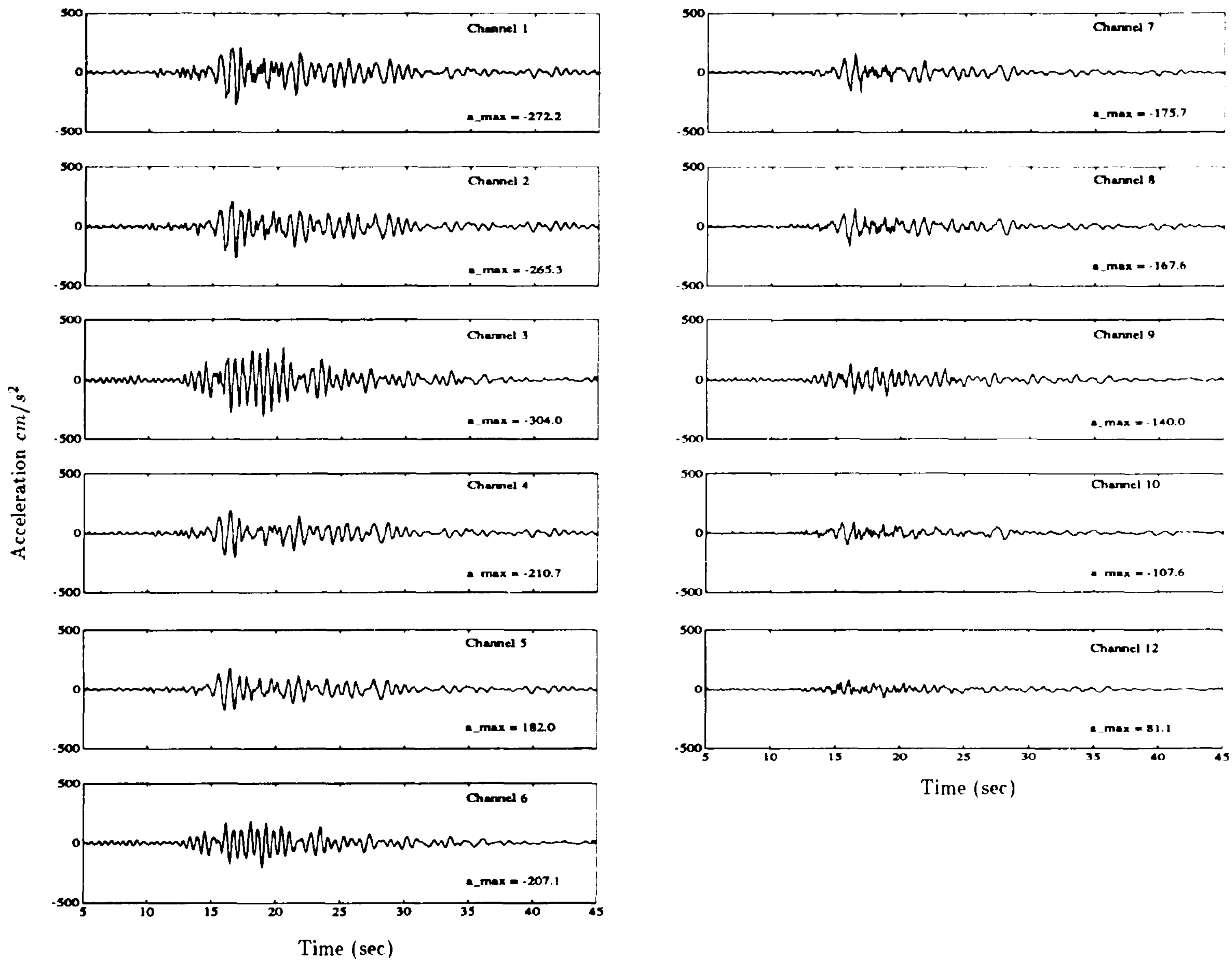

Figure 3: Recorded Motions in Building A During the Loma Prieta Earthquake

(a) Two-story Reinforced Concrete Building, Pomona, California

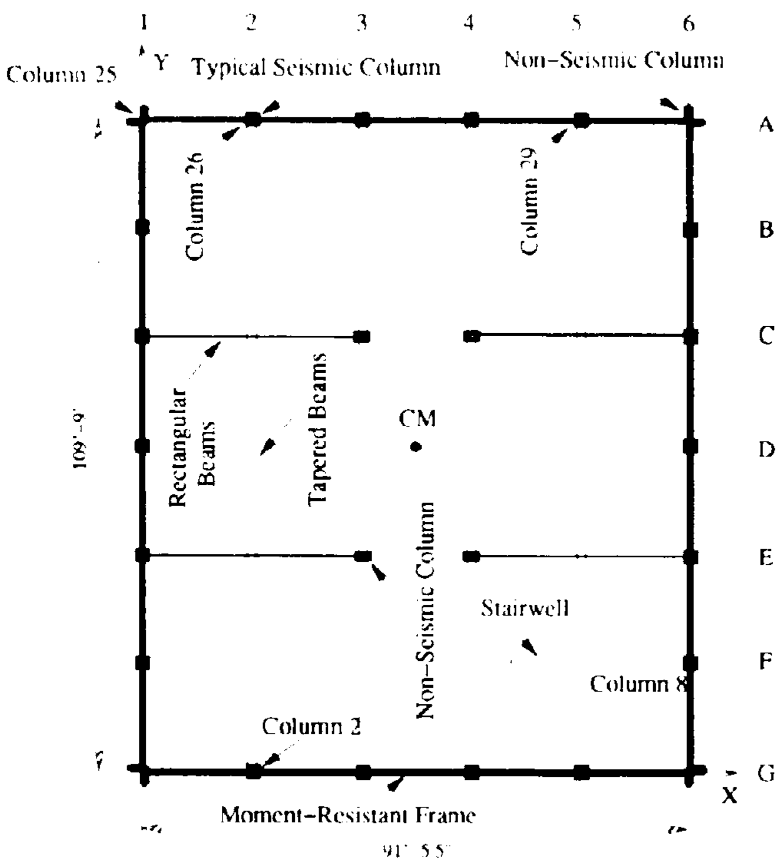

(b) Framing Plan

Figure 4: Photograph and Framing Plan of Building B

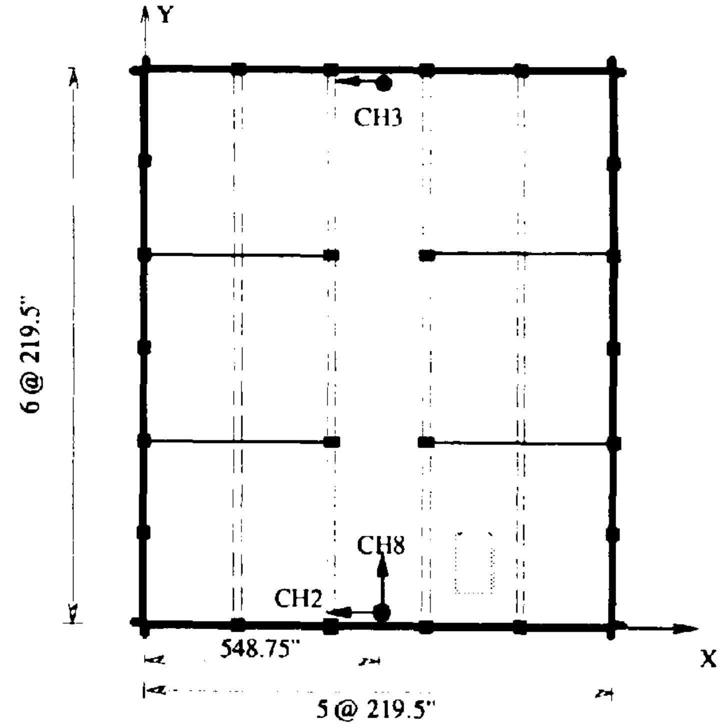

Roof

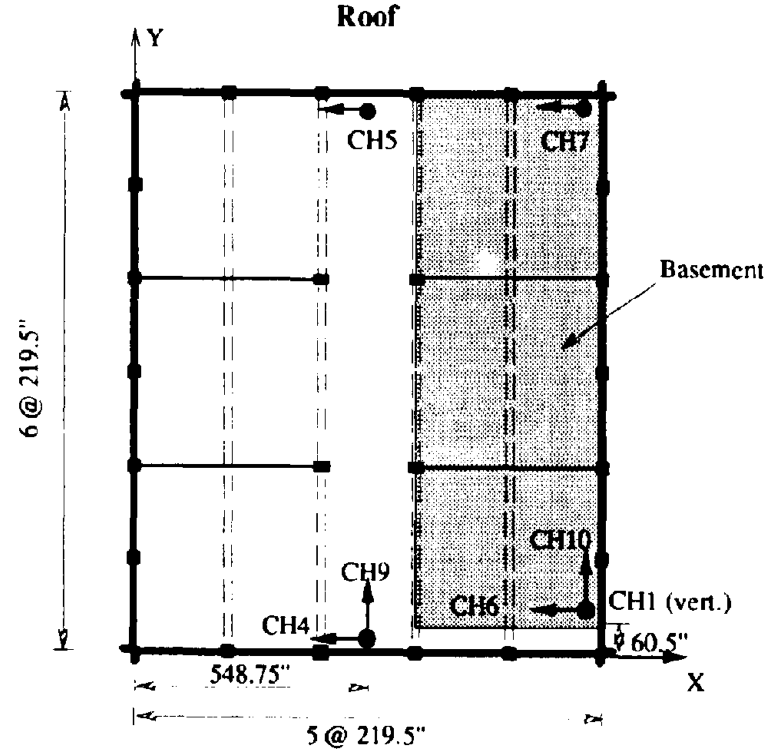

Second Floor and Basement

Figure 5: Accelerograph Channels

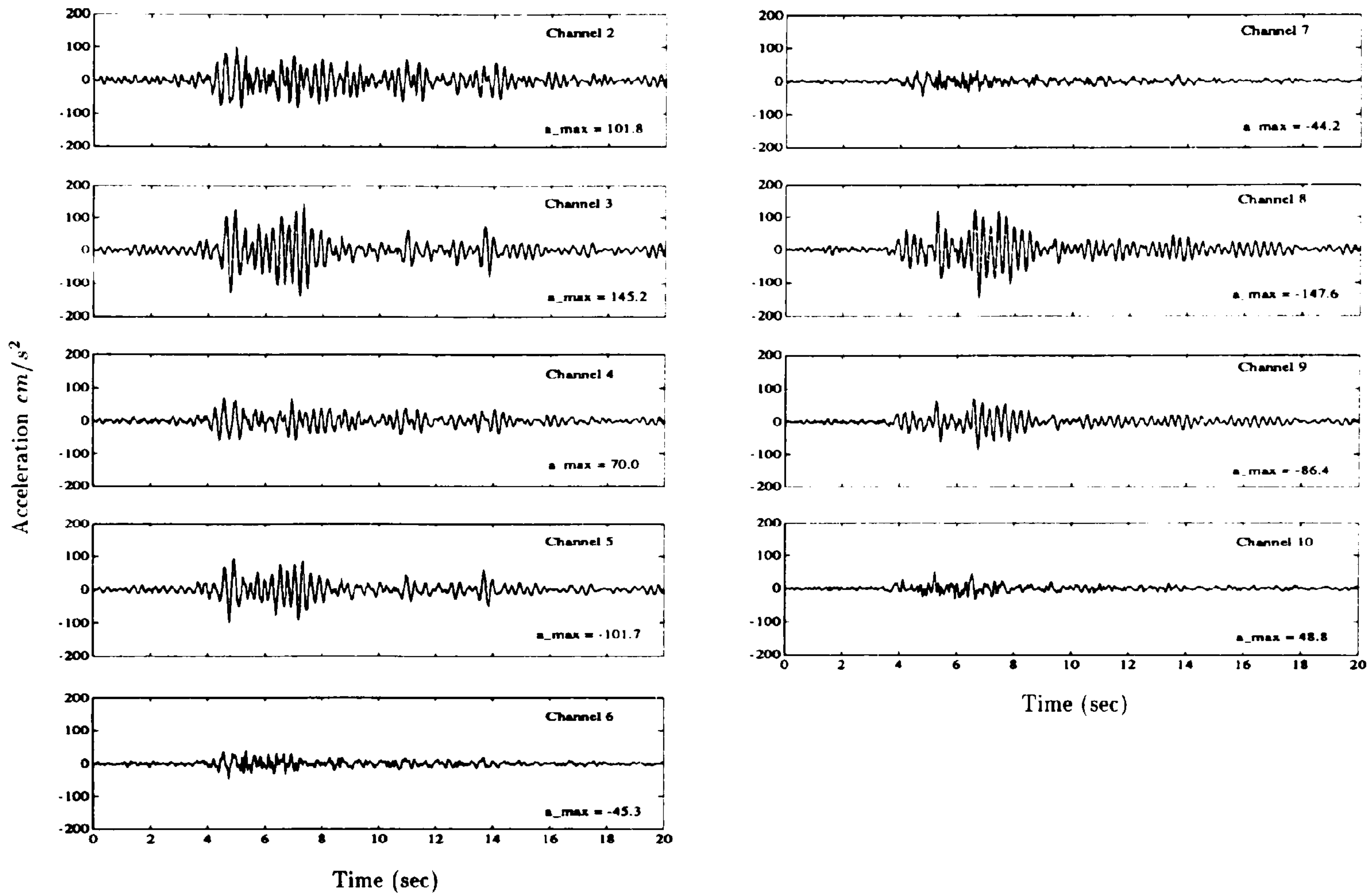

Figure 6: Recorded Motions in Building B During the Whittier Earthquake

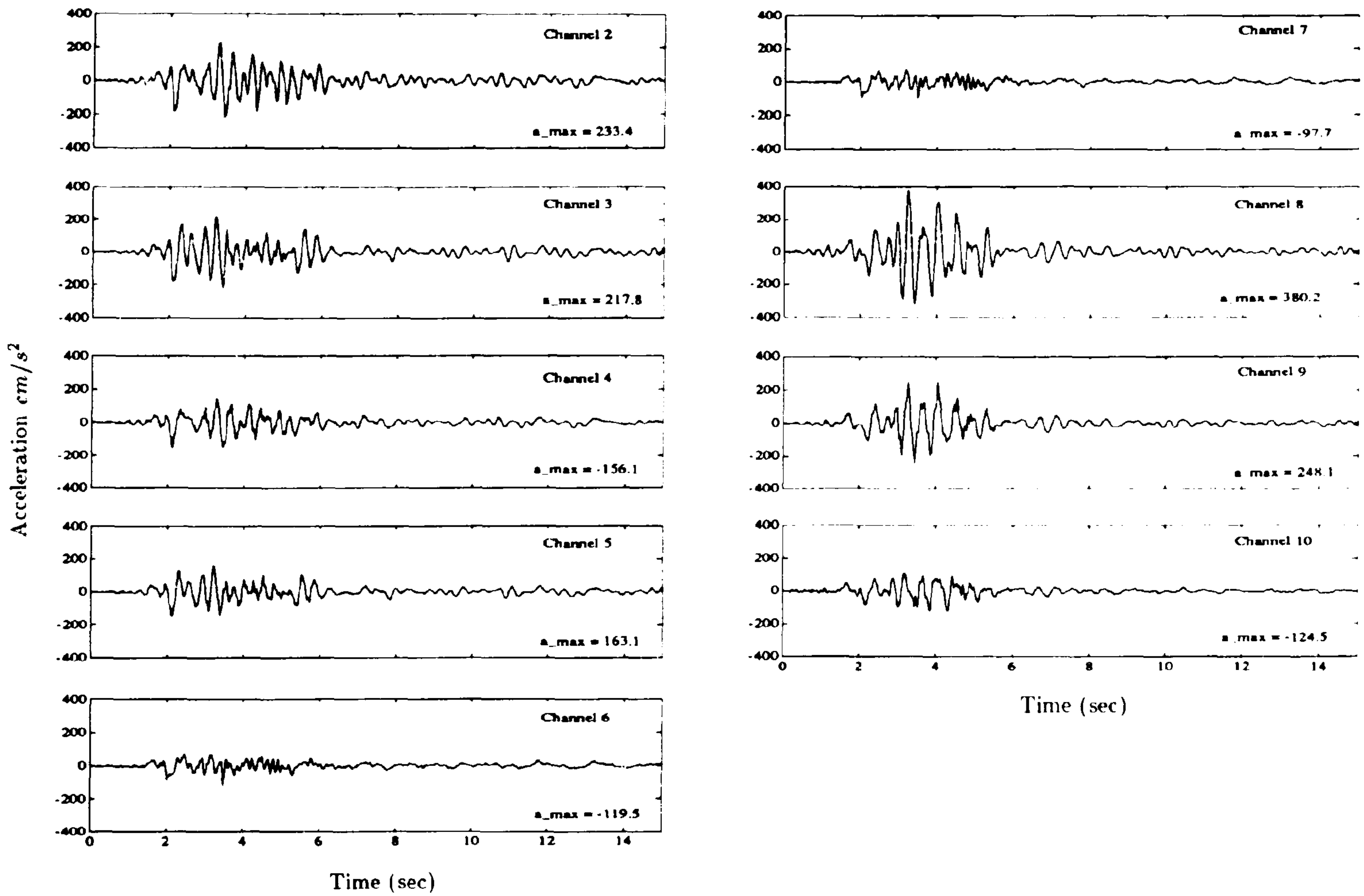

Figure 7: Recorded Motions in Building B During the Upland Earthquake

(a) Three-story Steel Frame Building, San Jose, California

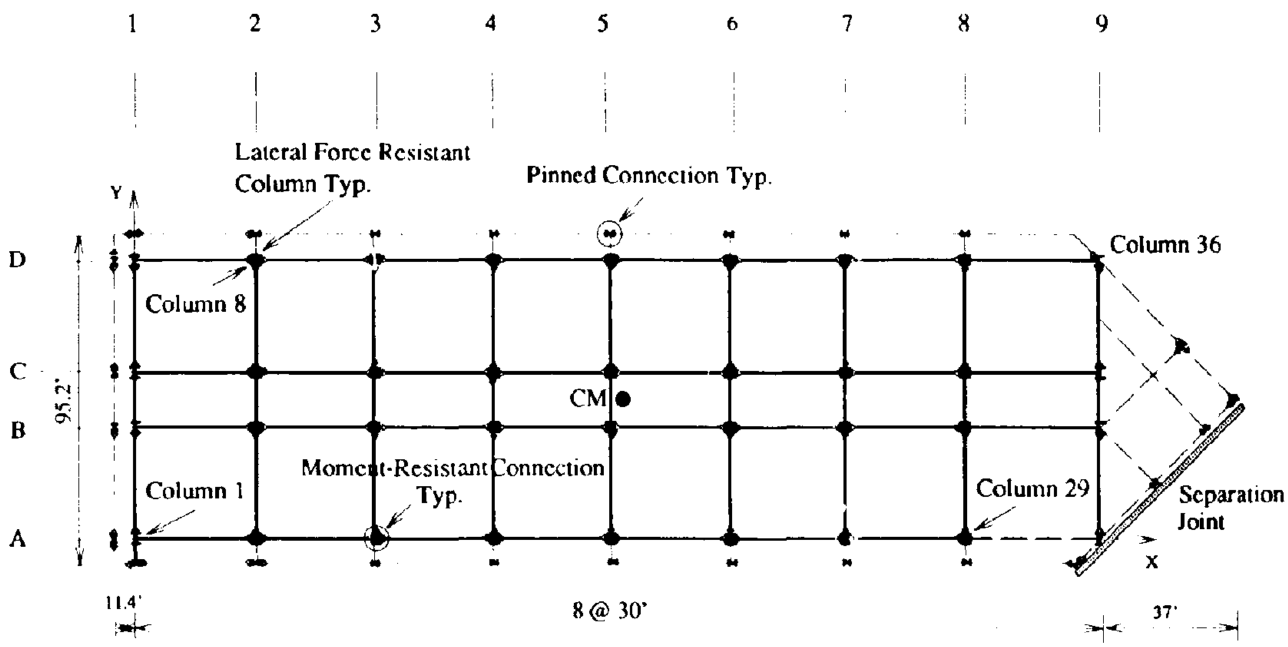

(b) Framing Plan

Figure 8: Photograph and Framing Plan of Building C

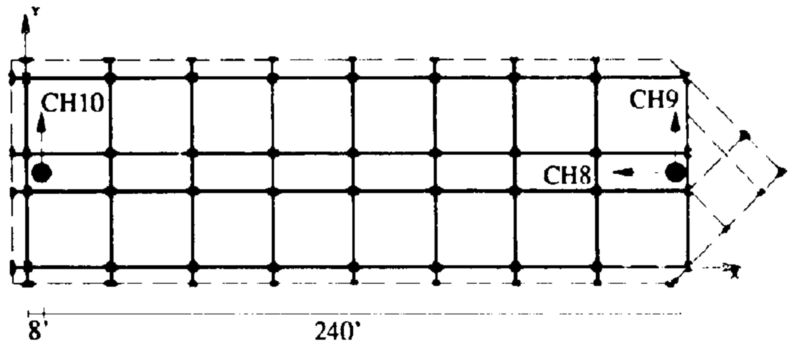

Roof

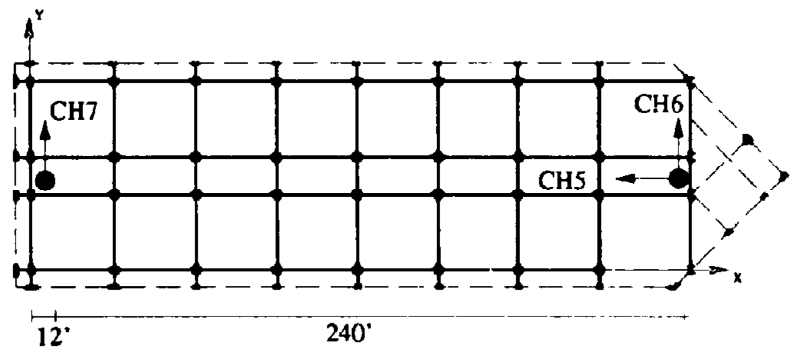

Third Floor

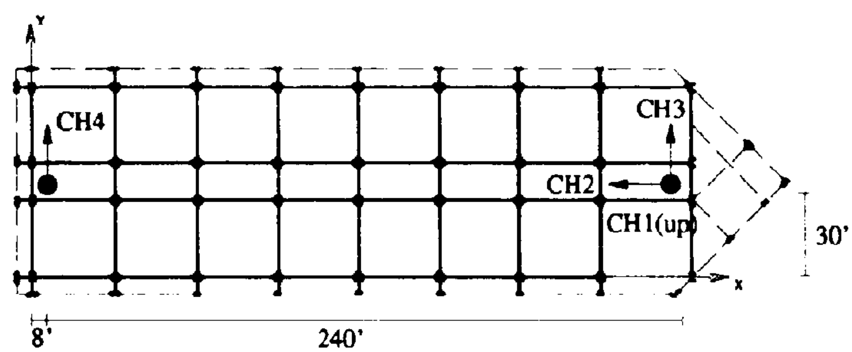

First Floor

Figure 9: Accelerograph Channels

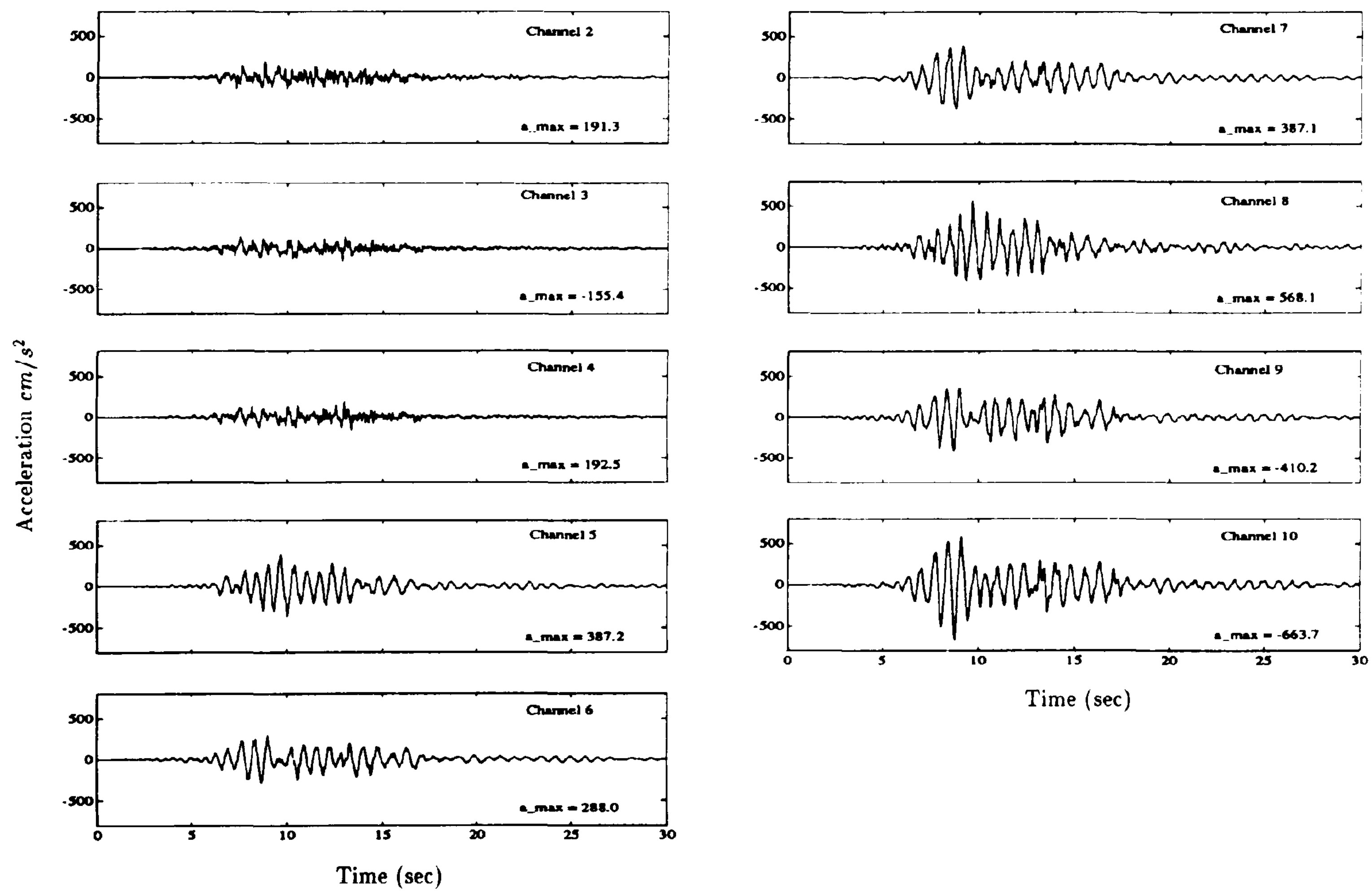

Figure 10: Recorded Motions in Building C During the Loma Prieta Earthquake

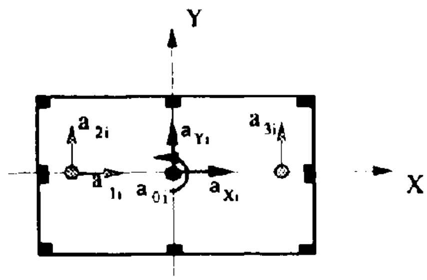

(a) Recorded Accelerations at ith Floor and Accelerations at the CM

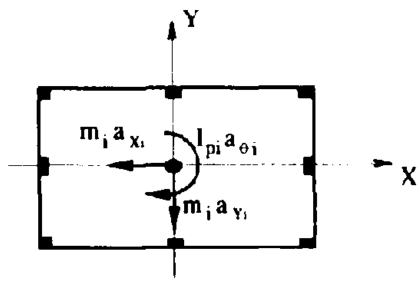

(b) Inertia Forces at ith Floor

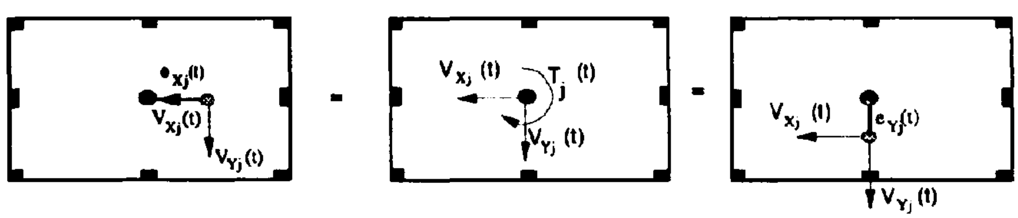

(c) Accidental Eccentricities for the jth Story

Figure 11: Dynamic Accidental Eccentricity

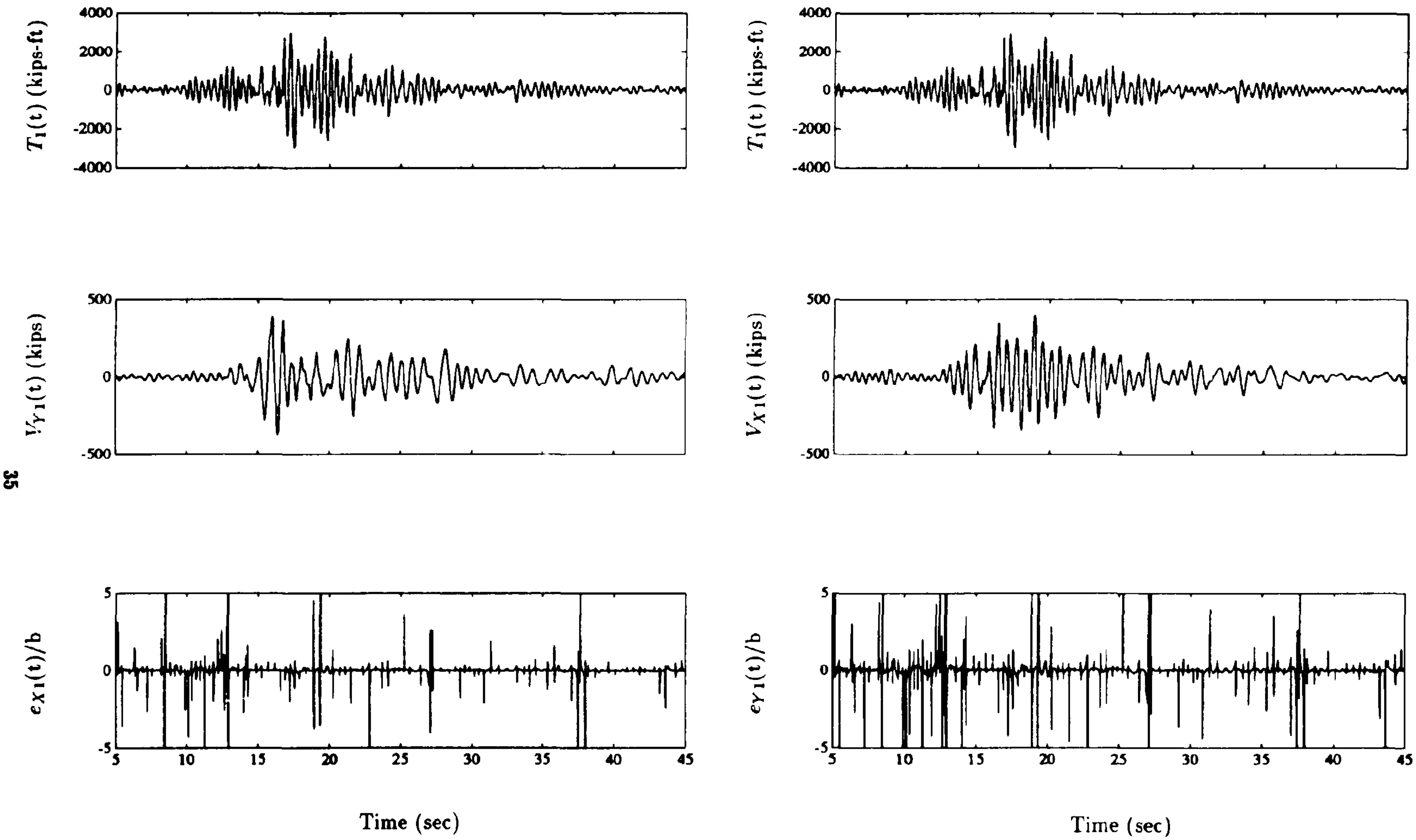

Figure 12: Base Shear, Base Torque and First Floor Accidental Eccentricities Computed from Recorded Accelerations in Building A During the Loma Prieta Earthquake

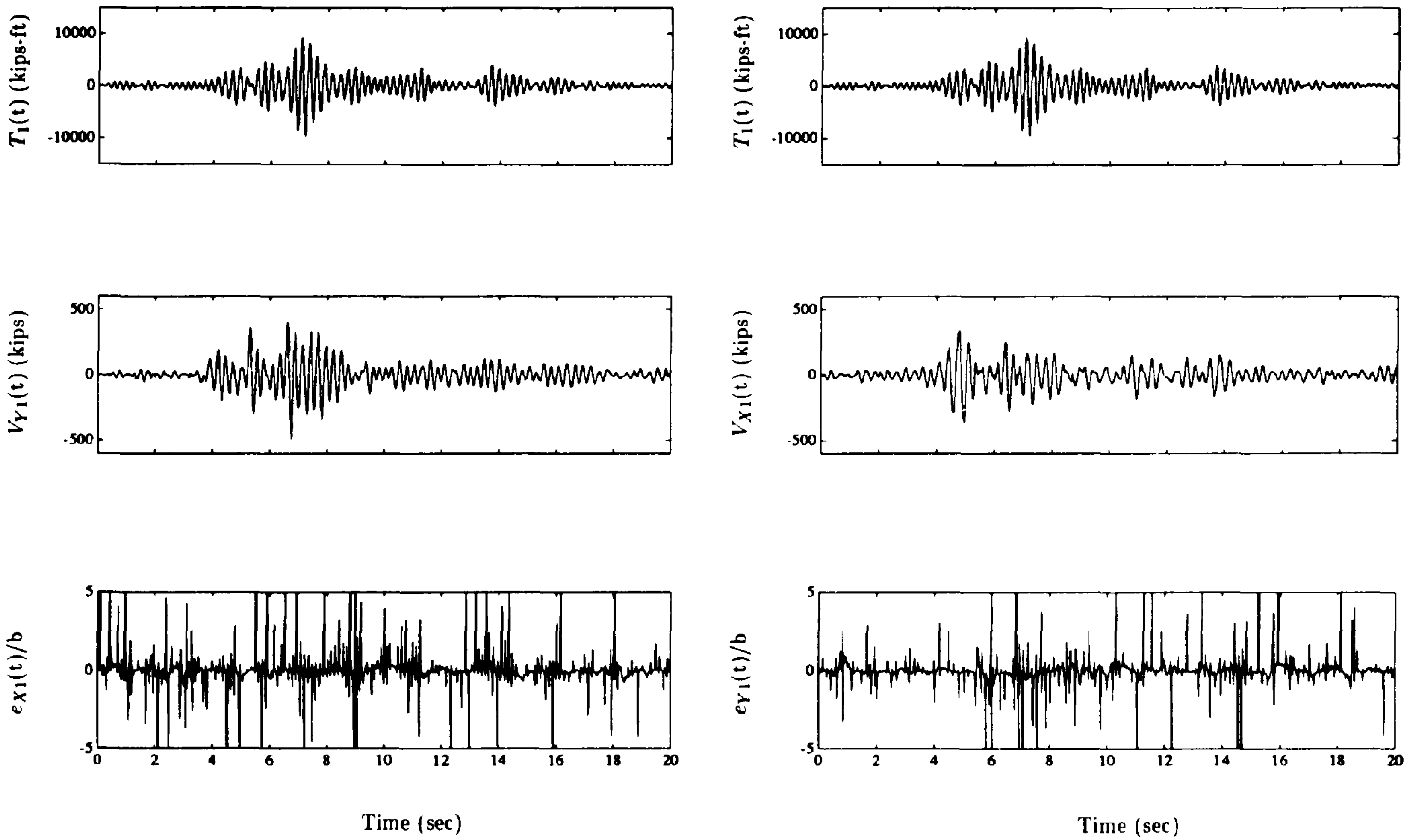

Figure 13: Base Shear, Base Torque and First Floor Accidental Eccentricities Computed from Recorded Accelerations in Building B During the Whittier Earthquake

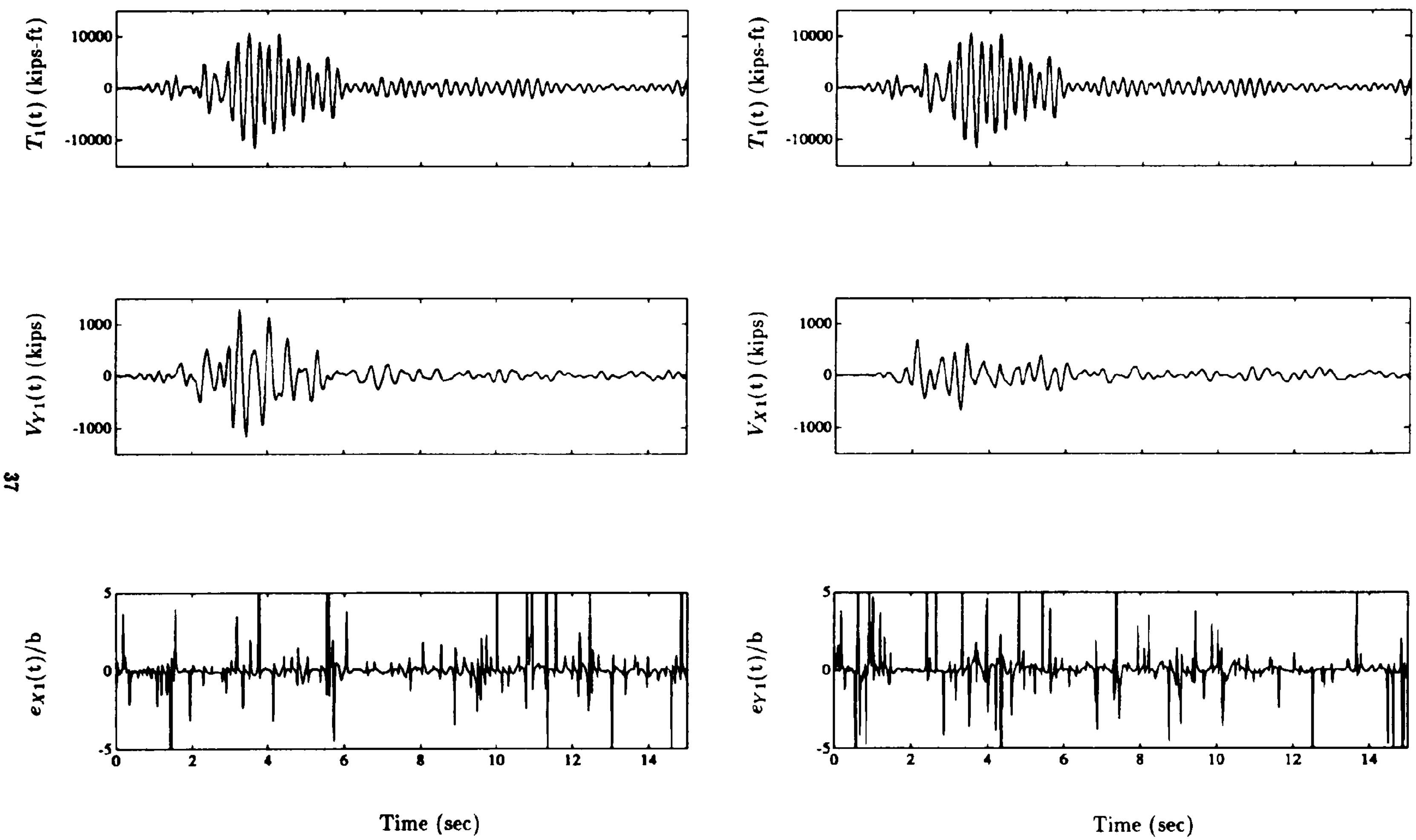

Figure 14: Base Shear, Base Torque and First Floor Accidental Eccentricities Computed from Recorded Accelerations in Building B During the Upland Earthquake

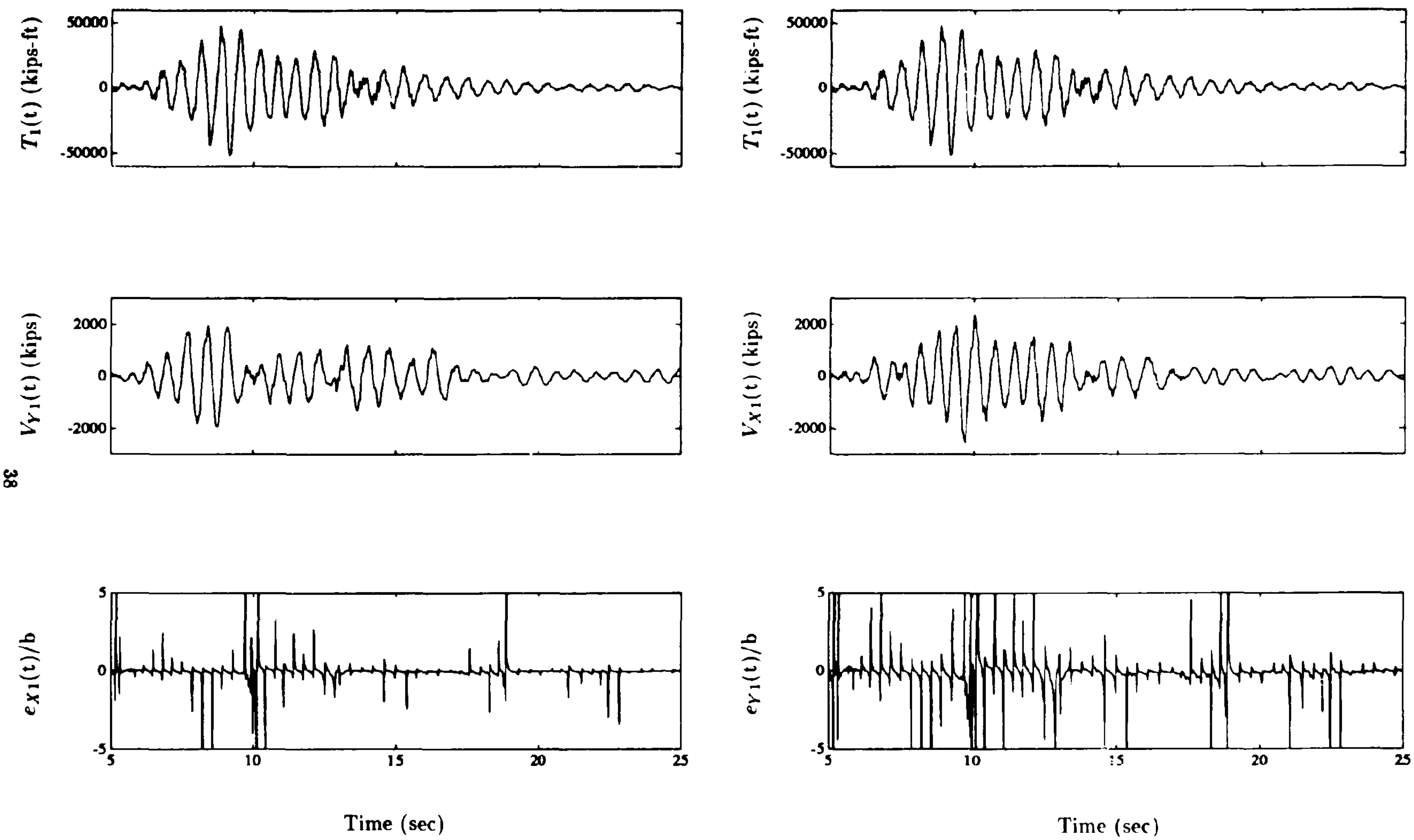

Figure 15: Base Shear, Base Torque and First Floor Accidental Eccentricities Computed from Recorded Accelerations in Building C During the Loma Prieta Earthquake

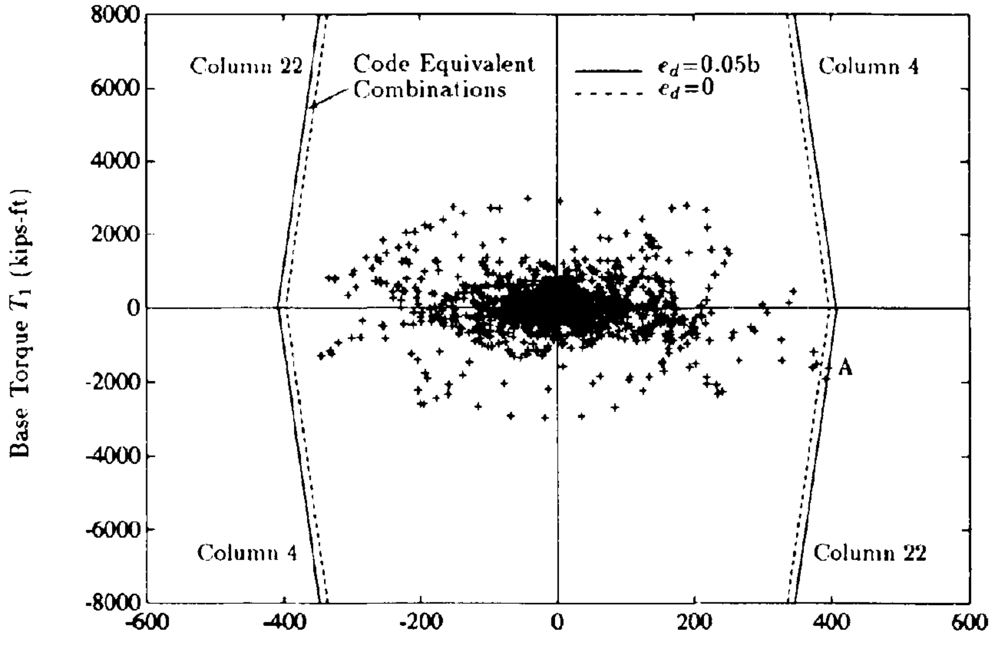

a) Base Shear V_{X1} (kips)

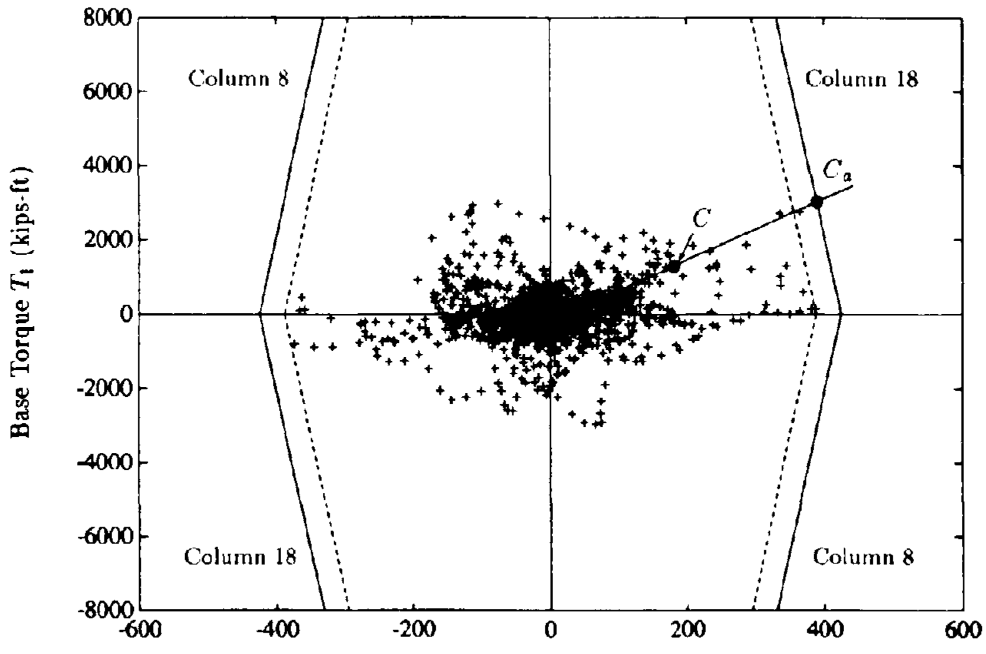

b) Base Shear V_{Y1} (kips)

Figure 16: Comparison of Dynamic Base Shear, Base Torque and "Code Equivalent Combinations" in Building A During the Loma Prieta Earthquake

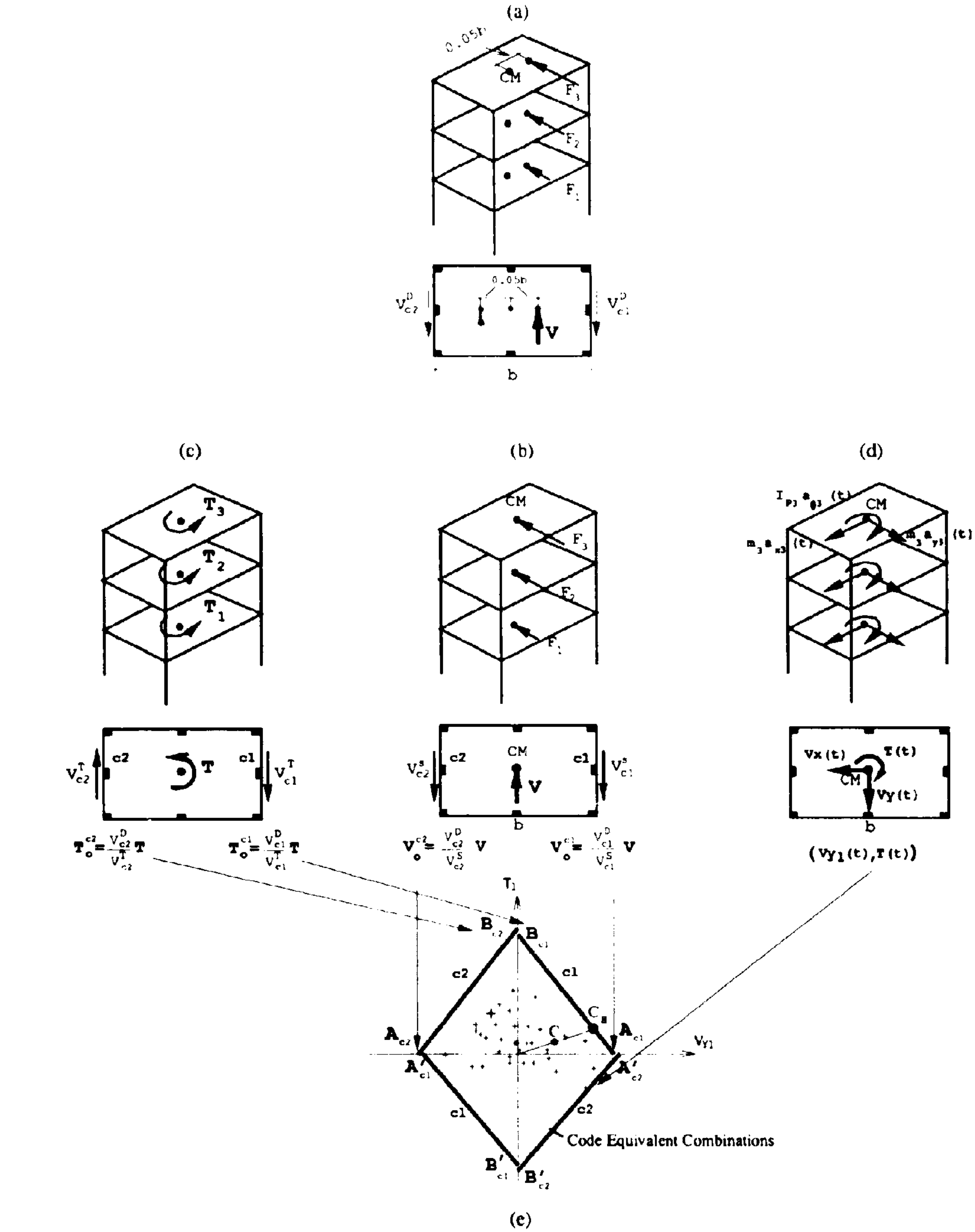

Figure 17: Computation of Design Member Forces, Base Shear, Base Torque, and Code Equivalent Combinations

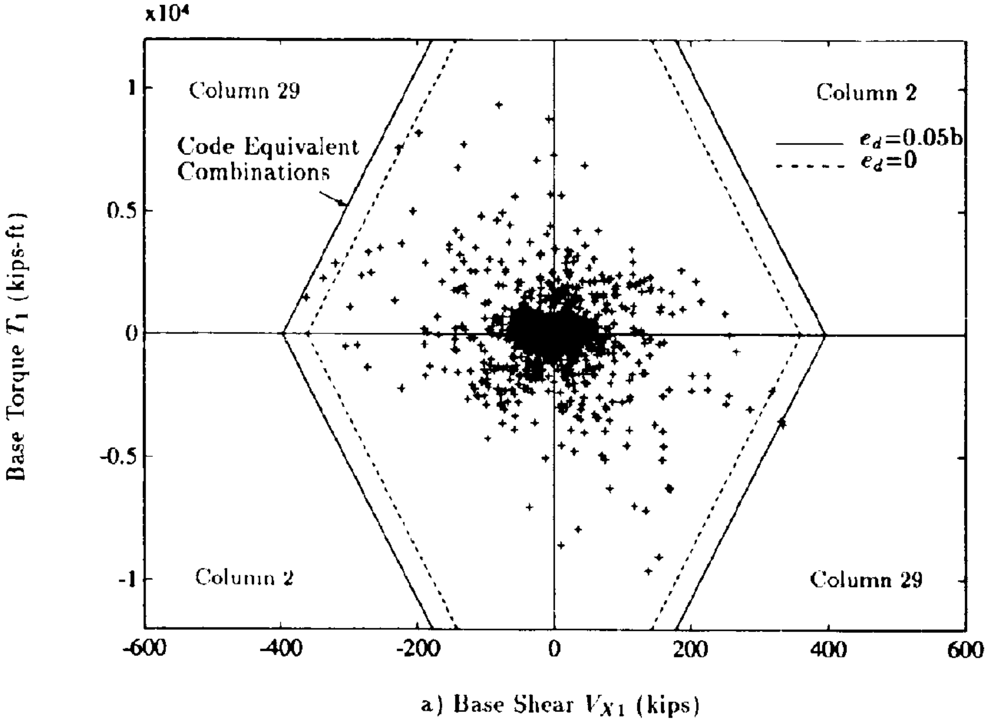

a) Base Shear V_{X1} (kips)

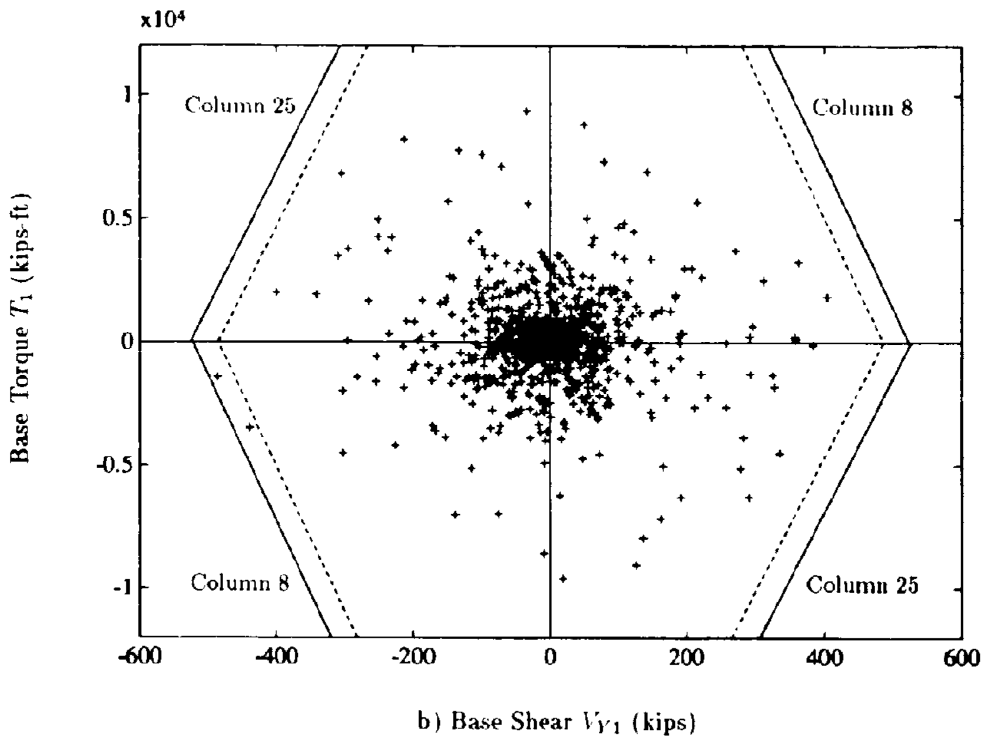

b) Base Shear V_{Y1} (kips)

Figure 18: Comparison of Dynamic Base Shear, Base Torque and "Code Equivalent Combinations" in Building B During the Whittier Earthquake

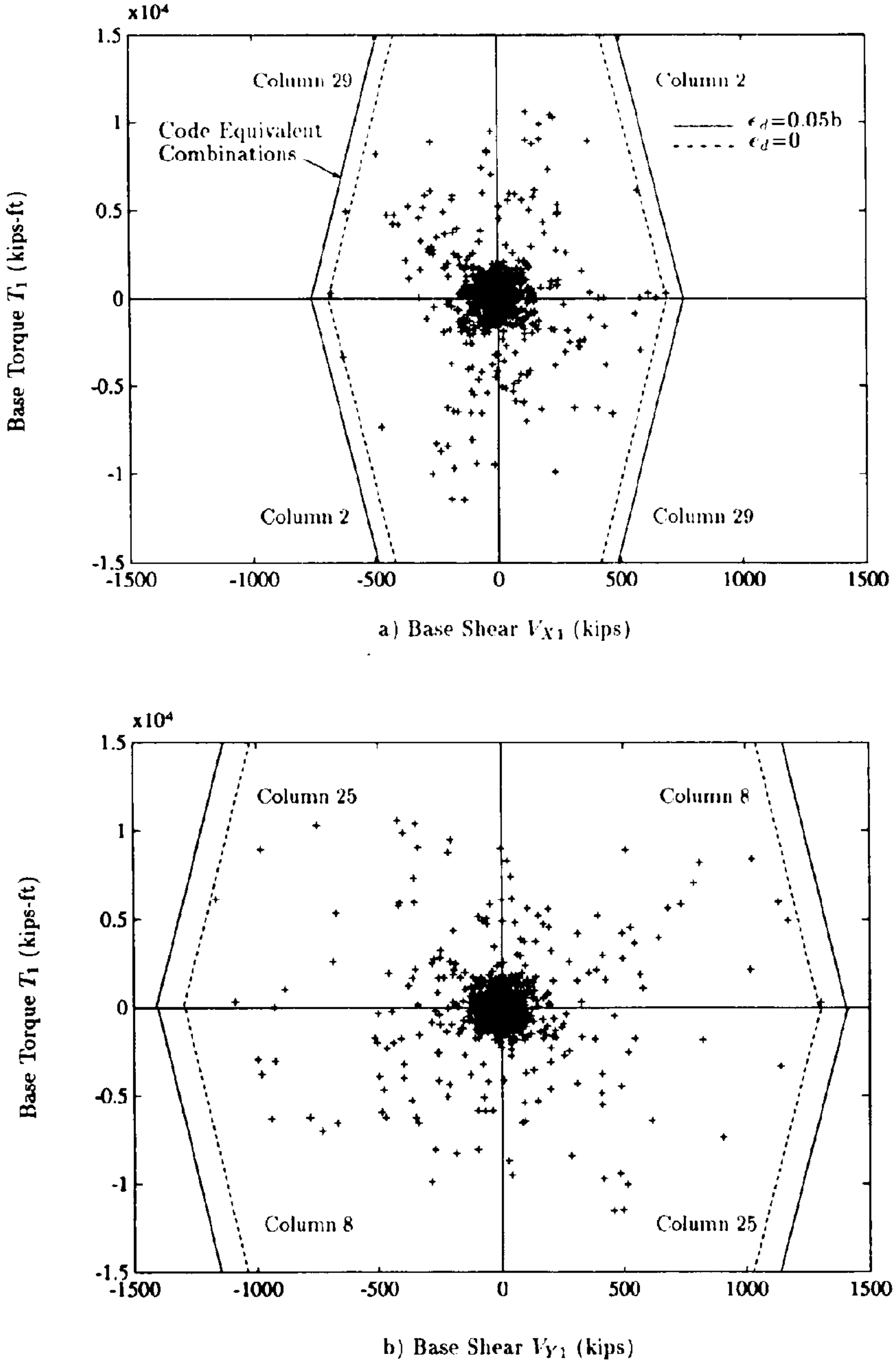

Figure 19: Comparison of Dynamic Base Shear, Base Torque and "Code Equivalent Combinations" in Building B During the Upland Earthquake

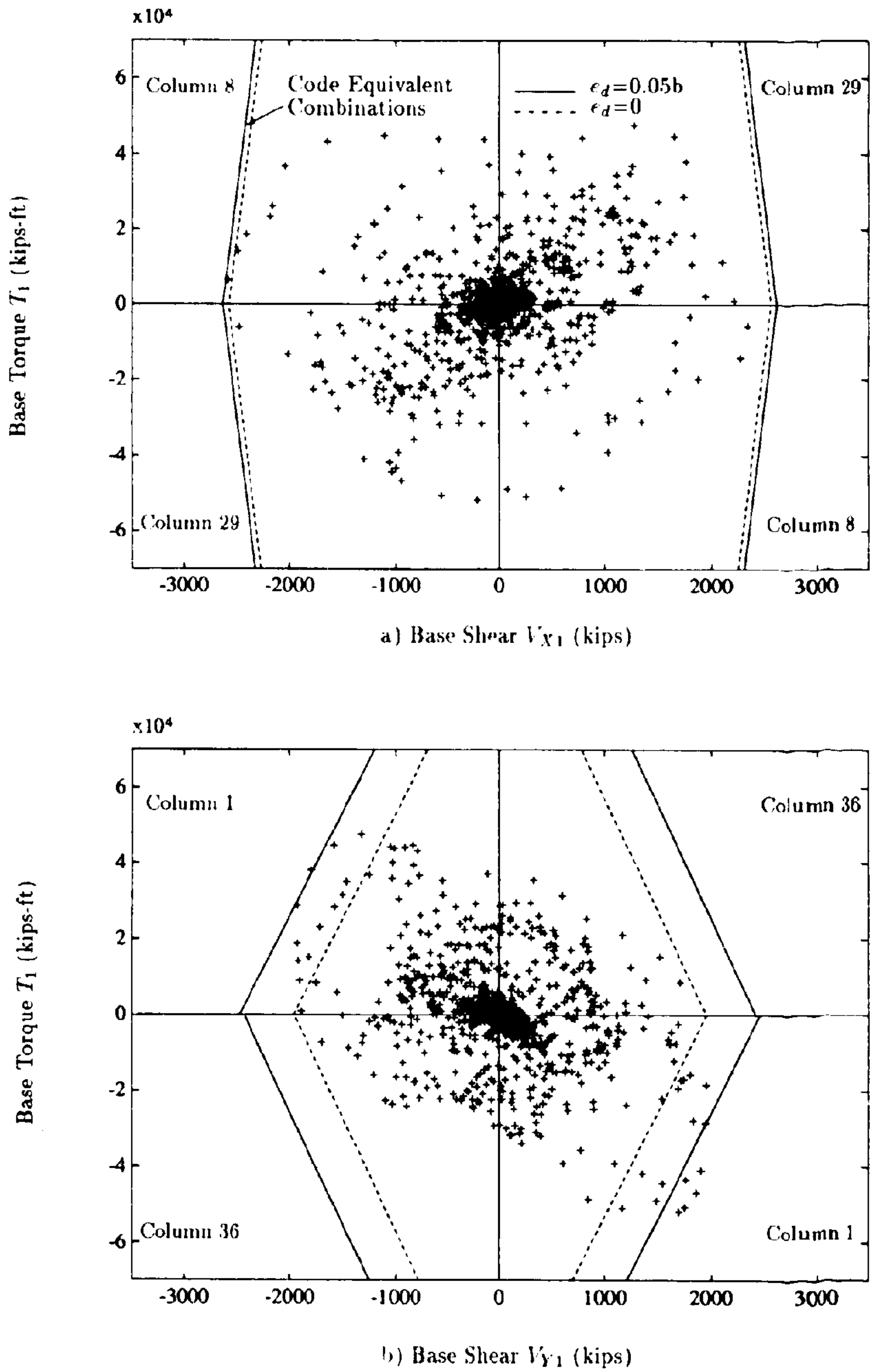

Figure 20: Comparison of Dynamic Base Shear, Base Torque and "Code Equivalent Combinations" in Building C During the Loma Prieta Earthquake

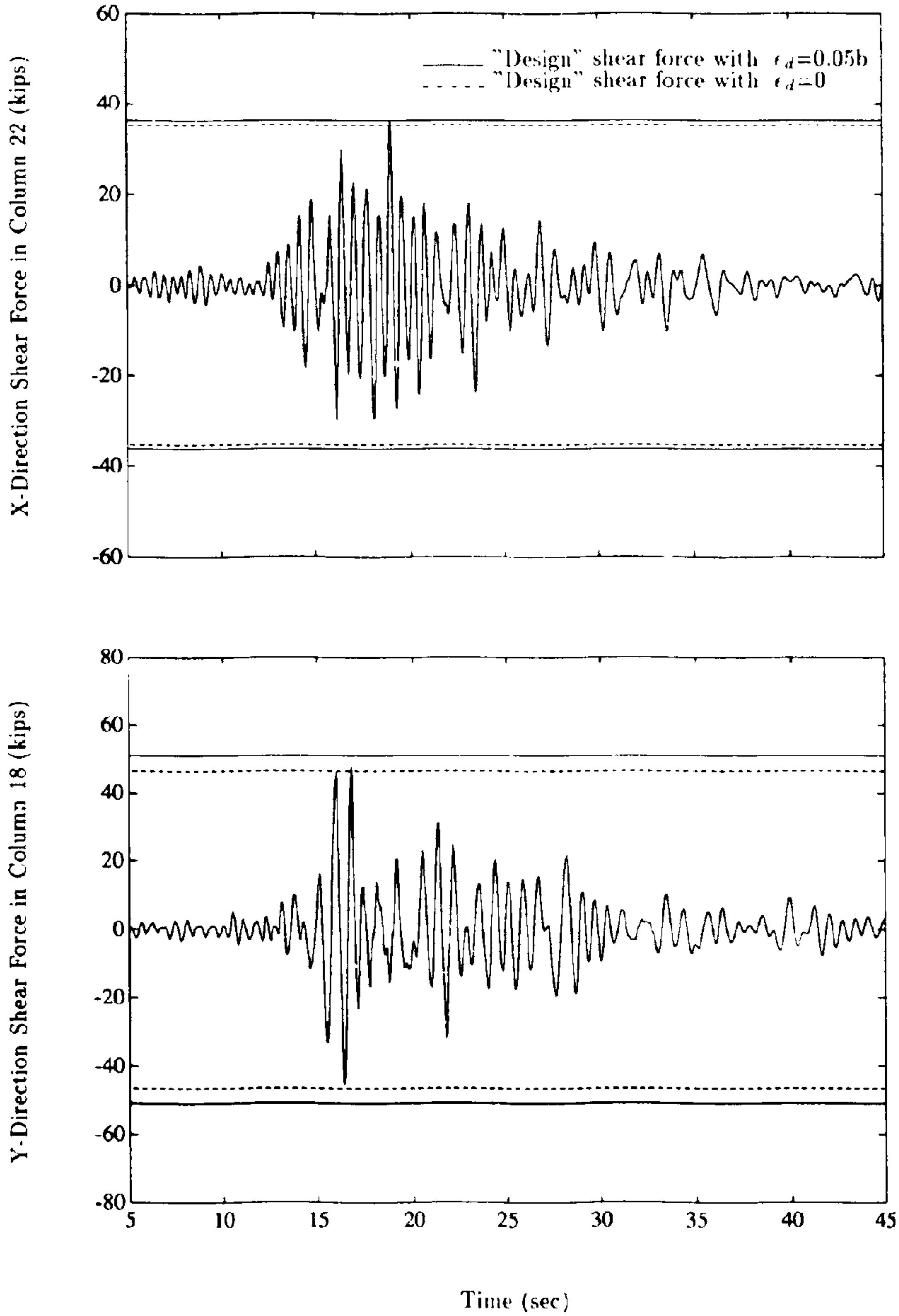

Figure 21: Comparison of Earthquake Induced Shears in Columns 22 and 18 with "Design" Shear Values for Building A

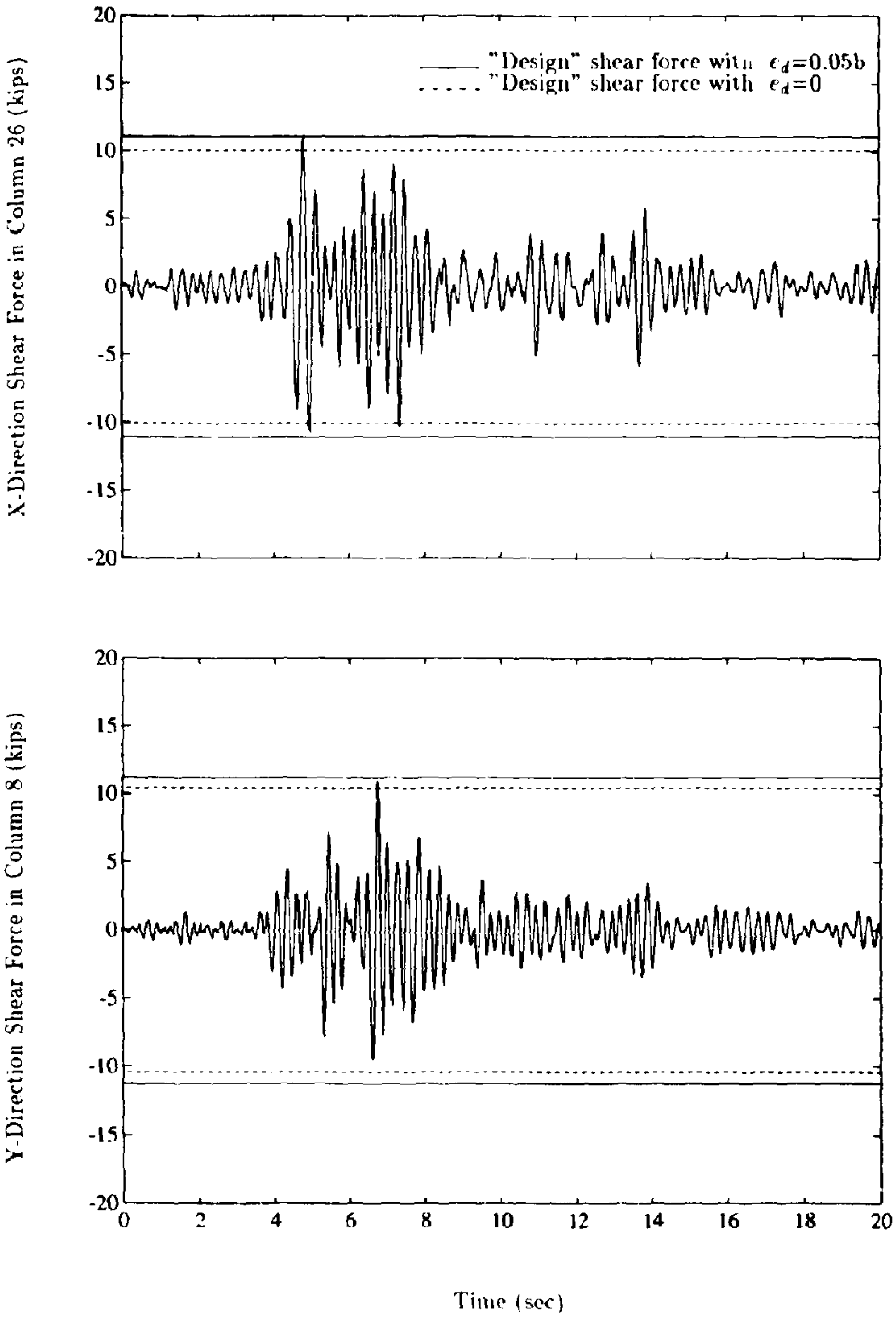

Figure 22: Comparison of Earthquake Induced Shears in Columns 26 and 8 with "Design" Shear Values for Building B and Whittier Earthquake

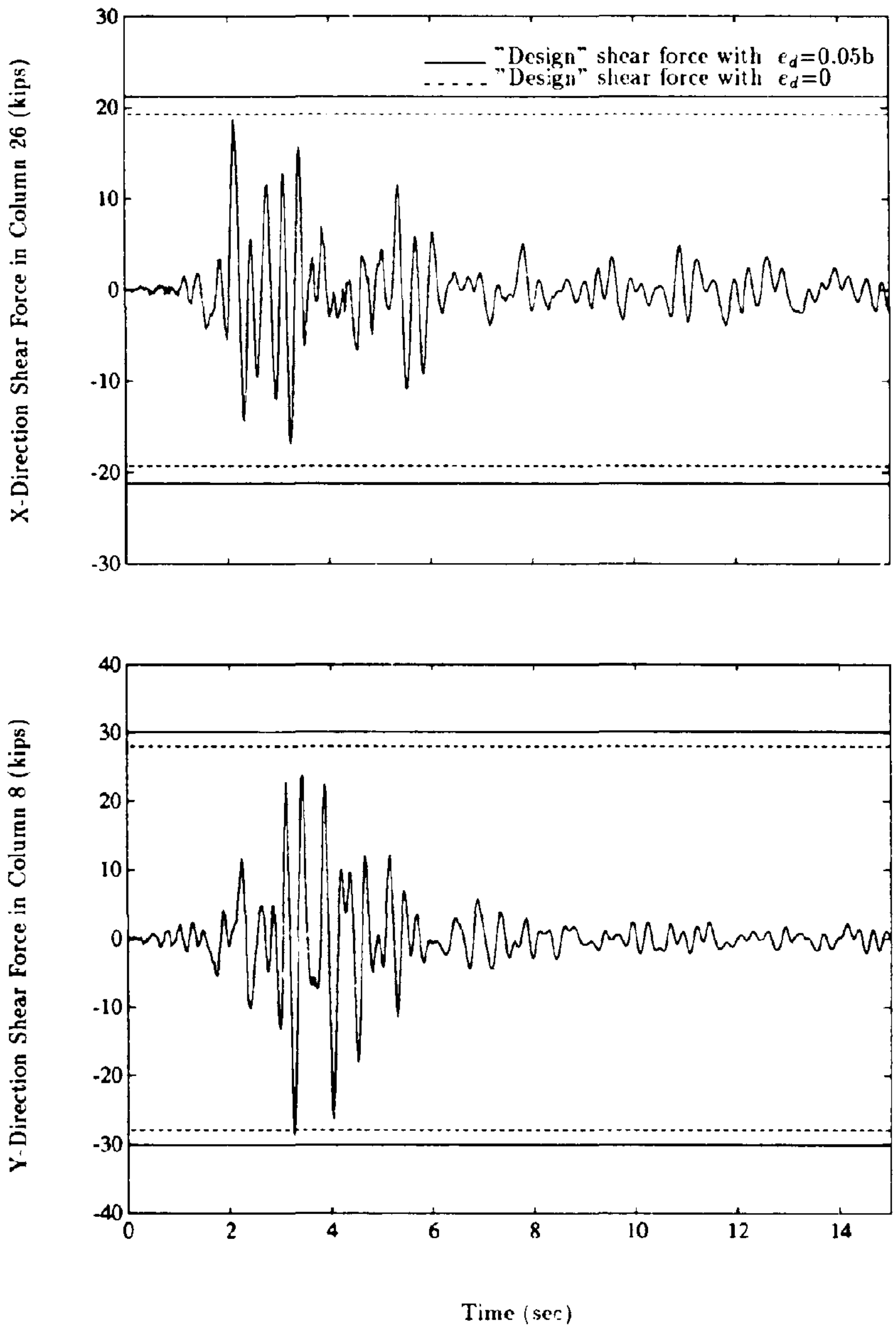

Figure 23: Comparison of Earthquake Induced Shears in Columns 26 and 8 with "Design" Shear Values for Building B and Upland Earthquake

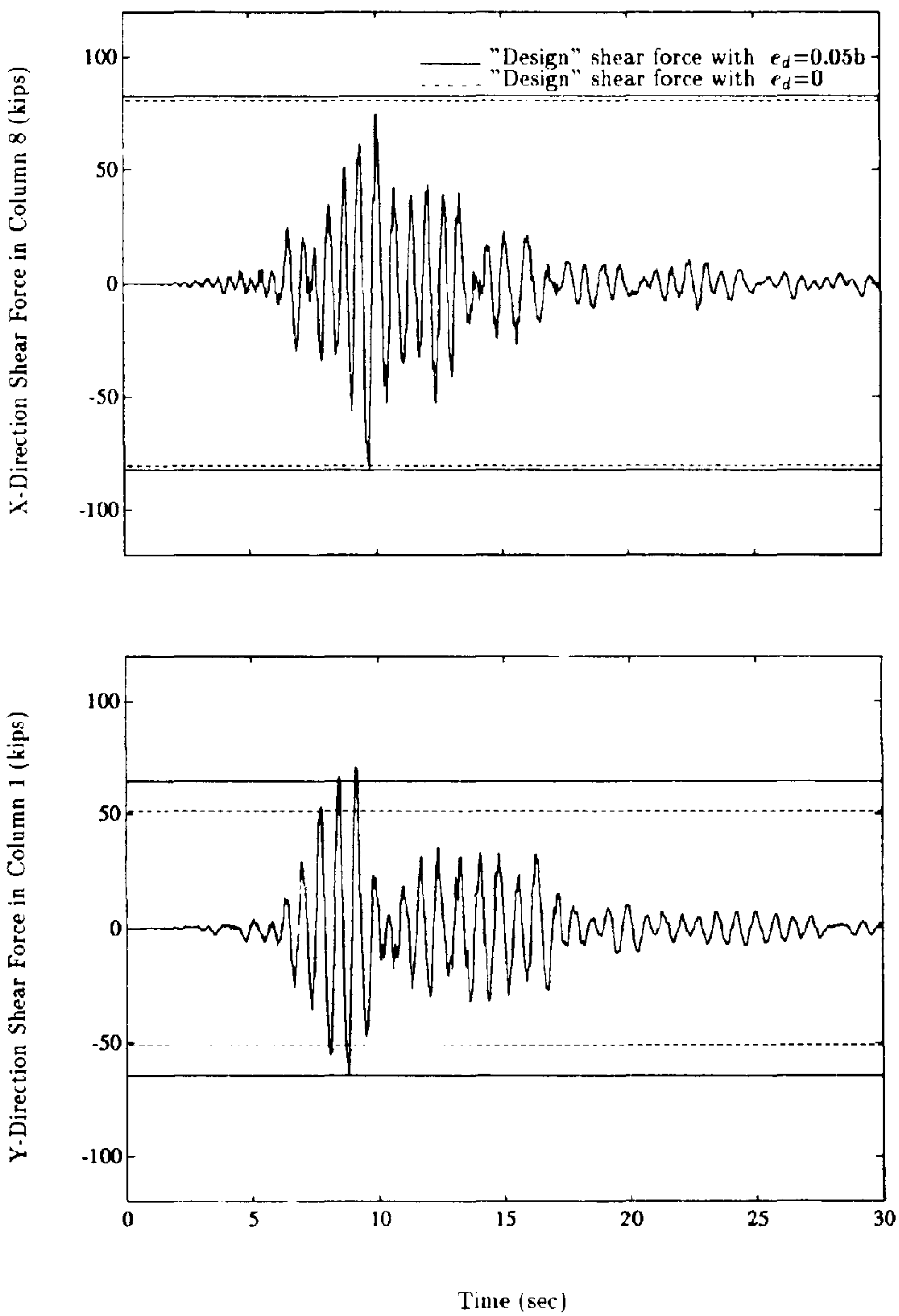

Figure 24: Comparison of Earthquake Induced Shears in Columns 8 and 1 with "Design" Shear Values for Building C

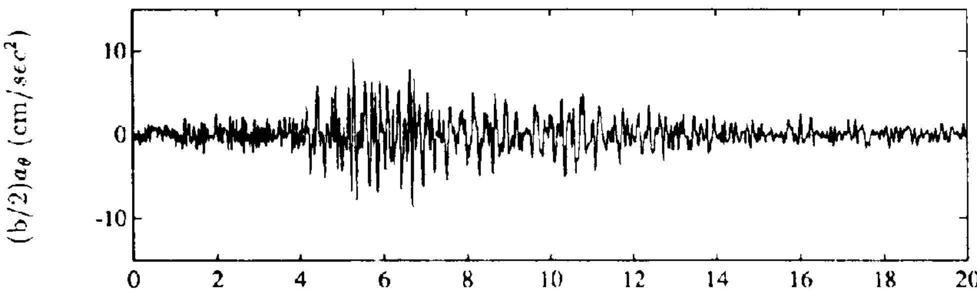

a) Building B, Whittier Earthquake

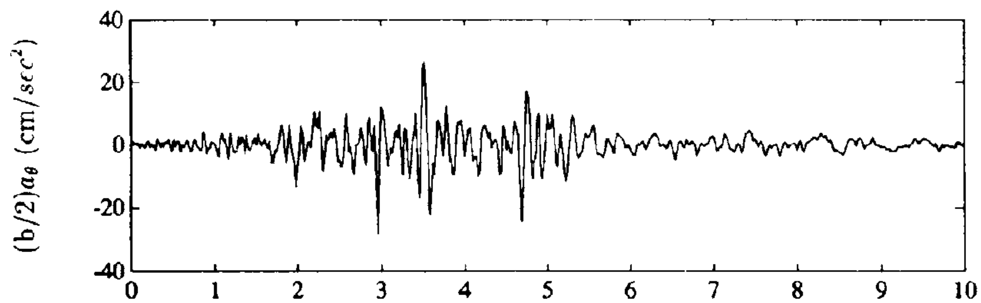

b) Building B, Upland Earthquake

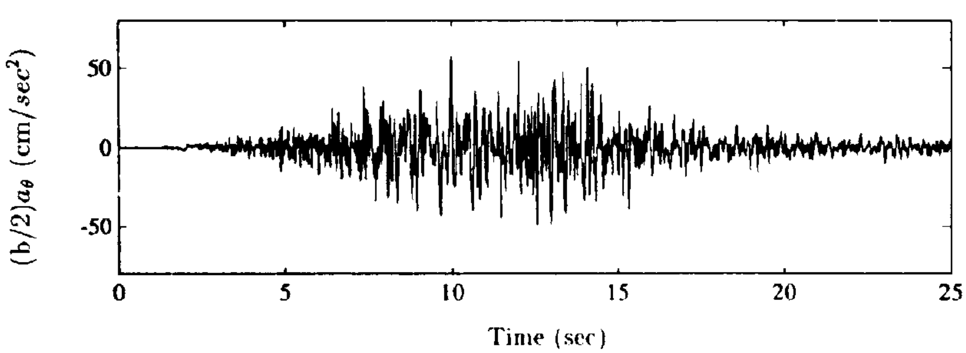

c) Building C, Loma Prieta Earthquake

Figure 25: Computed Rotational Accelerations at the Ground Level in Buildings B and C

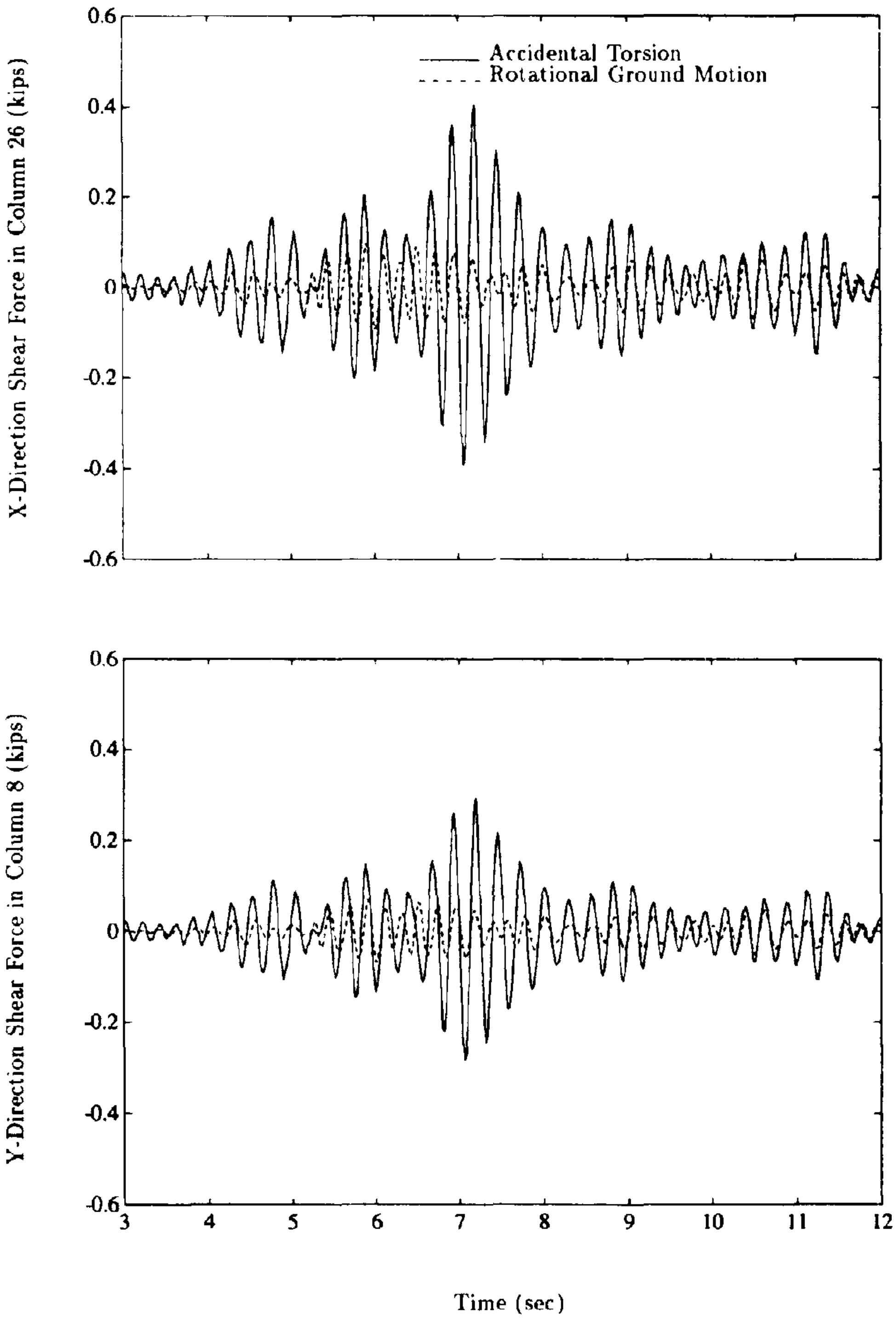

Figure 26: Comparison of Member Forces Due to Accidental Torsion and Due Only to the Rotational Ground Motion in Building B During the Whittier Earthquake

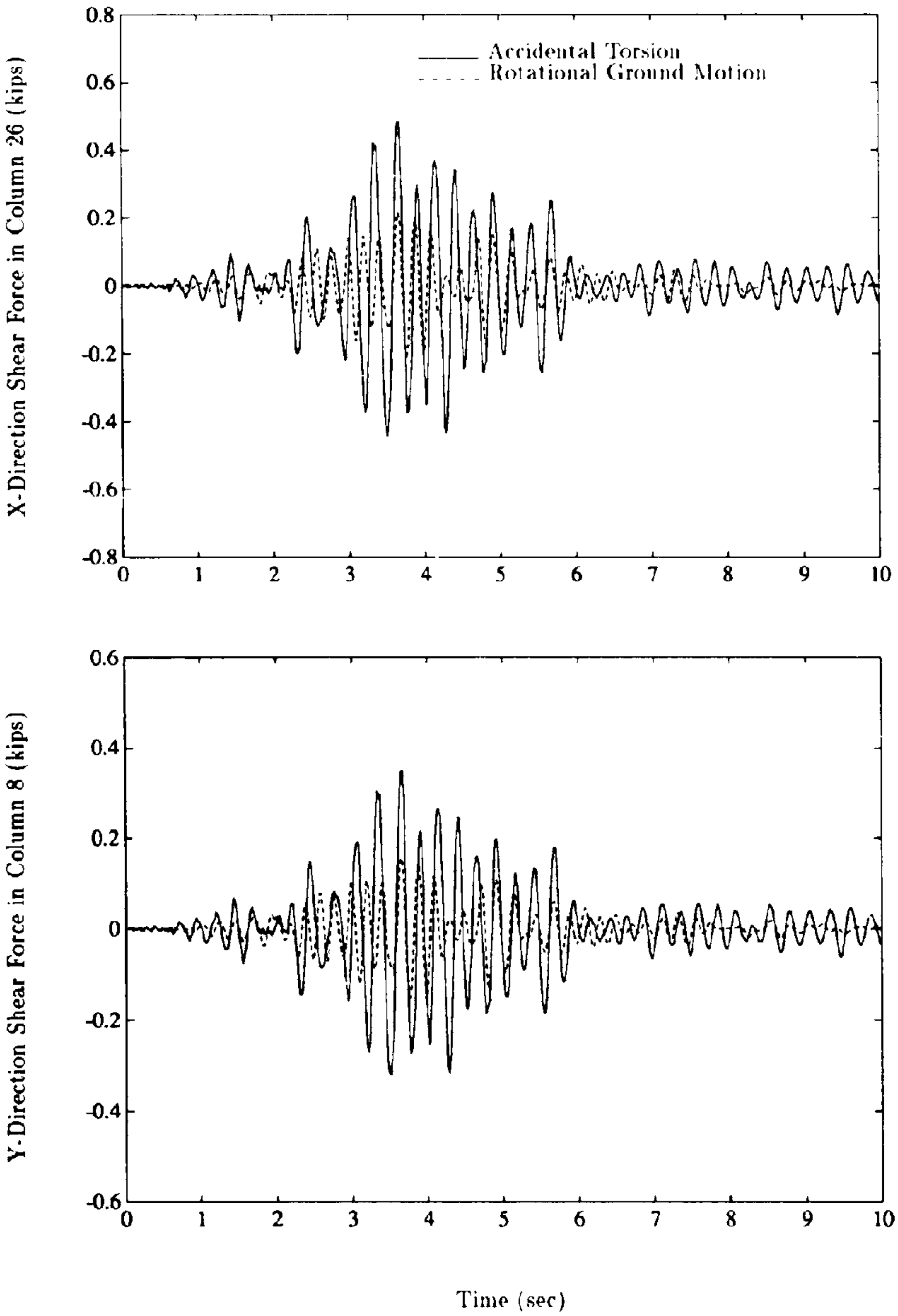

Figure 27: Comparison of Member Forces Due to Accidental Torsion and Due Only to the Rotational Ground Motion in Building B During the Upland Earthquake

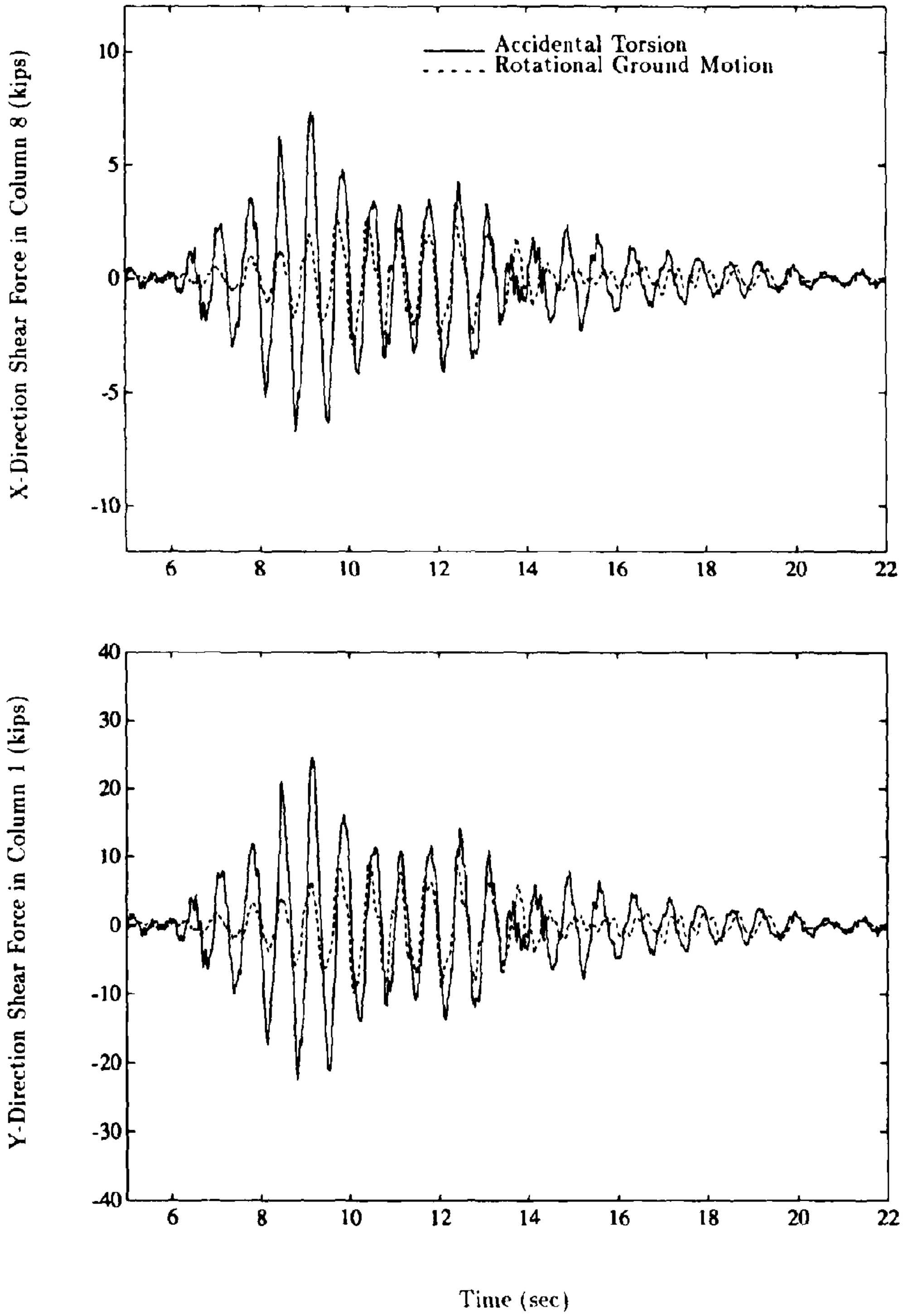

Figure 28: Comparison of Member Forces Due to Accidental Torsion and Due Only to the Rotational Ground Motion in Building C During the Loma Prieta Earthquake

Page Intentionally Left Blank

APPENDIX A: THREE STORY OFFICE BUILDING

(CSMIP STATION No. 58506)

A.1 Building and Recorded Motions

Identified as CSMIP station No. 58506, this building is located in Richmond, California. Records of motions of the building during the Loma Prieta earthquake are available. A brief description of the structure, the recorded motions and the natural vibration frequencies and mode shapes estimated from the records is presented in this section.

A.1.1 Brief Description of Building

A typical framing plan of this three-story steel building is shown in Figure A-1. The building is approximately 162 feet long, 77 feet wide and 45 feet high. The building has two lateral moment resisting frames in the X-direction (A and C) and two in the Y-direction (1 and 7). All other frames are designed to carry only gravitational loads. Beam-column connections in the structure are moment resisting and pinned as described in Section A.2. The floor decking system is formed by a steel corrugated metal deck filled with lightweight concrete. The roof deck is lighter but has additional insulating concrete. The foundation system consists of rectangular column footings interconnected by grade beams. In the Y-direction only footings for columns of frames 1 and 7 are interconnected.

For all practical and code design purposes, the building has a floor plan that is nominally-symmetric about two axes. The translational mass and rotational inertia for each floor is determined from the weight of the structural elements, partitions, ceilings and other miscellaneous contributions. The mass of columns and partitions in each story is distributed equally to the floors at the top and bottom of the story. No live load is considered in calculating the floor masses. The location of the center of mass (CM) for each floor was determined assuming that the dead loads are distributed uniformly over the plan. The coordinates of the CM, with the origin defined as shown in Figure A·1, are presented in Table A·1.

A.1.2 Recorded Motions

The locations of the accelerographs in the building are shown in plan in Figure A·2. These include three channels at the first, second, third floors and the roof level. The twelve strong motion records obtained during the Loma Prieta earthquake are shown in Figure A·3. The peak ground accelerations at the ground level are 0.083g in the X-direction and 0.11g in the Y-direction. These motions were amplified to 0.31g and 0.27g, respectively at the roof level. The building experienced no structural damage during the earthquake.

From the three channels of accelerations recorded at any level, the accelerations of the CM - - these are $a_x(t)$ and $a_y(t)$, the X and Y components of translational acceleration, and $a_\theta(t)$, the rotational acceleration about a vertical axis - - at the same level can be computed assuming a rigid floor diaphragm. This assumption seems valid for this building, given the large in-plane stiffness of the decking system compared with the lateral stiffness of the columns. Computed by this procedure, the accelerations $a_x(t)$, $a_y(t)$ and $a_\theta(t)$ at the CM of the second, third and roof levels are presented in Figure A·4. In the X-direction the peak acceleration at the ground level is 0.083g, which is amplified to 0.31g at the CM of the roof level; the amplification is from 0.11g to 0.27g in the Y-direction. The peak rotation at the roof level is $0.033 rad/s^2$. The rotational acceleration of the ground could not be obtained from the recorded accelerations because only two horizontal components of acceleration are available at the ground level.

A.1.3 Natural Vibration Frequencies and Modes

Examination of the motions recorded at the roof level by channels 1, 2 and 3 provides rough estimates of the fundamental natural vibration frequencies of the building: 1.64 Hz in the X-direction and 1.35 Hz in the Y-direction. The true (not pseudo) acceleration response spectra for the motions recorded at the roof level in the X-direction at channel 3 and in the Y-direction at channel 1 and 2 are shown in Figure A·5. The largest peak is obtained at 1.66 Hz for the X component of motion and 1.35 Hz for the Y component , which is consistent with the frequencies gleaned from direct examination of the records.

Figure A·6 shows the transfer functions for the X and Y components of the relative (to the ground) acceleration at the CM of the three floor levels and the corresponding motions at the ground level. Also shown in Figure A·6 is the amplitude of the Fourier transform of the total rotational component of acceleration at the roof, whose transfer function could not be obtained because the rotational ground motion is not known. The transfer functions and Fourier spectra were smoothed by a running average procedure with weights (1/4,1/2,1/4). The transfer functions for the X and Y translational motions have peaks at 1.60 Hz and 1.43 Hz, respectively. The amplitude Fourier spectrum for the total rotational motion shows a peak at 2.17 Hz. A vibration mode shape corresponding to a particular natural vibration frequency can be estimated from the ordinates at that frequency of the transfer functions at the various floor levels. Thus, the shapes of the two natural vibration modes in translation can be determined from the numerical data of Figure A·6: the X-translational mode from Figure A·6(a), and the Y-translational mode from Figure A·6(b). However, a torsional mode shape can be determined only approximately because the rotational ground motion is not known. The mode shapes are presented in Table A·2.

A.2 Structural Idealization of the Building

The building was idealized for analysis by the ETABS computer program, wherein the building mass is assumed to be lumped at the floor levels and the floor diaphragms are assumed to be rigid, an assumption which was also used in computing motions at the CM from the recorded motions. The building is treated as fixed at the level defined by the slab on grade. All structural elements were included in the structural idealization, i.e, even the elements that provide little lateral resistance are considered because they may contribute to the accidental eccentricities. The column lines and frame bays used for the ETABS model are defined in Figure A-10. Flexural and axial deformations are considered in defining the properties of columns, whereas only flexural deformations are considered for defining the stiffness properties of beams. The compatibility of axial deformations required in columns belonging to more than one moment resisting frame is considered by analyzing the structure as a single three dimensional frame with six degrees of freedom per joint (in contrast to the most common type of analysis that considers the structure as an assemblage of several two dimensional lateral-force resisting frames distributed across the building plan).

The framing plans idealized for analysis are shown in Figures A-7 to A-9, wherein the sizes of the columns and beams are noted. Each frame is modelled with appropriate beam-column joints: moment resistant (or rigid) connections, denoted in Figures A-7 to A-9 by small triangles next to the column, and pinned connections, columns without the small triangles. The structural analysis of this model is identified in the following as analysis case "A".

Two additional structural models of the building were studied to bound the effect of the true flexibility of the non moment-resistant connections. Figure A-11 shows a schematic detail of the two types of non moment-resistant connections used in the building. Beam-column connections connecting the beam web to the column web (Figure A-11(a)) are more flexible than those connecting the web of the beam to the flange of the column (Figure A-11(b)). Thus, a second structural idealization models all web-to-flange connections as moment-resistant and all web-to-web connections as pinned. The analysis of this model is denoted as case "B". In the third analysis case all beam-column connections are modelled as moment-resistant. This structural idealization, denoted as case "C", provides an upper bound for the true structural stiffness. In the case of moment-resistant connections, the portions of beams and columns within the beam-column panel zone are treated as rigid, consistent with the the rigidity of the connection.

The natural vibration frequencies and mode shapes of the idealized structural system computed by the ETABS program are presented in Table A-2. The agreement between these computed frequencies and those determined earlier from the recorded response of the building depends greatly on how the non moment-resistant connections are modelled. Analysis case "A" predicts natural frequencies for the system that are too low because this model underestimates the stiffness of the structure. Analysis case "B" provides better values of vibration frequencies, especially for the fundamental natural frequency in the X-direction because, as described earlier, the connections are modelled realistically which especially affects the lateral stiffness of frame B. Analysis case "C" provides a higher value for the frequency of vibration in the Y-direction because the assumption of moment-resistant connections slightly overestimates the stiffness in this direction. The resulting natural frequencies for this case are also in good agreement with the natural frequencies obtained from the analysis of the transfer functions.

Either structural model "B" or "C" could have been used for the analyses presented in Sections A.4 and A.5. Model "B" is selected mainly because it appears to be a more realistic representation of the expected behavior of the beam-column connections in the structure.

A.3 Dynamic Eccentricity

The story shears and torques are computed from the floor masses and accelerograms (Figure A-4) by Equations 1 to 3, wherein the acceleration records at all floor levels are available.

The accidental eccentricity at the "jth" floor has been defined by Equations 4 and 5 in terms of the story shears and story torques in the "jth" story. The latter are computed from Equations 1 to 3 wherein the floor masses are given by Table A-1 and the accelerations $a_{xj}(t), a_{yj}(t)$ and

$a_{\theta_j}(t)$ at the CM in Figure A·4. The computed base shear and base torque for the building are shown in Figure A·12. The maximum values for the base shear are 397 kips and 388 kips in the X and Y-directions, respectively, which are 18.2% and 17.8% of the total weight of the building. The accidental eccentricities $e_{Y1}(t)$ and $e_{X1}(t)$ determined from the base shear and torque by Equations 4 and 5 are also shown in Figure A·12.

A.4 Base Shear, Base Torque and Code-Equivalent Combinations

This section presents the implementation of the step-by-step procedure described in Section 5 for this building.

1. At each instant of time, the base shear was computed by Equations 1 to 3, where the floor masses are given in Table A·1 and the floor accelerations in Figure A·4. The "design" base shears for the analyses in the X and Y-directions are 397 kips and 388 kips, respectively, and correspond to the maximum values during the earthquake (Figure A·12).

2. The heightwise distribution of lateral forces at the three floor levels are computed from the code formula:

$$F_j = \frac{w_j h_j}{\sum_{i=1}^{3} w_i h_i}$$

j=1,2 and 3, using the floor masses and story heights in Table A·1. The lateral floor forces for this building are 0.28V, 0.49V and 0.23V for the second floor, third floor and roof , respectively, wherein V represents the "design" base shear determined in Step 1. In the X direction, V=397 kips and the associated lateral forces are 111, 196 and 90 kips at the second floor, third floor and roof, respectively. In the Y-direction V=388 kips and the lateral floor forces are 108, 192 and 88 kips. The X-lateral forces are applied at a distance of ±0.05b = ±0.05x77 = 3.85 ft. The Y-lateral forces are applied at a distance of ±0.05b = ±0.05x162

= 8.1 ft. The resulting "design" shear forces for selected columns in the first story of the building are shown in column 3 of Table A-3.

3. The lateral story forces determined in Step 2 are next applied at the CM of each floor. The resulting shear forces for selected columns in the first story of the building are presented in column 4 of Table A-3. The procedure for calculating the base shear that produces the same "design" member force as in Step 2 is described next for Column 8 (row 1) in the first story (Figure A-10). Step 2 provided 53.4 kips as the "design" shear force for this column in the Y-direction, whereas step 3 resulted in shear force of 48.8 kips. Thus, the ratio 53.4/48.8 represents the factor by which the "design" base shear, V=388 kips, in the Y-direction has to be amplified in order to obtain the "design" shear force of 53.4 kips in Column # 8 of the first story. The amplified base shear V_0=(53.4/48.8)388=424.5 kips (column 5 of Table A-3). Similar results for other columns in the first story are also presented in Table A-3.

4. Next we analyze the structure subjected to torques T_i=0.05bF_i where the lateral forces F_i were determined in step 2. The resulting force in a member is the difference of the two values for the member force determined in steps 2 and 3. Therefore, the resulting shear forces in the selected columns corresponding to this analysis are obtained as the difference of the values in columns 3 and 4 of Table A-3. The procedure for calculating the base torque that produces the same "design" shear force in a selected column as step 2 is described next for Column 8 in the first story. Step 2 provided 53.4 kips as the "design" shear force for this column, whereas step 4 resulted in a shear force of 4.6 kips. Therefore, the ratio 53.4/4.6 denotes the factor by which the base torque, T=388x8.1=3143 kip-ft, has to be amplified to produce the "design" force in Column 8 of the first story. The amplified base torque is T_0=(53.4/4.6)3143=36484[1]

[1]This value of torque differs slightly from the one presented in Table A-3 because of rounding of the numbers presented in the text

kip-ft. Similar results for other columns of the first floor are presented in Table A·3.

5. The code-equivalent combinations associated with column 8 in the first story are shown by solid straight lines in Figure A·13(b). Also shown by dashed lines are the code-equivalent combinations for zero accidental eccentricity. They have been calculated as described in steps 3 and 4 but using the value in column 4 of Table A·3 as the "design" member force associated with zero accidental eccentricity. Considering the first story Column 8 the corresponding base shear V=388 kips and the base torque is, T=388x8.1 kip-ft, amplified by the factor 48.8/4.6, resulting in 33341 kip-ft.

The values of base shear and torque for the X and Y-directions of analysis that were presented in Figure A·12 are plotted as pairs (V,T) for each instant of time in Figure A·13. For analysis in the Y-direction Figure A·13(b) shows that all base shear and base torque combinations fall inside the code-equivalent combinations. For analysis in the X-direction Figure A·13(a) shows that, except for a single instant, the base shear and base torque pairs determined in step 6 fall inside the code-equivalent combinations. The code-equivalent combinations are only slightly exceeded by a single combination of base shear and base torque in Column 22 (Figure A·13(a)). This combination is identified as point A in the figure. The value of "shear" in Column 22 corresponding to this combination of base shear and base torque is essentially identical (larger by less than 1%) to the code "design" value.

A.5 Time History of Member Forces

The member forces due to the static application of the floor inertia forces computed by Equations 1 to 3 were determined by first: (a) computing the influence coefficients defining the forces in selected members due to unit values of each of the nine floor inertia forces applied individually (Table A·4); and (b) multiplying at each instant of time the actual values of the floor inertia forces and the respective influence coefficients. Table A·4 presents the force influence coefficients for six columns in the first story of the building due to F_{xj} or F_{yj}=1000 kips, j=1,2 or 3; and $F_{\theta j}$=1000 kip-ft, j=1,2 or 3. In Table A·4, V is the shear force in the selected element and M the bending moment. The subscript attached to V or M indicates the element number according to Figure A·10 and the superscript indicates the direction of analysis. The time-history of element forces obtained by combining the products of the nine floor inertia forces (Figure A·4) by the corresponding influence coefficients (Table A·4) and divided by 1000 are presented in Figures A·14 and A·15. Also included in these figures are the "design" values for the member forces associated with accidental eccentricity 0.05b (solid horizontal line) and zero accidental eccentricity (dotted horizontal line).

Results of analysis of the building in the Y-direction (Figure A·15) show that at all time instants the member forces computed in step 4 are less than the "design" member forces. The same observation is true for the results of the analysis in the X-direction (Figure A·14) except that the "design" shear for Column 22 is exceeded once (this peak corresponds to point A in Figure A·13). The observed increase in shear force is negligible, being less than 1%.

Page Intentionally Left Blank

Table A·1: Building Properties

Floor	h (ft)	m_i (k-s^2/ft)	Ip_i (k-s^2-ft)	x_{gi} (ft)	y_{gi} (ft)
3rd	13.5	9.1652	25309	81	38.5
2nd	13.5	28.982	80031	81	38.5
1st	17.9	29.727	82089	81	38.5

Table A·2: Natural Vibration Frequencies and Modes Shapes of the Building

Vibration Properties	X-lateral mode		Y-lateral mode		Torsional mode	
	Recorded	Computed	Recorded	Computed	Recorded	Computed
Analysis "A" Frequency (Hz)	1.60	1.25	1.43	1.24	2.17	2.01
Mode Shape						
Roof	1.00	1.00	1.00	1.00	1.00	1.00
3^{rd}	0.71	0.74	0.72	0.76	0.72	0.78
2^{nd}	0.39	0.40	0.39	0.42	0.40	0.59
Analysis "B" Frequency (Hz)	1.60	1.66	1.43	1.32	2.17	2.21
Mode Shape						
Roof	1.00	1.00	1.00	1.00	1.00	1.00
3^{rd}	0.71	0.77	0.72	0.73	0.72	0.76
2^{nd}	0.39	0.57	0.39	0.38	0.40	0.43
Analysis "C" Frequency (Hz)	1.60	1.66	1.43	1.48	2.17	2.25
Mode Shape						
Roof	1.00	1.00	1.00	1.00	1.00	1.00
3^{rd}	0.71	0.77	0.72	0.75	0.72	0.76
2^{nd}	0.39	0.57	0.39	0.41	0.40	0.43

Table A-3: "Design" Member Forces in Selected Elements and Amplified Base Shear and Base Torque

Column #	Direction	Shear Force (k)	Shear Force (k)	Base Shear (k)	Base Torque (k-ft)
8	Y	53.4	48.8	424.5	36312
18	Y	51.0	46.6	424.5	36363
4	X	36.1	35.1	408.3	54194
22	X	36.3	35.3	408.4	53478
Column #	**Direction**	**Bend. Mom. (k-ft)**	**Bend. Mom. (k-ft)**	**Base Shear (k)**	**Base Torque (k-ft)**
8	Y	524.1	479.5	423.9	36903
18	Y	503.1	460.4	423.8	36985
4	X	350.0	340.1	408.4	53894
22	X	352.1	340.1	408.5	53252

Table A-4: Influence Force Coefficients for Selected Elements

Unit Story Forces	V_4^x(k)	V_{22}^x(k)	V_8^y(k)	V_{18}^y(k)
F_{x1}	8.8000e-02	8.7500e-02	-2.3700e-04	8.1200e-04
F_{y1}	-1.5200e-03	1.4900e-03	1.1800e-01	1.1200e-01
$F_{\theta 1}$	6.7000e-04	-6.5900e-04	-1.4530e-03	1.3740e-03
F_{x2}	8.9170e-02	8.8700e-02	-7.8300e-05	1.0900e-03
F_{y2}	-1.1900e-03	1.1700e-03	1.2800e-01	1.2300e-01
$F_{\theta 2}$	6.8200e-04	-6.6900e-04	-1.4770e-03	1.4120e-03
F_{x3}	8.9520e-01	8.9020e-01	-3.0600e-03	8.3200e-03
F_{y3}	-1.1500e-03	1.1330e-03	1.3000e-01	1.2500e-01
$F_{\theta 3}$	6.8600e-04	-6.7340e-04	-1.4830e-03	1.4170e-03
	M_4^x(k-ft)	M_{22}^x(k-ft)	M_8^y(k-ft)	M_{18}^y(k-ft)
F_{x1}	8.0000e-01	7.9630e-01	-3.1170e-03	·6.1940e-03
F_{y1}	-1.3260e-02	1.3030e-02	1.0800e+00	1.0250e+00
$F_{\theta 1}$	6.1130e-03	-6.0000e-03	-1.3200e-02	1.2480e-02
F_{x2}	8.8110e-01	8.7620e-01	-2.7920e-03	8.2830e-03
F_{y2}	-1.0770e-02	1.0580e-02	1.2810e+00	1.2340e+00
$F_{\theta 2}$	6.7690e-03	-6.6420e-03	-1.4520e-02	1.3950e-02
F_{x3}	8.9520e-01	8.9020e-01	-3.0600e-03	8.3200e-03
F_{y3}	-9.9600e-03	9.7950e-03	1.3300e+00	1.2850e+00
$F_{\theta 3}$	6.9070e-03	-6.7770e-03	-1.4780e-02	1.4230e-02

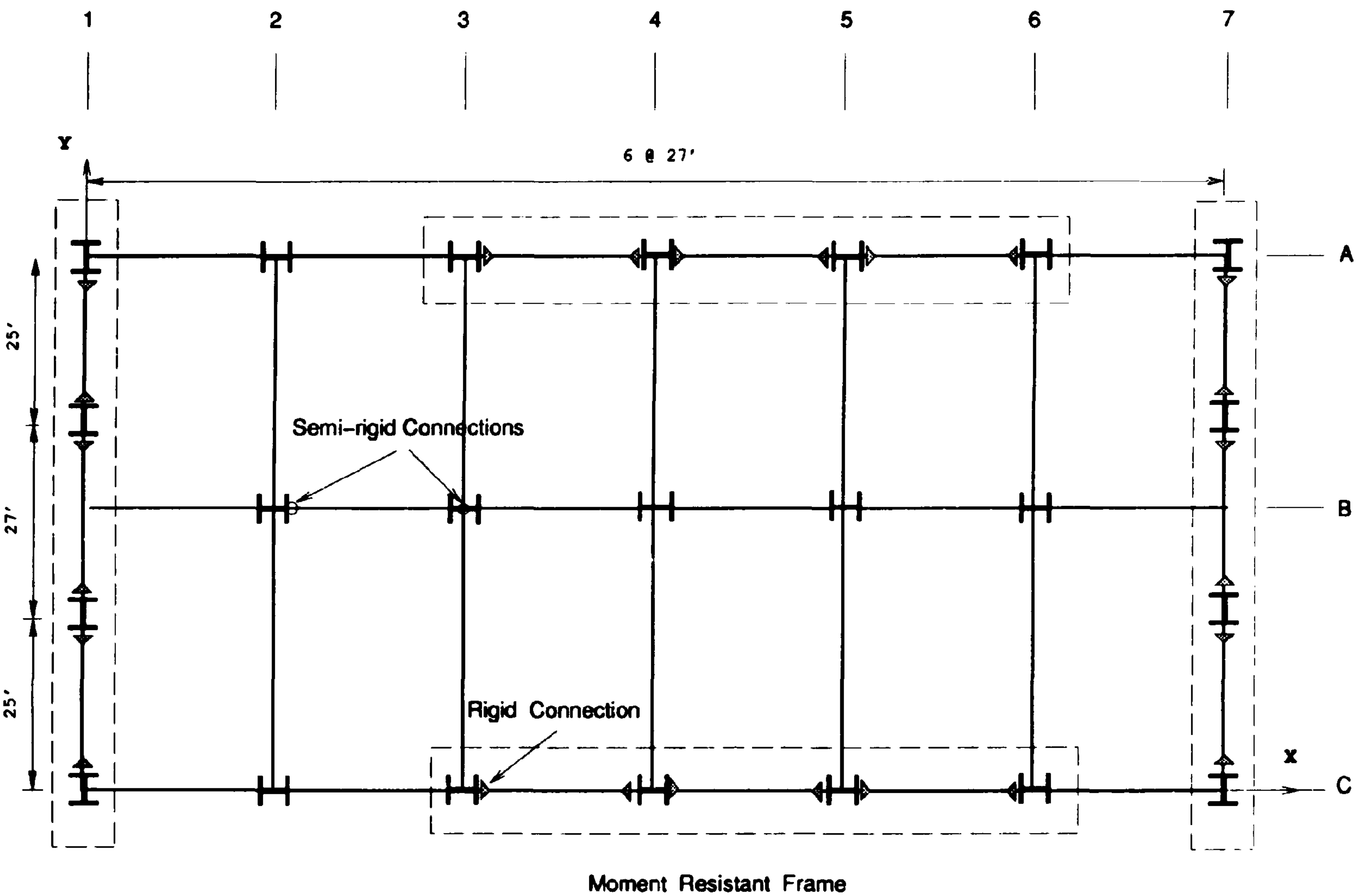

Figure A·1: Typical Framing Plan

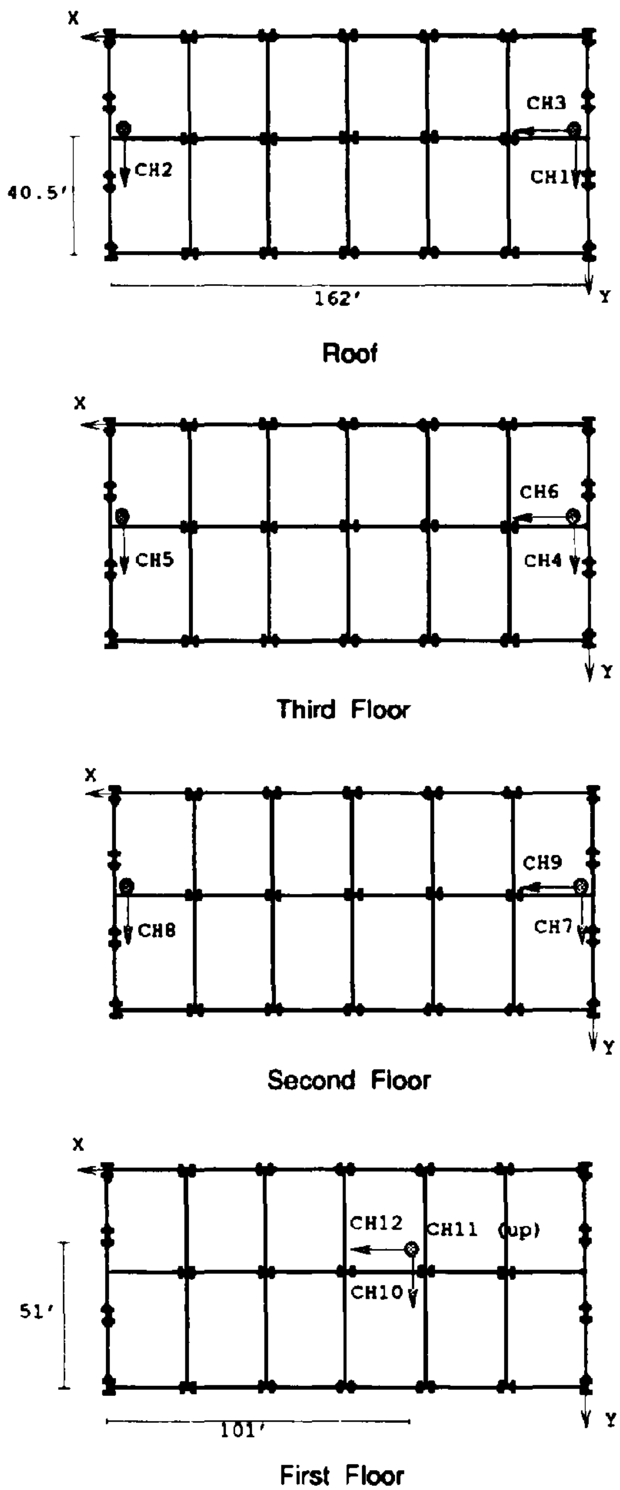

Figure A-2: Instrument Locations

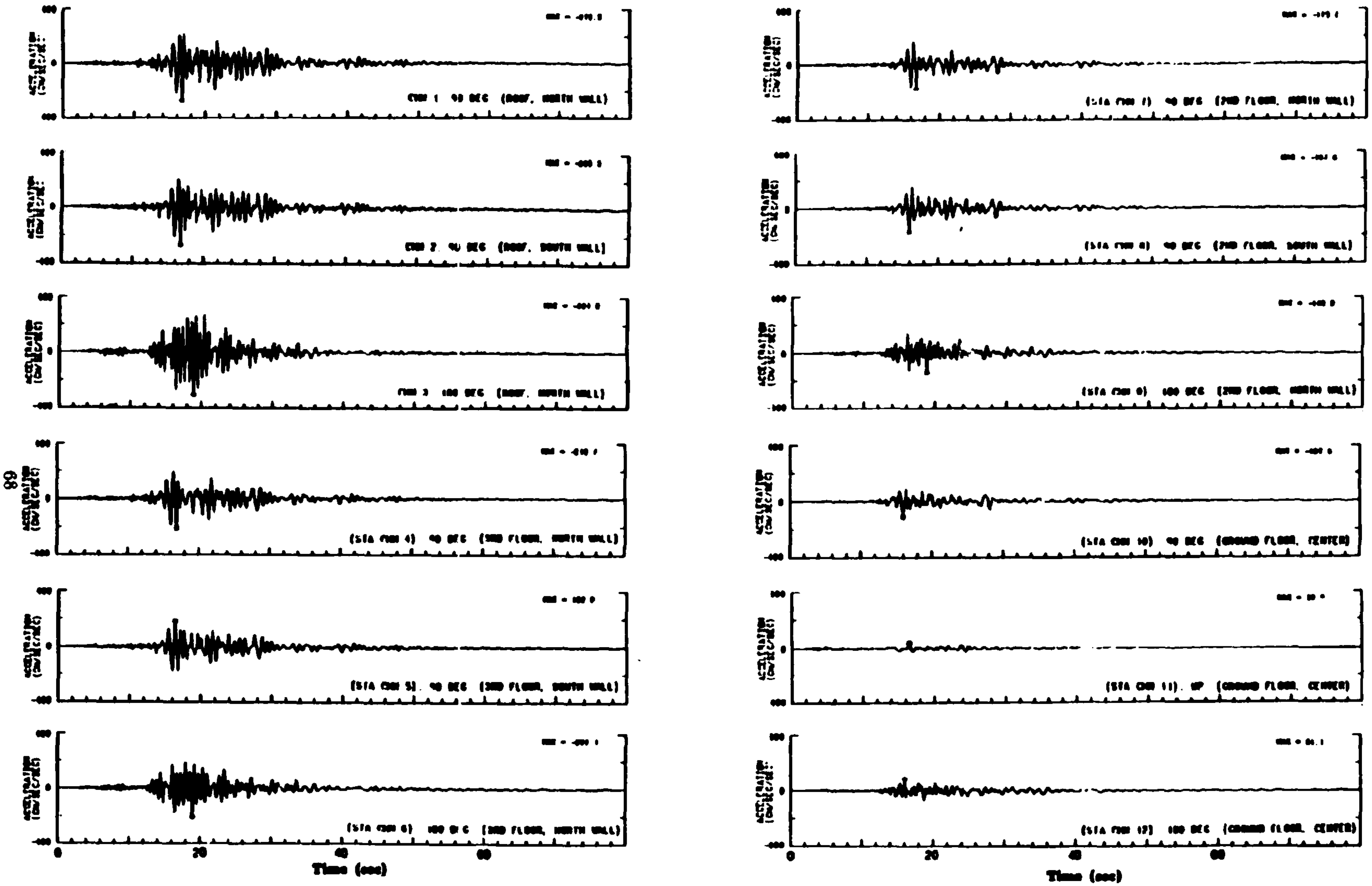

Figure A-3: Recorded Motions During the Loma Prieta Earthquake

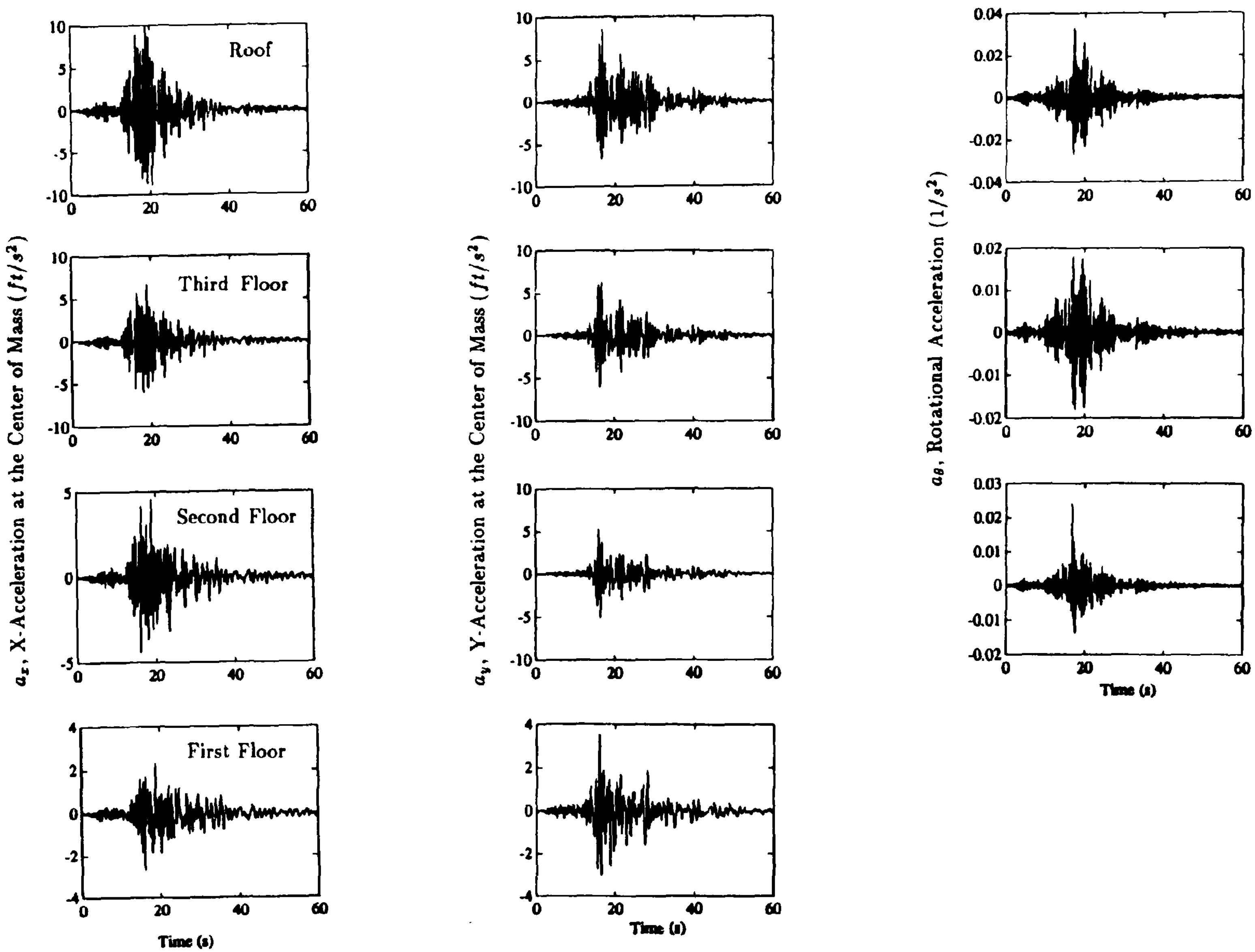

Figure A·4: Computed Motions at the CM of each Floor Level

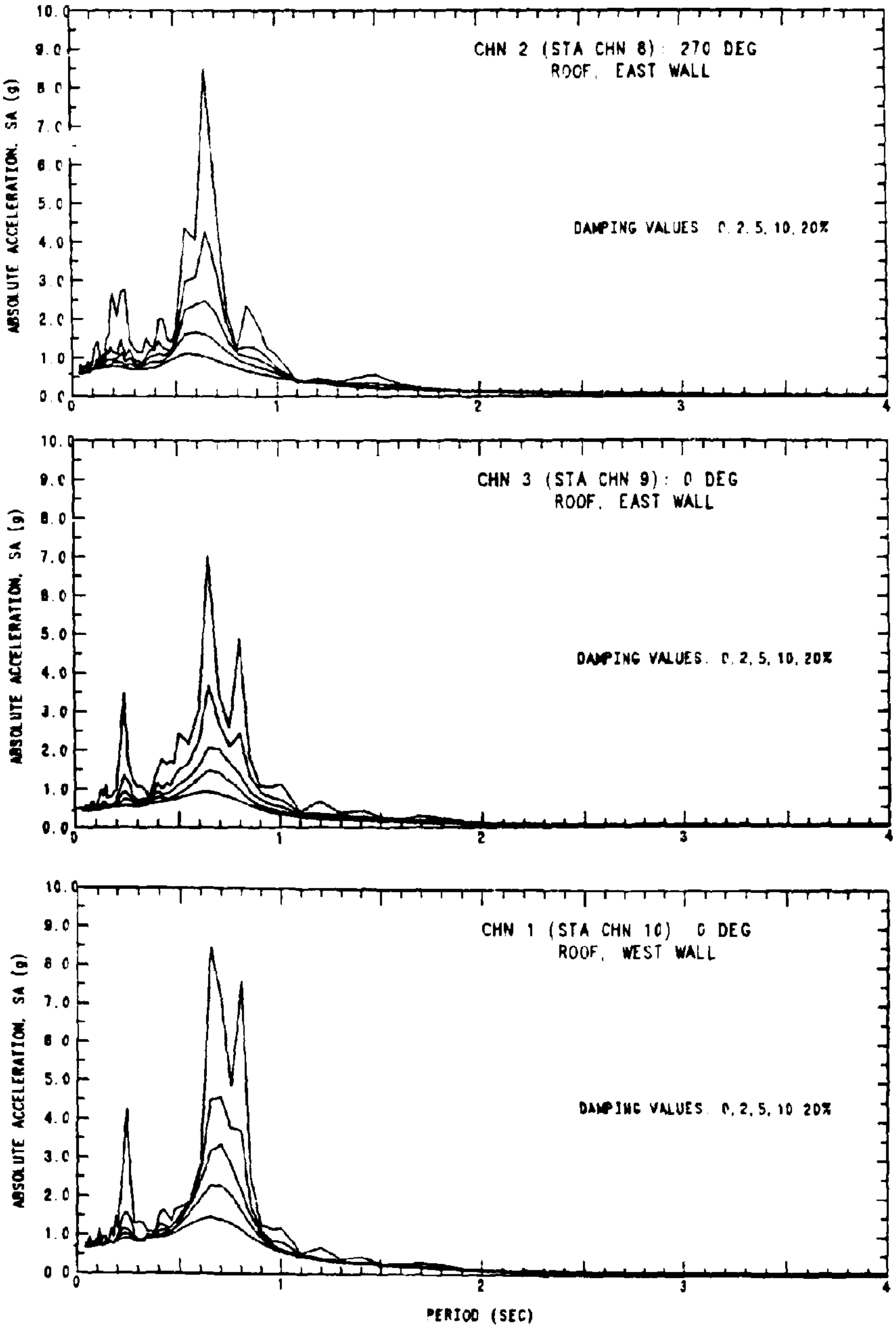

Figure A-5: Absolute Acceleration Spectra of Channels 1,2 and 3 at the Roof

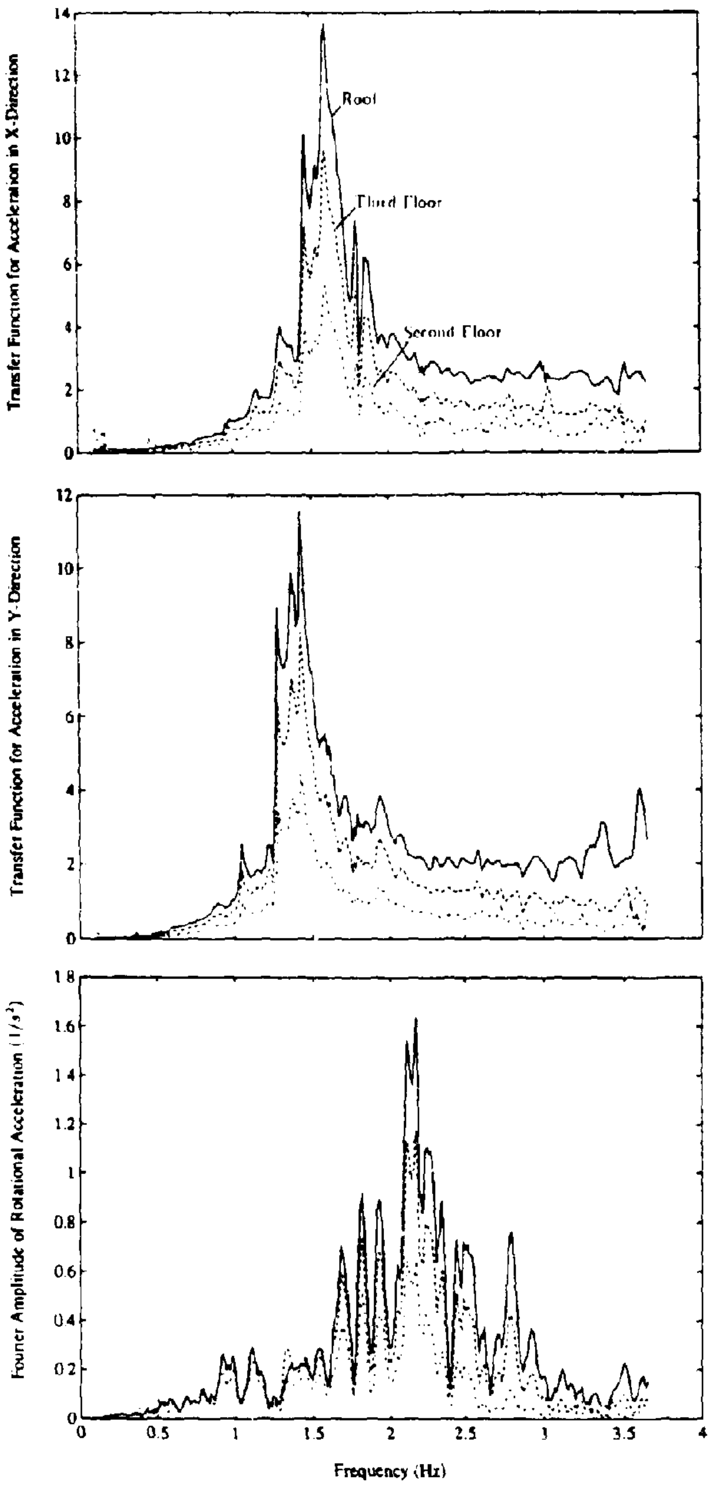

Figure A-6: Transfer Functions of the Roof Relative Floor Accelerations in the X and Y-Directions, and Fourier Amplitude of the Roof Rotational Acceleration

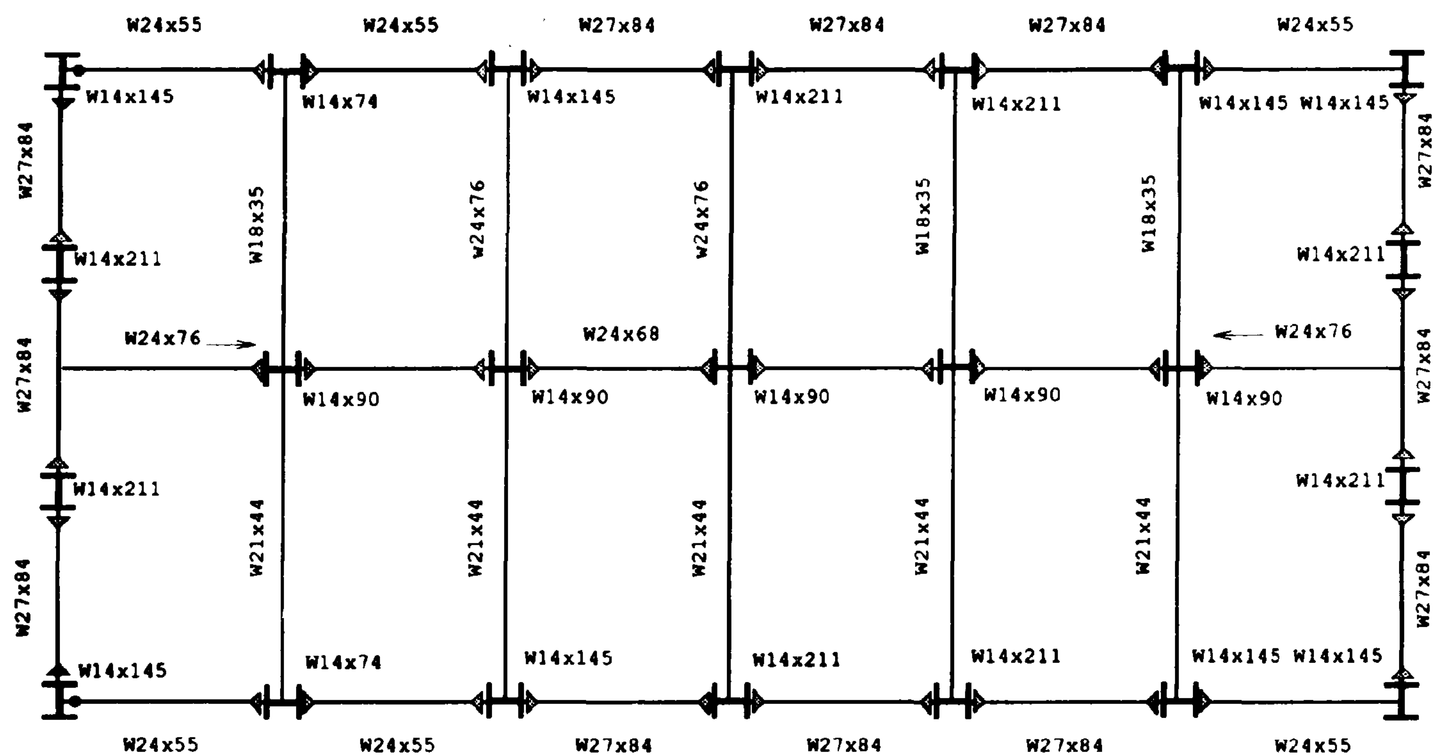

Figure A-7: Schematic Structural Plan of First Story

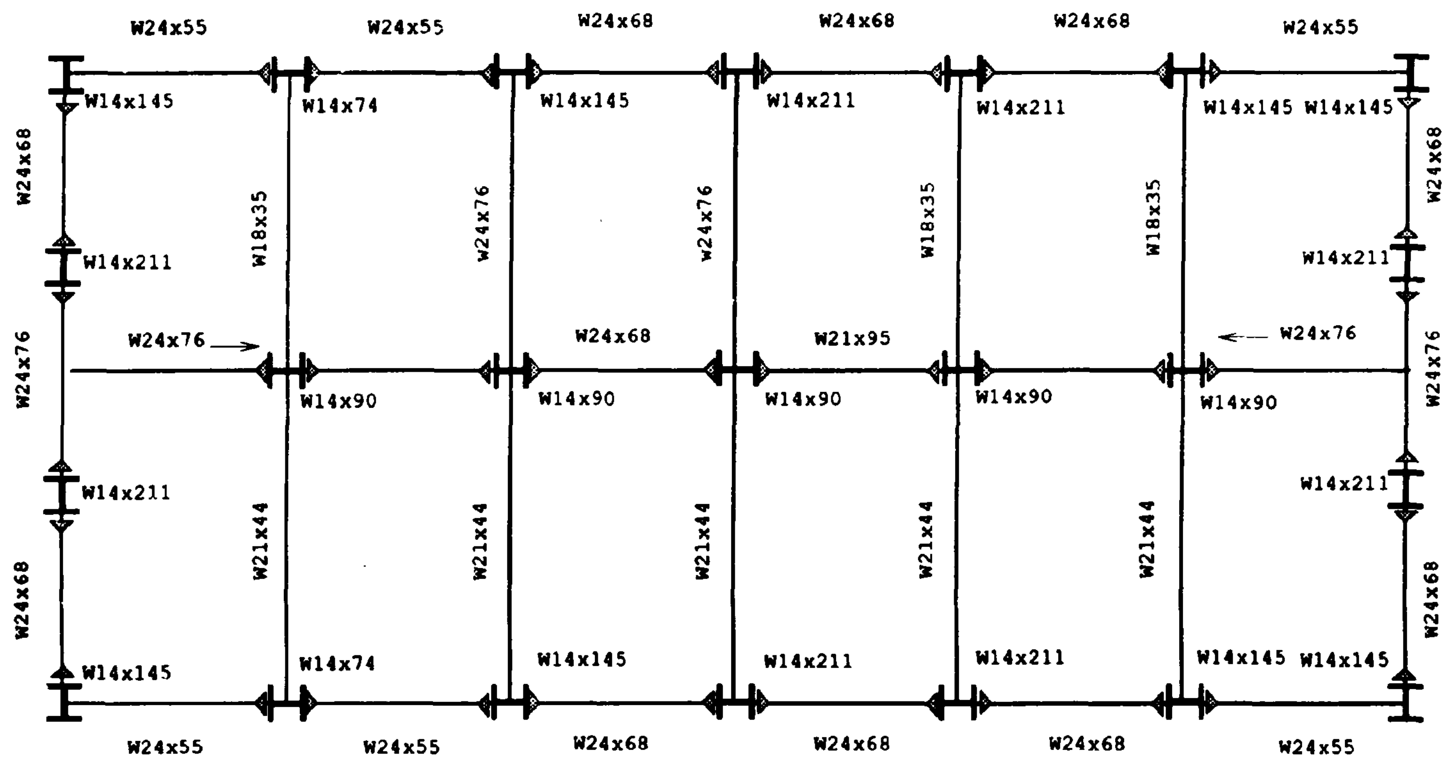

Figure A·8: Schematic Structural Plan of Second Story

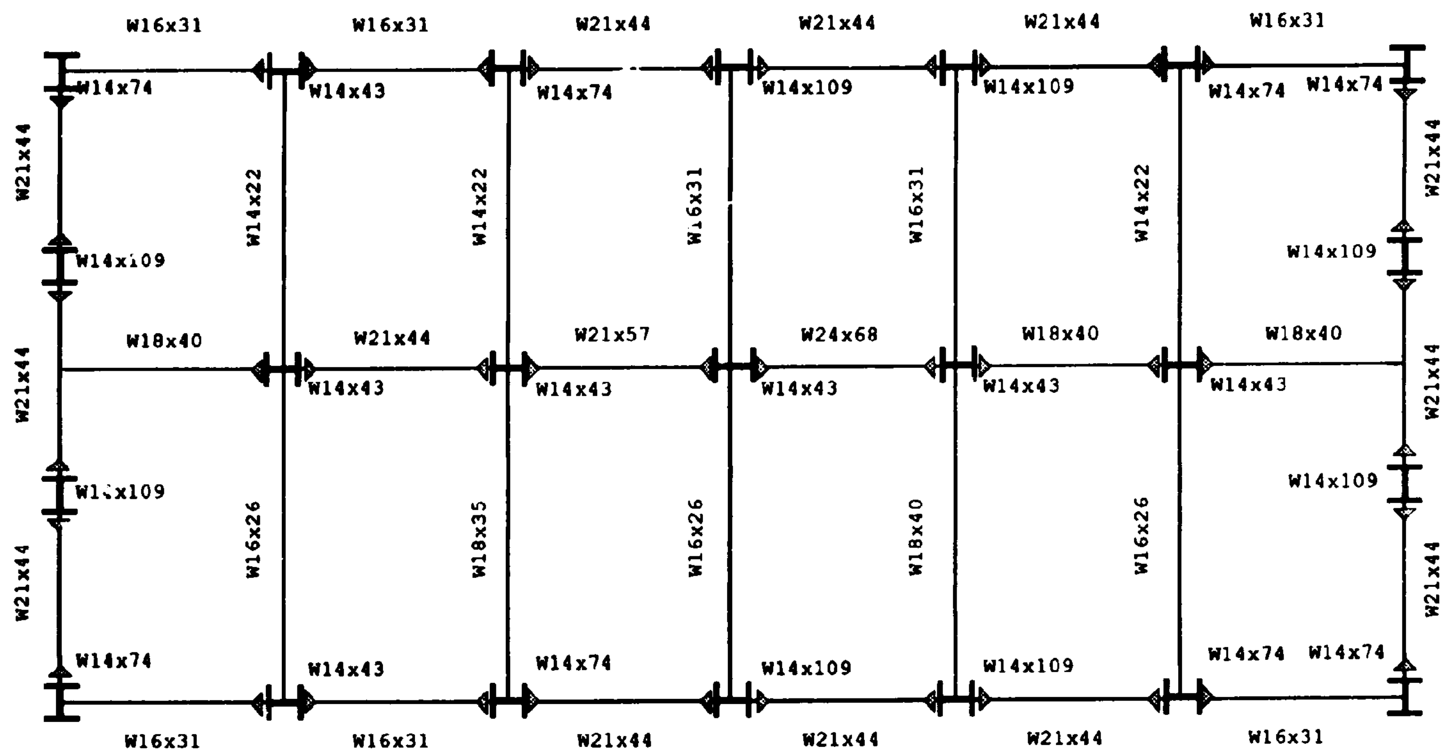

Figure A-9: Schematic Structural Plan of Third Story

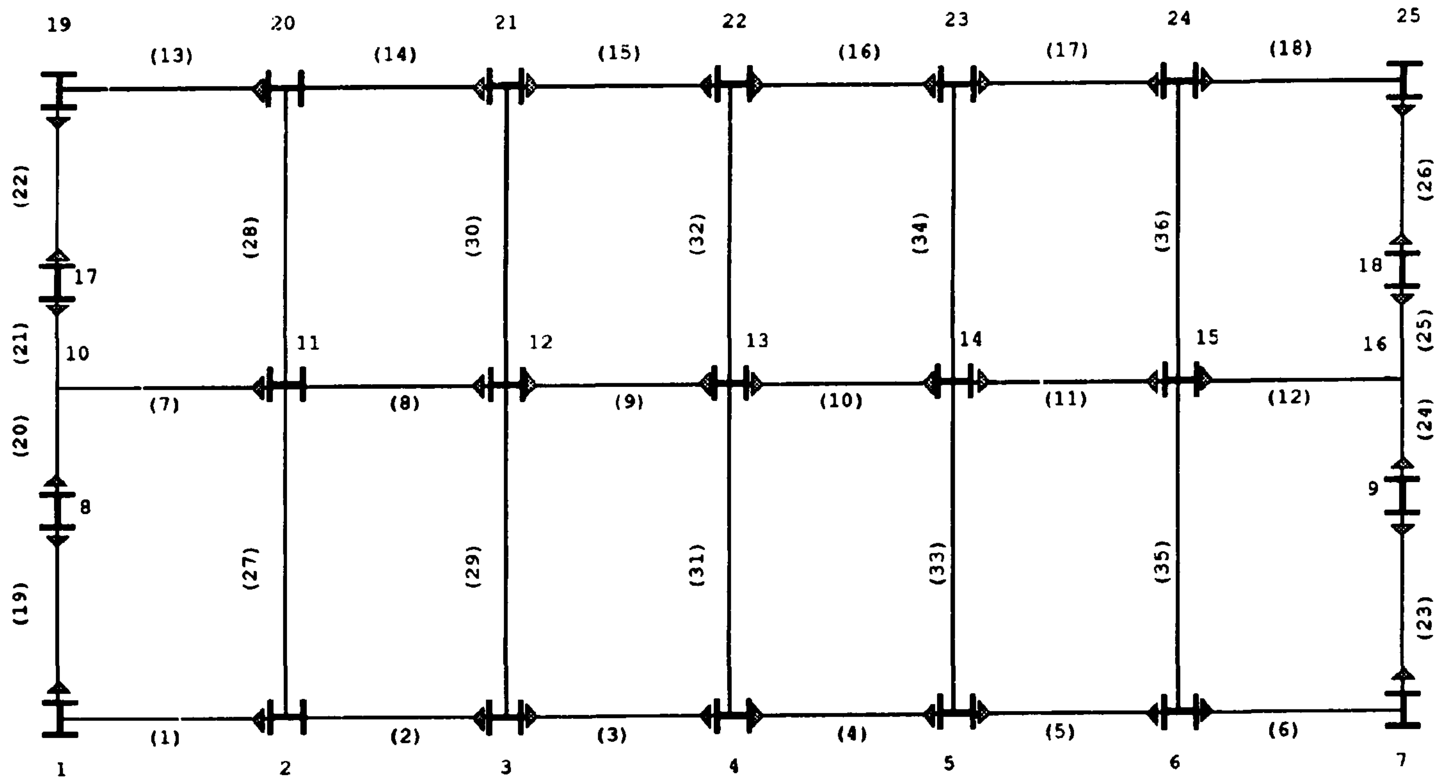

Figure A·10: Definition of Column Lines and Frame Bays for ETABS Model

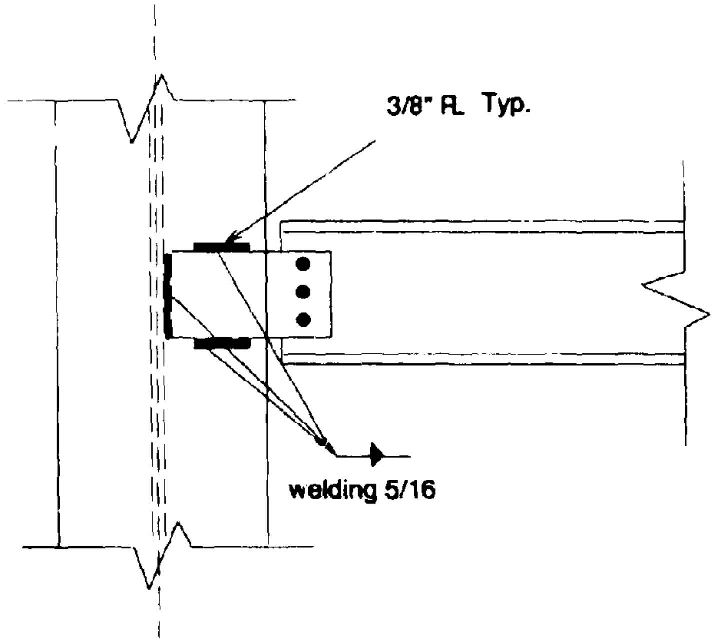

a) Web-to-Web Beam Column Connection

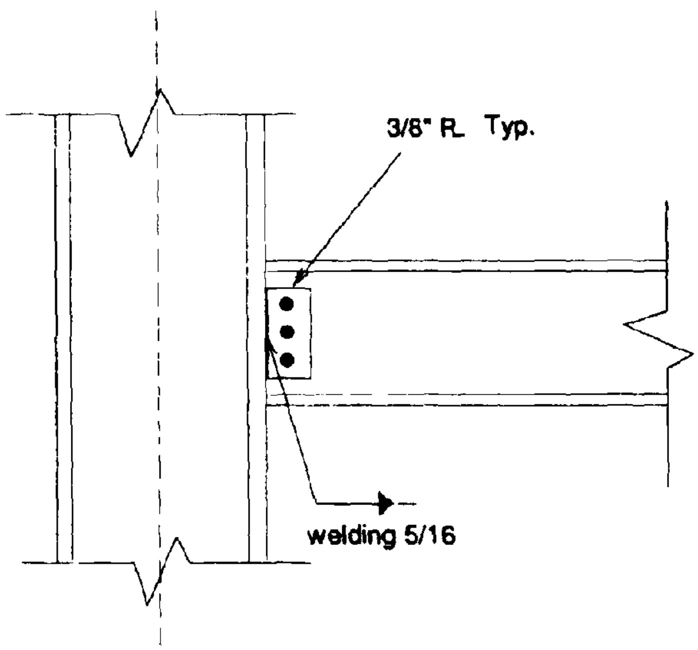

b) Web-to-Flange Bea Column Connection

Figure A-11: Semi-Rigid Beam-Column Connections

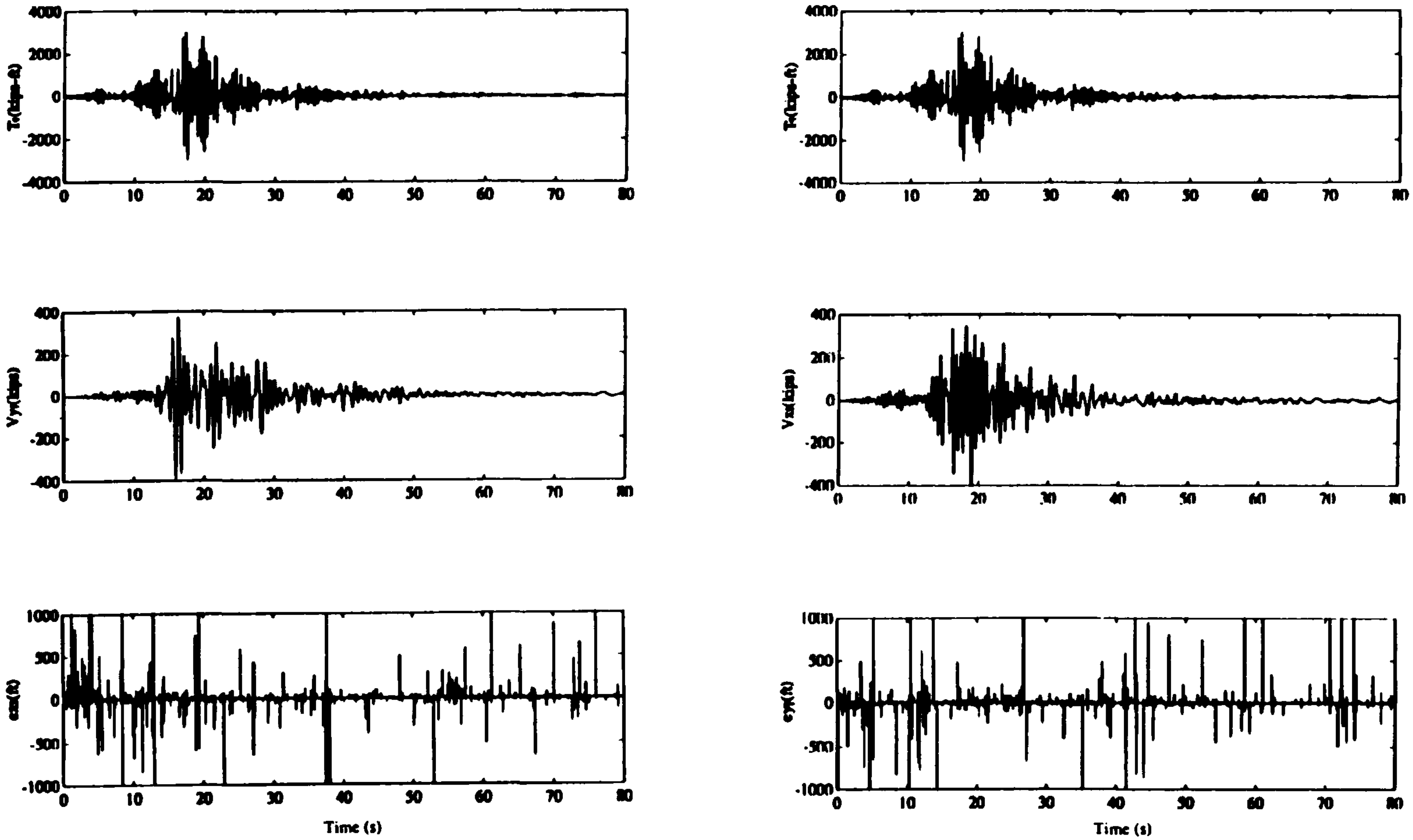

Figure A·12: Base Shear, Base Torque and First Floor Accidental Eccentricities Computed from Recorded Accelerations During the Loma Prieta Earthquake

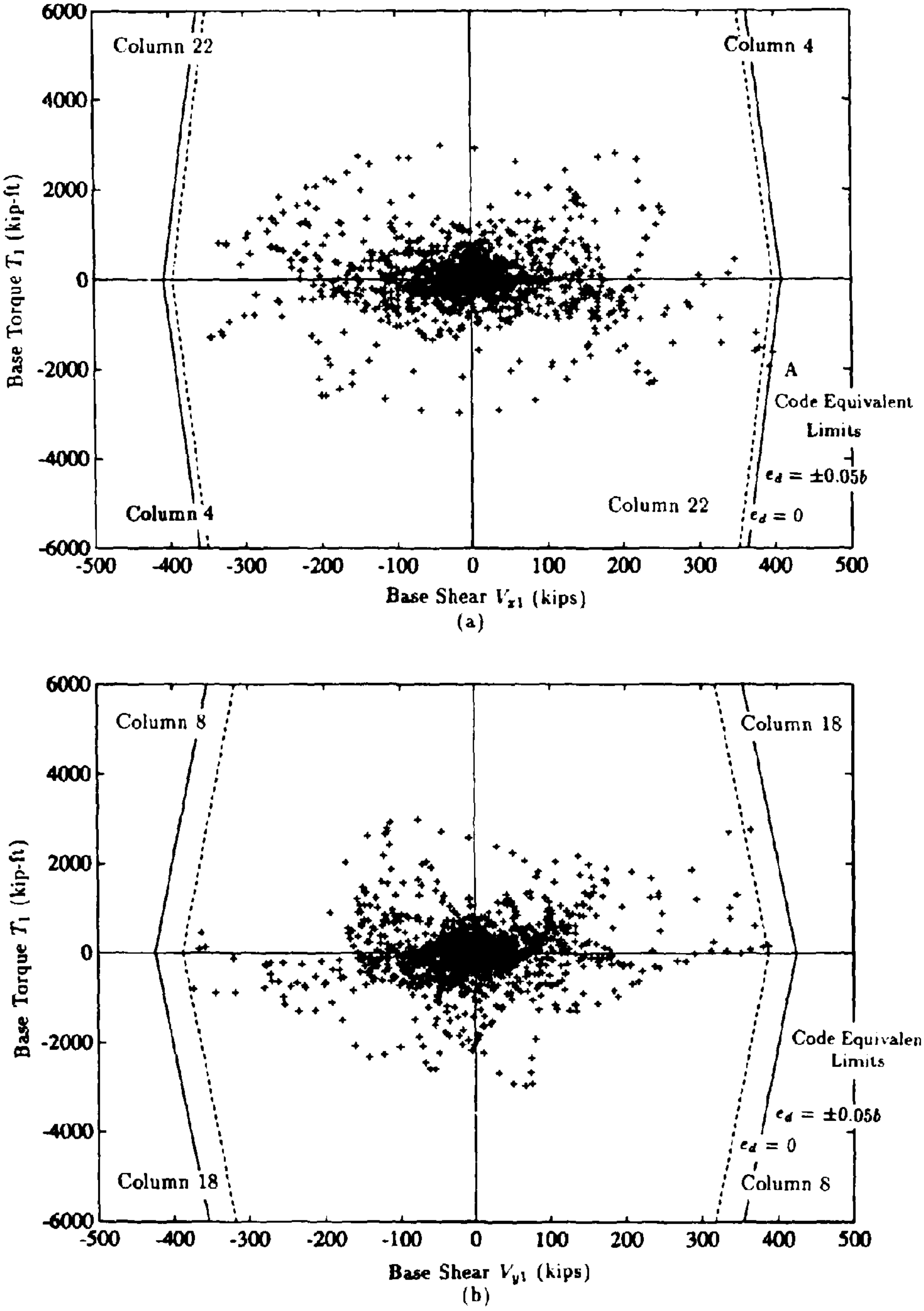

Figure A-13: Comparison of Dynamic Base Shear, Base Torque and "Code Equivalent Limits" Computed During the Loma Prieta Earthquake

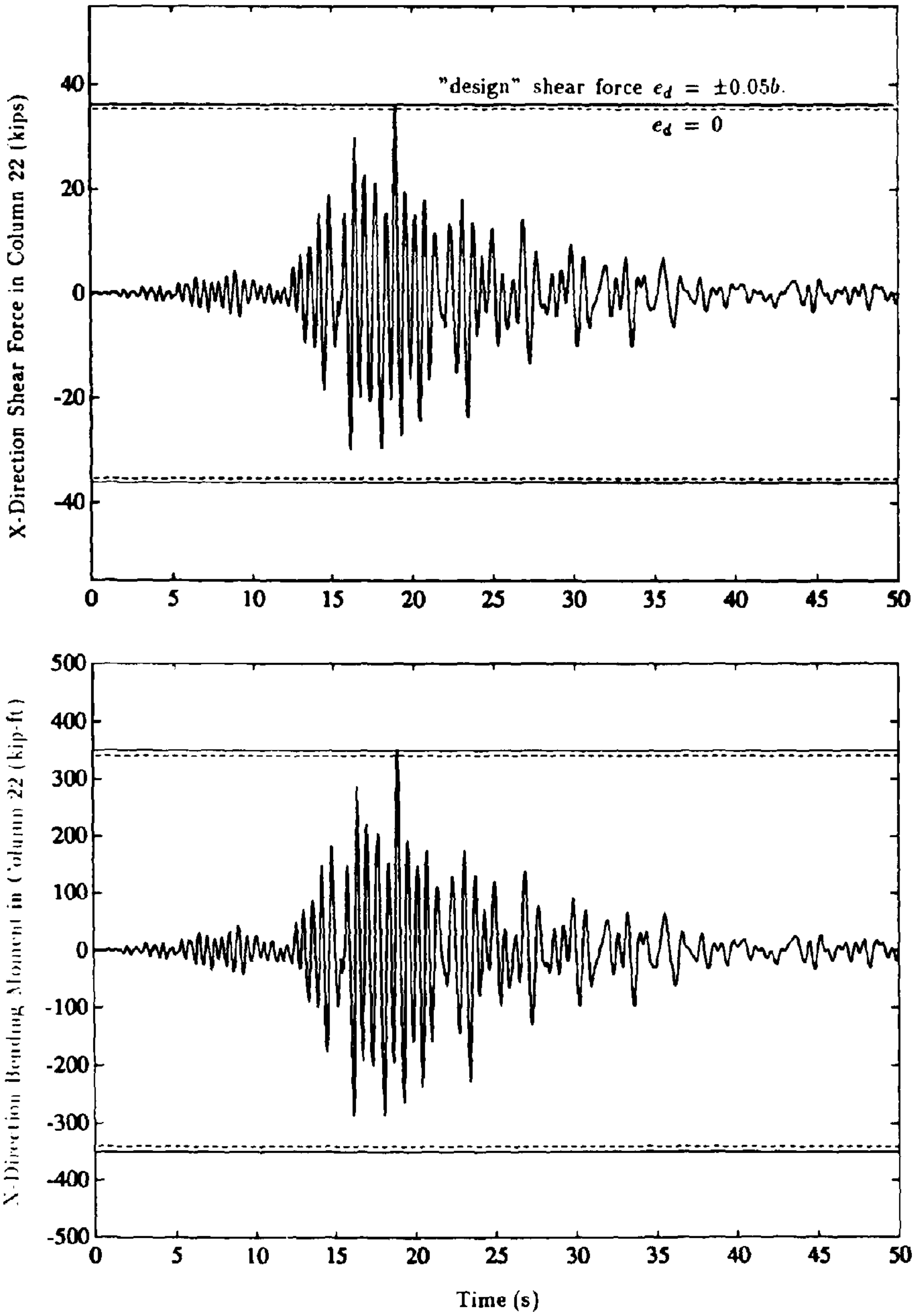

Figure A-14: Comparison of Earthquake Induced Shears and Bending Moments in Column 22 with "Design" Values

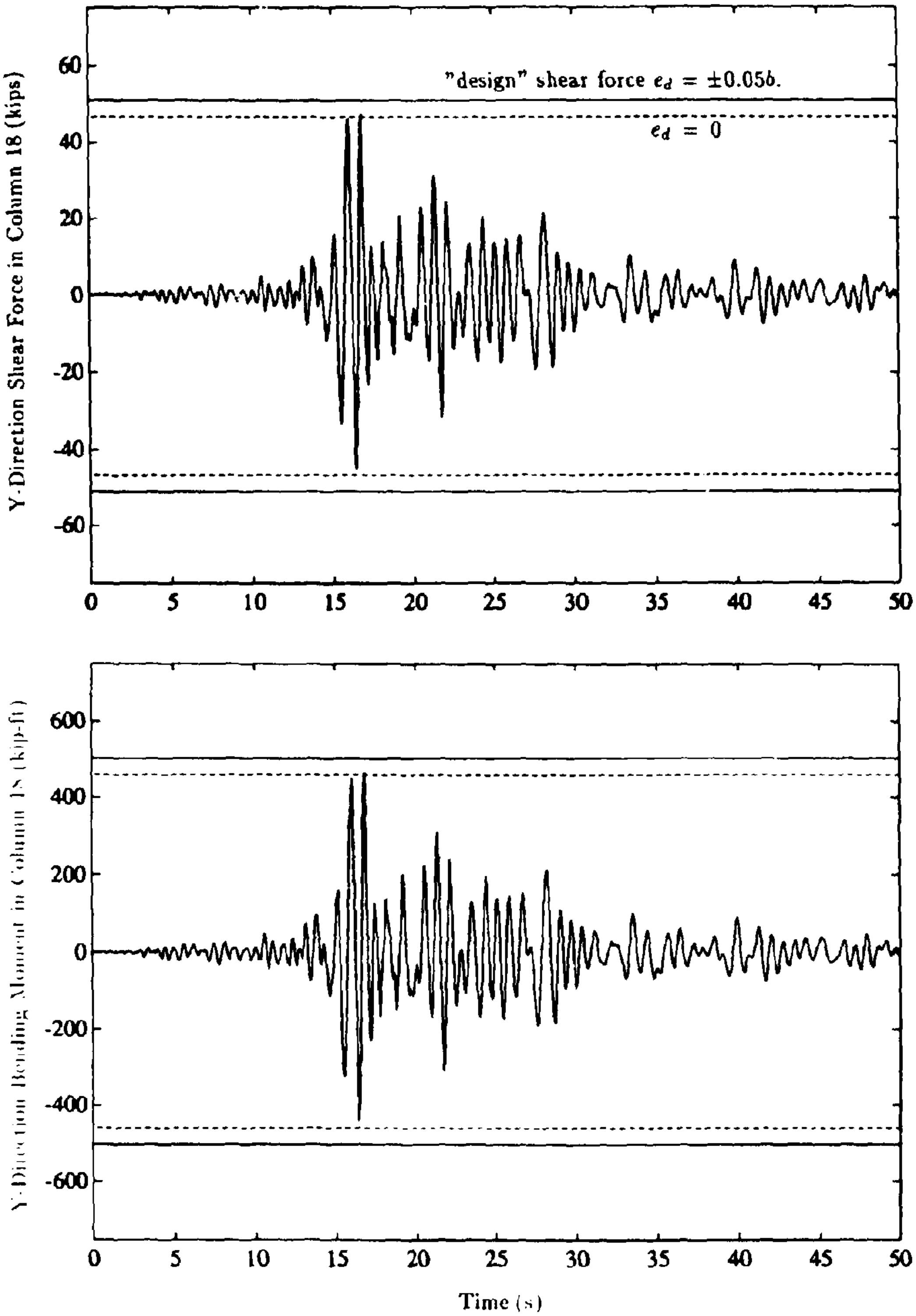

Figure A-15: Comparison of Earthquake Induced Shears and Bending Moments in Column 18 with "Design" Values

APPENDIX B: TWO STORY OFFICE BUILDING

(CSMIP STATION No. 23511)

B.1 Building and Recorded Motions

Identified as CSMIP station No. 23511, this building is located in Pomona, California. Records of motions of the building during the Whittier Narrows (October 1st, 1987) and the Upland (February 28th, 1990) earthquakes are available. A brief description of the structure, the recorded motions and the natural vibration frequencies and modes estimated from the records is presented in this section.

B.1.1 Brief Description of Building

The building is a reinforced concrete frame structure. It has two stories and a partial basement, and a light penthouse structure. A typical plan of this two-story concrete frame building is presented in Figure B-1. The figure shows that the building is approximately 110 feet long, 92 feet wide and 30 feet high (Figure B-1). The lateral force-resisting system in the building consists of peripheral columns interconnected by longitudinal and transverse beams(Figure B-1). In Figure B-1 dotted lines represent tapered beams (axis 2-5) and solid lines represent uniform beams. The "L" shaped corner columns as well as the interior columns are not designed with special seismic details. The floor decking system is formed by a 6" reinforced concrete slab. The building also includes walls in the stairwell system—concrete walls in the basement and masonry walls in upper stories (Figure B-1). Foundation of columns and interior walls are supported on piles.

For all practical and code design purposes, the building has a floor plan that is nominally-symmetric about two axes. The asymmetry resulting from additional non-structural elements distributed across the the plan is minimal. The translational mass and rotational inertia for each floor is determined from the weight of the structural elements, partitions, ceilings and other miscellaneous contributions. The mass of columns and partitions in each story is distributed equally to the floors at the top and bottom of the story. No live load is considered in calculating the floor masses. The location of the center of mass (CM) for each floor was determined according to the dead loads specified in the original structural drawings of the building. The coordinates of the CM, with the origin defined as shown in Figure B-1, are presented in Table B-1.

B.1.2 Recorded Motions

The locations of the accelerographs in the building are shown in plan in Figure B-2. These include three channels at the basement, second floor and roof. The nine strong motion records obtained during the Whittier and Upland earthquakes are shown in Figures B-3 and B-4.

The peak ground accelerations recorded at the basement level during the Whittier earthquake are 0.046g and 0.05g in the X and Y directions, respectively. These motions were both amplified to 0.15g in the X and Y-directions at the roof level. The peak ground accelerations recorded at the basement level during the Upland earthquake are 0.12g and 0.13g in the X and Y directions, respectively. These motions were amplified to 0.24g in the X-direction and 0.39g in the Y-direction at the roof level. The building experienced no structural damage during either earthquake.

From the three channels of accelerations recorded at any level, the accelerations of the CM -- these are $a_x(t)$ and $a_y(t)$, the X and Y components of translational acceleration of the CM, and $a_\theta(t)$, the rotational acceleration about a vertical axis -- at the same level can be computed assuming a rigid floor diaphragm. This assumption seems valid for this building, given the large in-plane stiffness of the reinforced concrete decking system compared with the lateral stiffness of the concrete columns. Computed by this procedure, the accelerations $a_x(t)$, $a_y(t)$ and $a_\theta(t)$ at the geometric center of the basement and the CM of the second floor and roof level are presented in Figures B-5 and B-6 for both earthquakes. During the Whittier earthquake (Figure B-5), the calculated peak acceleration in the X-direction at the geometric center of the basement is 0.046g which is amplified to 0.12g at the CM of the roof level; the amplification is from 0.052g to 0.15g in the Y-direction. The peak ground rotational acceleration at the geometric center of the basement is 0.0055 rad/s^2 which is amplified to 0.056 rad/s^2 at the roof level. During the Upland earthquake the calculated peak ground acceleration in the X-direction at the basement is 0.10g which is amplified to 0.20g at the roof level; the amplification is from 0.13g to 0.39g in the Y-direction. The peak ground rotational acceleration in this case of 0.017 rad/s^2 is amplified to 0.068 rad/s^2 at the roof level.

B.1.3 Natural Vibration Frequencies and Modes

Examination of the motions recorded at the roof level by channels 2, 3 and 8 during the Whittier earthquake provides rough estimates of the fundamental natural vibration frequencies of the building: 3.4 Hz in the X-direction and 3.7 Hz in the Y-direction. Examination of motions during the Upland earthquake gives very similar values for these frequencies. The true (not pseudo) acceleration response spectra for the motions recorded during the two earthquakes at the roof level in the X-direction at channels 2 and 3 and in the Y-direction at channel 8 are shown in Figures B-7 and B-8. For the Whittier earthquake peaks are obtained at frequencies of 3.1 Hz and 3.8 Hz in the X and Y-directions, respectively. However, the poor resolution of the peaks in the X-direction does not allow a reliable estimation of the natural frequency in that direction. For the Upland earthquake, Figure B-8 shows peaks around 3.3 Hz for the X-direction and 3.8 Hz for the Y-direction of motion. Thus, these results are consistent with the results gleaned from direct examination of the records.

Figures B-9 and B-10 show the transfer functions for the X, Y and Θ components of the relative (to the ground) accelerations at the CM of each floor level and the corresponding motions at the geometric center of the basement plan. The transfer functions were smoothed by a running average procedure with weights (1/4,1/2,1/4). The transfer functions for the X and Y translational motions for the Whittier earthquake (Figure B-9) have a peak at 3.49 Hz and 3.71 Hz. The transfer function for rotational motion in this figure shows a peak at 4.96 Hz. The frequency associated to the local peak value existing at 4.6 Hz in Figure B-9 was discarded as the torsional natural frequency mainly because the peak vanishes in the corresponding torsional transfer function for the Upland earthquake (Figure B-10). The transfer functions for the Upland earthquake (Figure B-10) show peaks at 3.34 Hz, 3.61 Hz and 4.81 Hz for the X, Y and Θ motions. A vibration mode shape corresponding to a particular natural vibration frequency can be estimated from the ordinates at that frequency of the transfer function at the various floor levels. Thus, the shapes of the first three natural vibration modes can be determined from the numerical data of Figure B-9 (or B-10): the X-translational mode shape from Figure B-9(a) (or Figure B-10(a)), the Y-translational mode shape from Figure B-9(b) (or Figure B-10(b)), and the torsional mode shape from Figure B-9(c) (or Figure B-10(c)). The mode shapes are presented in Table B-2 for both earthquakes.

B.2 Structural Idealization of the Building

The building was idealized for analysis by the ETABS computer program, wherein the building mass is assumed to be lumped at the floor levels and the floor diaphragms are assumed to be rigid, an assumption which was also used in computing motions at the CM from the recorded motions. The building is treated as fixed at the base of the columns given the rigidity of the foundation pile system. All structural elements were included in the final structural idealization, i.e, even the elements that provide little lateral resistance are considered because they may contribute to the accidental eccentricities. Flexural and axial deformations are considered in defining the properties of columns, whereas only flexural deformations are considered in defining the stiffness properties of beams. Shear deformations are also included for the case of walls (stairwell system).

The moment of inertia of a beam is computed as the gross inertia of the beam web. This definition of the moment of inertia in beams indirectly accounts for cracking of the cross section and variation of moment of inertia along the beam. Stiffness matrices for beams along axes 2,3,4 and 5 (Figure B-1) were determined considering the beam taper in addition to the moment of inertia considerations mentioned above. Column and wall inertia properties were calculated from their gross-section.

Compatibility of axial deformations required in columns belonging to more than one moment resisting frame was considered by analyzing the structure as a single three-dimensional frame with six degrees of freedom per joint (in contrast to the most common type of analysis that considers the structure as an ensemble of several two dimensional lateral force resisting frames distributed across the building plan).

The framing plans idealized for analysis are shown in Figures B-11 and B-12, wherein the sizes of the columns and beams are noted. The column lines and frame bays used for the ETABS model are defined in Figure B-11.

Five different idealizations of the structure were analyzed and the computed vibration properties were compared with the "actual" values obtained from earthquake records. The five models are:

- Model 1: This is the basic model and considers columns and beams as the only lateral load-resistant structural elements in the building. The natural vibration frequencies of the idealized structural system computed by the ETABS program are presented in the first row of Table B-3. These values differ considerably from the actual frequency values presented in Table B-2.

- Model 2: This model is identical to model 1 but includes the effect of the stairwell masonry walls. A prismatic strength of $f'_m = 1500psi$ is assumed for the masonry; modulus of elasticity $E_m = 750f'_m$ and shear modulus $G = 0.4E_m$. The natural vibration frequencies of this model are shown in Table B-3. This table shows that the walls affect primarily the fundamental natural frequency of the structure in the Y-direction.

- Model 3: This model builds over model 2 but includes the effective contribution of the slab (effective width) in the computation of the flexural stiffness of beams, i.e, the inertia of beams is calculated assuming cracked sections but considering the effective contribution of the slab. The ACI code effective width values were adopted to determine the slab contribution. Table B-3 shows that the slab has little contribution to the natural frequencies.

- Model 4: This model is identical to model 3 but includes the effect of the rigidity of the beam-column joints. The rigidity in the beam-column joints is accomplished by using rigid end zones in the columns and beams framing into the joint. The dimension of these rigid end zones in beams is variable but it is never taken more than half the width of the smallest column framing into the joint. Similarly, the length of the rigid end zones for columns is always less than half the minimum depth of the smallest beam framing into the joint. The increase on the lateral stiffness of the building, as a consequence of these rigid end zones in beams and columns, is important. Table B-3 shows the natural frequencies of this model, which are affected significantly by the rigidity of beam-column joints.

- Model 5: This final model is identical to model 4 but includes the as-built non-structural column details depicted in Figure B-13. The brick veneer shown in the figure has an important effect on the stiffness of the peripheral columns even though concrete and masonry were assumed to work separately. The natural vibration frequencies of the model are presented in Table B-3.

The agreement between the natural vibration frequencies of model 5 computed by the ETABS program and the "actual" frequencies (Table B-2) is satisfactory. The computed mode shapes of the final structural model are presented in Table B-2. The agreement between the mode shapes predicted by model 5 and those obtained from the analysis of the transfer functions (Figures B-9 and B-10) is also satisfactory.

B.3 Dynamic Eccentricity

The story shears and torques are computed from the floor masses and accelerograms (Figure B-5 and B-6) by Equations 1 to 3, wherein the acceleration records at all floor levels are needed. For this building all instruments recorded motions during the Whittier and Upland earthquakes.

The accidental eccentricity at the "jth" floor has been defined by Equations 4 and 5 in terms of the story shears and story torques in the "jth" story. The latter are computed from Equations [1-3] wherein the floor masses are given by Table B-1 and the accelerations $a_{xj}(t), a_{yj}(t)$ and $a_{\theta j}(t)$ at the CM in Figure B-5 and B-6. The computed base shear and torque for the building are shown in Figures B-14 and B-15. For the Whittier Narrows earthquake the maximum values for the base shear are 361 kips and 485 kips in the X and Y-directions, respectively, which are 9% and 12% of the total weight of the building. The maximum values of base shear and torque during the Upland earthquake are 692 kips and 1301 kips for the X and Y directions, respectively, which are 17% and 32% of the total weight of the structure. The accidental eccentricities $e_{Y1}(t)$ and $e_{X1}(t)$ determined from the base shear and torque by Equations 4 and 5 are also shown in Figures B-14 and B-15.

B.4 Base Shear, Base Torque and Code-Equivalent Combinations

This section presents the implementation of the step-by-step procedure described in Section 5 for this building.

1. At each instant of time, the base shear was computed by Equations 1 to 3 , where the floor masses are given in Table B-1 and the floor accelerations in Figures B-5 and B-6. The "design" base shears during the Whittier Narrows earthquake are 361 kips and 485 kips for the analyses in the X and Y-directions, respectively, and correspond to the maximum values during the

earthquake (Figure B-14). The "design" values of base shear during the Upland earthquake are 692 kips and 1301 kips in the X and Y-directions , respectively, and correspond to the maximum values of base shear in Figure B-15.

2. The heightwise distribution of lateral forces at the two floor levels are computed from the code formula:

$$F_j = \frac{w_j h_j}{\sum_{i=1}^{2} w_i h_i}$$

j=1 and 2, using the floor masses and the story heights presented in Table B-1. The lateral story forces for this building are 0.36V, 0.64V for the second floor and the roof level level, respectively, wherein V represents the "design" base shear determined in Step 1. In the X direction, V=361 kips during the Whittier earthquake and the associated lateral forces are 129 and 232 kips at the second floor and roof, respectively. In the Y-direction , V=485 kips and the lateral forces are 173 and 312 kips at the second floor and roof, respectively. Similarly, in the X-direction during the Upland earthquake, V=692 kips and the lateral forces are 247 and 445 kips at the second floor and roof, respectively. In the Y-direction, V=1301 kips and the lateral forces are 465 and 836 kips at the second floor and roof, respectively. The X-lateral forces are applied at a distance of ±0.05b = ±0.05x109.8 = ±5.59 ft. The Y-lateral forces are applied at a distance of ±0.05b = 0.05x91.4 ft = ±4.57 ft. The resulting "design" shear forces for the selected columns in the first story of the building are shown in column 3 of Table B-4.

3. The lateral story forces determined in Step 2 are next applied to the structure at the CM of each floor level. The resulting shear forces for selected columns in the first story of the building are presented in column 4 of Table B-4. The procedure for calculating the base shear that produces the same "design" member force as in Step 2 is described next for Column 1 in the first story and the Whittier earthquake (Figure B-16(b)). Step 2 provided 21.4 kips

as the "design" shear force force for this column in the X-direction, whereas step 3 resulted in shear force of 19.4 kips. Thus, the ratio 21.4/19.4 represents the factor by which the "design" base shear, V=361 kips, in the X-direction has to be amplified in order to obtain the "design" shear force of 21.4 kips in Column 1 of the first story. The amplified base shear V_0=(21.4/19.4)361=398 kips (column 5 of Table B-4). Similar results for the two earthquakes and for other columns in the first story are also presented in Table B-4.

4. Next we analyze the structure subjected to torques T_i=0.05bF_i where the lateral forces F_i were determined in step 2. The resulting force in a member is the difference of the two values for the member force determined in steps 2 and 3. Therefore, the resulting shear forces in the selected columns corresponding to this analysis are obtained as the difference of the values in columns 3 and 4 of Table B-4. The procedure for calculating the base torque that produces the same "design" shear force in a selected column as step 2 is described next for Column 1 in the first story and the Whittier earthquake. Step 2 provided 21.4 kips as the "design" shear force for this column, whereas step 4 resulted in a shear force of 2 kips. Therefore, the ratio 21.4/2 denotes the factor by which the base torque, T=361x5.49=1982 kip-ft, has to be amplified to produce the "design" force in Column 1 of the first story. The amplified base torque is T_0=(21.4/2)1982=21207[2] kip-ft. Similar results for the two earthquakes and other columns of the first floor are presented in Table B-4.

5. The code-equivalent combinations associated with column 1 in the first story are shown by solid straight lines in Figure B-16(b). Also shown by dashed lines are the code-equivalent combinations for zero accidental eccentricity. They have been calculated as described in steps 3 and 4 but using the value in column 4 of Table B-4 as the "design" member force associated

[2]This value of torque differs slightly from the one presented in Table B-4 because rounding of the numbers presented in the text

kip-in, j=1,2 or 3, for story torques. In Table B-5, V is the shear force in the selected element and M the bending moment. The subscript attached to V or M, indicates the element number according to Figure B-12 and the superscript indicates the direction of analysis. The time-history of element forces obtained by combining the products of the six floor inertia forces (Figure B-4) by the corresponding influence coefficients (Table B-5) and divided by 1000 are presented in Figures B-20 through B-29. Also included in these figures are the "design" values for the member forces associated with accidental eccentricity 0.05b (solid horizontal line) and zero accidental eccentricity (dotted horizontal line).

Results of analysis of the building in the X-direction (Figures B-20- B-21, and B-25-B-26) show that except for a single case (Figure B-25(a)) at all time instants the member forces computed in step 4 are less than the "design" member forces for the elements acting in the X-direction. The same observation is true for the results of the analysis in the Y-direction (Figures B-22-B-24, B-27-B-29) wherein at all time instants the elements forces computed in step 4 are less than the "design" member forces. These results are, in general, consistent with the results of Figures B-16 through B-19 presented in Section B.4. Figure B-25(a) shows that for Column 1 there are two peaks in the shear response history of the element that slightly exceed the "design" forces in the element. The maximum observed increase in the shear force in Column 1 is less than 4%, which for all design practical purposes is negligible.

Page Intentionally Left Blank

Table B-1: Building Properties

Floor	h_i (ft)	m_i (k-s^2/ft)	Ip_i (k-s^2-ft)	x_{gi} (ft)	y_{gi} (ft)
Roof	12.5	64.53	109753	45.73	54.88
2^{nd}	17.5	60.97	103698	45.73	54.88

Table B-2: Natural Vibration Frequencies and Modes Shapes of the Building

Vibration Properties	X-lateral mode		Y-lateral mode		Torsional mode	
	Recorded	Computed	Recorded	Computed	Recorded	Computed
Frequency (Hz)	3.49	3.51	3.71	3.72	4.96	4.90
Mode Shape						
Roof	1.00	1.00	1.00	1.00	1.00	1.00
2^{nd}	0.62	0.61	0.39 ?	0.60	0.57	0.64

(a) Whittier

Vibration Properties	X-lateral mode		Y-lateral mode		Torsional mode	
	Recorded	Computed	Recorded	Computed	Recorded	Computed
Frequency (Hz)	3.34	3.51	3.61	3.72	4.81	4.90
Mode Shape						
Roof	1.00	1.00	1.00	1.00	1.00	1.00
2^{nd}	0.64	0.61	0.55	0.60	0.52	0.64

(b) Upland

Table B-3: Variation of the Natural Frequencies of the Building with the Structural Model Considered

Structural Model	X-lateral mode	Y-lateral mode	Torsional mode
Model 1 Frequency (Hz)	2.44	2.44	3.65
Model 2 Frequency (Hz)	2.55	2.87	3.90
Model 3 Frequency (Hz)	2.66	2.98	4.06
Model 4 Frequency (Hz)	3.01	3.32	4.56
Model 5 Frequency (Hz)	3.51	3.72	4.90

Table B-4: "Design" Shear Forces in Selected Elements and Amplified Base Shear and Base Torque

Column #	Direction	Shear Force (k)	Shear Force (k)	Base Shear (k)	Base Torque (k-ft)
1	X	21.392	19.397	397.55	21215
2	X	10.044	9.132	396.43	21811
8	X	13.445	12.609	384.36	31838
25	X	23.606	21.415	397.35	21316
29	X	11.057	10.056	396.36	21851
1	Y	27.870	25.720	525.85	28769
2	Y	17.902	16.961	512.23	42199
3	Y	17.587	17.165	497.23	92440
6	Y	23.546	21.780	524.65	29581
8	Y	11.244	10.434	522.98	30789
25	Y	27.870	25.720	525.85	28769
27	Y	17.567	17.165	496.68	96788

(a) Whittier

Column #	Direction	Shear Force (k)	Shear Force (k)	Base Shear (k)	Base Torque (k-ft)
1	X	41.049	37.221	762.86	40707
2	X	19.273	17.525	760.72	41853
8	X	25.799	24.196	737.56	61093
25	X	45.298	41.094	762.49	40904
29	X	21.218	19.297	760.59	41930
1	Y	74.731	68.966	1410.0	77141
2	Y	48.003	45.479	1373.5	113150
3	Y	47.157	46.025	1333.3	247870
6	Y	63.137	58.400	1406.8	79318
8	Y	30.150	27.977	1402.3	82558
25	Y	74.731	68.966	1410.0	77141
27	Y	47.105	46.025	1331.8	259530

(b) Upland

Table B-5: Influence Force Coefficients for Selected Elements

Unit Forces (1000 k, k-in)	V_1^x(k)	V_1^y(k)	V_2^x(k)	V_2^y(k)	V_8^y(k)	V_{26}^x(k)	V_{23}^y (k)	V_3^y (k)
F_{x1}	-55.5600	2.3860	-23.5600	1.0210	0.8447	25.8200	1.0384	0.4588
F_{y1}	4.7490	54.6800	1.9350	36.8000	-19.9000	2.1090	23.1800	36.8300
$F_{\theta 1}$	-0.0876	-0.0837	-0.0365	-0.0371	-0.0288	-0.0399	-0.0349	-0.0163
F_{x2}	-52.8400	2.5500	-26.3200	1.1100	1.0100	29.0500	1.2600	0.4820
F_{y2}	4.6950	52.0600	2.0700	33.9300	-22.4100	2.2700	25.9200	34.5600
$F_{\theta 2}$	-0.0821	-0.0791	-0.0394	-0.0342	-0.0314	-0.0434	-0.0377	-0.0154
	M_1^x(k-in)	M_1^y(k-in)	M_2^x(k-in)	M_2^y(k-in)	M_8^y(k-in)	M_{26}^x(k-in)	M_{23}^y (k-in)	M_3^y (k-in)
F_{x1}	6.5035	0.2813	2.4571	0.1251	0.0886	2.6929	0.1079	0.0545
F_{y1}	0.5290	6.3993	0.1963	4.3718	2.0781	0.2143	2.4176	4.3718
$F_{\theta 1}$	-0.0101	-0.0096	-0.0038	-0.0044	-0.0030	-0.0041	-0.0036	-0.0019
F_{x2}	7.2656	0.3362	2.9371	0.1510	0.1120	3.2354	0.1367	0.0641
F_{y2}	0.5588	7.1568	0.2159	4.9125	2.5222	0.2364	2.8923	4.8885
$F_{\theta 2}$	-0.0109	-0.0104	-0.0043	-0.0047	-0.0035	-0.0048	-0.0041	-0.0020

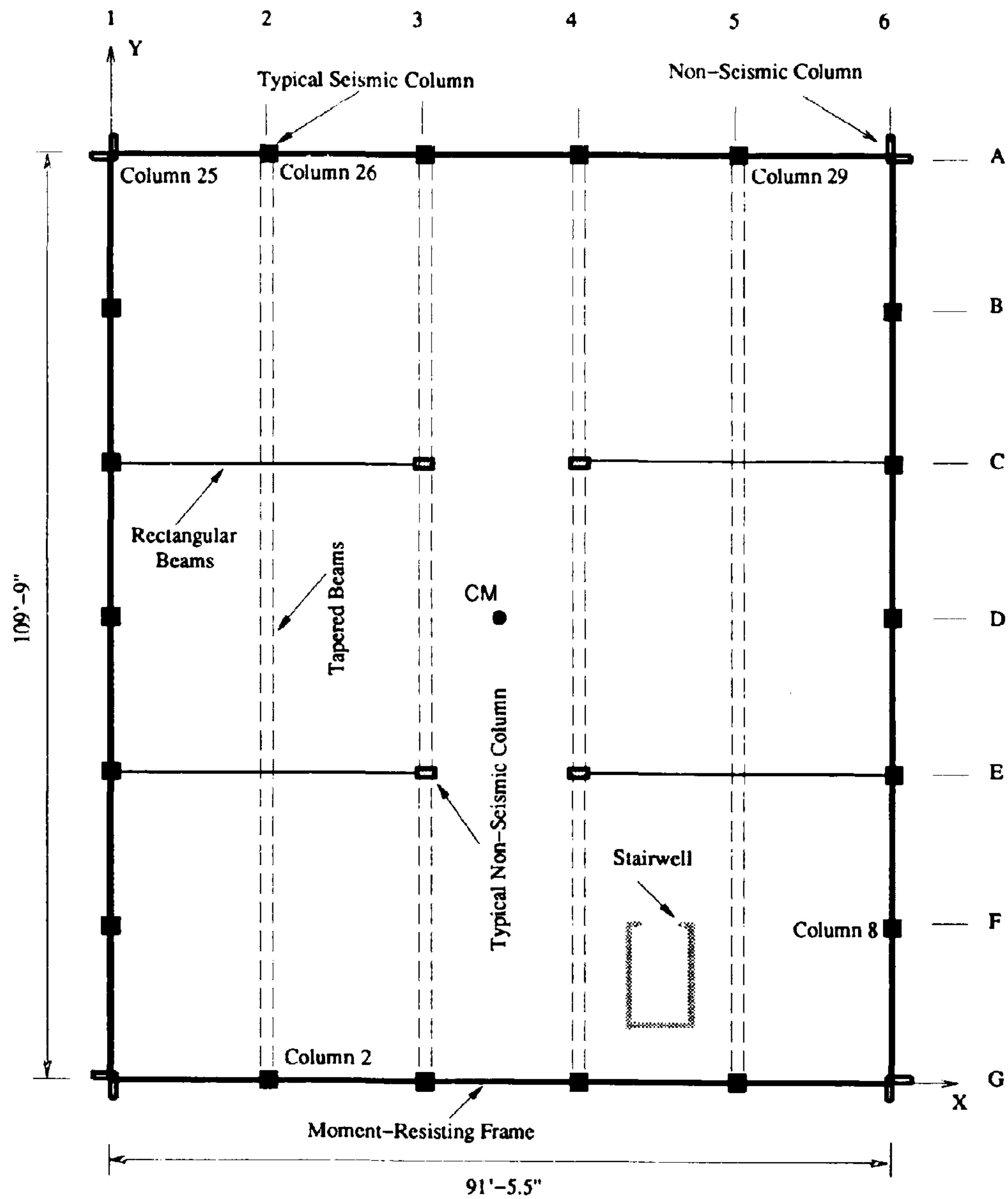

Figure B-1: Framing Plan of Building B

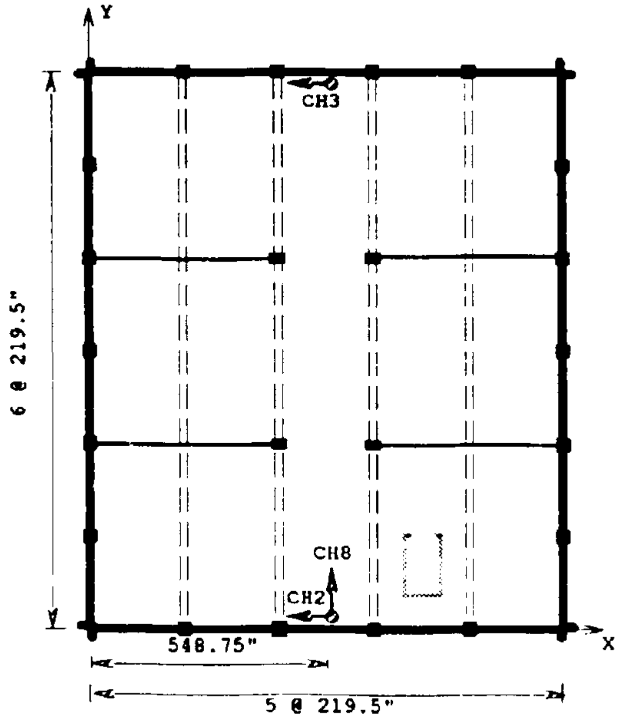

Roof

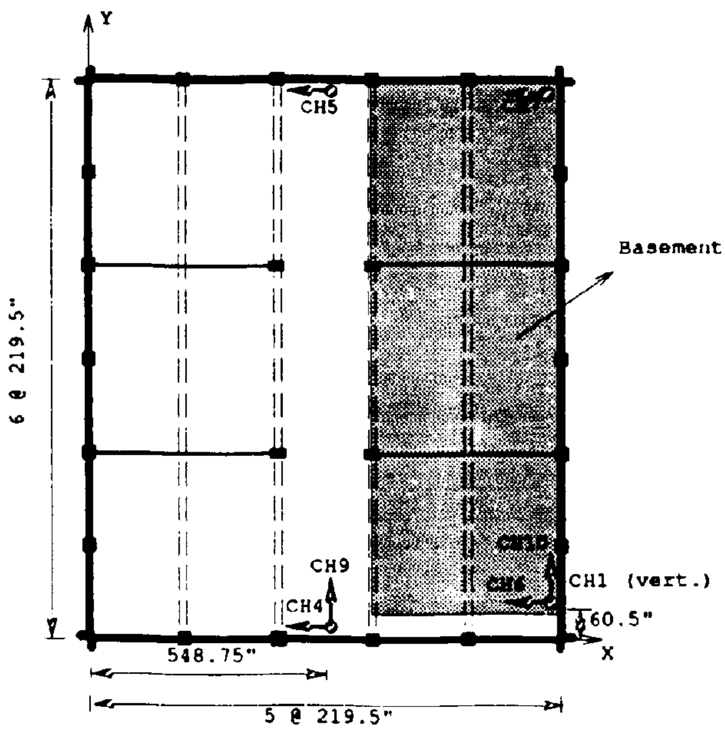

Second Floor and Basement

Figure B-2: Instrument Locations

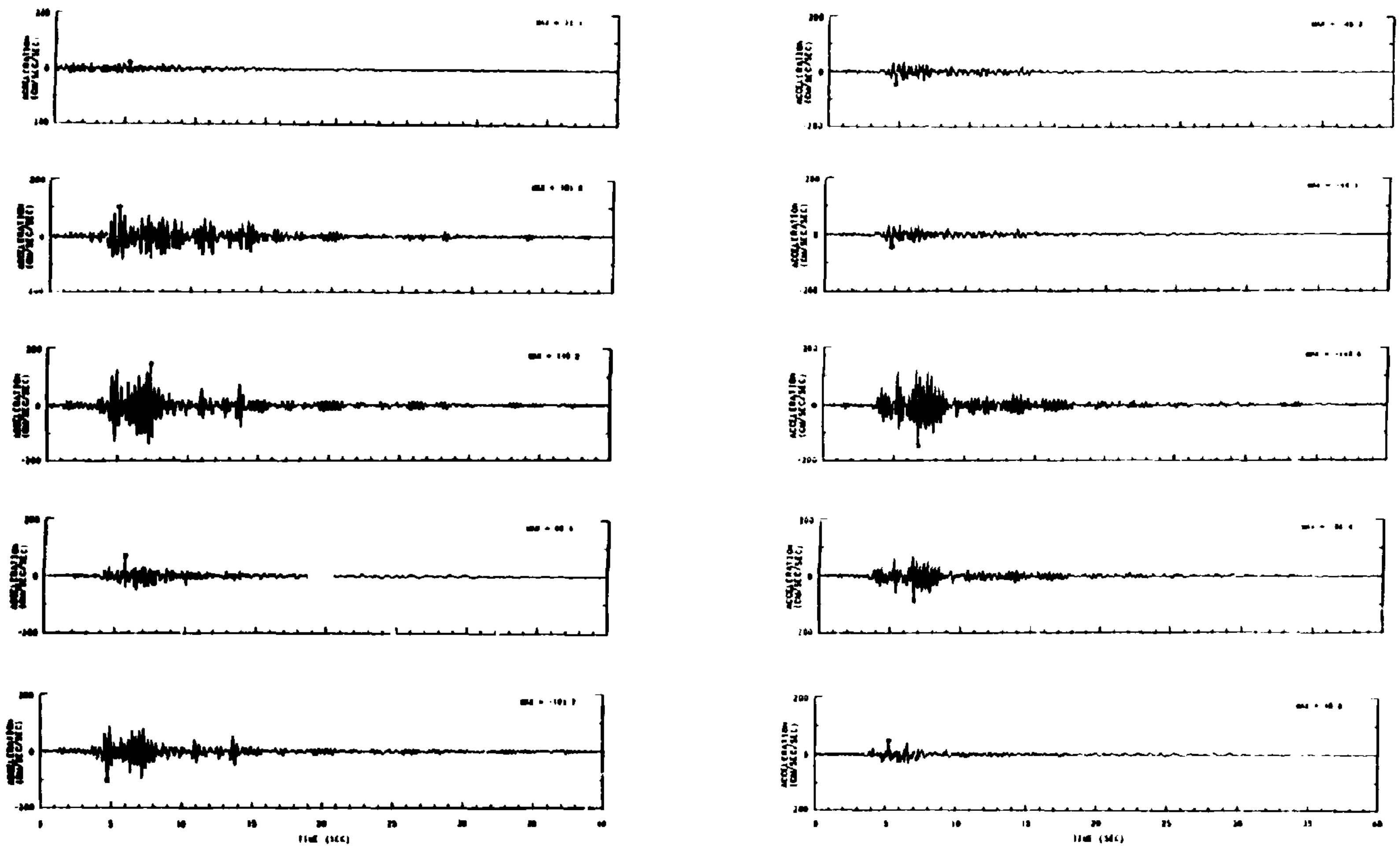

Figure B-3: Recorded Motions During the Whittier Earthquake

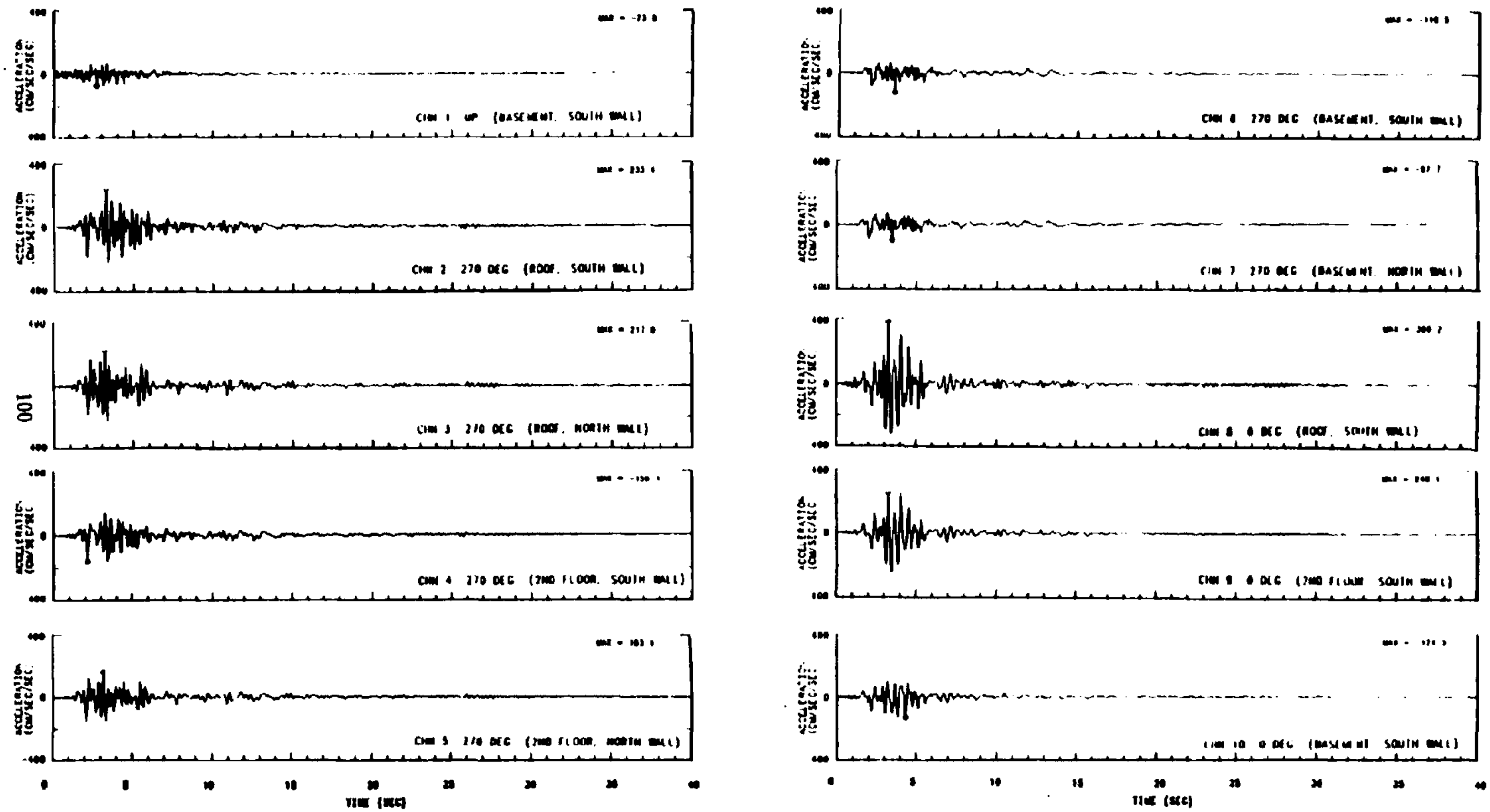

Figure B-4: Recorded Motions During the Upland Earthquake

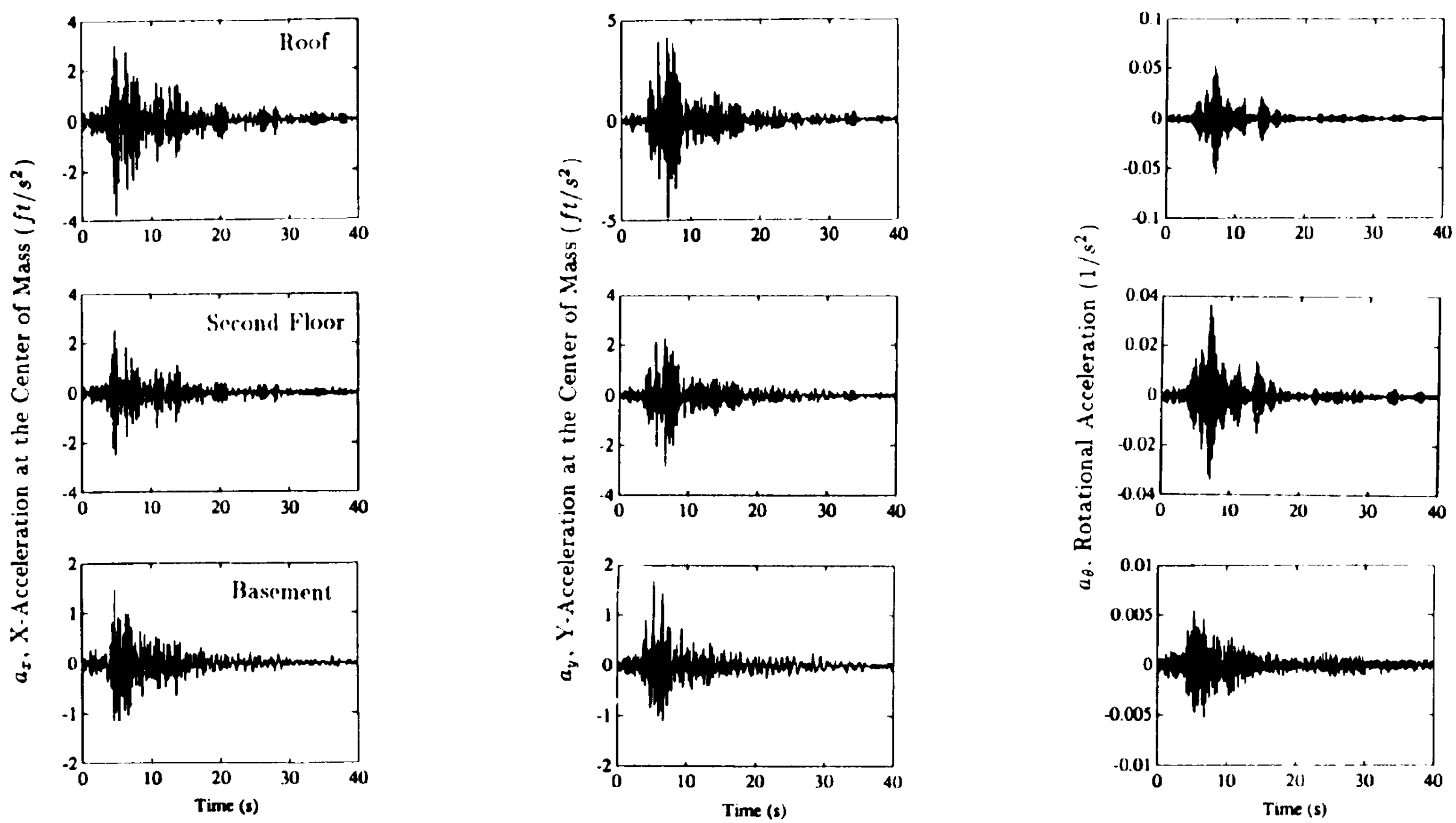

Figure B-5: Computed Motions at the CM of each Floor Level (Whittier Earthquake)

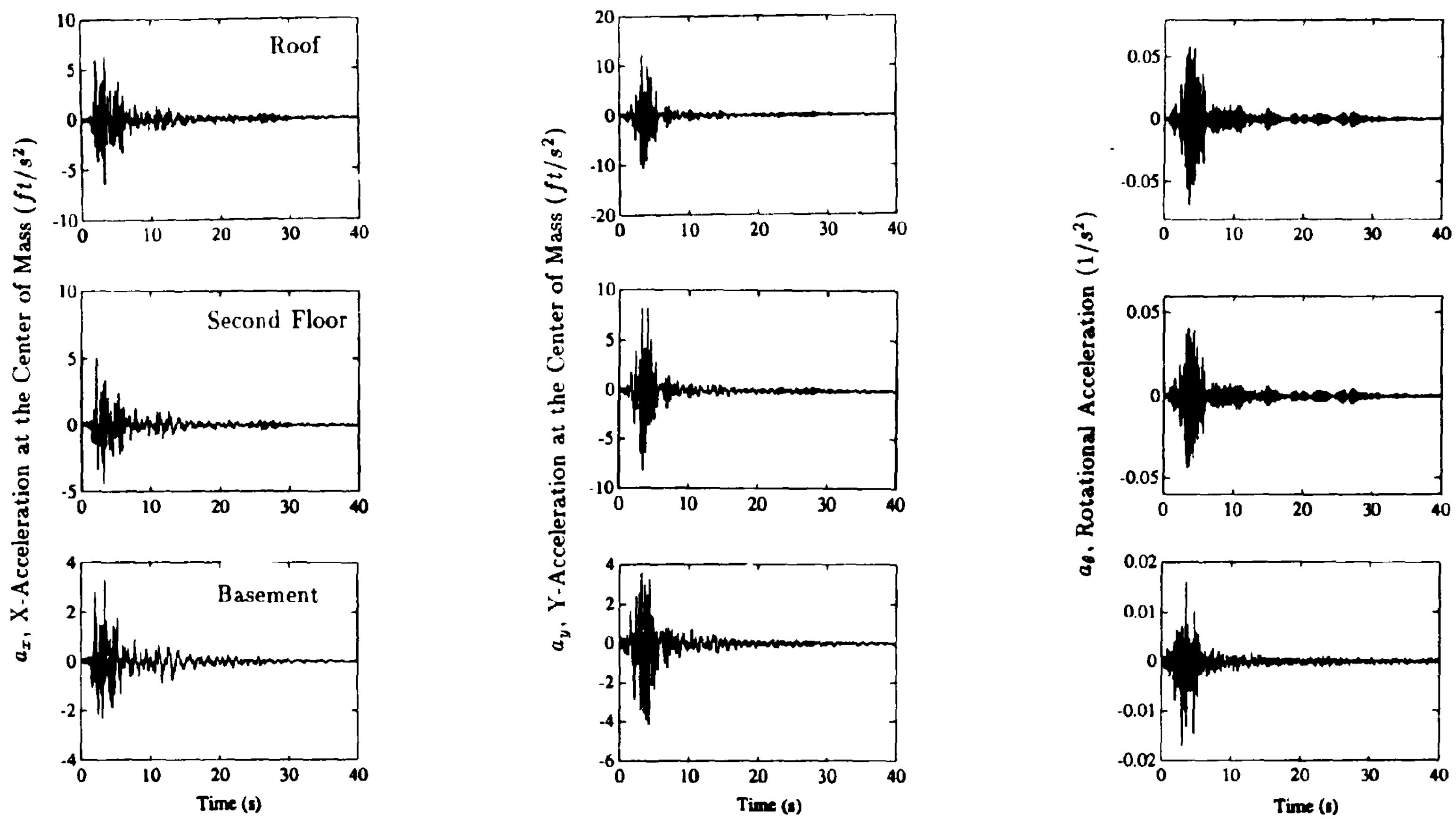

Figure B-6: Computed Motions at the CM of each Floor Level (Upland Earthquake)

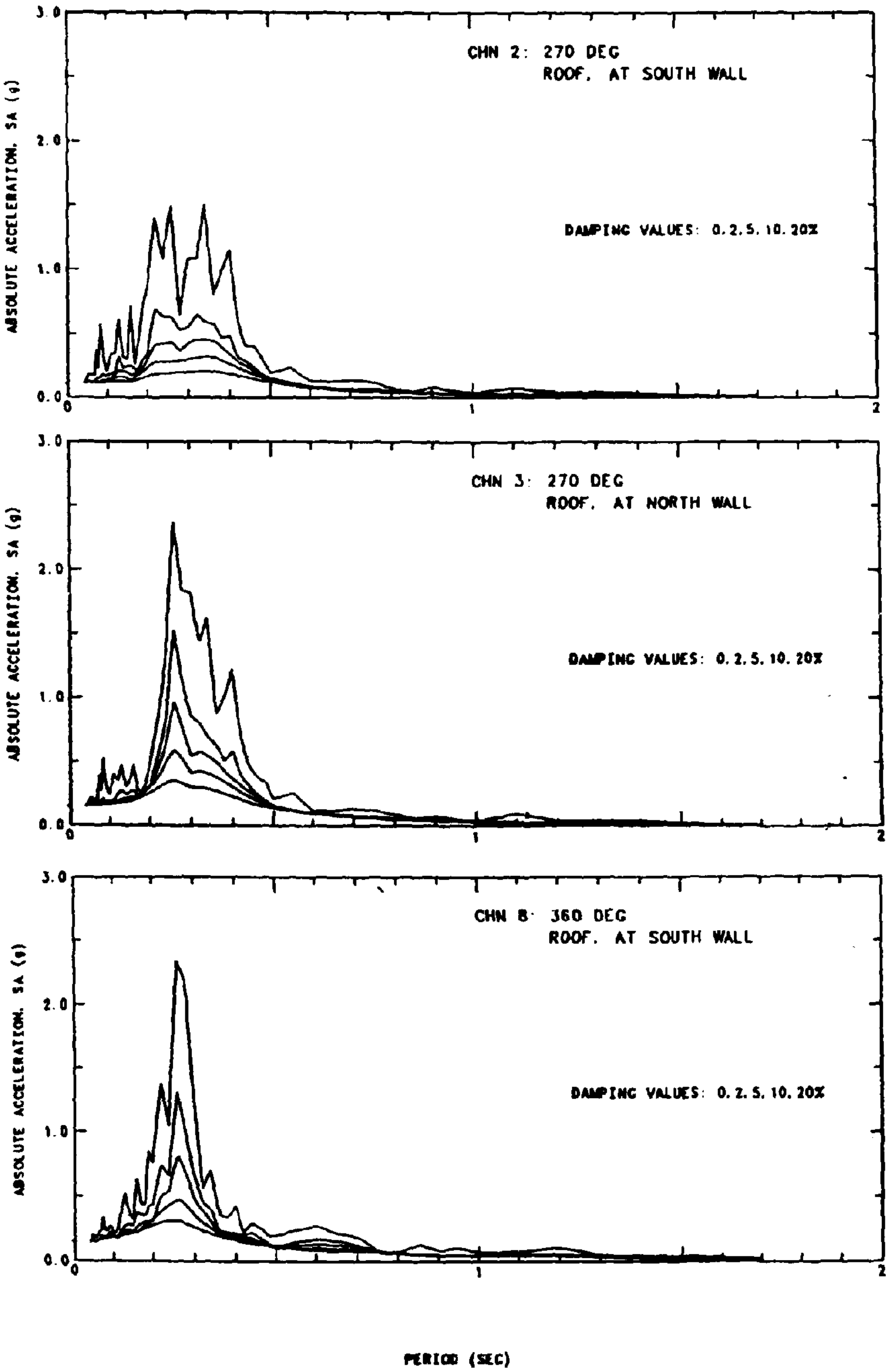

Figure B-7: Absolute Acceleration Spectra of Channels 2,3 and 8 at the Roof (Whittier Earthquake)

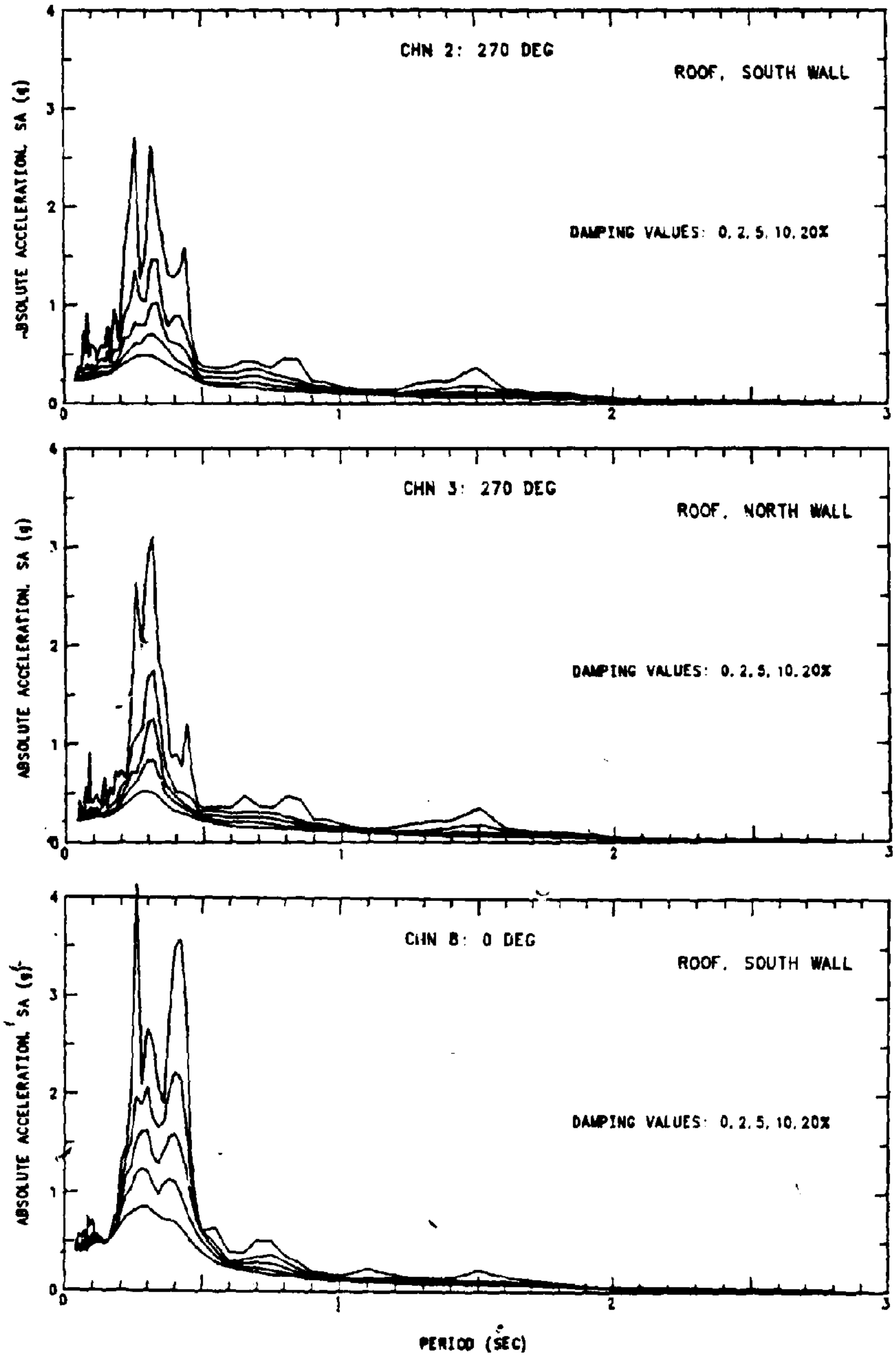

Figure B-8: Absolute Acceleration Spectra of Channels 2,3 and 8 at the Roof (Upland Earthquake)

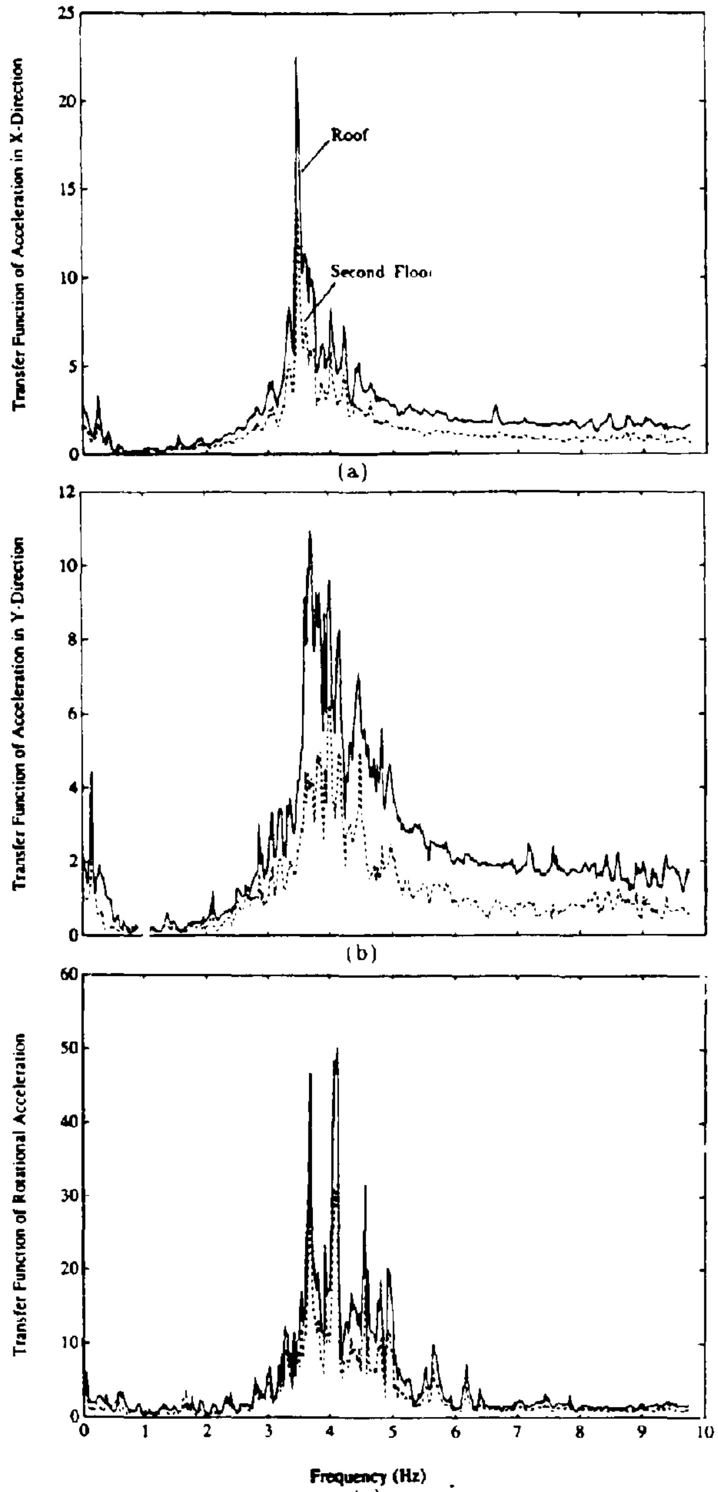

Figure B-9: Transfer Functions of the Roof Relative Floor Accelerations (Whittier Earthquake)

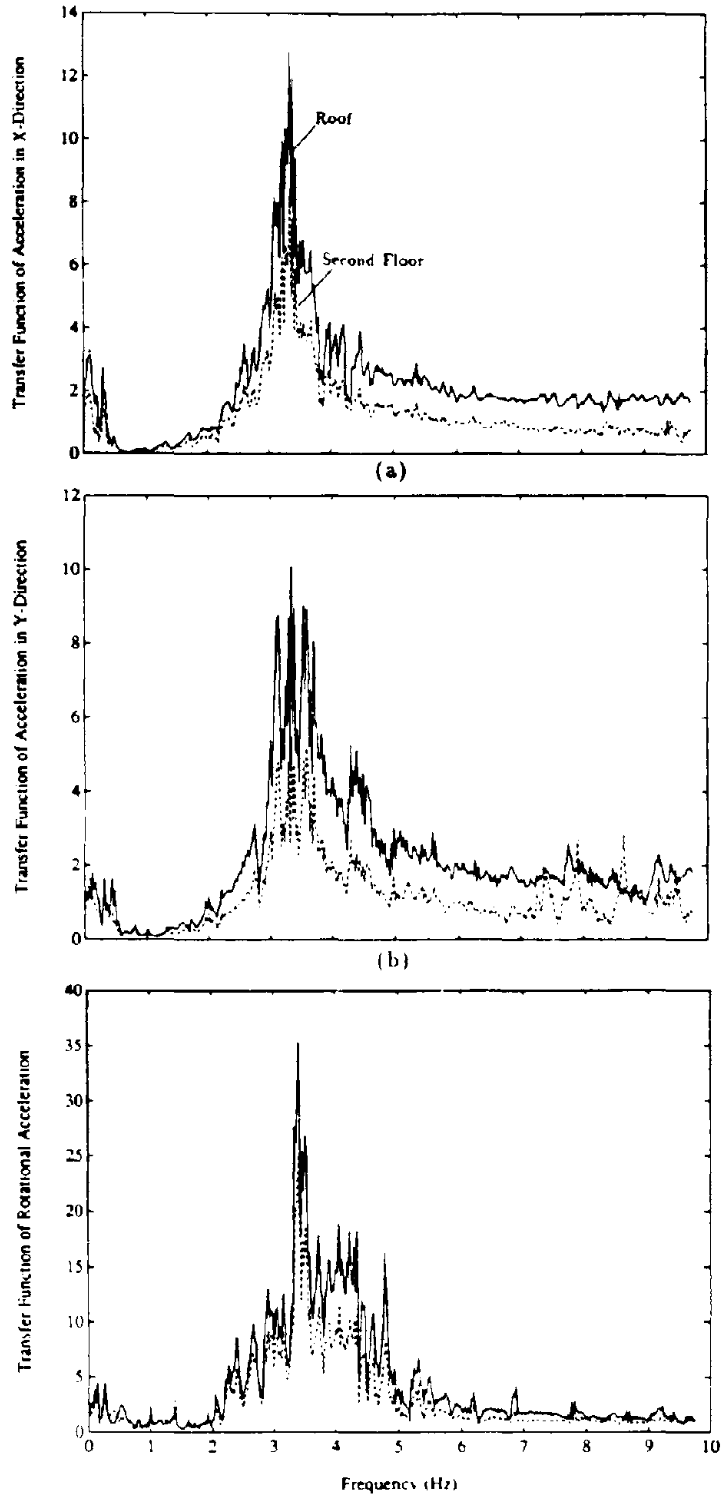

Figure B-10: Transfer Functions of the Roof Relative Floor Accelerations (Upland Earthquake)

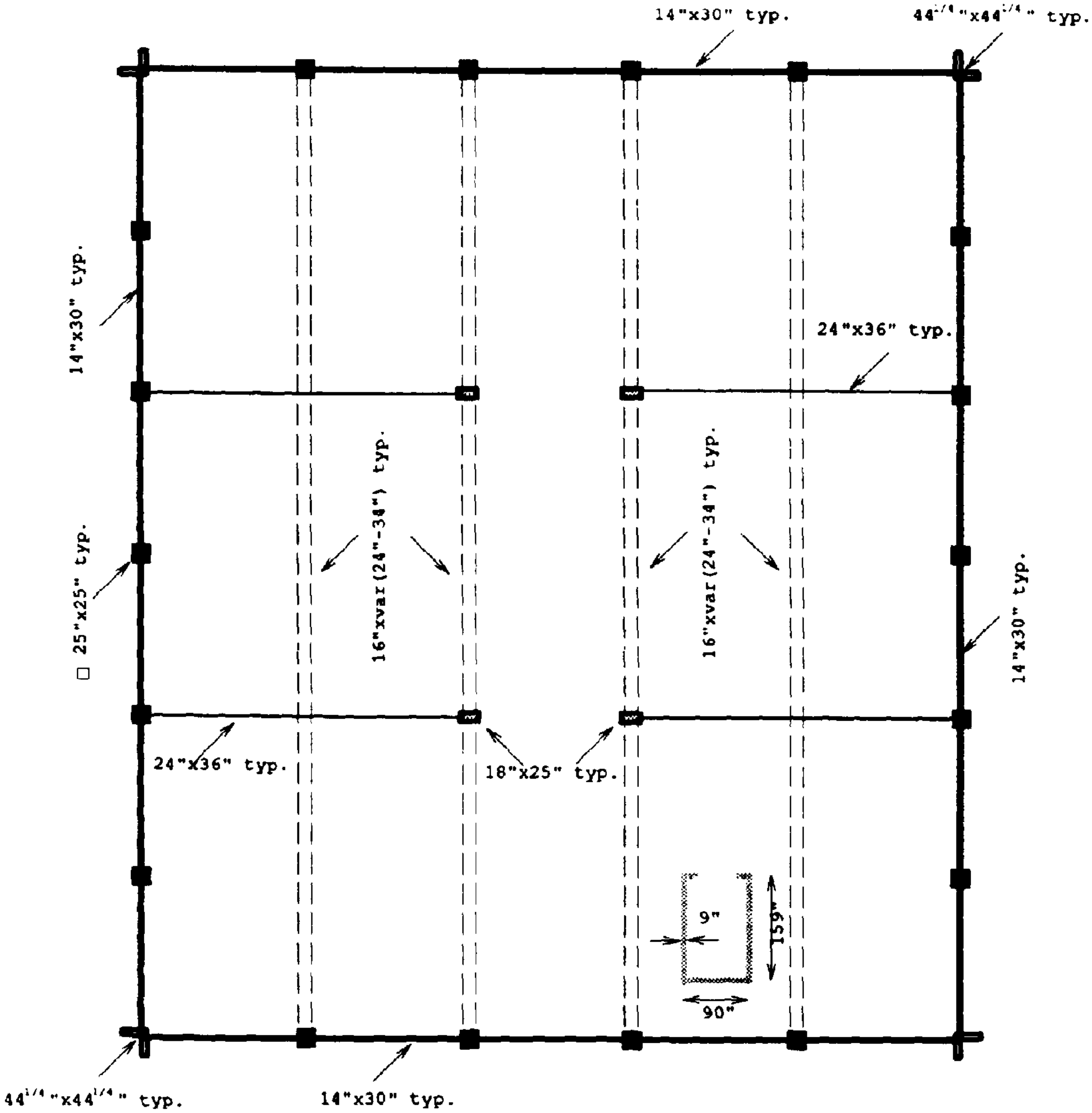

Figure B-11: Schematic Structural Plan of the First and Second Story

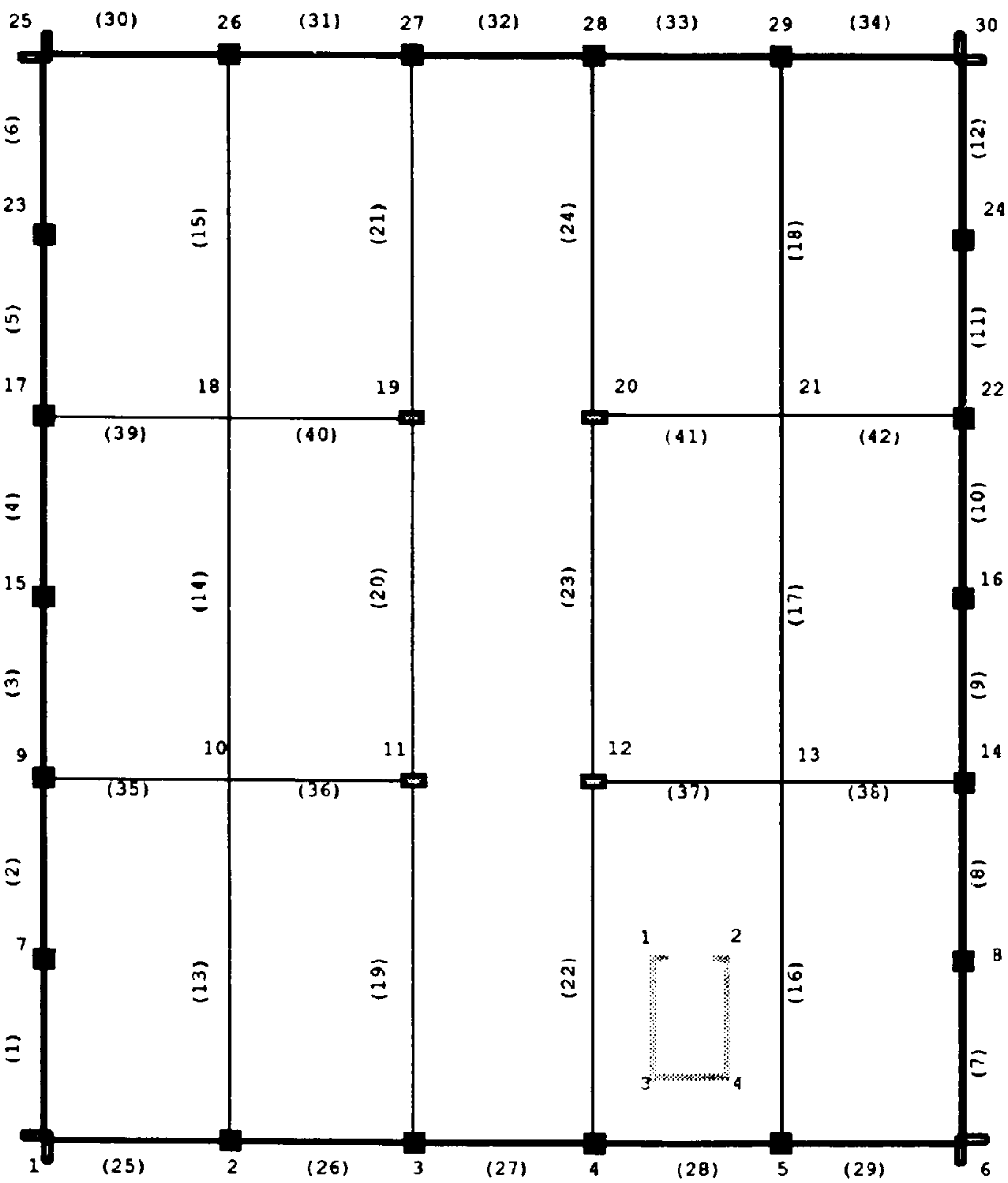

Figure B-12: Definition of Column Lines and Frame Bays for ETABS Model

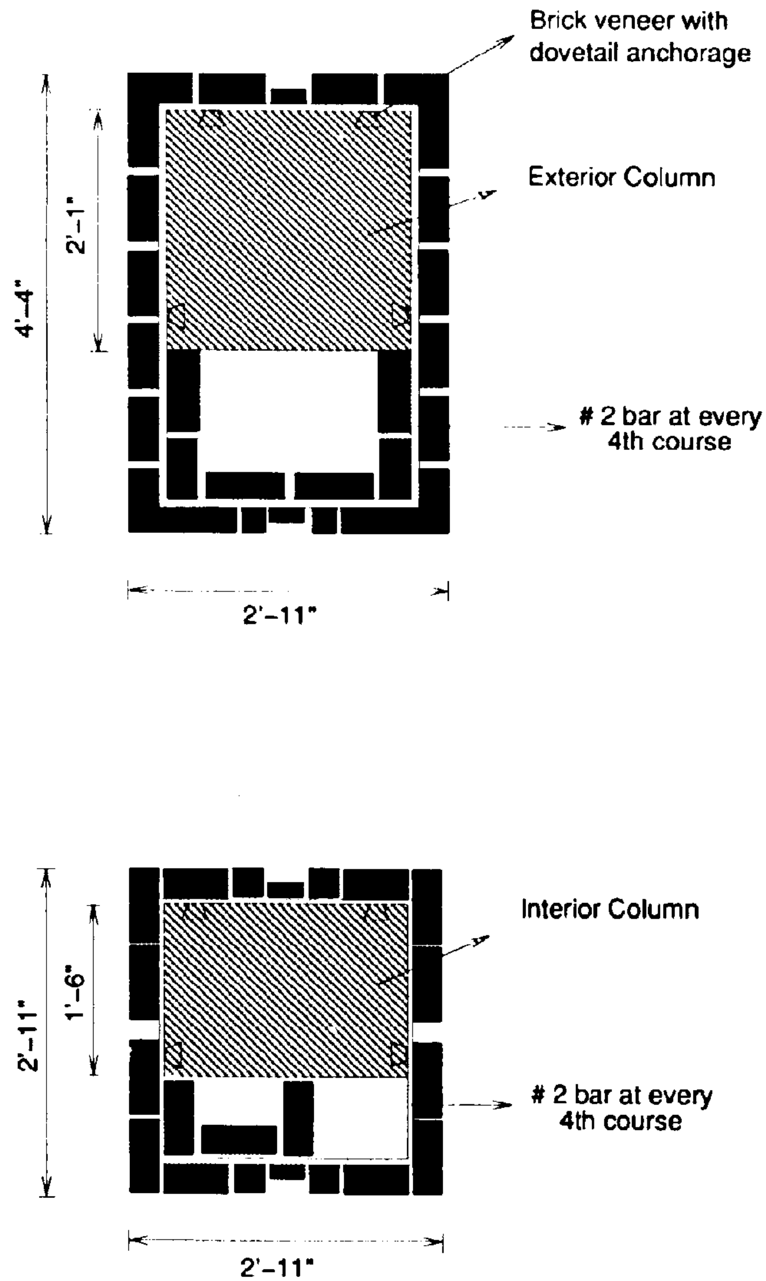

Figure B 13: Nonstructural Details in Peripheral and Interior Columns

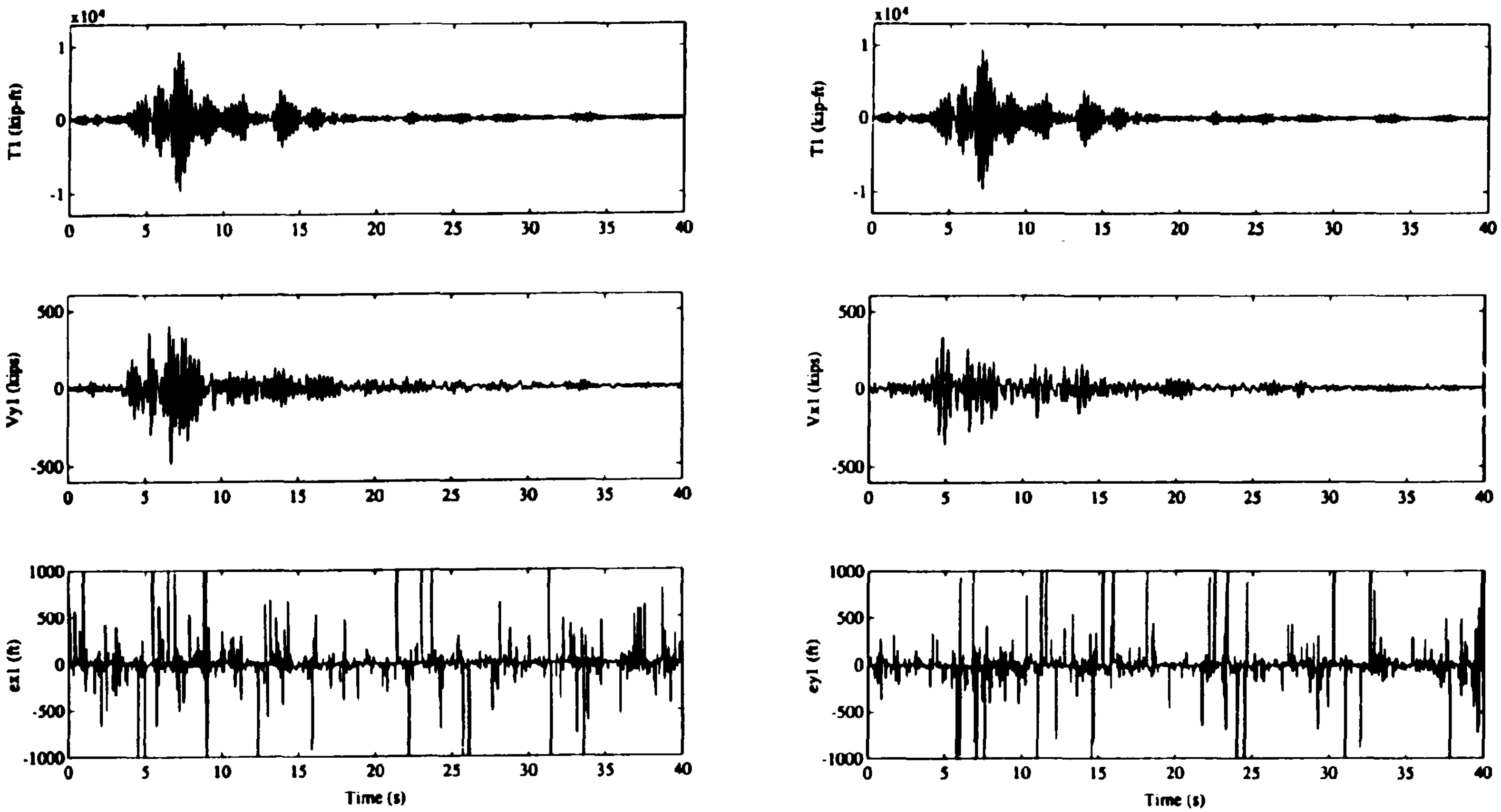

Figure B-14: Base Shear, Base Torque and First Floor Accidental Eccentricities Computed from Recorded Accelerations During the Whittier Earthquake

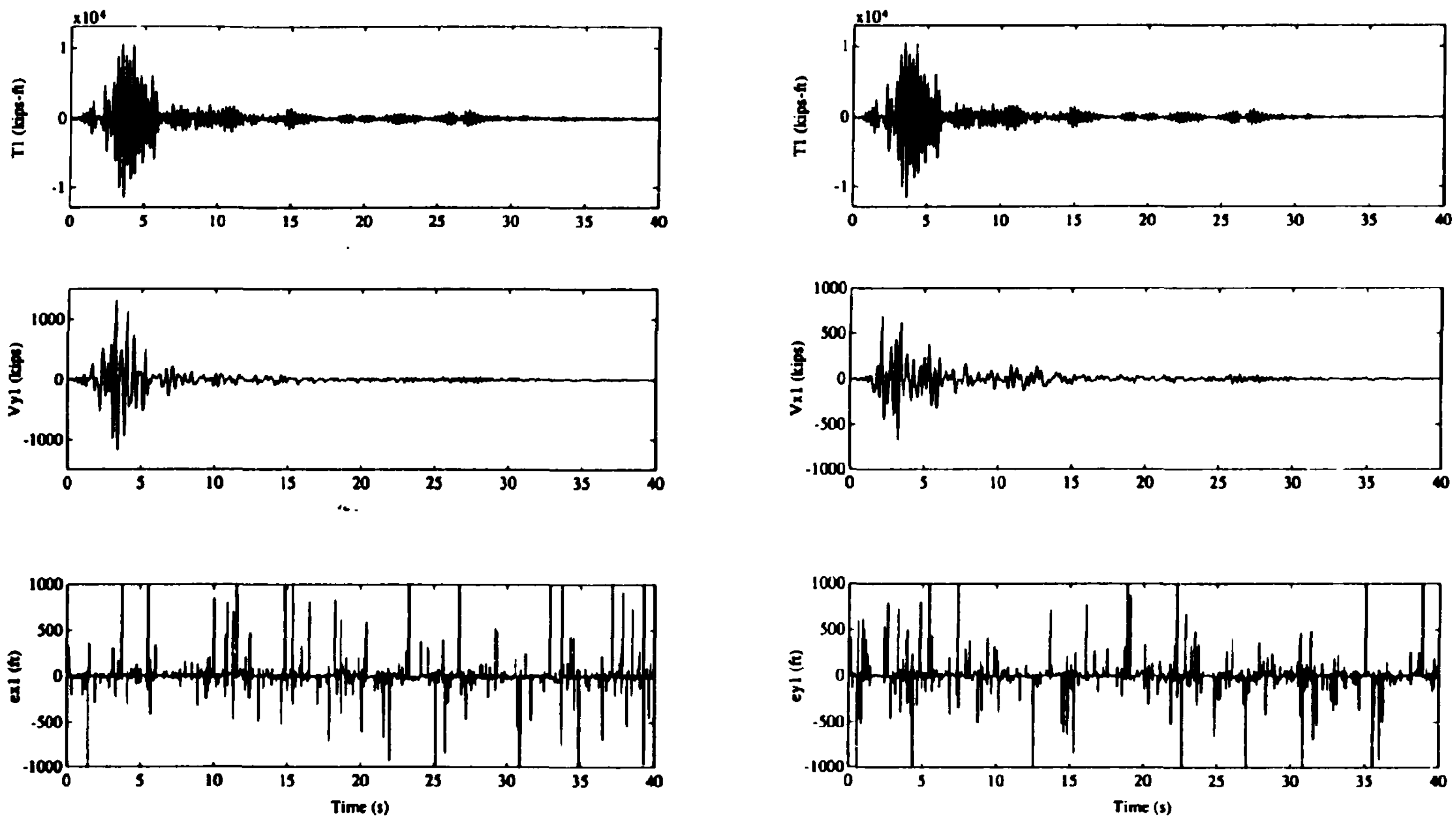

Figure B-15: Base Shear, Base Torque and First Floor Accidental Eccentricities Computed from Recorded Accelerations During the Upland Earthquake

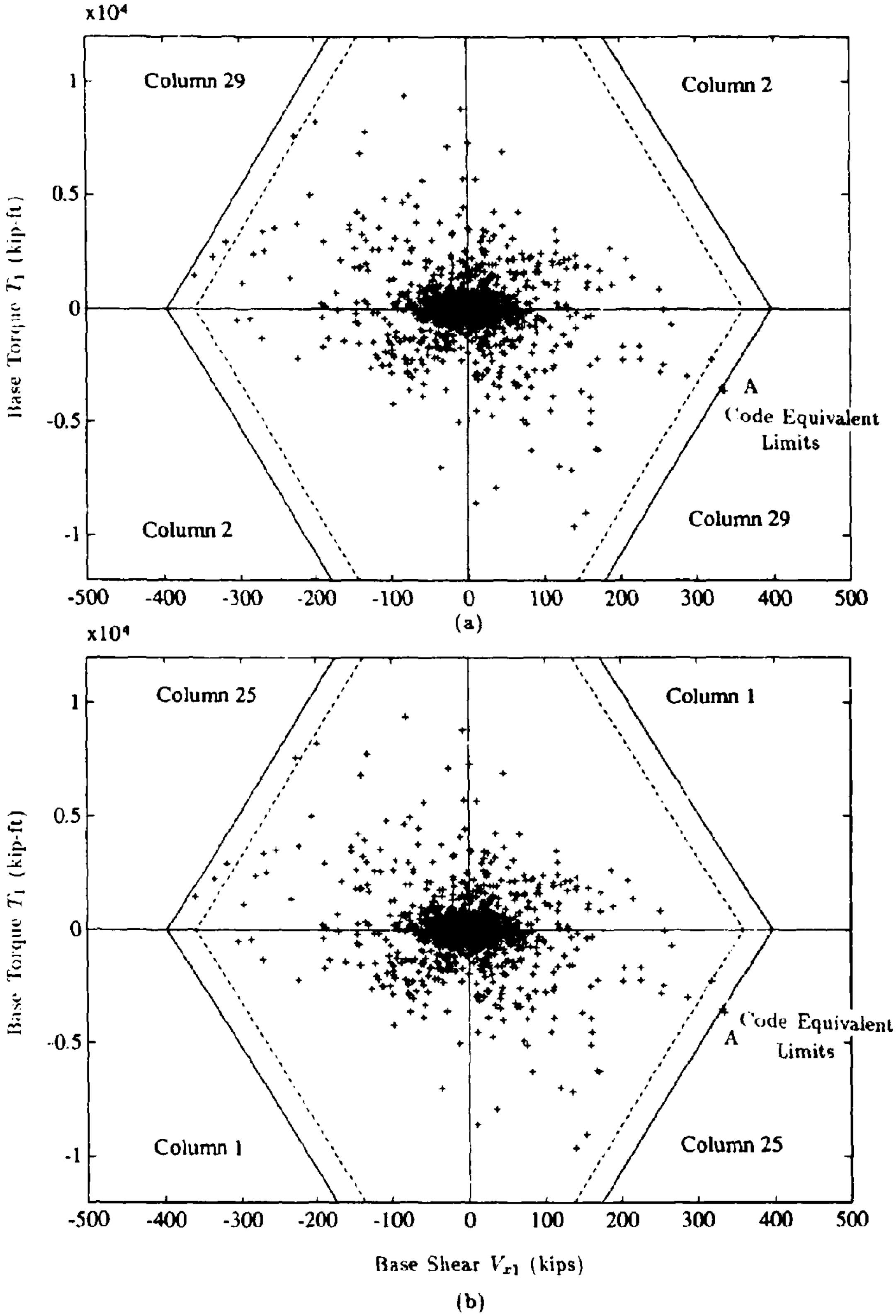

Figure B-16: Comparison of Dynamic Base Shear, Base Torque and "Code Equivalent Limits" for Elements in the X-Direction (Whittier Earthquake)

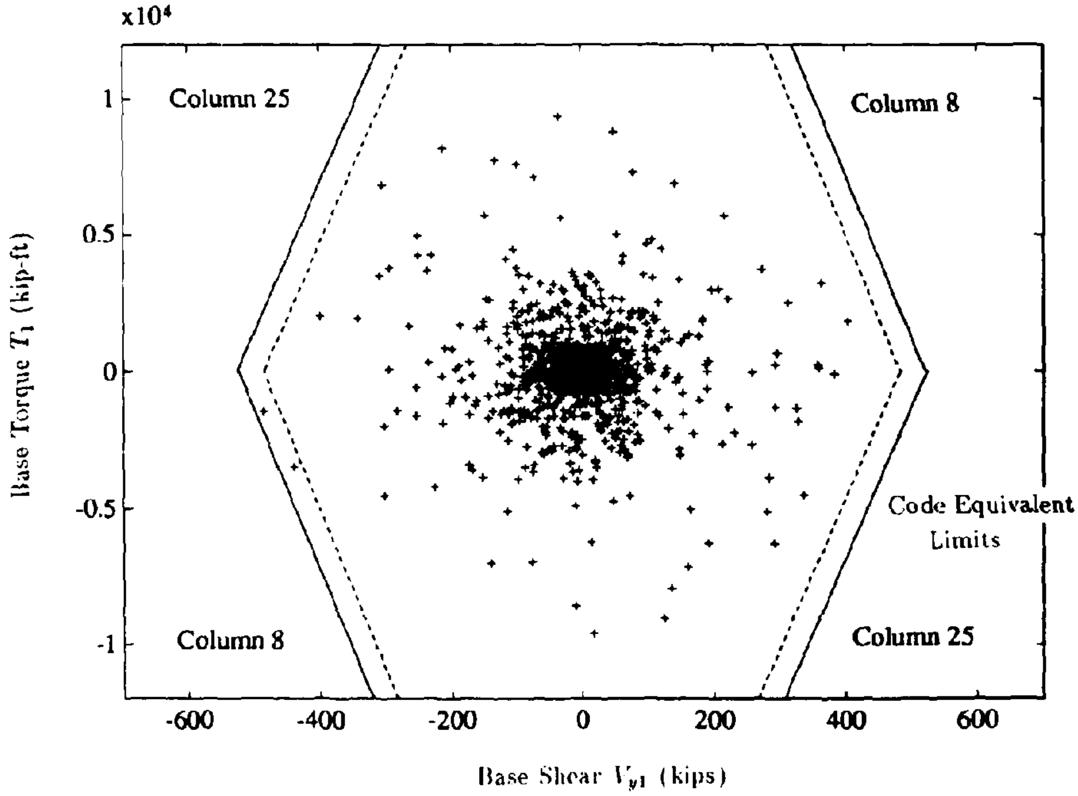

Figure B-17: Comparison of Dynamic Base Shear, Base Torque and "Code Equivalent Limits" for Elements in the Y-Direction (Whittier Earthquake)

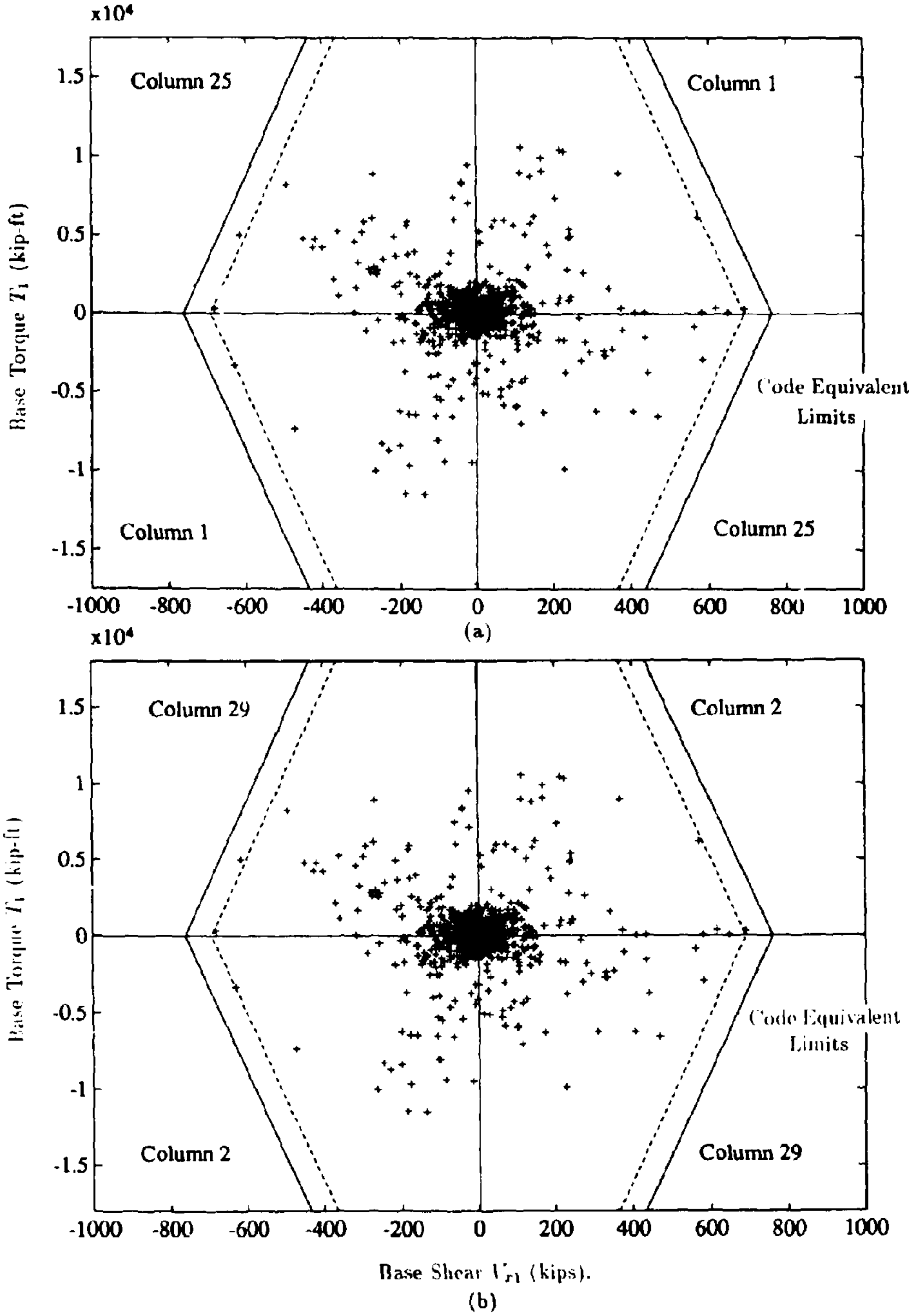

Figure B-18: Comparison of Dynamic Base Shear, Base Torque and "Code Equivalent Limits" for Elements in the X-Direction (Upland Earthquake)

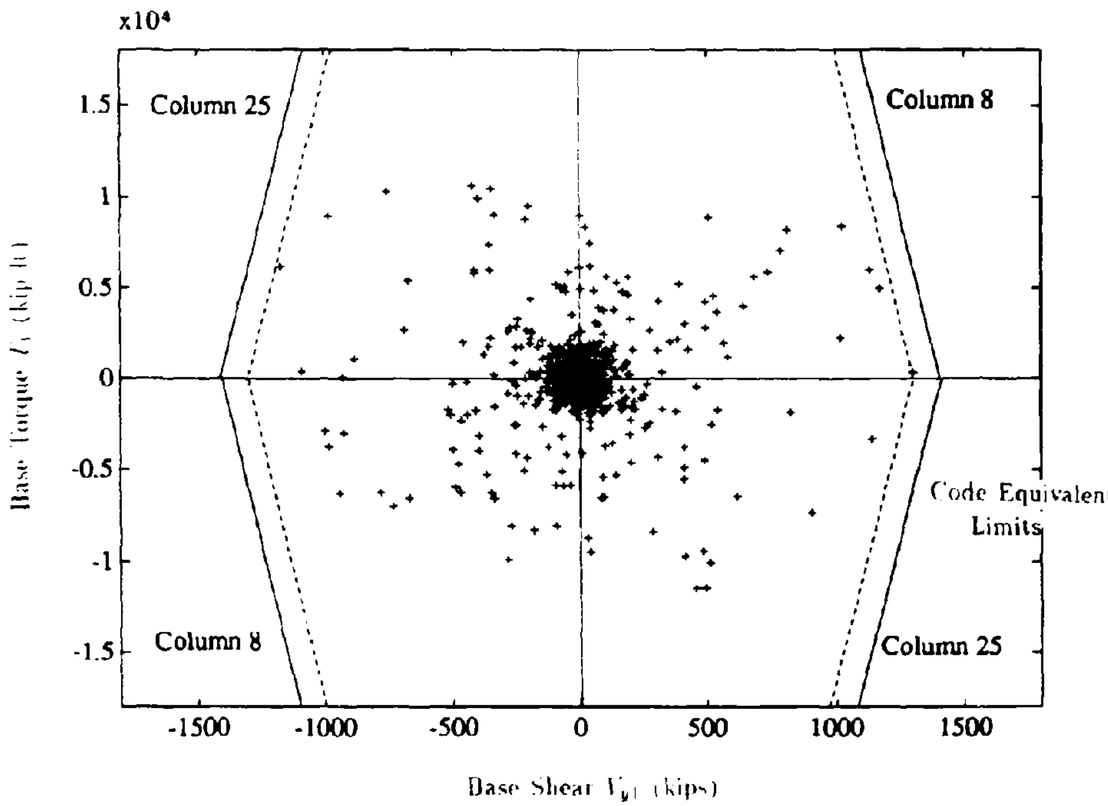

Figure B-19: Comparison of Dynamic Base Shear, Base Torque and "Code Equivalent Limits" for Elements in the Y-Direction (Upland Earthquake)

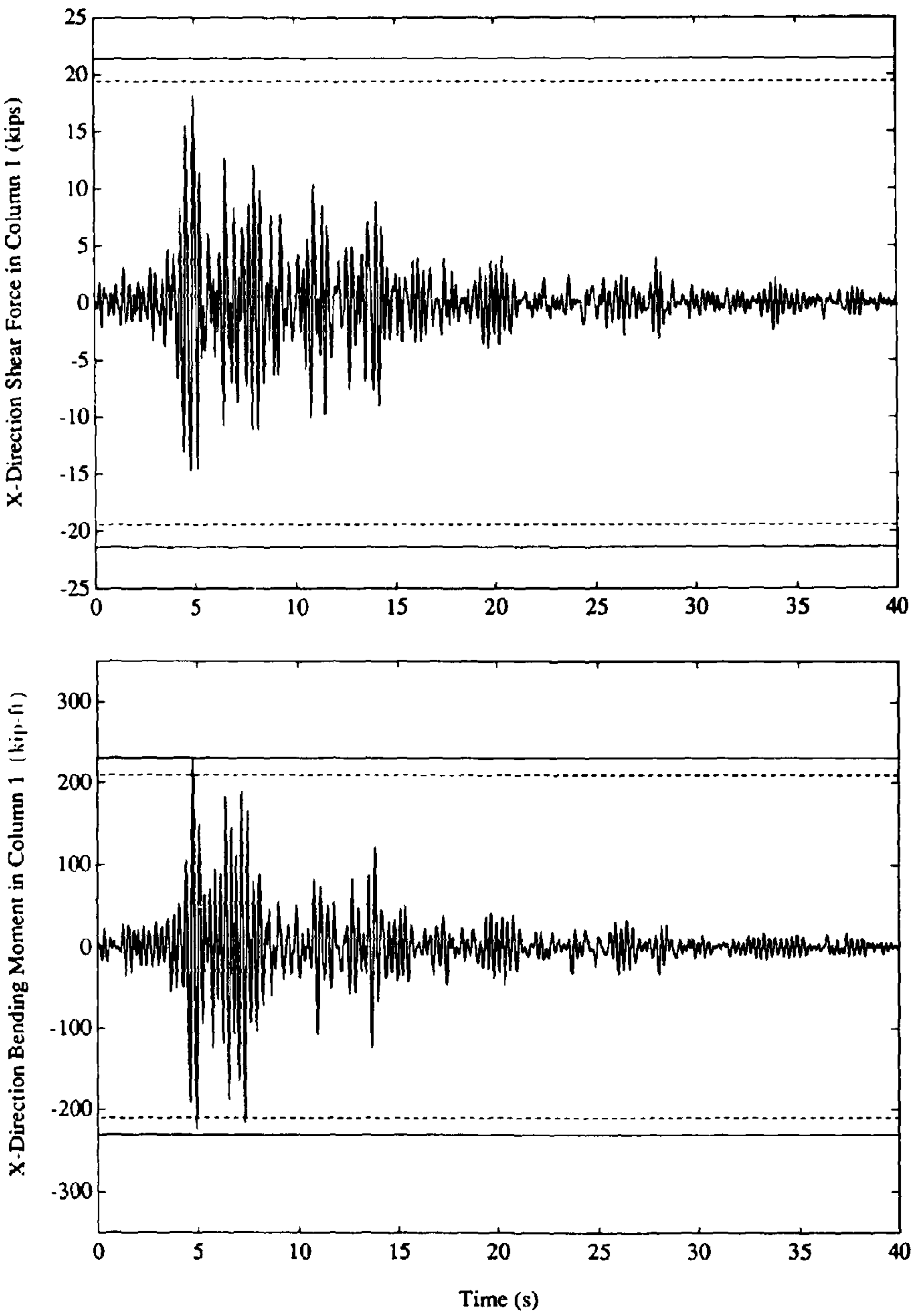

Figure B-20: Comparison of Earthquake Induced Shears and Bending Moments in Column 1 with "Design" Values in the X-Direction (Whittier Earthquake)

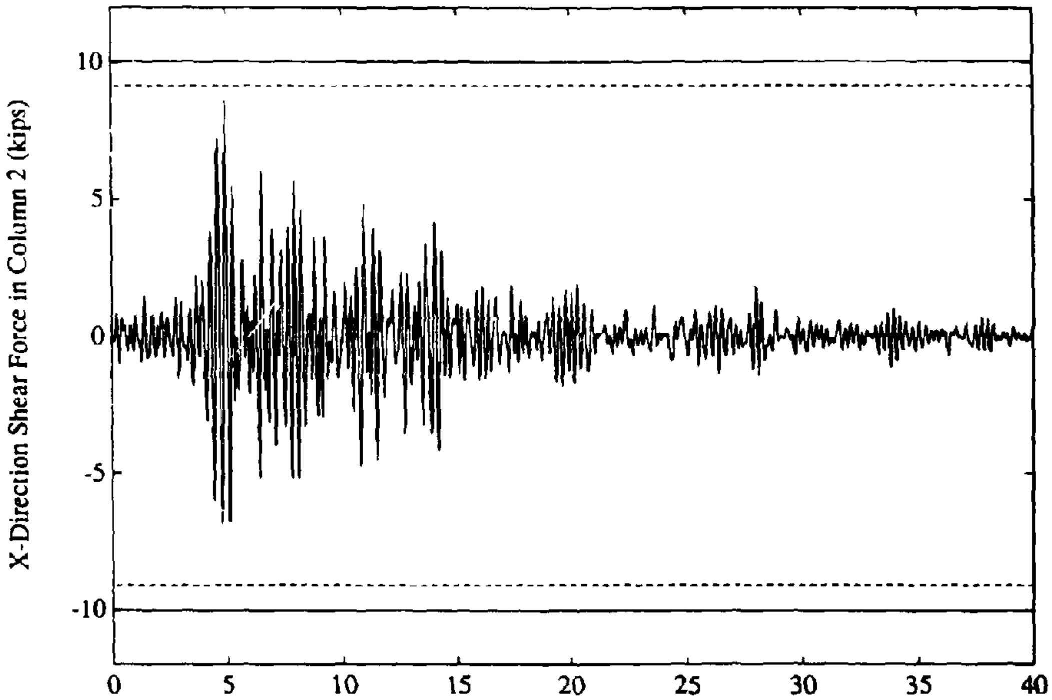

(a)

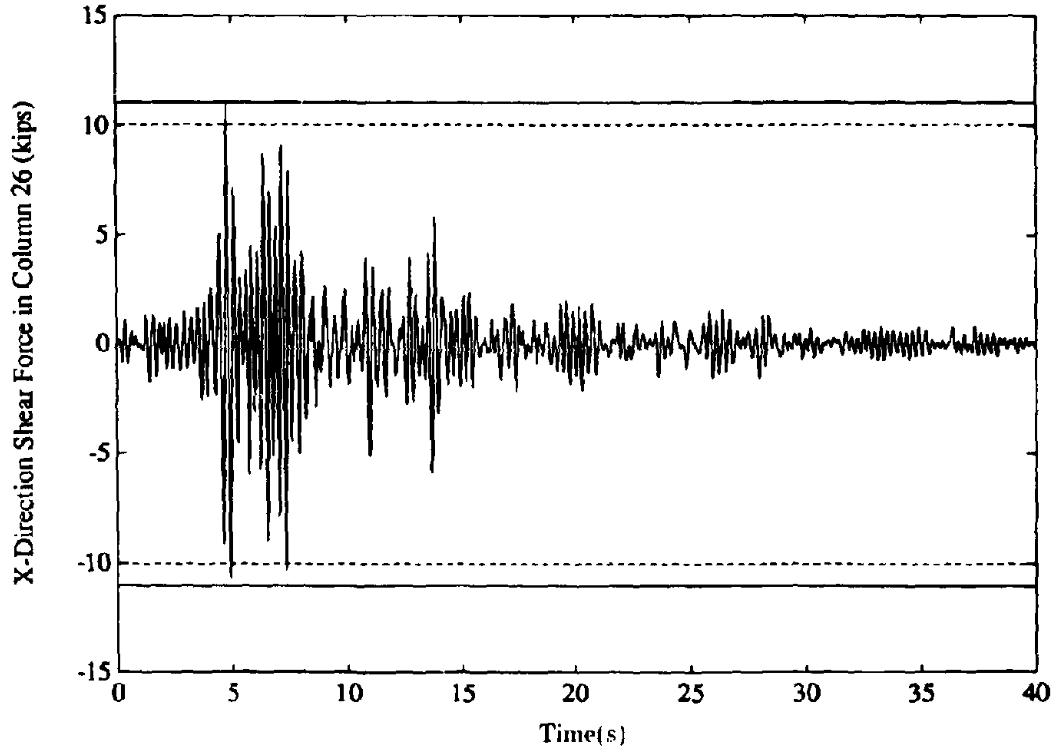

(b)

Figure B-21: Comparison of Earthquake Induced Shears in Columns 2 and 26 with "Design" Values in the X-Direction (Whittier Earthquake)

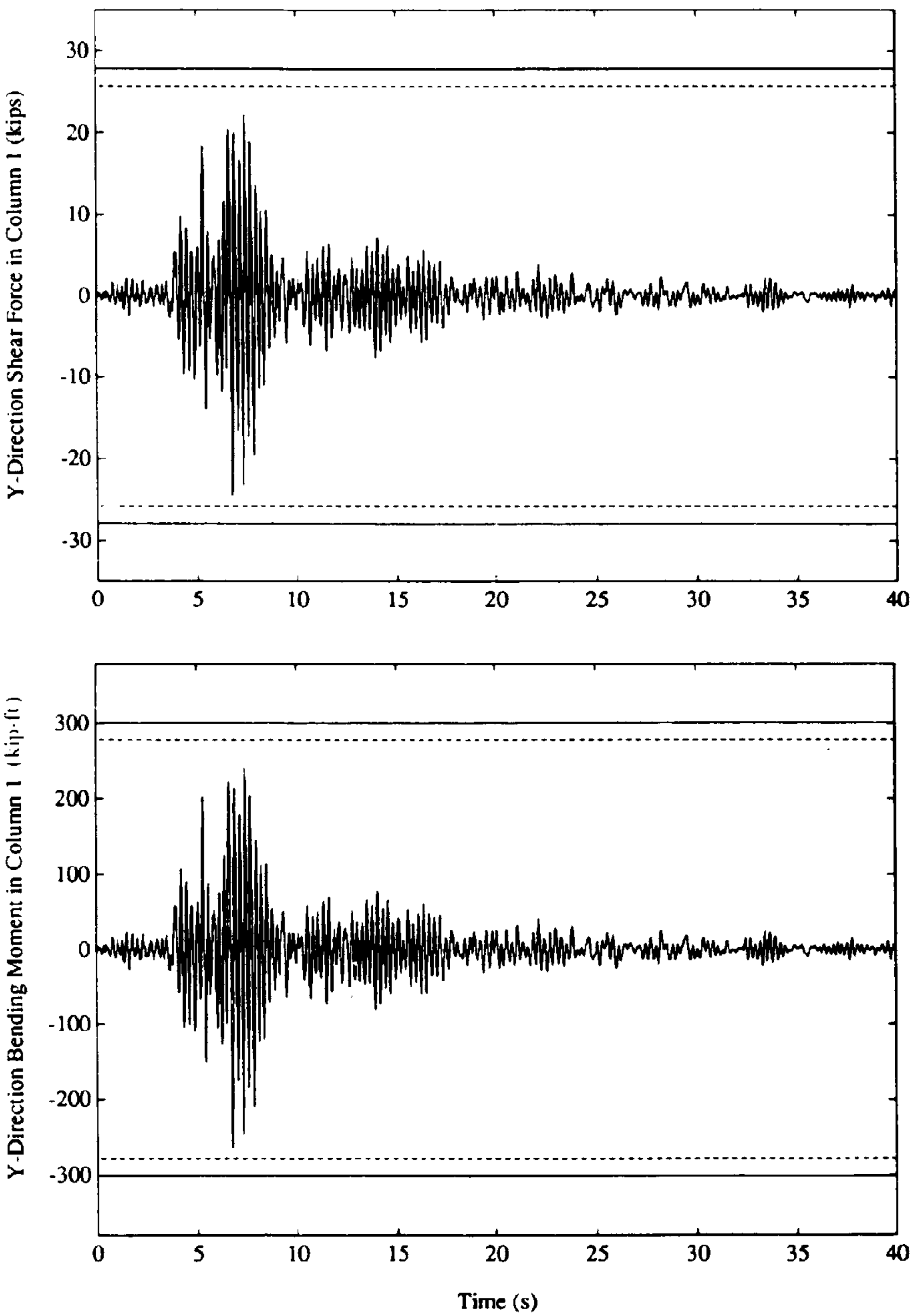

Figure B-22: Comparison of Earthquake Induced Shears and Bending Moments in Column 1 with "Design" Values in the Y-Direction (Whittier Earthquake)

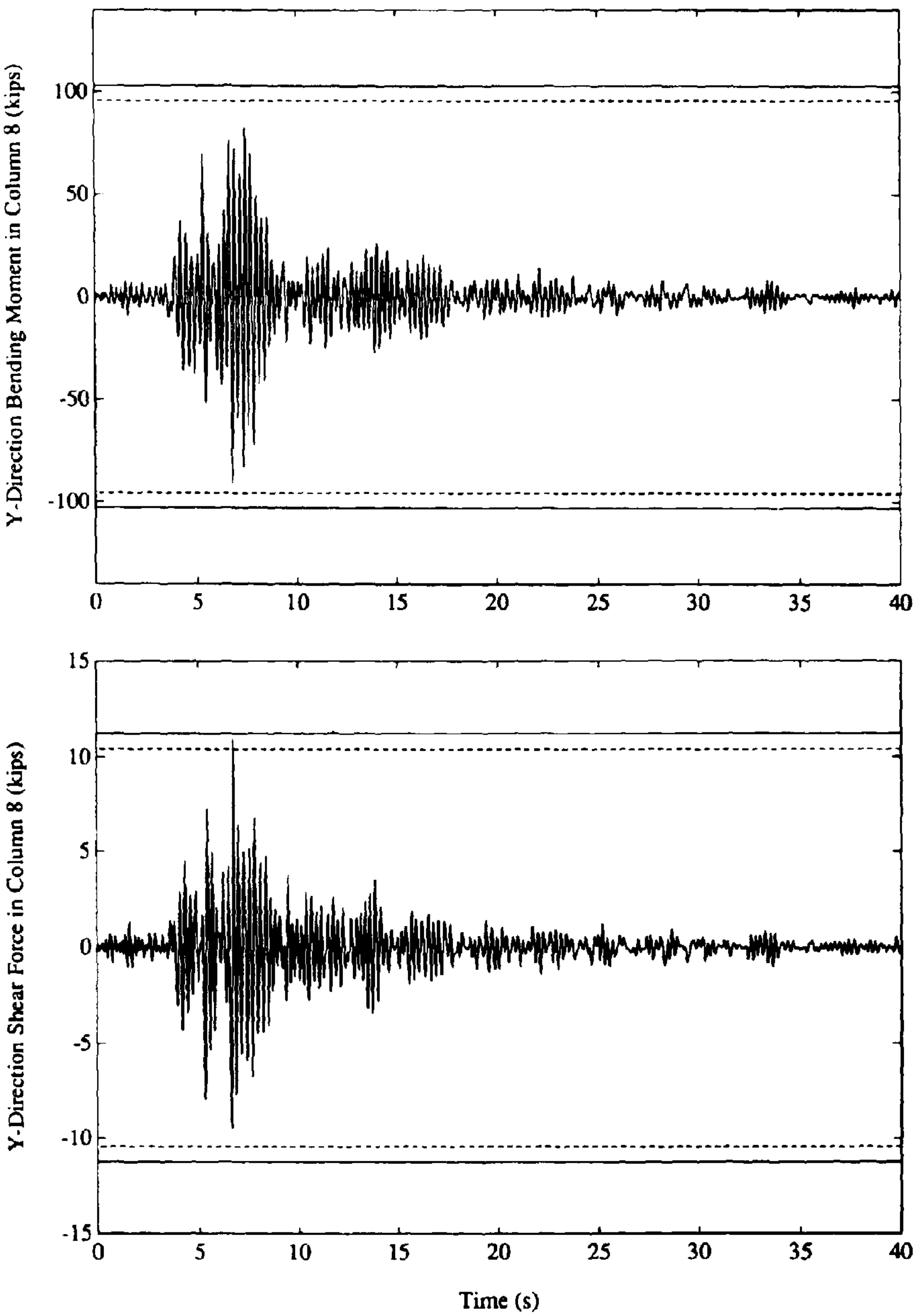

Figure B-23: Comparison of Earthquake Induced Shears and Bending Moments in Column 8 with "Design" Values in the Y-Direction (Whittier Earthquake)

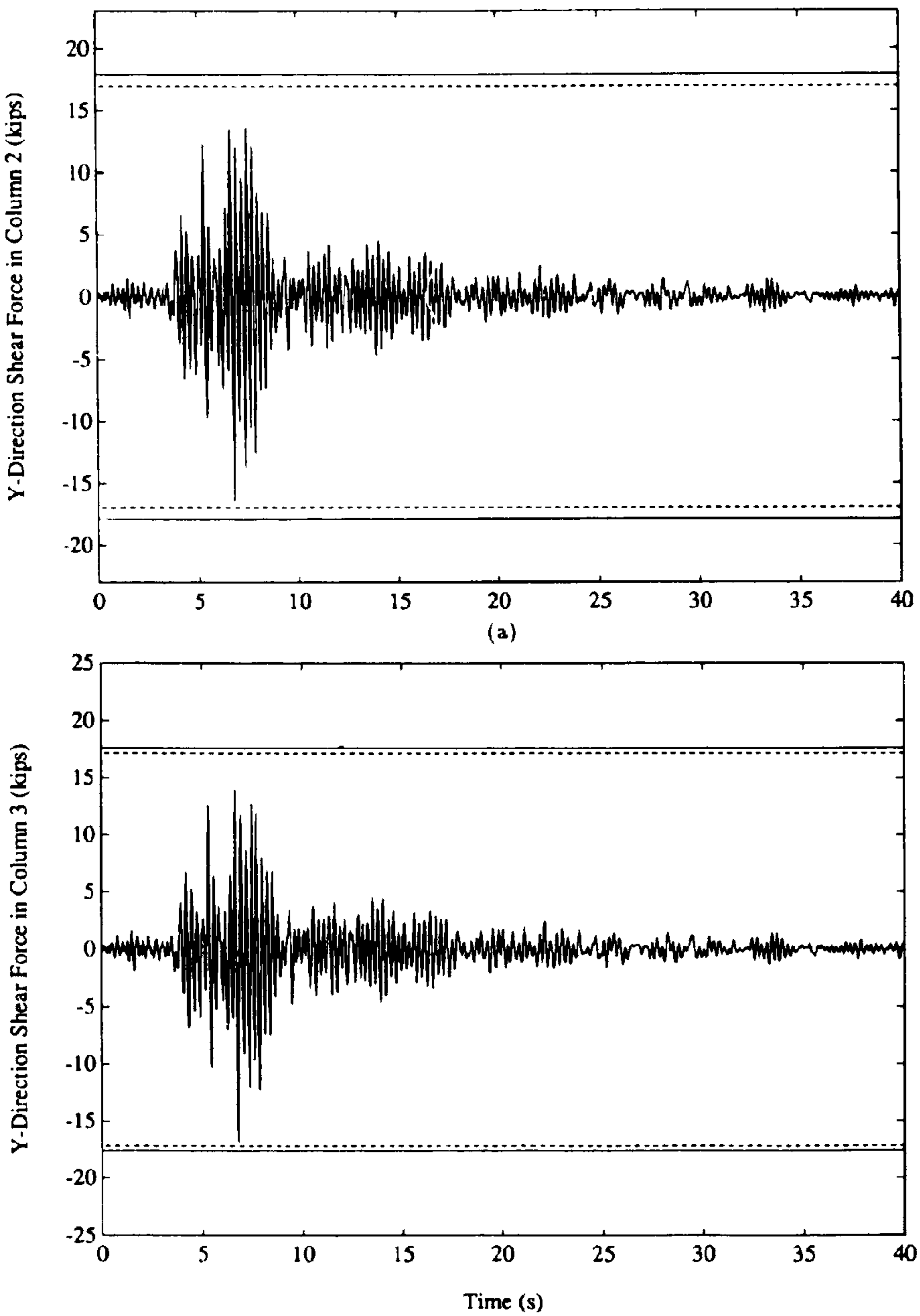

Figure B-24: Comparison of Earthquake Induced Shears in Columns 2 and 3 with "Design" Values in the Y-Direction (Whittier Earthquake)

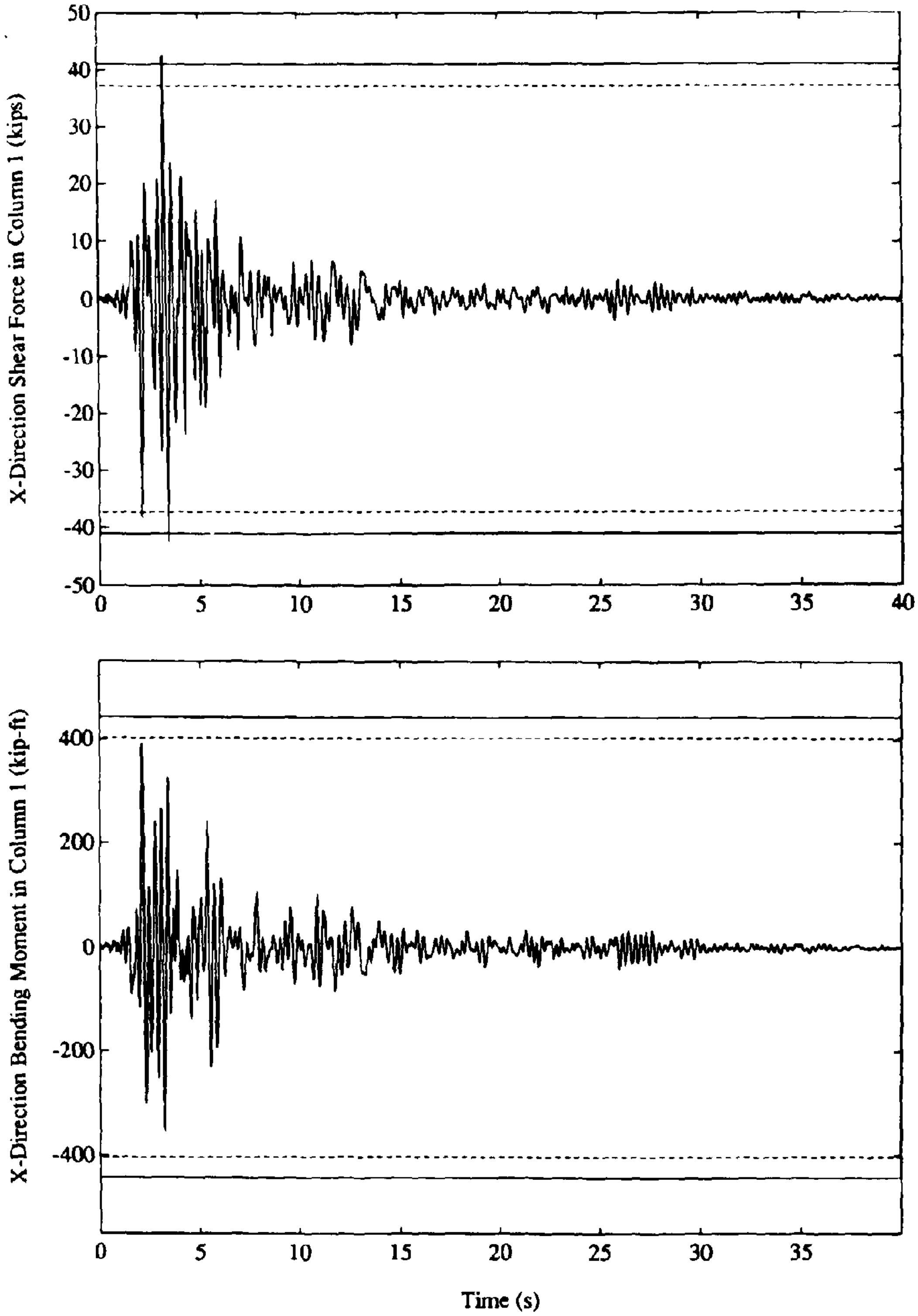

Figure B-25: Comparison of Earthquake Induced Shears and Bending Moments in Column 1 with "Design" Values in the X-Direction (Upland Earthquake)

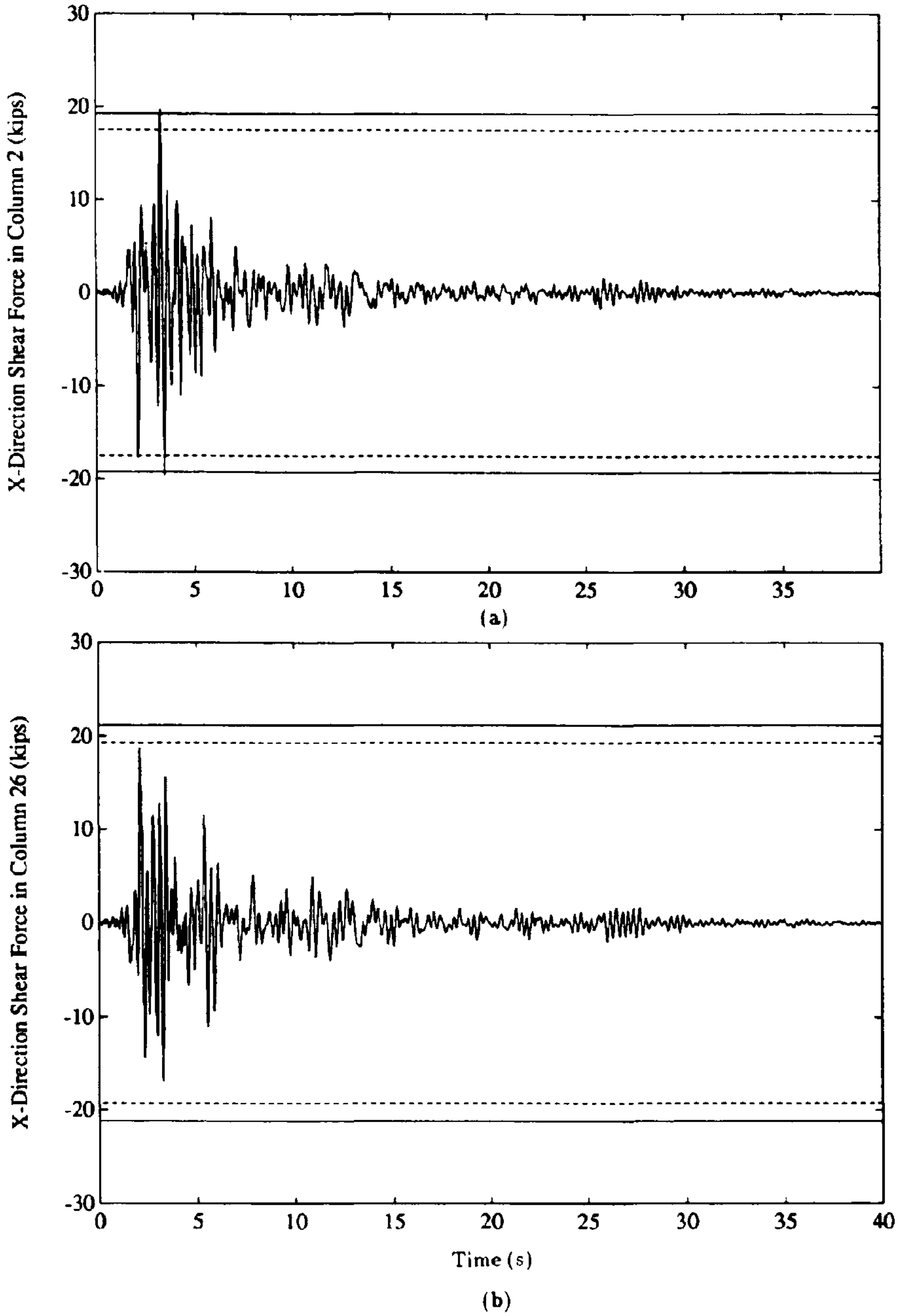

Figure B-26: Comparison of Earthquake Induced Shears in Columns 2 and 26 with "Design" Values in the X-Direction (Upland Earthquake)

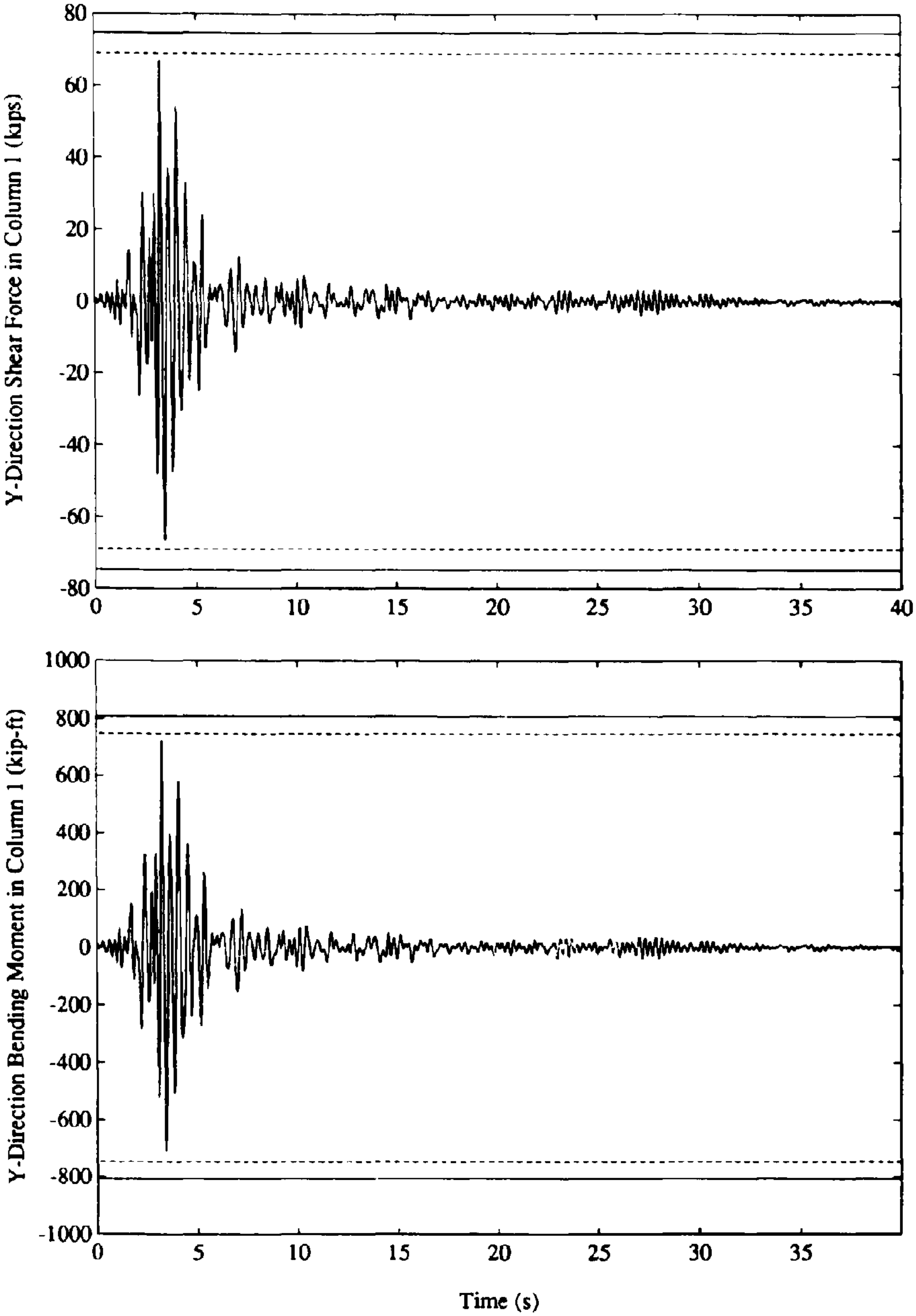

Figure B-27: Comparison of Earthquake Induced Shears and Bending Moments in Column 1 with "Design" Values in the Y-Direction (Upland Earthquake)

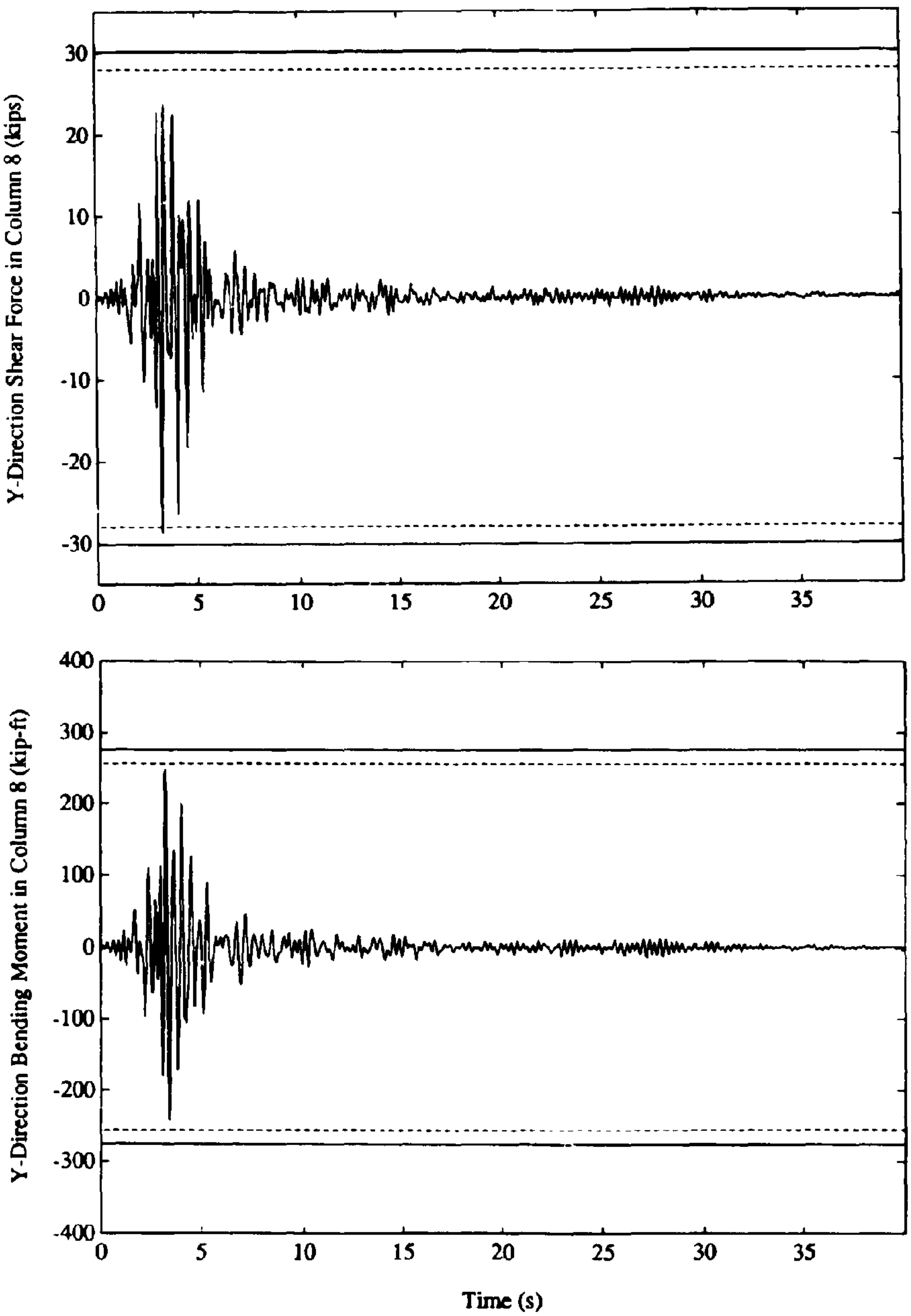

Figure B-28: Comparison of Earthquake Induced Shears and Bending Moments in Column 8 with "Design" Values in the Y-Direction (Upland Earthquake)

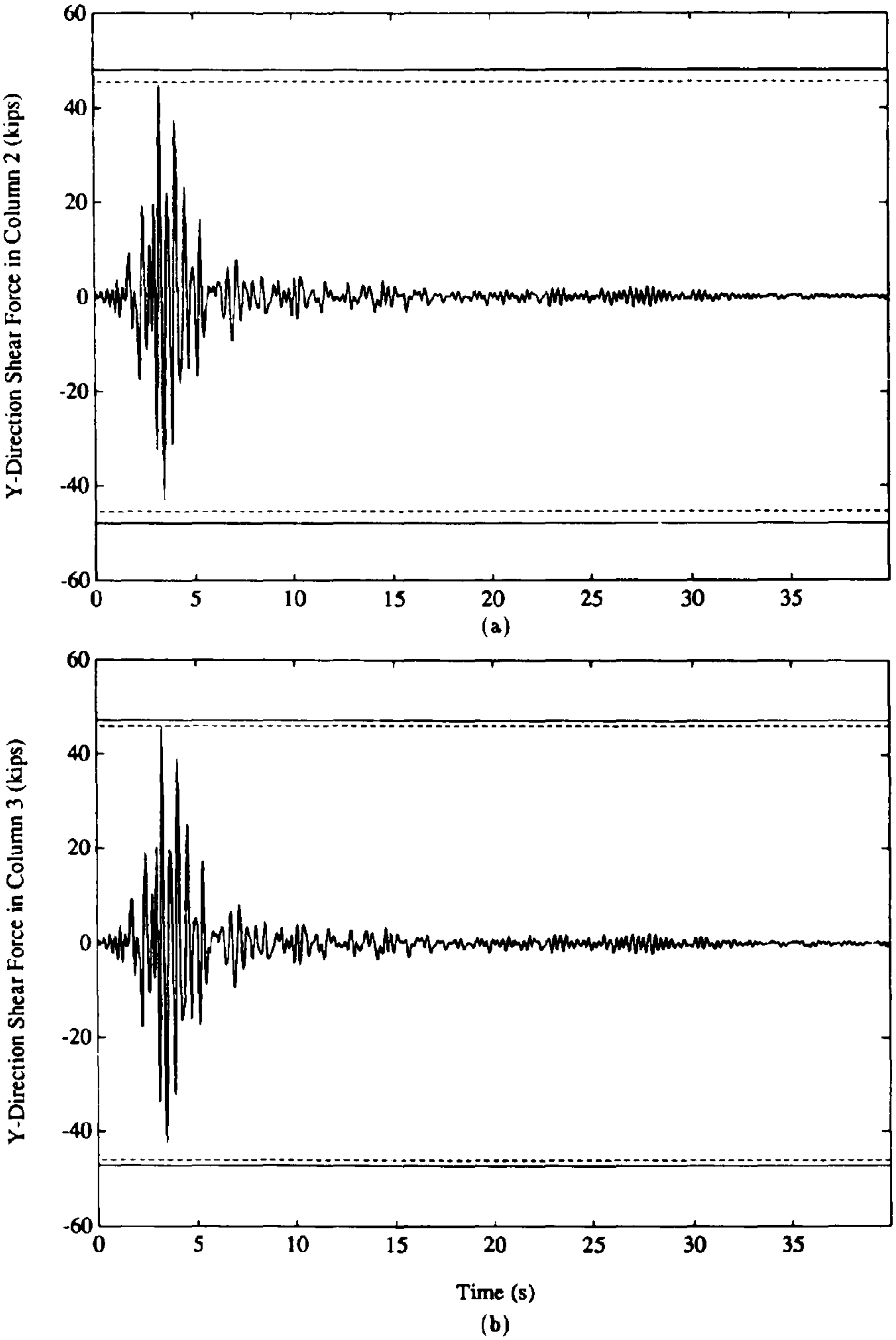

Figure B-29: Comparison of Earthquake Induced Shears in Columns 2 and 3 with "Design" Values in the Y-Direction (Upland Earthquake)

Page Intentionally Left Blank

APPENDIX C: THREE STORY OFFICE BUILDING

(CSMIP STATION No. 57562)

C.1 Building and Recorded Motions

Identified as CSMIP station No. 57562, this building is located in San Jose, California. Records of motions of the building during the Loma Prieta earthquake are available. A brief description of the structure, the recorded motions and the natural vibration frequencies and modes estimated from the records is presented in this section.

C.1.1 Brief Description of Building

The building considered is one of four similar wings, around a central building. Each wing is isolated from the central building by a separation joint and in principle there is no structural interaction between the wings and the central building. A typical plan of this three-story steel building shows that the building is approximately 288 feet long, 95 feet wide and 50 feet high (Figure C-1). The building has four lateral moment-resisting frames in the X-direction (A,B,C and D) and nine in the Y-direction (1 to 9). Most of beam-column connections of the structure are moment resisting but some are pinned as described in Section C.2. The triangular portion of the building plan (shown in lighter lines) is not part of any lateral moment-resisting frame of the structure and contributes minimally to the total lateral stiffness of the system. The floor decking system is formed by a steel corrugated metal deck filled with lightweight concrete. The foundation system consists of rectangular column footings interconnected by grade beams.

For all practical and code design purposes, the building has a floor plan that is nominally-symmetric about two axes. The asymmetry resulting from the additional mass or lateral stiffness provided by the triangular portions of the plan is minimal. The translational mass and rotational inertia for each floor is determined from the weight of structural elements, partitions, ceilings and other miscellaneous contributions. The mass of columns and partitions in each story is distributed equally to the floors at the top and bottom of the story. No live load is considered in calculating the floor masses. The locations of the center of mass (CM) for each floor was determined according to the distribution of dead loads specified in the original structural drawings of the building. The coordinates of the CM, with the origin defined as shown in Figure C-1, are presented in Table C-1.

C.1.2 Recorded Motions

The locations of the accelerographs in the building are shown in plan and elevation in Figure C-2. These include three channels at the ground, second, and third floors but none at the first floor. The ten strong motion records obtained during the Loma Prieta earthquake are shown in Figure C-3. The peak ground accelerations at the ground level are 0.2g in both lateral directions X and Y. These motions were amplified to 0.58g in the X-direction and 0.68g in the Y-direction at the roof level. The building experienced no structural damage during the earthquake.

From the three channels of accelerations recorded at any level, the accelerations of the CM at the same level - - these are $a_x(t)$ and $a_y(t)$, the X and Y components of translational acceleration and $a_\theta(t)$, the rotational acceleration about a vertical axis - - can be computed assuming a rigid floor diaphragm. This assumption seems valid for this building, given the large in-plane stiffness of the decking system compared with the lateral stiffness of the columns. Computed by this procedure, the accelerations $a_x(t)$, $a_y(t)$ and $a_\theta(t)$ at the geometric center of the ground plan and the CM of the second and third floor levels are presented in Figure C-4. Also shown are the accelerations at the CM of the second floor obtained from the recorded accelerations at the 3^{rd} floor and roof by the procedure described in Section C.3. These could not be obtained by the above procedure for lack of instrumental records at the first floor-level. In the X-direction the peak acceleration at the ground level is 0.2g which is amplified to 0.58g at the roof level; the amplification is from 0.17g to 0.53g in the Y-direction. The peak ground rotation of 0.014 rad/s^2 is amplified to 0.057 rad/s^2 at the roof level.

C.1.3 Natural Vibration Frequencies and Modes

Examination of the motions recorded at the roof level by channels 8, 9 and 10 provides rough estimates of the fundamental natural vibration frequencies of the building: 1.5 Hz in the X-direction and about the same value in the Y-direction. The true (not pseudo) acceleration response spectra for the motions recorded at the roof level in the X-direction at channel 8 and in the Y-direction at channels 9 and 10 are shown in Figure C-5. The major peak is around 1.5 Hz for both X and Y components of motion, which is consistent with the fundamental frequencies gleaned from direct examination of the records. Obviously the fundamental natural frequencies of the building in the two lateral directions are close. The second peak in all response spectra around 4 Hz indicates the possibility of another cluster of natural vibration frequencies.

Figure C-6 shows the transfer functions for the X, Y and Θ components of the relative (to the ground) acceleration at the CM of the three floor levels and the corresponding motions at the geometric center of the ground plan. The transfer functions were smoothened by a running average filtering procedure with weights (1/4,1/2,1/4). The transfer functions for the X and Y translational motions have a peak at 1.49 Hz and 1.44 Hz. The transfer function for rotational motion shows two peaks at 1.45 Hz and 1.54 Hz. An estimate of the fundamental natural vibration modes is provided by the relative values of the peaks in the transfer functions at the various floor levels. A vibration mode shape corresponding to a particular natural vibration frequency can be estimated from the ordinates at that frequency of the transfer functions at the various floor levels. Thus, the shapes of the first three natural vibration modes can be determined from the numerical data of Figure C-6: the X-translational mode from Figure C-6(a), the Y-translational mode from Figure C-6(b) and the torsional mode from Figure C-6(c). The mode shapes are presented in Table C-2.

C.2 Structural Idealization of the Building

The building was idealized for analysis by the ETABS computer program, wherein the building mass is assumed to be lumped at the floor levels and the floor diaphragms are assumed to be rigid, an assumption which was also used in computing motions at the CM from the recorded motions. The building is treated as fixed at the level defined by the slab on grade. All structural elements were included in the structural idealization, i.e, even the elements that provide little lateral resistance are considered because they may contribute to the accidental eccentricities. The column lines and frame bays used for the ETABS model are defined in Figure C-10. Flexural and axial deformations are considered in defining the properties of columns whereas only flexural deformations are necessary for defining the properties of beams. The compatibility of axial deformations required in columns belonging to more than one moment resisting frame is considered by analyzing the structure as a single three-dimensional frame with six degrees of freedom per joint (in contrast to the most common type of analysis that considers the structure as an assemblage of several two dimensional lateral-force-resisting frames distributed across the building plan).

The framing plans idealized for analysis are shown in Figures C-7 to C-9, wherein the sizes of the columns and beams are noted. Each frame is modelled with appropriate beam-column joints: moment resistant (or rigid) connections denoted in Figures C-7 to C-9 by small triangles next to the column, and pinned connections which are all the joints without the small triangle. In the case of moment-resistant connections, the portions of beams within the beam column panel zone are treated as rigid, consistent with the rigidity of the connection.

The natural vibration frequencies and mode shapes of the idealized structural system computed by the ETABS program are presented in Table C-2. The agreement between these computed frequencies and those determined earlier from the recorded response of the building is satisfactory. Consistent with the results from the recorded response, the structural idealization predicts closely spaced frequencies of the first triplet of modes and a second triplet around 4 Hz. Because the frequencies computed from the initial structural idealization agreed satisfactorily with the recorded frequencies no refinement of the idealization was necessary.

C.3 Dynamic Eccentricity

The story shears and torques are computed from the floor masses and accelerograms (Figure C-4) by Equations 1 to 3, wherein the acceleration records at all floor levels are needed. Unfortunately, the accelerations of the first floor of this building were not recorded during the earthquake for lack of instrumentation. Therefore, they must be estimated from the accelerations recorded at the other floors.

The acceleration at the centers of mass of the three floors, relative to the ground acceleration at the geometric center of the ground plan can be expressed in terms of the nine natural vibration modes of this 3-story building with three degrees of freedom at each floor:

$$\underline{\ddot{u}} = \sum_{n=1}^{9} \underline{\phi}_n \ddot{q}_n$$

$$\begin{bmatrix} \underline{\ddot{u}}_2 \\ \underline{\ddot{u}}_3 \\ \underline{\ddot{u}}_r \end{bmatrix} = \sum_{n=1}^{9} \begin{bmatrix} \underline{\phi}_{2n} \\ \underline{\phi}_{3n} \\ \underline{\phi}_{rn} \end{bmatrix} \ddot{q}_n \tag{6}$$

For this building, $\underline{\ddot{u}}_3$ and $\underline{\ddot{u}}_r$ the three components of acceleration of the CM at the third floor and roof, respectively, are readily computed by subtracting the ground accelerations at the geometric-center of the ground plan from the total accelerations at the CM of a floor which were determined from the three accelerations records from that floor (Figure C-4). The accelerations $\underline{\ddot{u}}_2$, of the second floor are to be determined from the six acceleration components $\underline{\ddot{u}}_3$ and $\underline{\ddot{u}}_r$. Thus, no more than six natural vibration modes can be included in Equation C-1, from which

$$\begin{bmatrix} \underline{\ddot{u}}_3 \\ \underline{\ddot{u}}_r \end{bmatrix} = \sum_{n=1}^{6} \begin{bmatrix} \underline{\phi}_{3n} \\ \underline{\phi}_{rn} \end{bmatrix} \ddot{q}_n \tag{7}$$

This system of six algebraic equations can be solved to determine $\ddot{q}_1, \ddot{q}_2, \ldots, \ddot{q}_6$. The total accelerations at the CM of the first floor are then computed by adding the ground acceleration at the geometric-center of the ground plan to the relative accelerations computed from:

$$\underline{\ddot{u}}_2 = \sum_{n=1}^{6} \underline{\phi}_{2n} \ddot{q}_n \tag{8}$$

Resulting from these computations, using the first six modes computed by the ETABS analysis, the X, Y and Θ components of the total acceleration at the CM of the second floor are presented in Figure C-4.

The accidental eccentricity at the "jth" floor has been defined by Equations 4 and 5 (Section 5) in terms of the story shears and story torques in the "jth" story. The latter are computed from Equations 1 to 3 wherein the floor masses are given by Table C-1 and the accelerations $a_{xj}(t), a_{yj}(t)$ and $a_{\theta j}(t)$ at the CM in Figure C-4. The computed base shear and torque for the building are shown in Figures C-11 and C-12. The maximum values for the base shear are 2575 kips and 1955 kips in the X and Y-directions, respectively which are 33% and 25% of the total weight of the building. The accidental eccentricities $e_{Y1}(t)$ and $e_{X1}(t)$ determined from the base shear and torque by Equations 4 and 5 are also shown in Figure C-11.

C.4 Base Shear, Base Torque and Code-Equivalent Combinations

This section presents the implementation of the step by step procedure described in Section 5 for this building:

1. At each instant of time, the base shear was computed by Equations 1 to 3, where the floor masses are given in Table C-1 and the floor accelerations in Figure C-4. The "design" base

shears for the analyses in the X and Y-directions are 2575 kips and 1955 kips, respectively, and correspond to the maximum values during the earthquake (Figures C-11).

2. The heightwise distribution of lateral forces at the three floor levels are computed from the code formula:

$$F_j = \frac{w_j h_j}{\sum_{i=1}^{3} w_i h_i}$$

j=1,2 and 3, using the floor masses and story heights in Table C-1. The lateral story forces for this building are 0.25V, 0.47V and 0.28V for the second floor, third floor and roof , respectively, wherein V represents the "design" base shear determined in Step 1. In the X-direction, V=2575 kips and the associated lateral forces are 644, 1210 and 721 kips at the second floor, third floor and roof, respectively. In the Y-direction, V=1955 kips and the lateral forces are 489, 919 and 547 kips at the second floor, third floor and roof. The X-lateral forces are applied at a distance of ±0.05b = ±0.05x96 = ± 4.8 ft. The Y-lateral forces are applied at a distance of ±0.05b = ±0.05x288 = 14.4 ft. The resulting "design" shear forces for selected columns in the first story of the building are shown in column 3 of Table C-3.

3. The lateral story forces determined in Step 2 are next applied to the structure at the CM of each floor. The resulting shear forces for selected columns in the first story of the building are presented in column 4 of Table C-3. The procedure for calculating the base shear that produces the same "design" member force as in Step 2 is described next for Column 1 in the first story (Figure C-13(b)). Step 2 provided 64.5 kips as the "design" shear force for this column in the Y-direction, whereas step 3 resulted in shear forces of 51.2 kips. Thus, the ratio 64.5/51.2 represents the factor by which the the "design" base shear, V=1955 kips, in the Y-direction has to be amplified in order to obtain the "design" shear force of 64.5 kips in Column 1 of the first story. The amplified base shear V_0= (64.5/51.2)1955=2465 kips (column 5 of Table C-3). Similar results for other columns in the first story are also presented in Table

C-3.

4. Next we analyze subjected to the story torques $T_i=0.05bF_i$ where the lateral forces F_i were determined in step 2. The resulting force in a member is the difference of the two values for the the member force determined in steps 2 and 3. Therefore,the resulting shear forces in the selected columns corresponding to this analysis are obtained as the difference of the values in columns 3 and 4 of Table C-3. The procedure for calculating the base torque that produces the same "design" shear force in a selected column as step 2 is described next for Column 1 in the first story. Step 2 provided 64.5 kips as the "design" shear force for this column, whereas step 4 resulted in a shear force of 13.3 kips. Therefore, the ratio 64.5/13.3 denotes the factor by which the base torque, T=1955x14.4=136648 kip-ft, has to be amplified to produce the "design" force in Column 1 of the first story. The amplified base torque is T_o=(64.5/13.3)28177=136648 kip-ft. Similar results for other columns of the first floor are presented in Table C-3.

5. The code-equivalent combinations associated with column 1 in the first story are shown by solid straight lines in Figure C-13(b). Also shown by dashed lines are the code-equivalent combinations for zero accidental eccentricity. They have been calculated as described in steps 3 and 4 but using the value in column 4 of Table C-3 as the "design" member force associated with zero accidental eccentricity. Considering the first story Column 1 the corresponding base shear is V=1955 kips and the base torque is, T=1955x14.4 kip-ft, amplified by the factor 51.2/13.3, resulting in 108375 kip-ft.

The values of base shear and torque for the X and Y-directions of analysis that were presented in Figure C-11 are plotted as pairs (V,T) for each instant of time in Figures C-12 and C-13. For analysis in the X-direction Figure C-12 shows that all base shear and base torque combinations fall inside the code-equivalent combinations. For analysis in the Y-direction Figure C-13 shows that, except for a very few time instants, the base shear and base torque pairs determined in step 6 fall inside the code-equivalent combinations.

The code-equivalent combinations are only slightly exceeded at a few time instants in those columns located farther towards the left of the center of mass of the first story. Figure C-13 shows that the "shear" force in first-story Column 1 (and columns 2,3 and 4) associated with the most critical base shear and base torque combination (Point A in Figure C-13(b)) is 10 percent bigger than the "design" shear force (64.5 kips). Figure C-13(a) also shows that for Column #5 (similar results for Columns #6,7 and 8) the most critical base shear and torque combination (Point A in Figure C-13(a)) produces an element shear which is 6.8 % bigger than the "design" shear for that column (68.8 kips).

C.5 Time History of Member Forces

The member forces due to the static application of the floor inertia forces computed by Equations 1 to 3 were determined by first: (a) computing the influence coefficients defining the forces in selected members due to unit values of each of the nine floor inertia forces applied individually (Table C-4); and (b) multiplying at each instant of time the actual values of the floor inertia forces and the respective influence coefficients. Table C-4 presents the influence force coefficients for six columns in the first story of the building due to F_{xj} or F_{yj}= 1000 kips, j=1,2 or 3; and $F_{\theta j}$= 1000 kip-ft, j=1,2 or 3, for story torques. In Table C-4, V is the shear force in the selected element and M the bending moment. The subscript attached to V or M, indicates the element number according to Figure C-10 and the superscript indicates the direction of analysis. The time-history of element forces obtained by combining the products of the nine floor inertia forces (Figure C-4) and the corresponding influence coefficients (Table C-4), which have been divided by 1000, are presented in Figures C-14 to C-17. Also included in these figures are the "design" values for the member forces associated with 0.05b (solid horizontal line) and zero (dotted horizontal line) accidental eccentricity.

Results of analysis of the building in the X-direction (Figures C-14 and C-15(a)) show that at all time instants the member forces computed in Step 4 are less than the "design" member forces. This is consistent with the results of Figure C-12 presented in section C.4. Figures C-15(b) and C-16 show that for Columns #8 and #1 (similar results for Columns #2 to 7) which are located at the left of the CM of the plan, the "design" shear and bending moment values in the Y-direction are slightly exceeded at a few time instants during the earthquake. The maximum shear value for Column 1 (Figure C-16) is 9.7 percent greater than its "design" value (64.5 kips). The maximum shear in Column 8 (Figure C-15(b)) exceeds the design value by 6.8 percent. These results are consistent with the five points falling outside the code-equivalent combinations in Figure C-13(b).

Table C-1: Building Properties

Floor	h_i (ft)	m_i (k-s^2/ft)	Ip_i (k-s^2-ft)	x_{gi} (ft)	y_{gi} (ft)
Roof	16	39.47	268057	120.6	36.2
3^{rd}	16	99.98	650501	122.6	36.2
2^{nd}	18	99.98	650501	122.6	36.2

Table C-2: Natural Vibration Frequencies and Modes Shapes of the Building

Vibration Properties	X-lateral mode		Y-lateral mode		Torsional mode	
	Recorded	Computed	Recorded	Computed	Recorded	Computed
Frequency (Hz)	1.49	1.42	1.44	1.44	1.45 - 1.54	1.49
Mode Shape						
Floor 3	1.00	1.00	1.00	1.00	1.00	1.00
Floor 2	0.80	0.70	0.70	0.67	0.67	0.66
Floor 1	0.44	0.33	0.33	0.30	0.31	0.30

Table C-3: "Design" Shear Forces in Selected Elements and Amplified Base Shear and Base Torque

Column #	Direction	Shear Force (k)	Shear Force (k)	Base Shear (k)	Base Torque (k-ft)
1	Y	64.5	51.2	2465.0	136648
4	Y	-64.5	-51.2	2465.0	136648
5	Y	68.8	57.7	2332.0	174508
8	Y	-68.8	-57.7	2332.0	174508
29	Y	72.1	61.0	2311.9	182753
32	Y	-72.1	-61.0	2311.9	182753
33	Y	68.4	55.1	2427.5	144913
36	Y	-68.4	-55.1	2427.5	144913
5	X	-82.2	-80.5	2629.6	593025
8	X	82.6	80.8	2630.2	586552
29	X	-72.7	-71.2	2629.2	596624
32	X	73.0	71.5	2630.0	588797

Table C-4: Influence Force Coefficients for Selected Elements

Unit Forces (1000 k, k-ft)	V_1^y(k)	V_{36}^y(k)	V_8^y(k)	V_{32}^y(k)	V_{32}^x(k)	V_8^x(k)
F_{x1}	0.1331	0.2388	-0.0910	0.1999	29.2420	31.4570
F_{y1}	26.4680	-29.1037	-27.7490	-29.7920	-0.4108	-0.4445
$F_{\theta 1}$	-0.4865	-0.4874	0.3774	-0.3783	-0.1342	-0.1444
F_{x2}	0.1387	0.2365	-0.1064	0.2163	27.2780	31.3700
F_{y2}	25.9070	-28.4200	-29.5600	-31.6860	-0.3649	-0.4299
$F_{\theta 2}$	-0.4706	-0.4711	0.3975	-0.3981	-0.1213	-0.1409
F_{x3}	0.1379	0.2343	-0.1131	0.2261	27.2000	31.3500
F_{y3}	26.3400	-26.9600	-31.0600	-31.5900	-0.1187	-0.1476
$F_{\theta 3}$	-0.4623	-0.4627	0.4063	-0.4069	-0.1188	-0.1393
	M_1^y(k-ft)	M_{36}^y(k-ft)	M_8^y(k-ft)	M_{32}^y(k-ft)	M_{32}^x(k-ft)	M_8^x(k-ft)
F_{x1}	1.4332	2.5359	-0.9440	2.0458	14.2500	327.5400
F_{y1}	279.0000	-306.6670	-282.7890	-303.5370	-4.4111	-4.6134
$F_{\theta 1}$	-5.1179	-5.1264	3.8400	-3.8486	-1.4450	-1.5065
F_{x2}	1.7883	2.9891	-1.2506	2.4969	350.2100	374.7600
F_{y2}	320.8200	-351.8500	-337.3300	-361.4900	-4.7987	-5.1886
$F_{\theta 2}$	-5.8156	-5.8218	4.5292	-4.5360	-1.5993	-1.7167
F_{x3}	1.9403	3.1908	-1.3960	2.7163	361.4400	386.3000
F_{y3}	345.2000	-353.0700	-365.7000	-371.9000	-1.6400	-1.8100
$F_{\theta 3}$	-6.0185	6.0235	4.7634	-4.7695	-1.6585	-1.7813

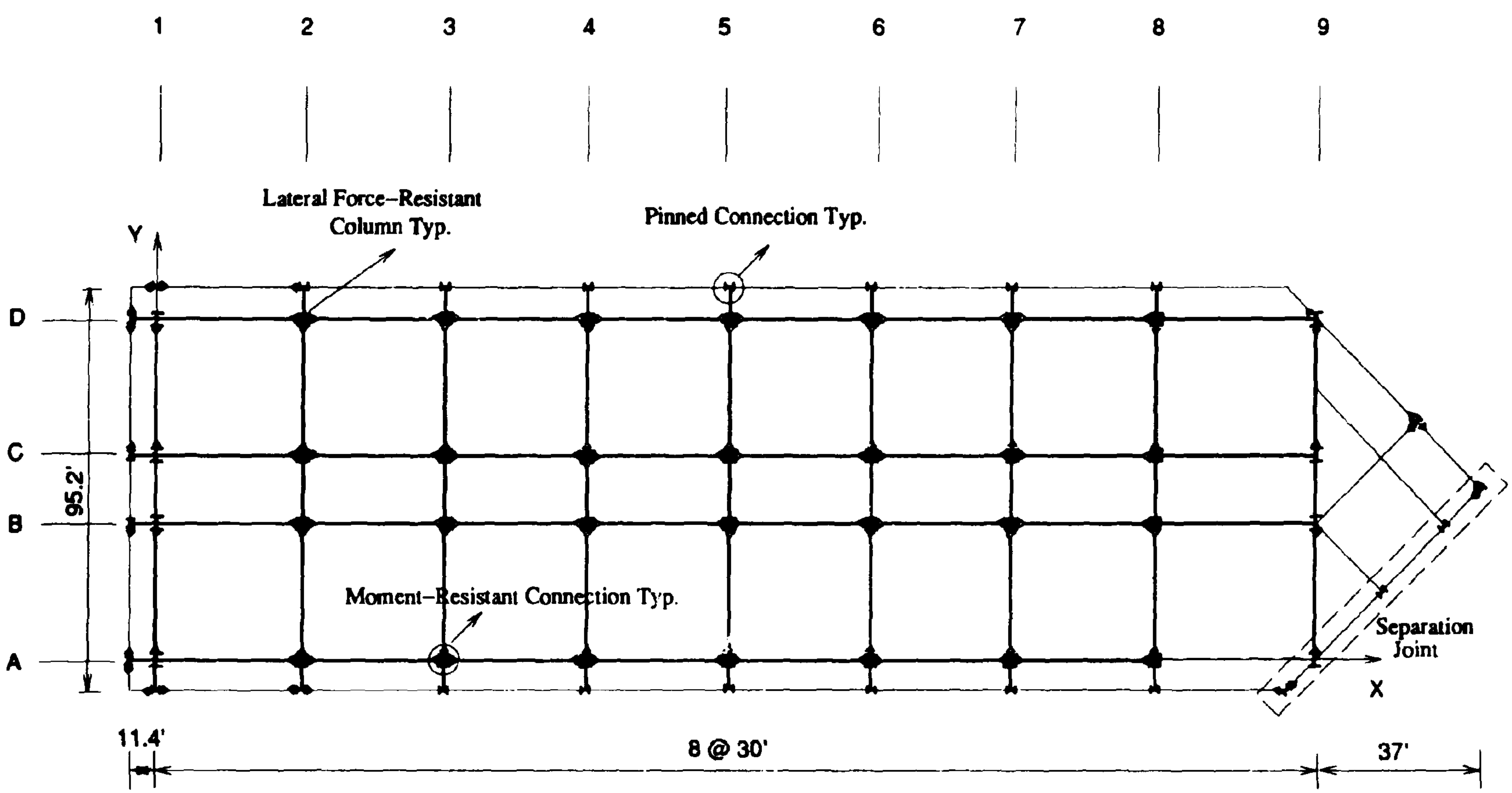

Figure C-1: Typical Framing Plan of Building C

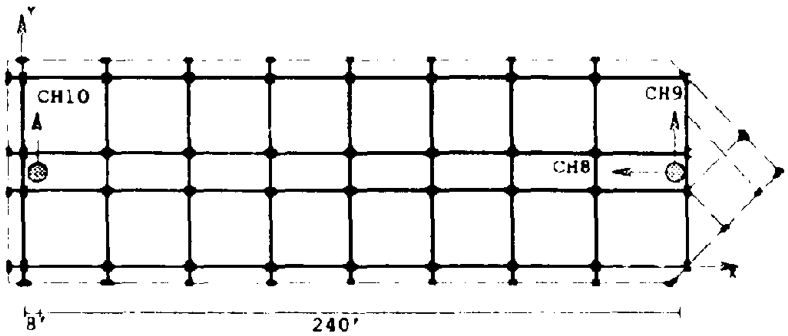

Roof

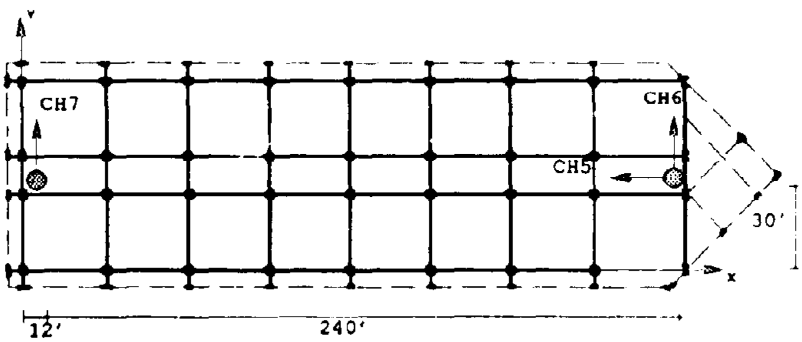

Third Floor

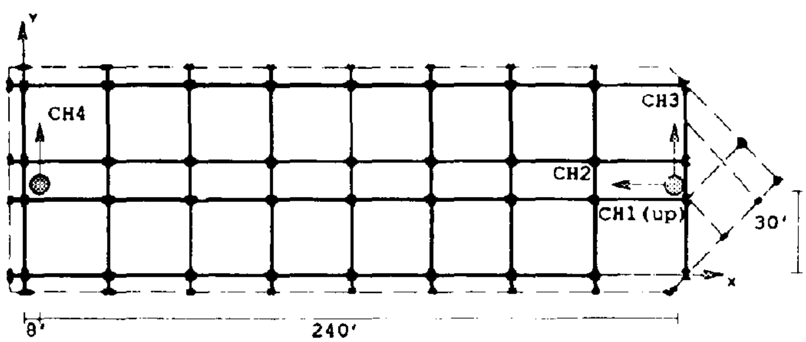

First Floor

Figure C-2: Instrument Locations (Building C)

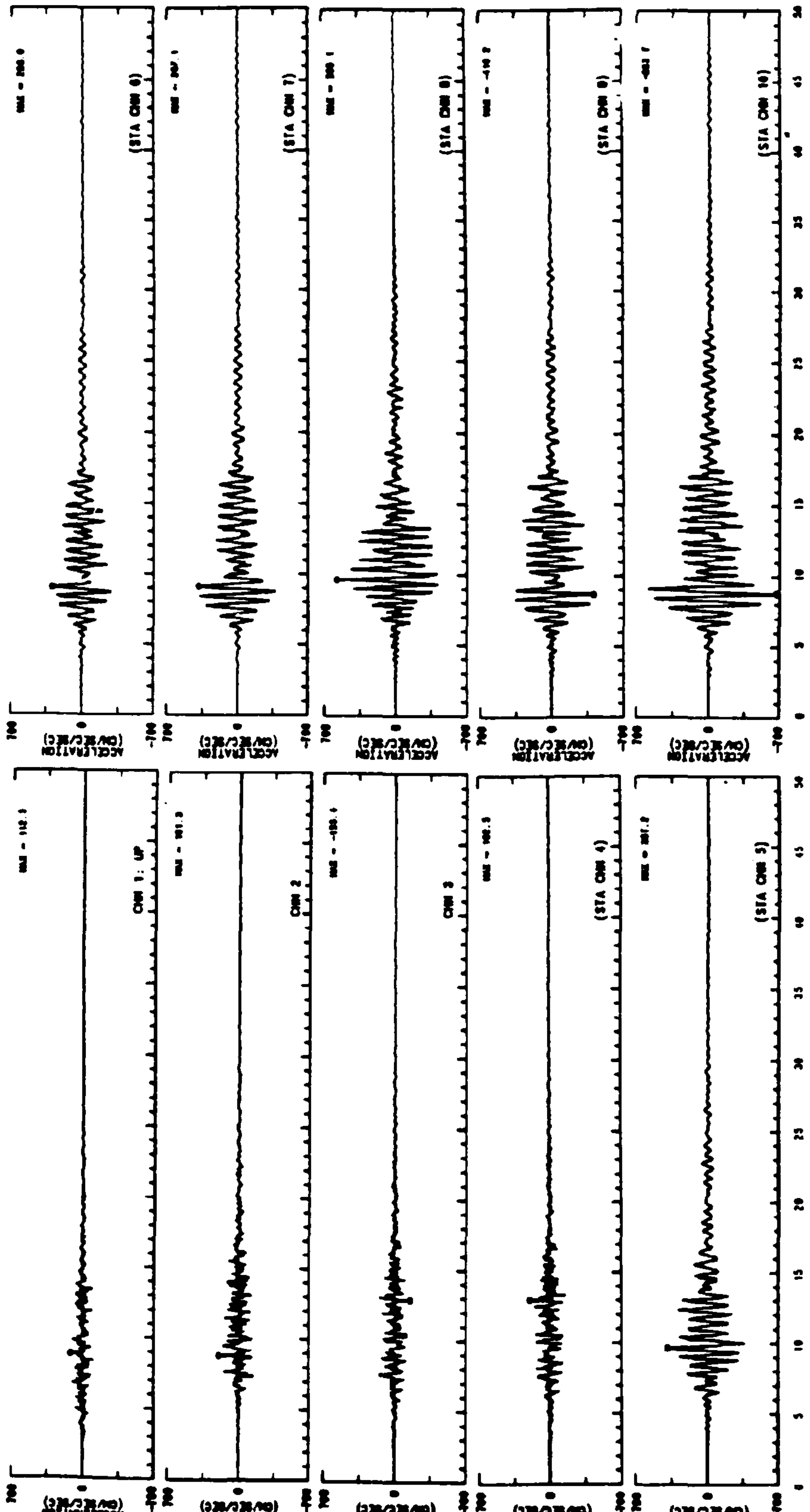

Figure C-3: Recorded Motions During the Loma Prieta Earthquake

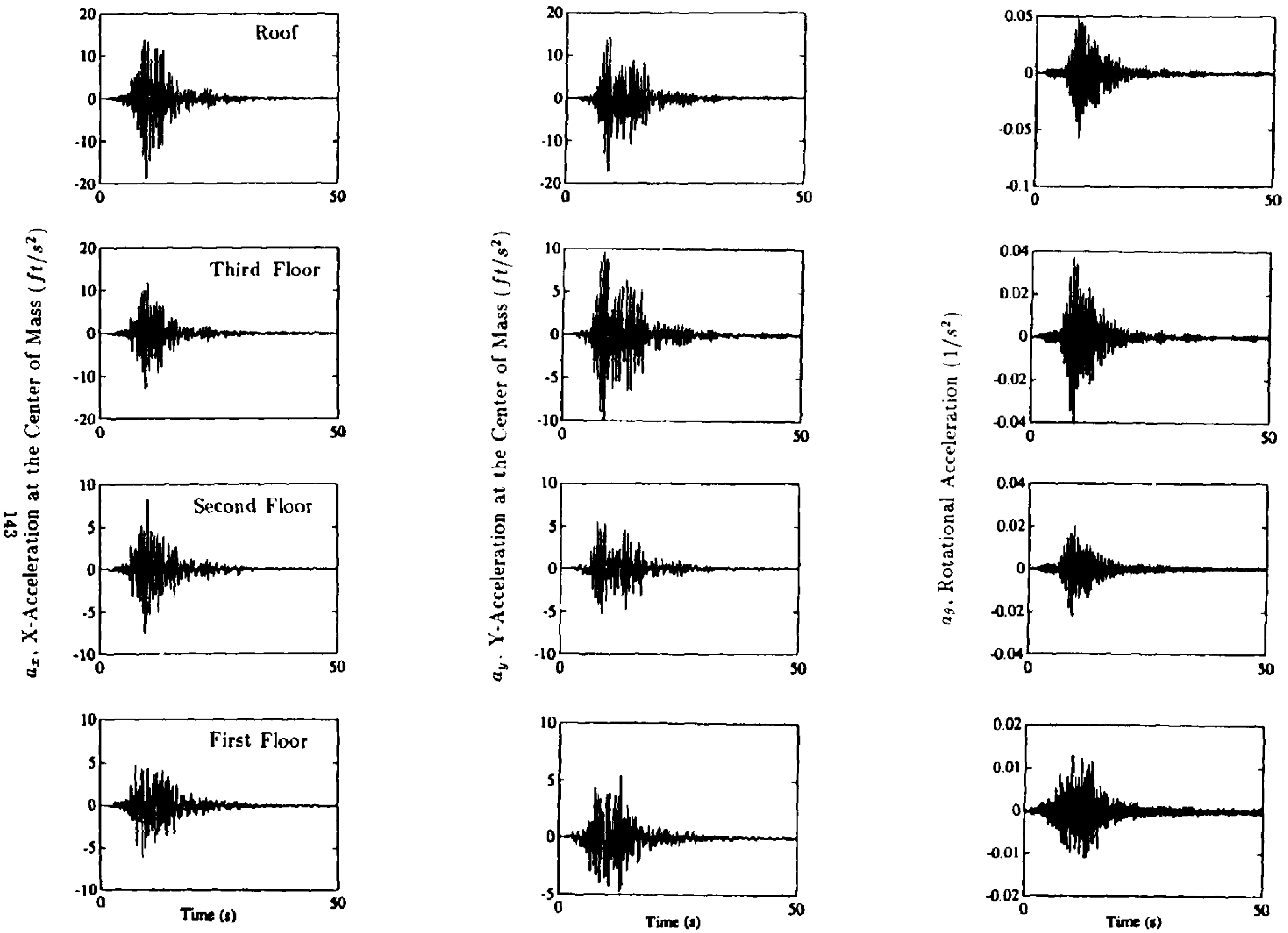

Figure C-4: Computed Motions at the CM of each Floor Level

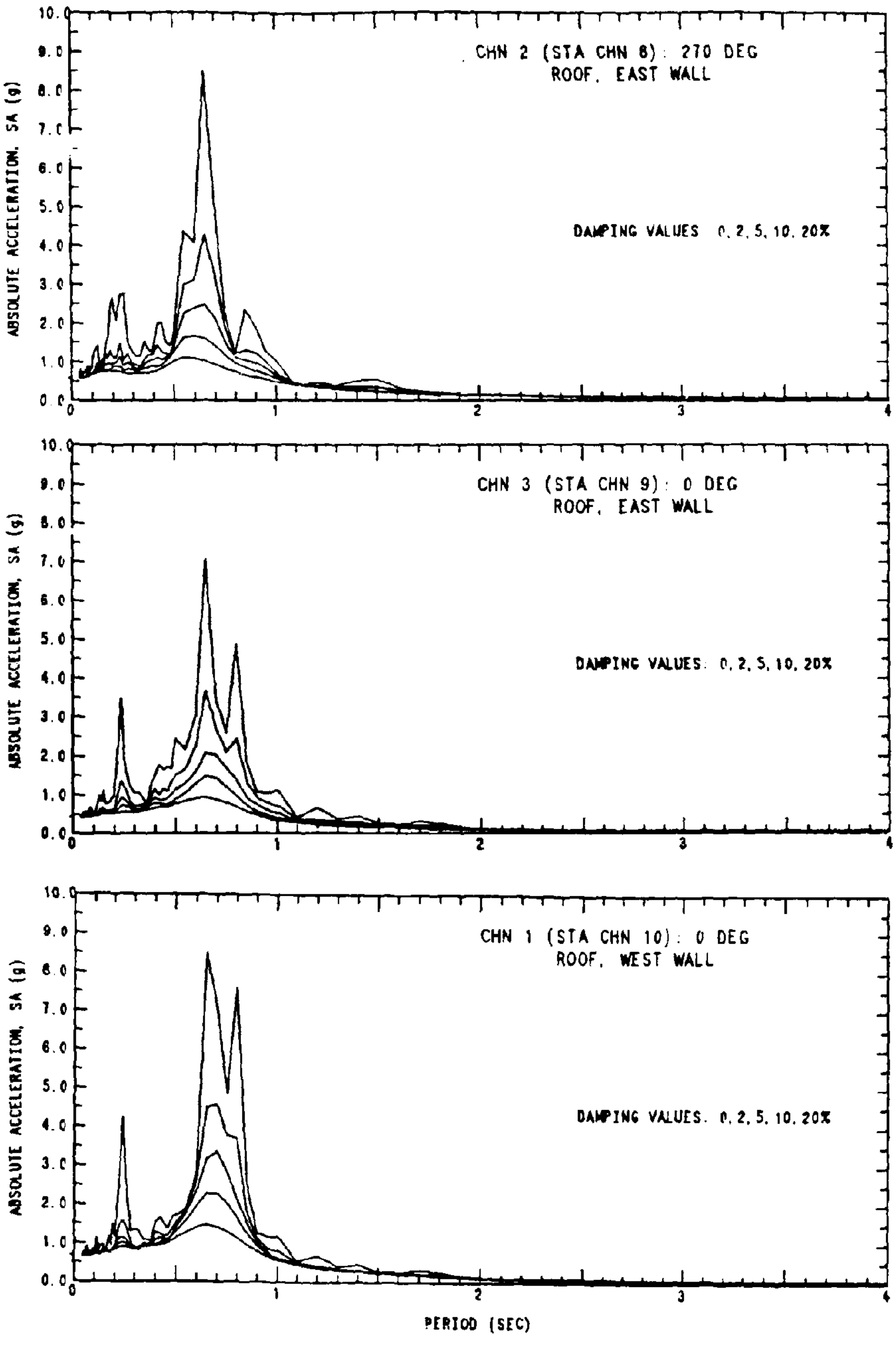

Figure C-5: Absolute Acceleration Spectra of Channels 1, 2, and 3

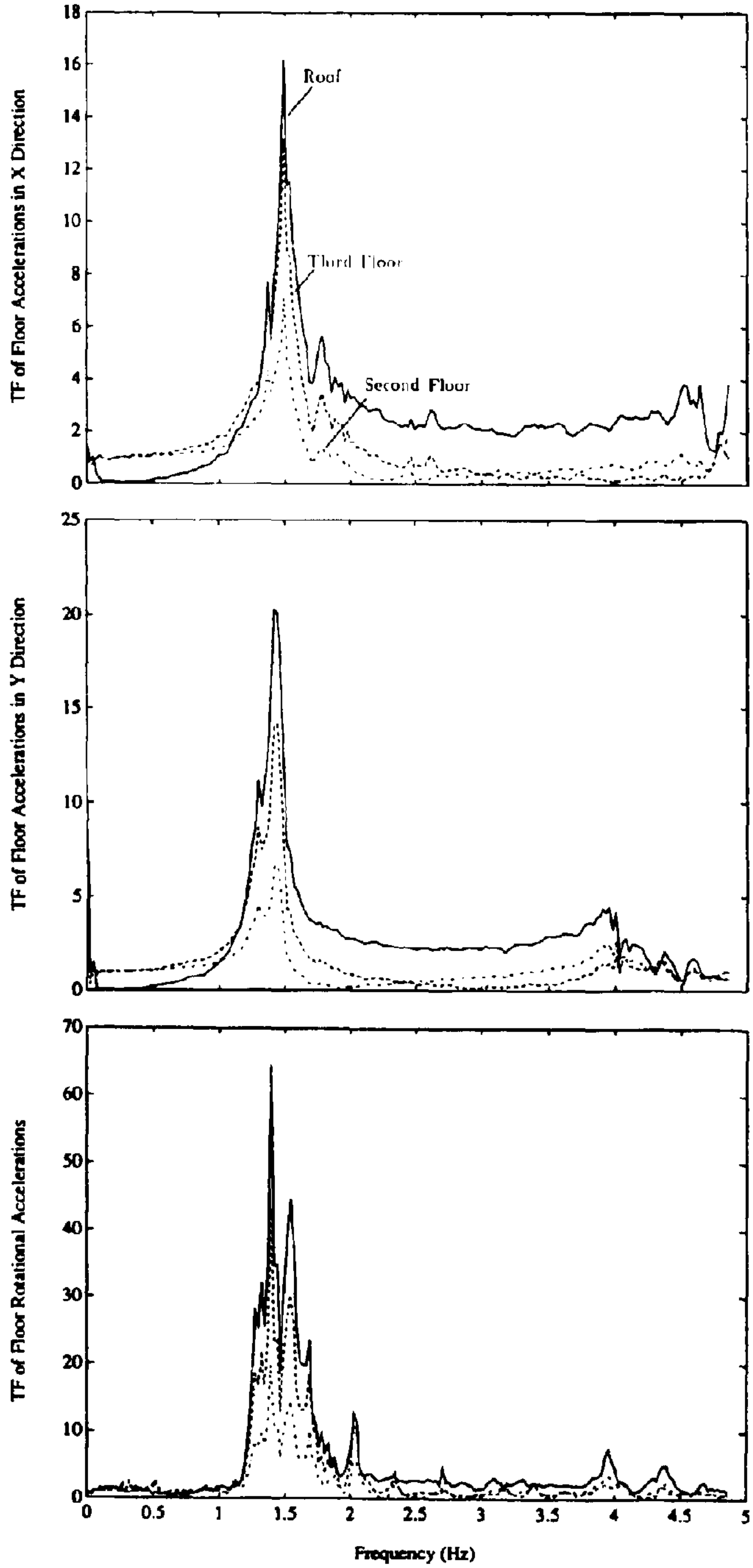

Figure C-6: Transfer Functions of the Roof Relative Floor Accelerations

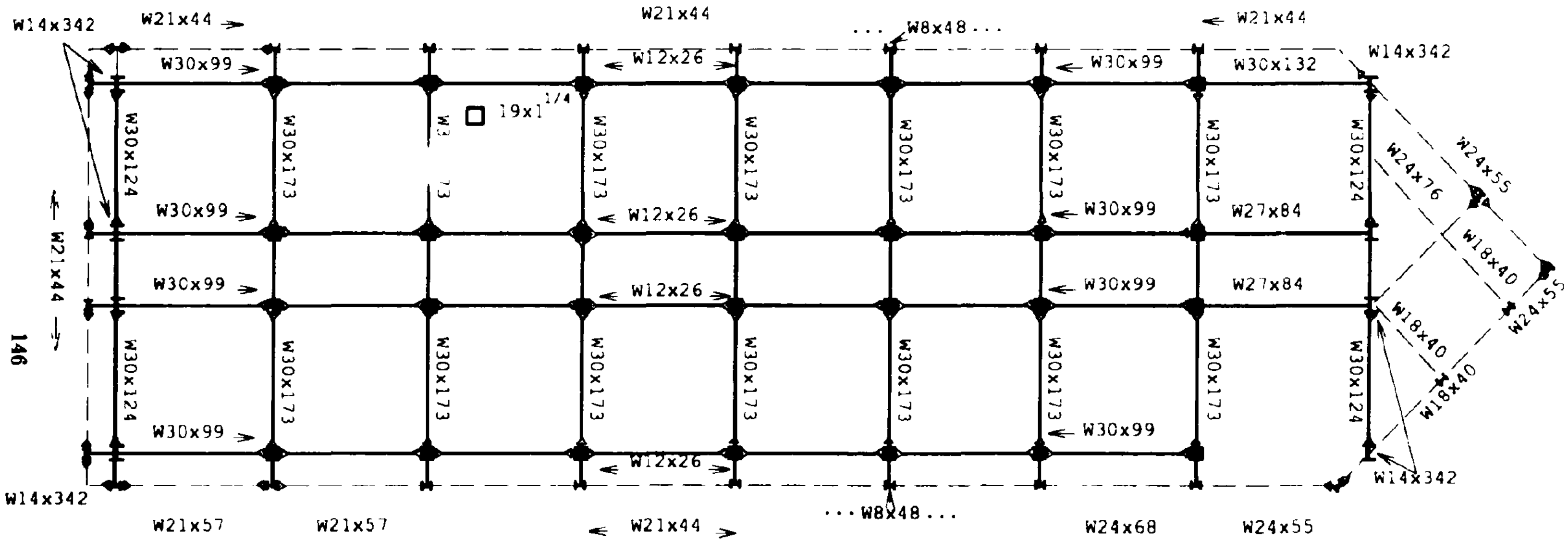

Figure C·7: Schematic Structural Plan of First Story

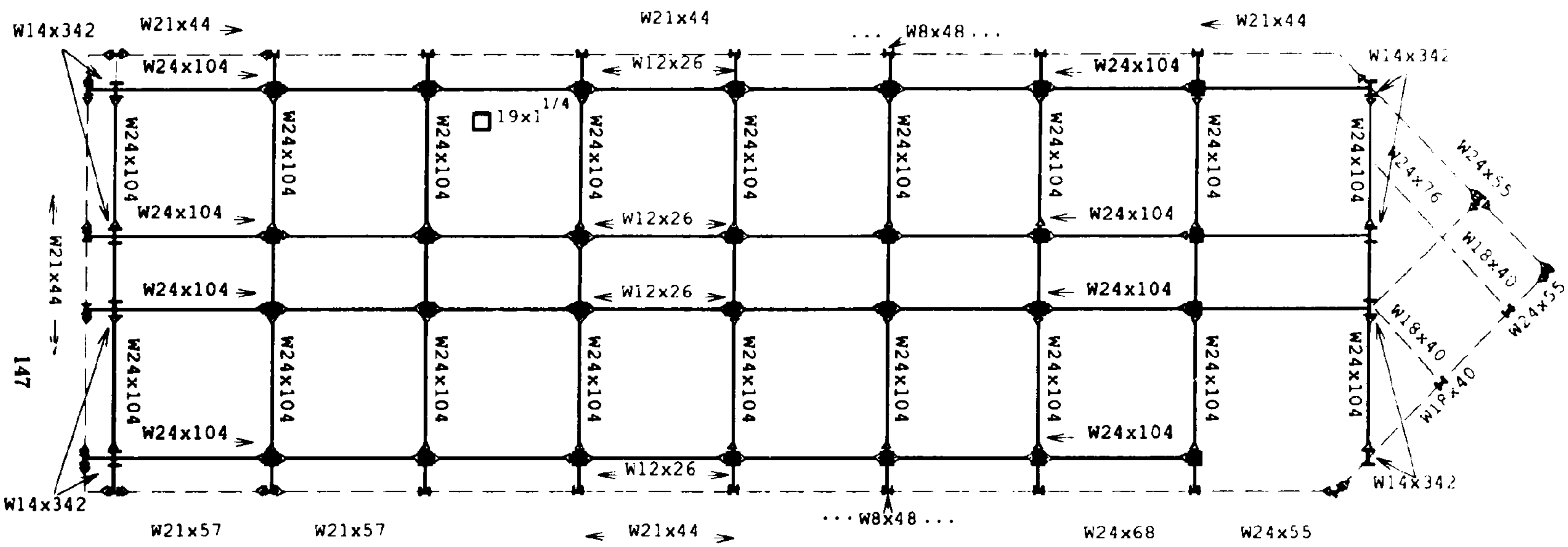

Figure C-8: Schematic Structural Plan of Second Story

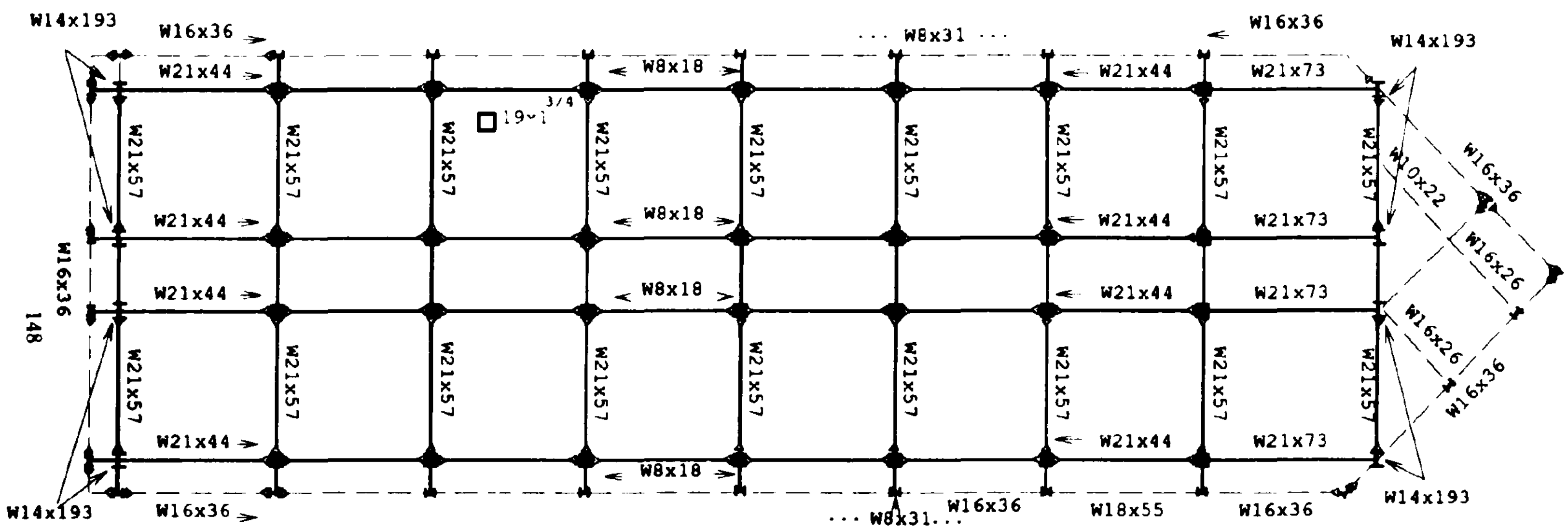

Figure C-9: Schematic Structural Plan of Third Story

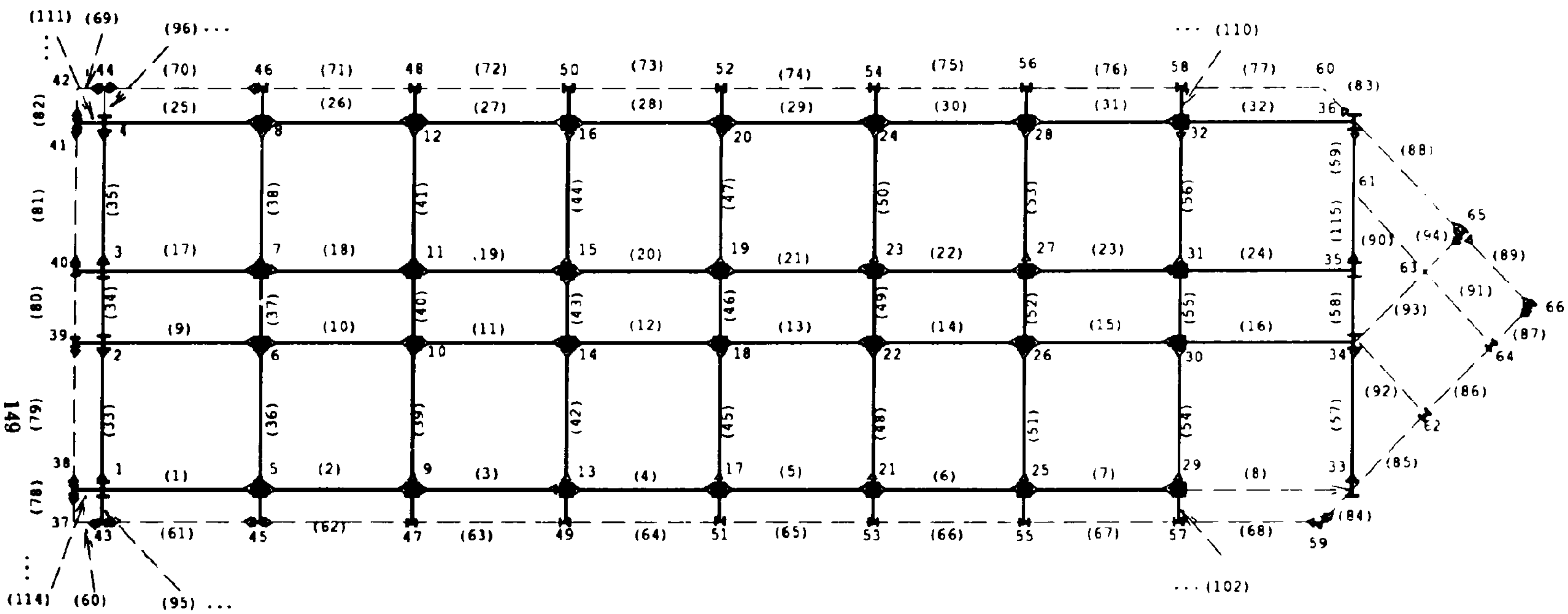

Figure C·10: Definition of Column Lines and Frame Bays for ETABS Model

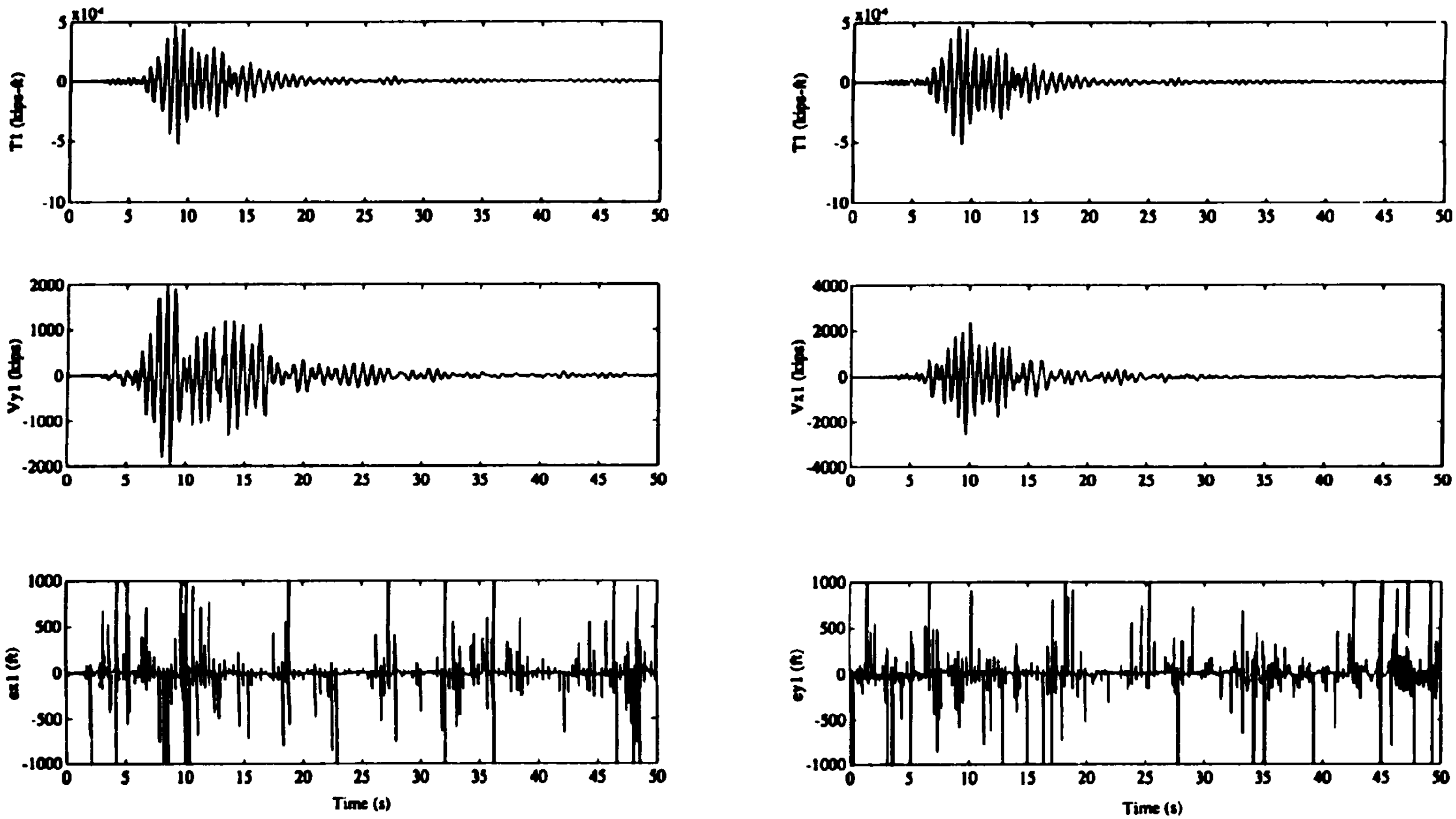

Figure C-11: Base Shear, Base Torque and First Floor Accidental Eccentricities Computed from Recorded Accelerations During the Loma Prieta Earthquake

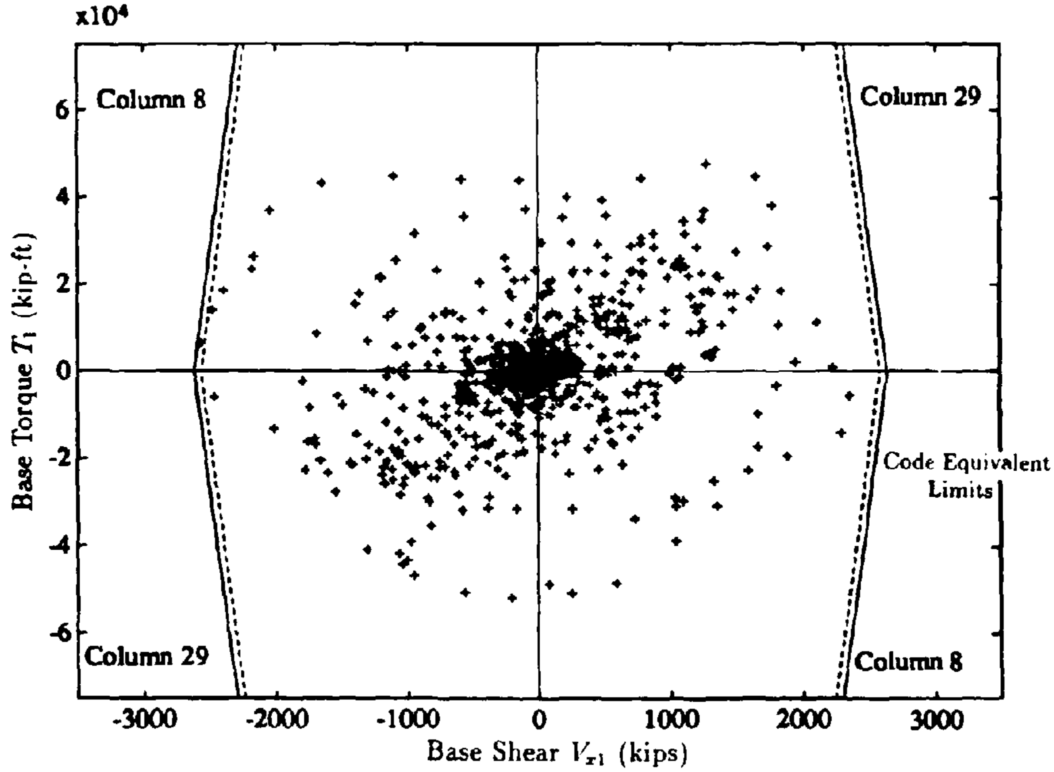

Figure C-12: Comparison of Dynamic Base Shear, Base Torque and "Code Equivalent Limits" for Elements in the X-Direction

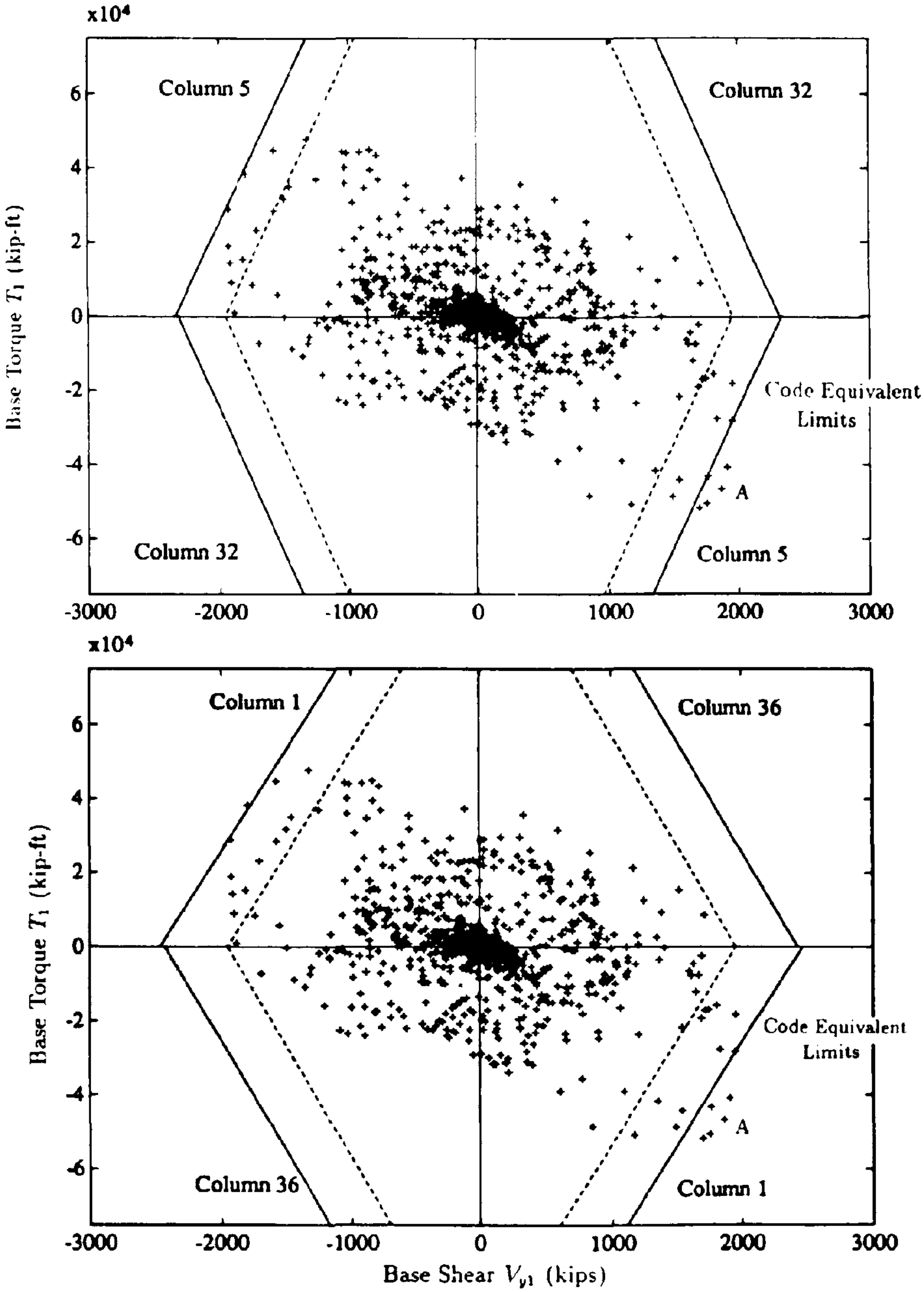

Figure C-13: Comparison of Dynamic Base Shear, Ba e Torque and "Code Equivalent Limits" for Elements in the Y-Direction

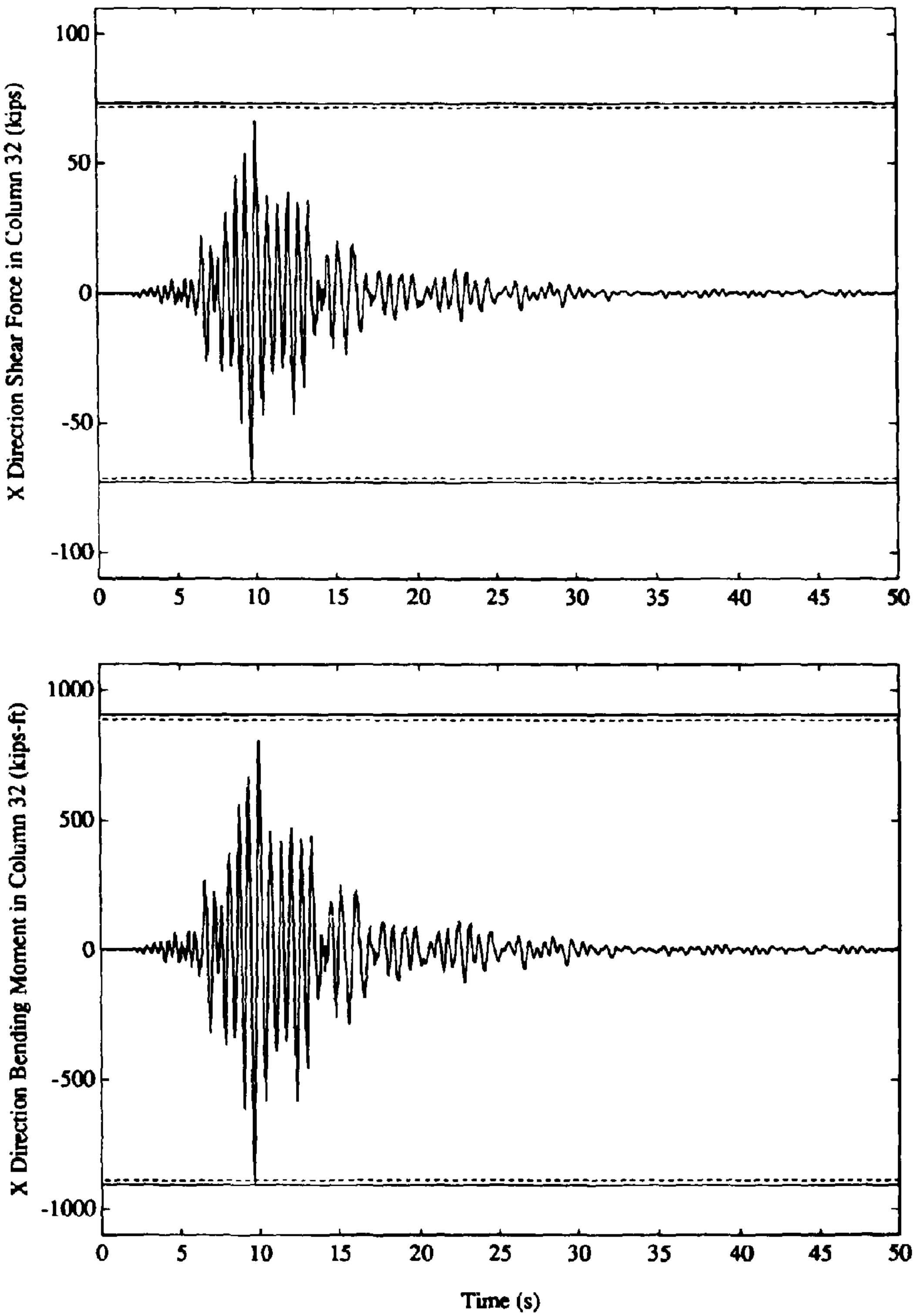

Figure C-14: Comparison of Earthquake Induced Shears and Bending Moments in Column 32 with "Design" Values in the X-Direction

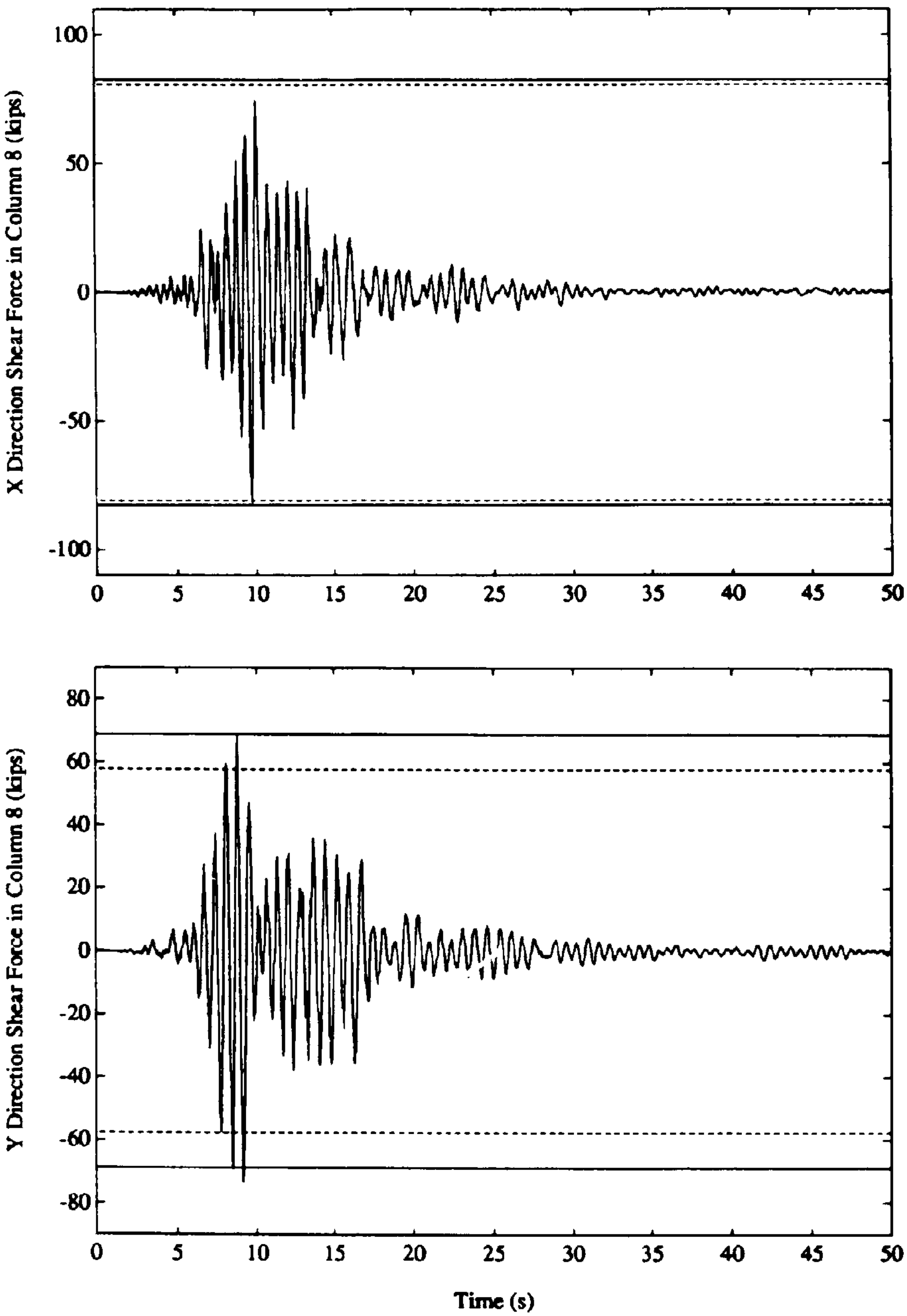

Figure C-15: Comparison of Earthquake Induced Shears in Column 8 with "Design" Values in the X and Y-Directions

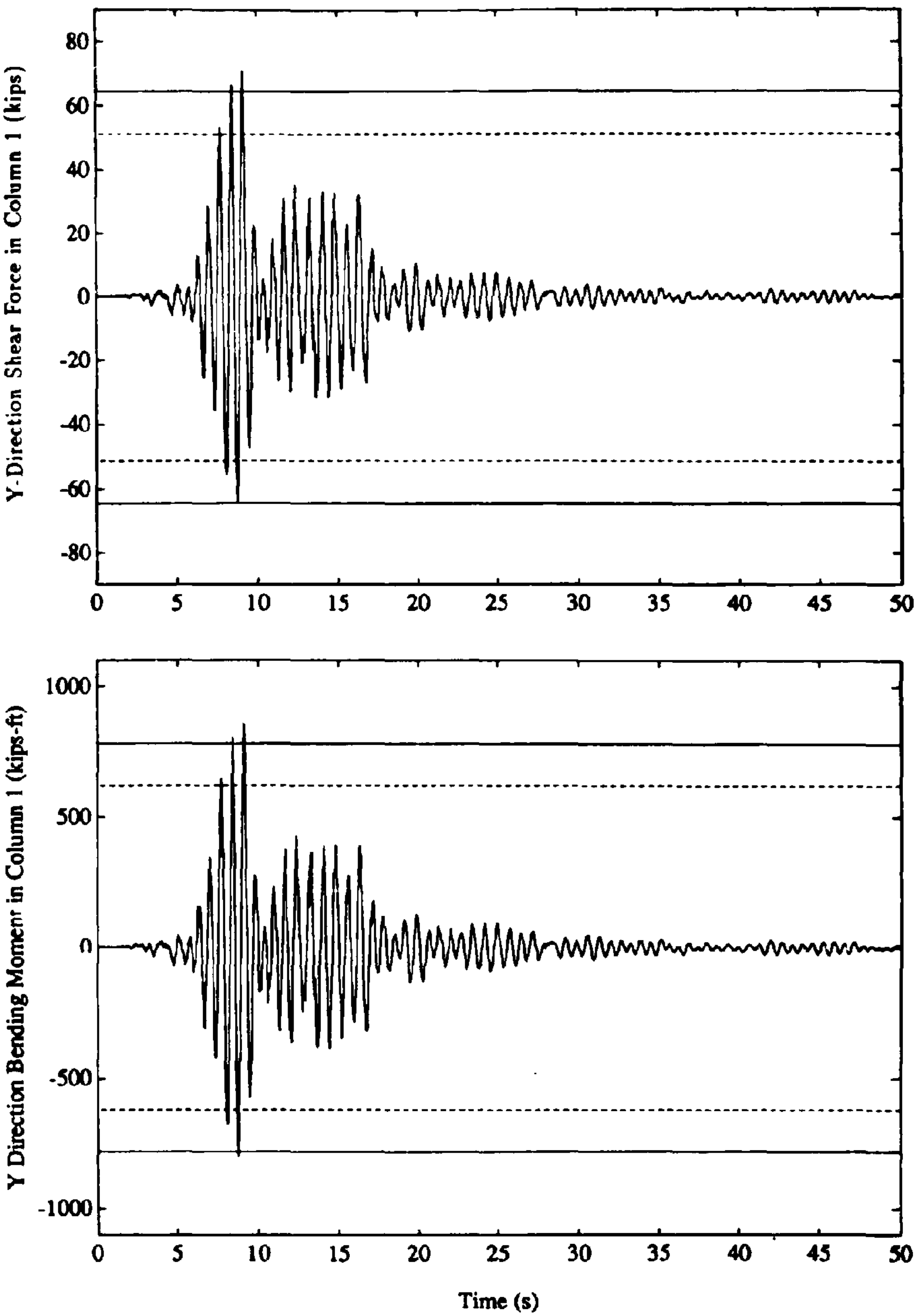

Figure C-16: Comparison of Earthquake Induced Shears and Bending Moments in Column 1 with "Design" Values in the Y-Direction

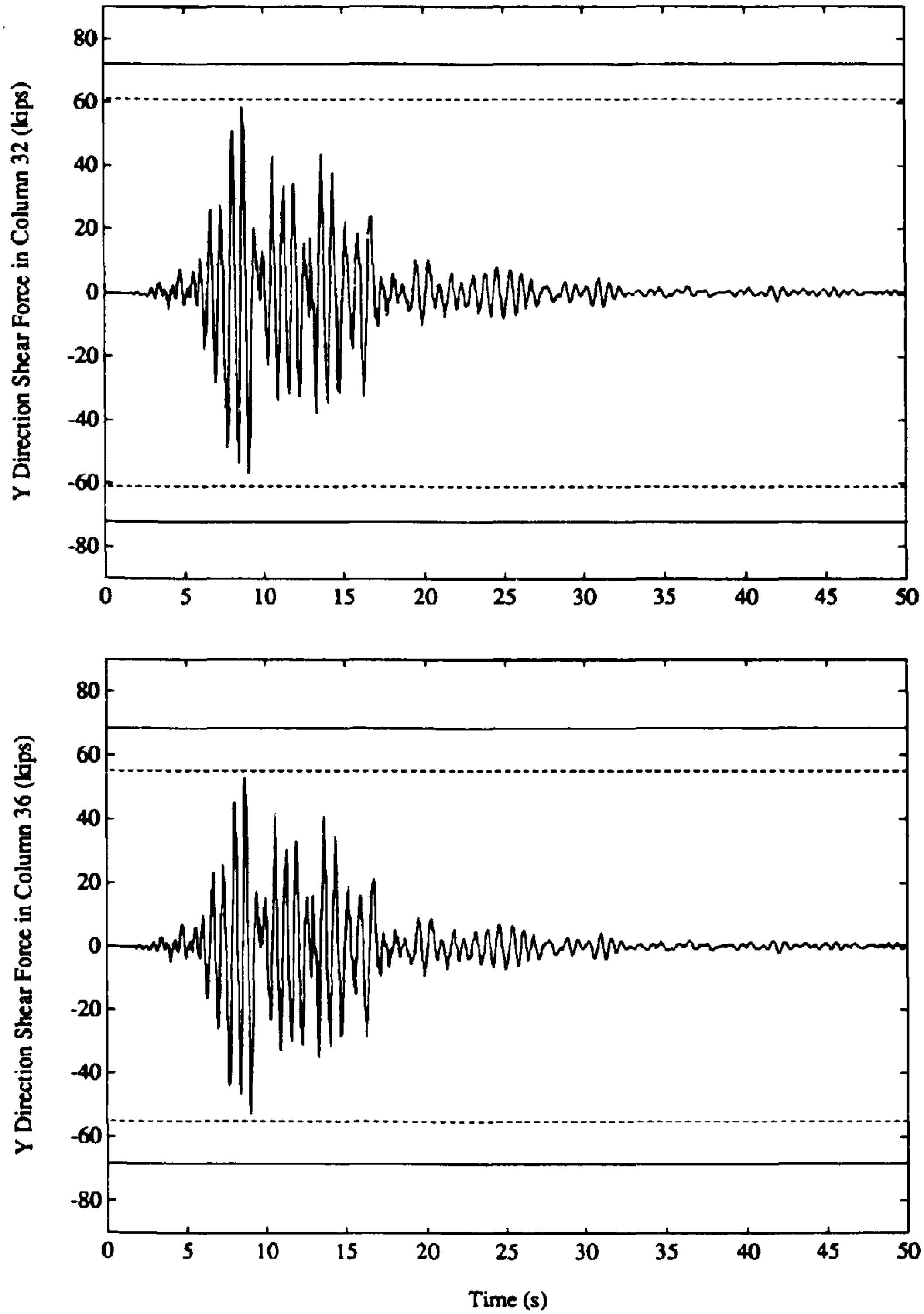

Figure C-17: Comparison of Earthquake Induced Shears in Columns 32 and 36 with "Design" Values in the Y-Direction

EARTHQUAKE ENGINEERING RESEARCH CENTER REPORT SERIES

EERC reports are available from the National Information Service for Earthquake Engineering (NISEE) and from the National Technical Information Service (NTIS). Numbers in parentheses are Accession Numbers assigned by the National Technical Information Service; these are followed by a price code. Contact NTIS, 5285 Port Royal Road, Springfield Virginia, 22161 for more information. Reports without Accession Numbers were not available from NTIS at the time of printing. For a current complete list of EERC reports (from EERC 67-1) and availablity information, please contact University of California, EERC, NISEE, 1301 South 46th Street, Richmond, California 94804.

UCB/EERC-82/01 "Dynamic Behavior of Ground for Seismic Analysis of Lifeline Systems," by Sato, T. and Der Kiureghian, A., January 1982, (PB82 218 926)A05.

UCB/EERC-82/02 "Shaking Table Tests of a Tubular Steel Frame Model," by Ghanaat, Y. and Clough, R.W., January 1982, (PB82 220 161)A07.

UCB/EERC-82/03 "Behavior of a Piping System under Seismic Excitation: Experimental Investigations of a Spatial Piping System supported by Mechanical Shock Arrestors," by Schneider, S., Lee, H.-M. and Godden, W. G., May 1982, (PB83 172 544)A09.

UCB/EERC-82/04 "New Approaches for the Dynamic Analysis of Large Structural Systems," by Wilson, E.L., June 1982, (PB83 148 080)A05.

UCB/EERC-82/05 "Model Study of Effects of Damage on the Vibration Properties of Steel Offshore Platforms," by Shahrivar, F. and Bouwkamp, J.G., June 1982, (PB83 148 742)A10.

UCB/EERC-82/06 "States of the Art and Practice in the Optimum Seismic Design and Analytical Response Prediction of R/C Frame Wall Structures," by Aktan, A.E. and Bertero, V.V., July 1982, (PB83 147 736)A05.

UCB/EERC-82/07 "Further Study of the Earthquake Response of a Broad Cylindrical Liquid-Storage Tank Model," by Manos, G.C. and Clough, R.W., July 1982, (PB83 147 744)A11.

UCB/EERC-82/08 "An Evaluation of the Design and Analytical Seismic Response of a Seven Story Reinforced Concrete Frame," by Charney, F.A. and Bertero, V.V., July 1982, (PB83 157 628)A09.

UCB/EERC-82/09 "Fluid-Structure Interactions: Added Mass Computations for Incompressible Fluid," by Kuo, J.S.-H., August 1982, (PB83 156 281)A07.

UCB/EERC-82/10 "Joint-Opening Nonlinear Mechanism: Interface Smeared Crack Model," by Kuo, J.S.-H., August 1982, (PB83 149 195)A05.

UCB/EERC-82/11 "Dynamic Response Analysis of Techi Dam," by Clough, R.W., Stephen, R.M. and Kuo, J.S.-H., August 1982, (PB83 147 496)A06.

UCB/EERC-82/12 "Prediction of the Seismic Response of R/C Frame-Coupled Wall Structures," by Aktan, A.E., Bertero, V.V. and Piazzo, M., August 1982, (PB83 149 203)A09.

UCB/EERC-82/13 "Preliminary Report on the Smart 1 Strong Motion Array in Taiwan," by Bolt, B.A., Loh, C.H., Penzien, J. and Tsai, Y.B., August 1982, (PB83 159 400)A10.

UCB/EERC-82/14 "Seismic Behavior of an Eccentrically X-Braced Steel Structure," by Yang, M.S., September 1982, (PB83 260 778)A12.

UCB/EERC-82/15 "The Performance of Stairways in Earthquakes," by Roha, C., Axley, J.W. and Bertero, V.V., September 1982, (PB83 157 693)A07.

UCB/EERC-82/16 "The Behavior of Submerged Multiple Bodies in Earthquakes," by Liao, W.-G., September 1982, (PB83 158 709)A07.

UCB/EERC-82/17 "Effects of Concrete Types and Loading Conditions on Local Bond-Slip Relationships," by Cowell, A.D., Popov, E.P. and Bertero, V.V., September 1982, (PB83 153 577)A04.

UCB/EERC-82/18 "Mechanical Behavior of Shear Wall Vertical Boundary Members: An Experimental Investigation," by Wagner, M.T. and Bertero, V.V., October 1982, (PB83 159 764)A05.

UCB/EERC-82/19 "Experimental Studies of Multi-support Seismic Loading on Piping Systems," by Kelly, J.M. and Cowell, A.D., November 1982, (PB90 262 684)A07.

UCB/EERC-82/20 "Generalized Plastic Hinge Concepts for 3D Beam-Column Elements," by Chen, P. F.-S. and Powell, G.H., November 1982, (PB83 247 981)A13.

UCB/EERC-82/21 "ANSR-III: General Computer Program for Nonlinear Structural Analysis," by Oughourlian, C.V. and Powell, G.H., November 1982, (PB83 251 330)A12.

UCB/EERC-82/22 "Solution Strategies for Statically Loaded Nonlinear Structures," by Simons, J.W. and Powell, G.H., November 1982, (PB83 197 970)A06.

UCB/EERC-82/23 "Analytical Model of Deformed Bar Anchorages under Generalized Excitations," by Ciampi, V., Eligehausen, R., Bertero, V.V. and Popov, E.P., November 1982, (PB83 169 532)A06.

UCB/EERC-82/24 "A Mathematical Model for the Response of Masonry Walls to Dynamic Excitations," by Sucuoglu, H., Mengi, Y. and McNiven, H.D., November 1982, (PB83 169 011)A07.

UCB/EERC-82/25 "Earthquake Response Considerations of Broad Liquid Storage Tanks," by Cambra, F.J., November 1982, (PB83 251 215)A09.

UCB/EERC-82/26 "Computational Models for Cyclic Plasticity, Rate Dependence and Creep," by Mosaddad, B. and Powell, G.H., November 1982, (PB83 245 829)A08.

UCB/EERC-82/27 "Inelastic Analysis of Piping and Tubular Structures," by Mahasuverachai, M. and Powell, G.H., November 1982, (PB83 249 987)A07.

UCB/EERC-83/01 "The Economic Feasibility of Seismic Rehabilitation of Buildings by Base Isolation," by Kelly, J.M., January 1983, (PB83 197 988)A05.

UCB/EERC-83/02 "Seismic Moment Connections for Moment-Resisting Steel Frames.," by Popov, E.P., January 1983, (PB83 195 412)A04.

UCB/EERC-83/03 "Design of Links and Beam-to-Column Connections for Eccentrically Braced Steel Frames," by Popov, E.P. and Malley, J.O., January 1983, (PB83 194 811)A04.

UCB/EERC-83/04 "Numerical Techniques for the Evaluation of Soil-Structure Interaction Effects in the Time Domain," by Bayo, E. and Wilson, E.L., February 1983, (PB83 245 605)A09.

UCB/EERC-83/05 "A Transducer for Measuring the Internal Forces in the Columns of a Frame-Wall Reinforced Concrete Structure," by Sause, R. and Bertero, V.V., May 1983, (PB84 119 494)A06.

UCB/EERC-83/06 "Dynamic Interactions Between Floating Ice and Offshore Structures," by Croteau, P., May 1983, (PB84 119 486)A16.

UCB/EERC-83/07 "Dynamic Analysis of Multiply Tuned and Arbitrarily Supported Secondary Systems," by Igusa, T. and Der Kiureghian, A., July 1983, (PB84 118 272)A11.

UCB/EERC-83/08 "A Laboratory Study of Submerged Multi-body Systems in Earthquakes," by Ansari, G.R., June 1983, (PB83 261 842)A17.

UCB/EERC-83/09 "Effects of Transient Foundation Uplift on Earthquake Response of Structures," by Yim, C.-S. and Chopra, A.K., June 1983, (PB83 261 396)A07.

UCB/EERC-83/10 "Optimal Design of Friction-Braced Frames under Seismic Loading," by Austin, M.A. and Pister, K.S., June 1983, (PB84 119 288)A06.

UCB/EERC-83/11 "Shaking Table Study of Single-Story Masonry Houses: Dynamic Performance under Three Component Seismic Input and Recommendations," by Manos, G.C., Clough, R.W. and Mayes, R.L., July 1983, (UCB/EERC-83/11)A08.

UCB/EERC-83/12 "Experimental Error Propagation in Pseudodynamic Testing," by Shing, P.B. and Mahin, S.A., June 1983, (PB84 119 270)A09.

UCB/EERC-83/13 "Experimental and Analytical Predictions of the Mechanical Characteristics of a 1/5-scale Model of a 7-story R/C Frame-Wall Building Structure," by Aktan, A.E., Bertero, V.V., Chowdhury, A.A. and Nagashima, T., June 1983, (PB84 119 213)A07.

UCB/EERC-83/14 "Shaking Table Tests of Large-Panel Precast Concrete Building System Assemblages," by Oliva, M.G. and Clough, R.W., June 1983, (PB86 110 210/AS)A11.

UCB/EERC-83/15 "Seismic Behavior of Active Beam Links in Eccentrically Braced Frames," by Hjelmstad, K.D. and Popov, E.P., July 1983, (PB84 119 676)A09.

UCB/EERC-83/16 "System Identification of Structures with Joint Rotation," by Dimsdale, J.S., July 1983, (PB84 192 210)A06.

UCB/EERC-83/17 "Construction of Inelastic Response Spectra for Single-Degree-of-Freedom Systems," by Mahin, S. and Lin, J., June 1983, (PB84 208 834)A05.

UCB/EERC-83/18 "Interactive Computer Analysis Methods for Predicting the Inelastic Cyclic Behaviour of Structural Sections," by Kaba, S. and Mahin, S., July 1983, (PB84 192 012)A06.

UCB/EERC-83/19 "Effects of Bond Deterioration on Hysteretic Behavior of Reinforced Concrete Joints," by Filippou, F.C., Popov, E.P. and Bertero, V.V., August 1983, (PB84 192 020)A10.

UCB/EERC-83/20 "Correlation of Analytical and Experimental Responses of Large-Panel Precast Building Systems," by Oliva, M.G., Clough, R.W., Velkov, M. and Gavrilovic, P., May 1988, (PB90 262 692)A06.

UCB/EERC-83/21 "Mechanical Characteristics of Materials Used in a 1/5 Scale Model of a 7-Story Reinforced Concrete Test Structure," by Bertero, V.V., Aktan, A.E., Harris, H.G. and Chowdhury, A.A., October 1983, (PB84 193 697)A05.

UCB/EERC-83/22 "Hybrid Modelling of Soil-Structure Interaction in Layered Media," by Tzong, T.-J. and Penzien, J., October 1983, (PB84 192 178)A08.

UCB/EERC-83/23 "Local Bond Stress-Slip Relationships of Deformed Bars under Generalized Excitations," by Eligehausen, R., Popov, E.P. and Bertero, V.V., October 1983, (PB84 192 848)A09.

UCB/EERC-83/24 "Design Considerations for Shear Links in Eccentrically Braced Frames," by Malley, J.O. and Popov, E.P., November 1983, (PB84 192 186)A07.

UCB/EERC-84/01 "Pseudodynamic Test Method for Seismic Performance Evaluation: Theory and Implementation," by Shing, P.-S.B. and Mahin, S.A., January 1984, (PB84 190 644)A08.

UCB/EERC-84/02 "Dynamic Response Behavior of Kiang Hong Dian Dam," by Clough, R.W., Chang, K.-T., Chen, H.-Q. and Stephen, R.M., April 1984, (PB84 209 402)A08.

UCB/EERC-84/03 "Refined Modelling of Reinforced Concrete Columns for Seismic Analysis," by Kaba, S.A. and Mahin, S.A., April 1984, (PB84 234 384)A06.

UCB/EERC-84/04 "A New Floor Response Spectrum Method for Seismic Analysis of Multiply Supported Secondary Systems," by Asfura, A. and Der Kiureghian, A., June 1984, (PB84 239 417)A06.

UCB/EERC-84/05 "Earthquake Simulation Tests and Associated Studies of a 1/5th-scale Model of a 7-Story R/C Frame-Wall Test Structure," by Bertero, V.V., Aktan, A.E., Charney, F.A. and Sause, R., June 1984, (PB84 239 409)A09.

UCB/EERC-84/06 "Unassigned," by Unassigned, 1984.

UCB/EERC-84/07 "Behavior of Interior and Exterior Flat-Plate Connections Subjected to Inelastic Load Reversals," by Zee, H.L. and Moehle, J.P., August 1984, (PB86 117 629/AS)A07.

UCB/EERC-84/08 "Experimental Study of the Seismic Behavior of a Two-Story Flat-Plate Structure," by Moehle, J.P. and Diebold, J.W., August 1984, (PB86 122 553/AS)A12.

UCB/EERC-84/09 "Phenomenological Modeling of Steel Braces under Cyclic Loading," by Ikeda, K., Mahin, S.A. and Dermitzakis, S.N., May 1984, (PB86 132 198/AS)A08.

UCB/EERC-84/10 "Earthquake Analysis and Response of Concrete Gravity Dams," by Fenves, G.L. and Chopra, A.K., August 1984, (PB85 193 902/AS)A11.

UCB/EERC-84/11 "EAGD-84: A Computer Program for Earthquake Analysis of Concrete Gravity Dams," by Fenves, G.L. and Chopra, A.K., August 1984, (PB85 193 613/AS)A05.

UCB/EERC-84/12 "A Refined Physical Theory Model for Predicting the Seismic Behavior of Braced Steel Frames," by Ikeda, K. and Mahin, S.A., July 1984, (PB85 191 450/AS)A09.

UCB/EERC-84/13 "Earthquake Engineering Research at Berkeley - 1984," by EERC, August 1984, (PB85 197 341/AS)A10.

UCB/EERC-84/14 "Moduli and Damping Factors for Dynamic Analyses of Cohesionless Soils," by Seed, H.B., Wong, R.T., Idriss, I.M. and Tokimatsu, K., September 1984, (PB85 191 468/AS)A04.

UCB/EERC-84/15 "The Influence of SPT Procedures in Soil Liquefaction Resistance Evaluations," by Seed, H.B., Tokimatsu, K., Harder, L.F. and Chung, R.M., October 1984, (PB85 191 732/AS)A04.

UCB/EERC-84/16 "Simplified Procedures for the Evaluation of Settlements in Sands Due to Earthquake Shaking," by Tokimatsu, K. and Seed, H.B., October 1984, (PB85 197 887/AS)A03.

UCB/EERC-84/17 "Evaluation of Energy Absorption Characteristics of Highway Bridges Under Seismic Conditions - Volume I (PB90 262 627)A16 and Volume II (Appendices) (PB90 262 635)A13," by Imbsen, R.A. and Penzien, J., September 1986.

UCB/EERC-84/18 "Structure-Foundation Interactions under Dynamic Loads," by Liu, W.D. and Penzien, J., November 1984, (PB87 124 889/AS)A11.

UCB/EERC-84/19 "Seismic Modelling of Deep Foundations," by Chen, C.-H. and Penzien, J., November 1984, (PB87 124 798/AS)A07.

UCB/EERC-84/20 "Dynamic Response Behavior of Quan Shui Dam," by Clough, R.W., Chang, K.-T., Chen, H.-Q., Stephen, R.M., Ghanaat, Y. and Qi, J.-H., November 1984, (PB86 115177/AS)A07.

UCB/EERC-85/01 "Simplified Methods of Analysis for Earthquake Resistant Design of Buildings," by Cruz, E.F. and Chopra, A.K., February 1985, (PB86 112299/AS)A12.

UCB/EERC-85/02 "Estimation of Seismic Wave Coherency and Rupture Velocity using the SMART 1 Strong-Motion Array Recordings," by Abrahamson, N.A., March 1985, (PB86 214 343)A07.

UCB/EERC-85/03 "Dynamic Properties of a Thirty Story Condominium Tower Building," by Stephen, R.M., Wilson, E.L. and Stander, N., April 1985, (PB86 118965/AS)A06.

UCB/EERC-85/04 "Development of Substructuring Techniques for On-Line Computer Controlled Seismic Performance Testing," by Dermitzakis, S. and Mahin, S., February 1985, (PB86 132941/AS)A08.

UCB/EERC-85/05 "A Simple Model for Reinforcing Bar Anchorages under Cyclic Excitations," by Filippou, F.C., March 1985, (PB86 112 919/AS)A05.

UCB/EERC-85/06 "Racking Behavior of Wood-framed Gypsum Panels under Dynamic Load," by Oliva, M.G., June 1985, (PB90 262 643)A04.

UCB/EERC-85/07 "Earthquake Analysis and Response of Concrete Arch Dams," by Fok, K.-L. and Chopra, A.K., June 1985, (PB86 139672/AS)A10.

UCB/EERC-85/08 "Effect of Inelastic Behavior on the Analysis and Design of Earthquake Resistant Structures," by Lin, J.P. and Mahin, S.A., June 1985, (PB86 135340/AS)A08.

UCB/EERC-85/09 "Earthquake Simulator Testing of a Base-Isolated Bridge Deck," by Kelly, J.M., Buckle, I.G. and Tsai, H.-C., January 1986, (PB87 124 152/AS)A06.

UCB/EERC-85/10 "Simplified Analysis for Earthquake Resistant Design of Concrete Gravity Dams," by Fenves, G.L. and Chopra, A.K., June 1986, (PB87 124 160/AS)A08.

UCB/EERC-85/11 "Dynamic Interaction Effects in Arch Dams," by Clough, R.W., Chang, K.-T., Chen, H.-Q. and Ghanaat, Y., October 1985, (PB86 135027/AS)A05.

UCB/EERC-85/12 "Dynamic Response of Long Valley Dam in the Mammoth Lake Earthquake Series of May 25-27, 1980," by Lai, S. and Seed, H.B., November 1985, (PB86 142304/AS)A05.

UCB/EERC-85/13 "A Methodology for Computer-Aided Design of Earthquake-Resistant Steel Structures," by Austin, M.A., Pister, K.S. and Mahin, S.A., December 1985, (PB86 159480/AS)A10.

UCB/EERC-85/14 "Response of Tension-Leg Platforms to Vertical Seismic Excitations," by Liou, G.-S., Penzien, J. and Yeung, R.W., December 1985, (PB87 124 871/AS)A08.

UCB/EERC-85/15 "Cyclic Loading Tests of Masonry Single Piers: Volume 4 - Additional Tests with Height to Width Ratio of 1," by Sveinsson, B., McNiven, H.D. and Sucuoglu, H., December 1985, (PB87 165031/AS)A08.

UCB/EERC-85/16 "An Experimental Program for Studying the Dynamic Response of a Steel Frame with a Variety of Infill Partitions," by Yanev, B. and McNiven, H.D., December 1985, (PB90 262 676)A05.

UCB/EERC-86/01 "A Study of Seismically Resistant Eccentrically Braced Steel Frame Systems," by Kasai, K. and Popov, E.P., January 1986, (PB87 124 178/AS)A14.

UCB/EERC-86/02 "Design Problems in Soil Liquefaction," by Seed, H.B., February 1986, (PB87 124 186/AS)A03.

UCB/EERC-86/03 "Implications of Recent Earthquakes and Research on Earthquake-Resistant Design and Construction of Buildings," by Bertero, V.V., March 1986, (PB87 124 194/AS)A05.

UCB/EERC-86/04 "The Use of Load Dependent Vectors for Dynamic and Earthquake Analyses," by Leger, P., Wilson, E.L. and Clough, R.W., March 1986, (PB87 124 202/AS)A12.

UCB/EERC-86/05 "Two Beam-To-Column Web Connections," by Tsai, K.-C. and Popov, E.P., April 1986, (PB87 124 301/AS)A04.

UCB/EERC-86/06 "Determination of Penetration Resistance for Coarse-Grained Soils using the Becker Hammer Drill," by Harder, L.F. and Seed, H.B., May 1986, (PB87 124 210/AS)A07.

UCB/EERC-86/07 "A Mathematical Model for Predicting the Nonlinear Response of Unreinforced Masonry Walls to In-Plane Earthquake Excitations," by Mengi, Y. and McNiven, H.D., May 1986, (PB87 124 780/AS)A06.

UCB/EERC-86/08 "The 19 September 1985 Mexico Earthquake: Building Behavior," by Bertero, V.V., July 1986.

UCB/EERC-86/09 "EACD-3D: A Computer Program for Three-Dimensional Earthquake Analysis of Concrete Dams," by Fok, K.-L., Hall, J.F. and Chopra, A.K., July 1986, (PB87 124 228/AS)A08.

UCB/EERC-86/10 "Earthquake Simulation Tests and Associated Studies of a 0.3-Scale Model of a Six-Story Concentrically Braced Steel Structure," by Uang, C.-M. and Bertero, V.V., December 1986, (PB87 163 564/AS)A17.

UCB/EERC-86/11 "Mechanical Characteristics of Base Isolation Bearings for a Bridge Deck Model Test," by Kelly, J.M., Buckle, I.G. and Koh, C.-G., November 1987, (PB90 262 668)A04.

UCB/EERC-86/12 "Effects of Axial Load on Elastomeric Isolation Bearings," by Koh, C.-G. and Kelly, J.M., November 1987.

UCB/EERC-87/01 "The FPS Earthquake Resisting System: Experimental Report," by Zayas, V.A., Low, S.S. and Mahin, S.A., June 1987, (PB88 170 287)A06.

UCB/EERC-87/02 "Earthquake Simulator Tests and Associated Studies of a 0.3-Scale Model of a Six-Story Eccentrically Braced Steel Structure," by Whittaker, A., Uang, C.-M. and Bertero, V.V., July 1987, (PB88 166 707/AS)A18.

UCB/EERC-87/03 "A Displacement Control and Uplift Restraint Device for Base-Isolated Structures," by Kelly, J.M., Griffith, M.C. and Aiken, I.D., April 1987, (PB88 169 933)A04.

UCB/EERC-87/04 "Earthquake Simulator Testing of a Combined Sliding Bearing and Rubber Bearing Isolation System," by Kelly, J.M. and Chalhoub, M.S., December 1990.

UCB/EERC-87/05 "Three-Dimensional Inelastic Analysis of Reinforced Concrete Frame-Wall Structures," by Moazzami, S. and Bertero, V.V., May 1987, (PB88 169 586/AS)A08.

UCB/EERC-87/06 "Experiments on Eccentrically Braced Frames with Composite Floors," by Ricles, J. and Popov, E., June 1987, (PB88 173 067/AS)A14.

UCB/EERC-87/07 "Dynamic Analysis of Seismically Resistant Eccentrically Braced Frames," by Ricles, J. and Popov, E., June 1987, (PB88 173 075/AS)A16.

UCB/EERC-87/08 "Undrained Cyclic Triaxial Testing of Gravels-The Effect of Membrane Compliance," by Evans, M.D. and Seed, H.B., July 1987, (PB88 173 257)A19.

UCB/EERC-87/09 "Hybrid Solution Techniques for Generalized Pseudo-Dynamic Testing," by Thewalt, C. and Mahin, S.A., July 1987, (PB 88 179 007)A07.

UCB/EERC-87/10 "Ultimate Behavior of Butt Welded Splices in Heavy Rolled Steel Sections," by Bruneau, M., Mahin, S.A. and Popov, E.P., September 1987, (PB90 254 285)A07.

UCB/EERC-87/11 "Residual Strength of Sand from Dam Failures in the Chilean Earthquake of March 3, 1985," by De Alba, P., Seed, H.B., Retamal, E. and Seed, R.B., September 1987, (PB88 174 321/AS)A03.

UCB/EERC-87/12 "Inelastic Seismic Response of Structures with Mass or Stiffness Eccentricities in Plan," by Bruneau, M. and Mahin, S.A., September 1987, (PB90 262 650/AS)A14.

UCB/EERC-87/13 "CSTRUCT: An Interactive Computer Environment for the Design and Analysis of Earthquake Resistant Steel Structures," by Austin, M.A., Mahin, S.A. and Pister, K.S., September 1987, (PB88 173 339/AS)A06.

UCB/EERC-87/14 "Experimental Study of Reinforced Concrete Columns Subjected to Multi-Axial Loading," by Low, S.S. and Moehle, J.P., September 1987, (PB88 174 347/AS)A07.

UCB/EERC-87/15 "Relationships between Soil Conditions and Earthquake Ground Motions in Mexico City in the Earthquake of Sept. 19, 1985," by Seed, H.B., Romo, M.P., Sun, J., Jaime, A. and Lysmer, J., October 1987, (PB88 178 991)A06.

UCB/EERC-87/16 "Experimental Study of Seismic Response of R. C. Setback Buildings," by Shahrooz, B.M. and Moehle, J.P., October 1987, (PB88 176 359)A16.

UCB/EERC-87/17 "The Effect of Slabs on the Flexural Behavior of Beams," by Pantazopoulou, S.J. and Moehle, J.P., October 1987, (PB90 262 700)A07.

UCB/EERC-87/18 "Design Procedure for R-FBI Bearings," by Mostaghel, N. and Kelly, J.M., November 1987, (PB90 262 718)A04.

UCB/EERC-87/19 "Analytical Models for Predicting the Lateral Response of R C Shear Walls: Evaluation of their Reliability," by Vulcano, A. and Bertero, V.V., November 1987, (PB88 178 983)A05.

UCB/EERC-87/20 "Earthquake Response of Torsionally-Coupled Buildings," by Hejal, R. and Chopra, A.K., December 1987.

UCB/EERC-87/21 "Dynamic Reservoir Interaction with Monticello Dam," by Clough, R.W., Ghanaat, Y. and Qiu, X-F., December 1987, (PB88 179 023)A07.

UCB/EERC-87/22 "Strength Evaluation of Coarse-Grained Soils," by Siddiqi, F.H., Seed, R.B., Chan, C.K., Seed, H.B. and Pyke, R.M., December 1987, (PB88 179 031)A04.

UCB/EERC-88/01 "Seismic Behavior of Concentrically Braced Steel Frames," by Khatib, I., Mahin, S.A. and Pister, K.S., January 1988, (PB91 210 898/AS)A11.

UCB/EERC-88/02 "Experimental Evaluation of Seismic Isolation of Medium-Rise Structures Subject to Uplift," by Griffith, M.C., Kelly, J.M., Coveney, V.A. and Koh, C.G., January 1988, (PB91 217 950/AS)A09.

UCB/EERC-88/03 "Cyclic Behavior of Steel Double Angle Connections," by Astaneh-Asl, A. and Nader, M.N., January 1988, (PB91 210 872)A05.

UCB/EERC-88/04 "Re-evaluation of the Slide in the Lower San Fernando Dam in the Earthquake of Feb. 9, 1971," by Seed, H.B., Seed, R.B., Harder, L.F. and Jong, H.-L., April 1988, (PB91 212 456/AS)A07.

UCB/EERC-88/05 "Experimental Evaluation of Seismic Isolation of a Nine-Story Braced Steel Frame Subject to Uplift," by Griffith, M.C., Kelly, J.M. and Aiken, I.D., May 1988, (PB91 217 968/AS)A07.

UCB/EERC-88/06 "DRAIN-2DX User Guide.," by Allahabadi, R. and Powell, G.H., March 1988, (PB91 212 530)A12.

UCB/EERC-88/07 "Theoretical and Experimental Studies of Cylindrical Water Tanks in Base-Isolated Structures," by Chalhoub, M.S. and Kelly, J.M., April 1988, (PB91 217 976/AS)A05.

UCB/EERC-88/08 "Analysis of Near-Source Waves: Separation of Wave Types Using Strong Motion Array Recording," by Darragh, R.B., June 1988, (PB91 212 621)A08.

UCB/EERC-88/09 "Alternatives to Standard Mode Superposition for Analysis of Non-Classically Damped Systems," by Kusainov, A.A. and Clough, R.W., June 1988, (PB91 217 992/AS)A04.

UCB/EERC-88/10 "The Landslide at the Port of Nice on October 16, 1979," by Seed, H.B., Seed, R.B., Schlosser, F., Blondeau, F. and Juran, I., June 1988, (PB91 210 914)A05.

UCB/EERC-88/11 "Liquefaction Potential of Sand Deposits Under Low Levels of Excitation," by Carter, D.P. and Seed, H.B., August 1988, (PB91 210 880)A15.

UCB/EERC-88/12 "Nonlinear Analysis of Reinforced Concrete Frames Under Cyclic Load Reversals," by Filippou, F.C. and Issa, A., September 1988, (PB91 212 589)A07.

UCB/EERC-88/13 "Implications of Recorded Earthquake Ground Motions on Seismic Design of Building Structures," by Uang, C.-M. and Bertero, V.V., November 1988, (PB91 212 548)A06.

UCB/EERC-88/14 "An Experimental Study of the Behavior of Dual Steel Systems," by Whittaker, A.S., Uang, C.-M. and Bertero, V.V., September 1988, (PB91 212 712)A16.

UCB/EERC-88/15 "Dynamic Moduli and Damping Ratios for Cohesive Soils," by Sun, J.I., Golesorkhi, R. and Seed, H.B., August 1988, (PB91 210 922)A04.

UCB/EERC-88/16 "Reinforced Concrete Flat Plates Under Lateral Load: An Experimental Study Including Biaxial Effects," by Pan, A. and Moehle, J.P., October 1988, (PB91 210 856)A13.

UCB/EERC-88/17 "Earthquake Engineering Research at Berkeley - 1988," by EERC, November 1988, (PB91 210 864)A10.

UCB/EERC-88/18 "Use of Energy as a Design Criterion in Earthquake-Resistant Design," by Uang, C.-M. and Bertero, V.V., November 1988, (PB91 210 906/AS)A04.

UCB/EERC-88/19 "Steel Beam-Column Joints in Seismic Moment Resisting Frames," by Tsai, K.-C. and Popov, E.P., November 1988, (PB91 217 984/AS)A20.

UCB/EERC-88/20 "Base Isolation in Japan, 1988," by Kelly, J.M., December 1988, (PB91 212 449)A05.

UCB/EERC-89/01 "Behavior of Long Links in Eccentrically Braced Frames," by Engelhardt, M.D. and Popov, E.P., January 1989, (PB92 143 056)A18.

UCB/EERC-89/02 "Earthquake Simulator Testing of Steel Plate Added Damping and Stiffness Elements," by Whittaker, A., Bertero, V.V., Alonso, J. and Thompson, C., January 1989, (PB91 229 252/AS)A10.

UCB/EERC-89/03 "Implications of Site Effects in the Mexico City Earthquake of Sept. 19, 1985 for Earthquake-Resistant Design Criteria in the San Francisco Bay Area of California," by Seed, H.B. and Sun, J.I., March 1989, (PB91 229 369/AS)A07.

UCB/EERC-89/04 "Earthquake Analysis and Response of Intake-Outlet Towers," by Goyal, A. and Chopra, A.K., July 1989, (PB91 229 286/AS)A19.

UCB/EERC-89/05 "The 1985 Chile Earthquake: An Evaluation of Structural Requirements for Bearing Wall Buildings," by Wallace, J.W. and Moehle, J.P., July 1989, (PB91 218 008/AS)A13.

UCB/EERC-89/06 "Effects of Spatial Variation of Ground Motions on Large Multiply-Supported Structures," by Hao, H., July 1989, (PB91 229 161/AS)A08.

UCB/EERC-89/07 "EADAP - Enhanced Arch Dam Analysis Program: Users's Manual," by Ghanaat, Y. and Clough, R.W., August 1989, (PB91 212 522)A06.

UCB/EERC-89/08 "Seismic Performance of Steel Moment Frames Plastically Designed by Least Squares Stress Fields," by Ohi, K. and Mahin, S.A., August 1989, (PB91 212 597)A05.

UCB/EERC-89/09 "Feasibility and Performance Studies on Improving the Earthquake Resistance of New and Existing Buildings Using the Friction Pendulum System," by Zayas, V., Low, S., Mahin, S.A. and Bozzo, L., July 1989, (PB92 143 064)A14.

UCB/EERC-89/10 "Measurement and Elimination of Membrane Compliance Effects in Undrained Triaxial Testing," by Nicholson, P.G., Seed, R.B. and Anwar, H., September 1989, (PB92 139 641/AS)A13.

UCB/EERC-89/11 "Static Tilt Behavior of Unanchored Cylindrical Tanks," by Lau, D.T. and Clough, R.W., September 1989, (PB92 143 049)A10.

UCB/EERC-89/12 "ADAP-88: A Computer Program for Nonlinear Earthquake Analysis of Concrete Arch Dams," by Fenves, G.L., Mojtahedi, S. and Reimer, R.B., September 1989, (PB92 139 674/AS)A07.

UCB/EERC-89/13 "Mechanics of Low Shape Factor Elastomeric Seismic Isolation Bearings," by Aiken, I.D., Kelly, J.M. and Tajirian, F.F., November 1989, (PB92 139 732/AS)A09.

UCB/EERC-89/14 "Preliminary Report on the Seismological and Engineering Aspects of the October 17, 1989 Santa Cruz (Loma Prieta) Earthquake," by EERC, October 1989, (PB92 139 682/AS)A04.

UCB/EERC-89/15 "Experimental Studies of a Single Story Steel Structure Tested with Fixed, Semi-Rigid and Flexible Connections," by Nader, M.N. and Astaneh-Asl, A., August 1989, (PB91 229 211/AS)A10.

UCB/EERC-89/16 "Collapse of the Cypress Street Viaduct as a Result of the Loma Prieta Earthquake," by Nims, D.K., Miranda, E., Aiken, I.D., Whittaker, A.S. and Bertero, V.V., November 1989, (PB91 217 935/AS)A05.

UCB/EERC-90/01 "Mechanics of High-Shape Factor Elastomeric Seismic Isolation Bearings," by Kelly, J.M., Aiken, I.D. and Tajirian, F.F., March 1990.

UCB/EERC-90/02 "Javid's Paradox: The Influence of Preform on the Modes of Vibrating Beams," by Kelly, J.M., Sackman, J.L. and Javid, A., May 1990, (PB91 217 943/AS)A03.

UCB/EERC-90/03 "Earthquake Simulator Testing and Analytical Studies of Two Energy-Absorbing Systems for Multistory Structures," by Aiken, I.D. and Kelly, J.M., October 1990, (PB92 192 988)A13.

UCB/EERC-90/04 "Damage to the San Francisco-Oakland Bay Bridge During the October 17, 1989 Earthquake," by Astaneh-Asl, A., June 1990.

UCB/EERC-90/05 "Preliminary Report on the Principal Geotechnical Aspects of the October 17, 1989 Loma Prieta Earthquake," by Seed, R.B., Dickenson, S.E., Riemer, M.F., Bray, J.D., Sitar, N., Mitchell, J.K., Idriss, I.M., Kayen, R.E., Kropp, A., Harder, L.F., Jr. and Power, M.S., April 1990, (PB 192 970)A08.

UCB/EERC-90/06 "Models of Critical Regions in Reinforced Concrete Frames Under Seismic Excitations," by Zulfiqar, N. and Filippou, F.C., May 1990.

UCB/EERC-90/07 "A Unified Earthquake-Resistant Design Method for Steel Frames Using ARMA Models," by Takewaki, I., Conte, J.P., Mahin, S.A. and Pister, K.S., June 1990.

UCB/EERC-90/08 "Soil Conditions and Earthquake Hazard Mitigation in the Marina District of San Francisco," by Mitchell, J.K., Masood, T., Kayen, R.E. and Seed, R.B., May 1990, (PB 193 267/AS)A04.

UCB/EERC-90/09 "Influence of the Earthquake Ground Motion Process and Structural Properties on Response Characteristics of Simple Structures," by Conte, J.P., Pister, K.S. and Mahin, S.A., July 1990, (PB92 143 064)A15.

UCB/EERC-90/10 "Experimental Testing of the Resilient-Friction Base Isolation System," by Clark, P.W. and Kelly, J.M., July 1990, (PB92 143 072)A08.

UCB/EERC-90/11 "Seismic Hazard Analysis: Improved Models, Uncertainties and Sensitivities," by Araya, R. and Der Kiureghian, A., March 1988.

UCB/EERC-90/12 "Effects of Torsion on the Linear and Nonlinear Seismic Response of Structures," by Sedarat, H. and Bertero, V.V., September 1989, (PB92 193 002/AS)A15.

UCB/EERC-90/13 "The Effects of Tectonic Movements on Stresses and Deformations in Earth Embankments," by Bray, J. D., Seed, R. B. and Seed, H. B., September 1989.

UCB/EERC-90/14 "Inelastic Seismic Response of One-Story, Asymmetric-Plan Systems," by Goel, R.K. and Chopra, A.K., October 1990.

UCB/EERC-90/15 "Dynamic Crack Propagation: A Model for Near-Field Ground Motion.," by Seyyedian, H. and Kelly, J.M., 1990.

UCB/EERC-90/16 "Sensitivity of Long-Period Response Spectra to System Initial Conditions," by Blasquez, R., Ventura, C. and Kelly, J.M., 1990.

UCB/EERC-90/17 "Behavior of Peak Values and Spectral Ordinates of Near-Source Strong Ground-Motion over a Dense Array," by Niazi, M., June 1990.

UCB/EERC-90/18 "Material Characterization of Elastomers used in Earthquake Base Isolation," by Papoulia, K.D. and Kelly, J.M., 1990.

UCB/EERC-90/19 "Cyclic Behavior of Steel Top-and-Bottom Plate Moment Connections," by Harriott, J.D. and Astaneh-Asl, A., August 1990, (PB91 229 260/AS)A05.

UCB/EERC-90/20 "Seismic Response Evaluation of an Instrumented Six Story Steel Building," by Shen, J.-H. and Astaneh-Asl, A., December 1990, (PB91 229 294/AS)A04.

UCB/EERC-90/21 "Observations and Implications of Tests on the Cypress Street Viaduct Test Structure," by Bollo, M., Mahin, S.A., Moehle, J.P., Stephen, R.M. and Qi, X., December 1990.

UCB/EERC-91/01 "Experimental Evaluation of Nitinol for Energy Dissipation in Structures," by Nims, D.K., Sasaki, K.K. and Kelly, J.M., 1991.

UCB/EERC-91/02 "Displacement Design Approach for Reinforced Concrete Structures Subjected to Earthquakes," by Qi, X. and Moehle, J.P., January 1991, (PB93 114 569/AS)A09.

UCB/EERC-91/03 "A Long-Period Isolation System Using Low-Modulus High-Damping Isolators for Nuclear Facilities at Soft-Soil Sites," by Kelly, J.M., March 1991, (PB93 114 577/AS)A10.

UCB/EERC-91/04 "Dynamic and Failure Characteristics of Bridgestone Isolation Bearings," by Kelly, J.M., April 1991, (PB93 114 528)A05.

UCB/EERC-91/05 "Base Sliding Response of Concrete Gravity Dams to Earthquakes," by Chopra, A.K. and Zhang, L., May 1991, (PB93 114 544/AS)A05.

UCB/EERC-91/06 "Computation of Spatially Varying Ground Motion and Foundation-Rock Impedance Matrices for Seismic Analysis of Arch Dams," by Zhang, L. and Chopra, A.K., May 1991, (PB93 114 825)A07.

UCB/EERC-91/07 "Estimation of Seismic Source Processes Using Strong Motion Array Data," by Chiou, S.-J., July 1991, (PB93 114 551/AS)A08.

UCB/EERC-91/08 "A Response Spectrum Method for Multiple-Support Seismic Excitations," by Der Kiureghian, A. and Neuenhofer, A., August 1991, (PB93 114 536)A04.

UCB/EERC-91/09 "A Preliminary Study on Energy Dissipating Cladding-to-Frame Connection," by Cohen, J.M. and Powell, G.H., September 1991, (PB93 114 510)A05.

UCB/EERC-91/10 "Evaluation of Seismic Performance of a Ten-Story RC Building During the Whittier Narrows Earthquake," by Miranda, E. and Bertero, V.V., October 1991, + (PB93 114 783)A06.

UCB/EERC-91/11 "Seismic Performance of an Instrumented Six Story Steel Building," by Anderson, J.C. and Bertero, V.V., November 1991.

UCB/EERC-91/12 "Performance of Improved Ground During the Loma Prieta Earthquake," by Mitchell, J.K. and Wentz, Jr., F.J., October 1991, (PB93 114 791)A06.

UCB/EERC-91/13 "Shaking Table - Structure Interaction," by Rinawi, A.M. and Clough, R.W., October 1991, (PB93 114 917)A13.

UCB/EERC-91/14 "Cyclic Response of RC Beam-Column Knee Joints: Test and Retrofit," by Mazzoni, S., Moehle, J.P. and Thewalt, C.R., October 1991, (PB93 120 277)A03.

UCB/EERC-91/15 "Design Guidelines for Ductility and Drift Limits: Review of State-of-the-Practice and State-of-the-Art in Ductility and Drift-Based Earthquake-Resistant Design of Buildings," by Bertero, V.V., Anderson, J.C., Krawinkler, H., Miranda, E. and The CUREe and The Kajima Research Teams, July 1991, (PB93 120 269)A08.

UCB/EERC-91/16 "Evaluation of the Seismic Performance of a Thirty-Story RC Building," by Anderson, J.C., Miranda, E., Bertero, V.V. and The Kajima Project Research Team, July 1991, (PB93 114 841)A12.

UCB/EERC-91/17 "A Fiber Beam-Column Element for Seismic Response Analysis of Reinforced Concrete Structures," by Taucer, F., Spacone, E. and Filippou, F.C., December 1991.

UCB/EERC-91/18 "Investigation of the Seismic Response of a Lightly-Damped Torsionally-Coupled Building," by Boroschek, R. and Mahin, S.A., December 1991, (PB93 120 335)A13.

UCB/EERC-92/01 "Studies of a 49-Story Instrumented Steel Structure Shaken During the Loma Prieta Earthquake," by Chen, C.-C., Bonowitz, D. and Astaneh-Asl, A., February 1992.

UCB/EERC-92/02 "Response of the Dumbarton Bridge in the Loma Prieta Earthquake," by Fenves, G.L., Filippou, F.C. and Sze, D.T., January 1992, (PB93 120 319)A09.

UCB/EERC-92/03 "Models for Nonlinear Earthquake Analysis of Brick Masonry Buildings," by Mengi, Y., McNiven, H.D. and Tanrikulu, A.K., March 1992, (PB93 120 293)A08.

UCB/EERC-92/04 "Shear Strength and Deformability of RC Bridge Columns Subjected to Inelastic Cyclic Displacements," by Aschheim, M. and Moehle, J.P., March 1992, (PB93 120 327)A06.

UCB/EERC-92/05 "Parameter Study of Joint Opening Effects on Earthquake Response of Arch Dams," by Fenves, G.L., Mojtahedi, S. and Reimer, R.B., April 1992, (PB93 120 301)A04.

UCB/EERC-92/06 "Seismic Behavior and Design of Semi-Rigid Steel Frames," by Nader, M.N. and Astaneh-Asl, A., May 1992.

UCB/EERC-92/07 "A Beam Element for Seismic Damage Analysis," by Spacone, E., Ciampi, V. and Filippou, F.C., August 1992.

UCB/EERC-92/08 "Nonlinear Static and Dynamic Analysis of Reinforced Concrete Subassemblages," by Filippou, F.C., D'Ambrisi, A. and Issa, A., August 1992.

UCB/EERC-92/09 "Evaluation of Code Accidental-Torsion Provisions Using Earthquake Records from Three Nominally Symmetric-Plan Buildings," by De la Llera, J.C. and Chopra, A.K., September 1992.